ADVANCES IN MOLTEN SALT CHEMISTRY
Volume 1

CONTRIBUTORS TO THIS VOLUME

C. R. Boston
Metals and Ceramics Division
Oak Ridge National Laboratory
Oak Ridge, Tennessee

John W. Hastie
National Bureau of Standards
Washington, D. C.

Ronald E. Hester
Department of Chemistry
University of York
York, England

Yizhak Marcus
Department of Inorganic and Analytical Chemistry
The Hebrew University of Jerusalem
Jerusalem, Israel

D. A. J. Swinkels
Senior Research Officer
Broken Hill Proprietary Co., Ltd.
Central Research Laboratory
Shortland, New South Wales, Australia

ADVANCES IN MOLTEN SALT CHEMISTRY Volume 1

Edited by

J. BRAUNSTEIN
Oak Ridge National Laboratory
Oak Ridge, Tennessee

GLEB MAMANTOV
The University of Tennessee
Knoxville, Tennessee

and

G. P. SMITH
Oak Ridge National Laboratory
Oak Ridge, Tennessee

PLENUM PRESS • NEW YORK–LONDON • 1971

Library of Congress Catalog Card Number 78-131884
ISBN 978-1-4757-0506-5 ISBN 978-1-4757-0504-1 (eBook)
DOI 10.1007/978-1-4757-0504-1

A Division of Plenum Publishing Corporation
227 West 17th Street, New York, N.Y. 10011

United Kingdom edition published by Plenum Press, London
A Division of Plenum Publishing Company, Ltd.
Davis House (4th Floor), 8 Scrubs Lane, Harlesden, NW10 6SE, England

ARTICLES PLANNED FOR FUTURE VOLUMES

High Temperature Coordination Chemistry of Group VIII
K. E. Johnson, University of Saskatchewan at Regina, and J. R. Dickinson, University of Virginia

Molten Organic Salts
J. E. Lind, Stanford University

Optical Interferometry Applied to the Study of Molten Salts
A. Lunden and S. E. Gustafsson, Chalmers Institute of Technology, Sweden

Gas Solubility in Molten Salts
P. E. Field, Virginia Polytechnic Institute

Electrode Kinetics of Molten Salts
D. Inman and A. D. Graves, Imperial College, London

FOREWORD

Molten salts are investigated by very diverse techniques and for differing purposes, and the results are reported in widely scattered journals. There is a need to keep investigators aware of progress in other specialties and to provide students with source and background material. *Advances in Molten Salt Chemistry* hopes to fill these needs by providing reviews of recent progress presented, insofar as is reasonable, with enough background material and commentary to be comprehensible to a nonspecialist. We prefer a discussion of underlying principles, to the extent that they are known, and we encourage authors to comment critically on the reliability of data, the utility of models, and the cogency of ideas and theories.

We take a broad view of the suitability of topics for inclusion in this series. Both fundamental and technological advances have a place here, as do studies on materials related to molten salts (like liquid silicates, very concentrated aqueous solutions, solutions of salts in liquid metals, and solid electrolytes).

We intend this series to serve the needs of those who investigate or use molten salts. We welcome suggestions of topics and suitable authors, as well as comments on the strengths and shortcomings of what is published.

J. BRAUNSTEIN
G. MAMANTOV
G. P. SMITH

PREFACE

Subjects chosen for this volume are among those which have been of interest to molten salt chemists over the years. Structural investigations are discussed in the first chapter, on vibrational spectroscopy of molten salts, and in the last chapter, on mass spectrometry of vapors above molten salts. The second chapter deals with the important area of liquid–liquid extraction including technological applications as well as theoretical aspects. Chapter 3 deals with the haloaluminates, a class of molten salts with a rich chemistry, and Chapter 4, on batteries and fuel cells, covers one of the significant areas of technological application of molten salts. In future volumes we hope to maintain a balance among theoretical, experimental, and applied topics in molten salts and peripheral areas.

We thank our many colleagues for their suggestions and cooperation. Special thanks are due Drs. D. M. Moulton and R. A. Strehlow of Oak Ridge National Laboratory for their valuable comments.

J. B., G. M., G. P. S.

CONTENTS

Chapter 3

MOLTEN SALT CHEMISTRY OF THE HALOALUMINATES

C. R. Boston

Chapter 4

MOLTEN SALT BATTERIES AND FUEL CELLS

D. A. J. SWINKELS

Chapter 5

THERMODYNAMIC STUDIES, BY MASS SPECTROMETRY, OF MOLTEN MIXED HALIDE SYSTEMS

J. W. HASTIE

Chapter 1

VIBRATIONAL ASPECTS OF MOLTEN SALTS

Ronald E. Hester
Department of Chemistry
University of York
York, England

1. PRINCIPLES OF INFRARED AND RAMAN SPECTROSCOPY

1.1. Introduction

Vibrational spectroscopy provides perhaps the most direct information on the nature of chemical species present in molten salts and on the interactions of these species with one another. Equipment is now available in many laboratories for absorption studies in the normal infrared region (say 400–4000 cm^{-1}) and in the far infrared (say 30–400 cm^{-1}) and for Raman scattering with frequency shifts over the whole range *ca.* 20–4000 cm^{-1}. In recent years a number of workers have devised methods of constructing furnace assemblies suitable for molten salt studies within the design limitations imposed by commercially available infrared and Raman spectrometers, and it is the purpose of this chapter to review these experiments and to assess the results and interpretations made.

The only other technique that provides similar information to that obtainable from vibrational spectroscopy is that of inelastic scattering of slow neutrons. Very little work has so far been attempted in applying this technique to molten salts,[1] and it is self-evident that only very few workers will have access to the equipment needed.

1.2. Molecular Vibrations

As a good approximation, it is generally assumed that the vibrational part of the internal energy of a molecule can be separated from the electronic and rotational contributions. Moreover, it is common practice to neglect the anharmonicity of molecular vibrations. These simplifications greatly ease the burden of formulating expressions for the energies and activities of vibrational modes in polyatomic molecules.

For a diatomic molecule in its electronic ground state, the assumption of a harmonic potential function of the form $U = (f/2)(r - r_e)^2$, where f is the bond force constant and r and r_e are, respectively, an arbitrary and the equilibrium internuclear distances, results in the following expression for the vibrational energy levels:

$$E_v = h\nu(v + \tfrac{1}{2})$$

The quantum-mechanical selection rule governing transitions between these (equally spaced) energy levels is $v = \pm 1$ only, resulting in the spectroscopic inactivity of all modes other than the *fundamental* (and "hot band modes" of the same energy as the fundamental, corresponding to transitions from vibrationally excited states). The bond force constant is related to this fundamental mode frequency by $\nu = (1/2\pi)\sqrt{f/\mu}$, where μ is the reduced mass of the molecule.

This ideally simple situation breaks down in practice due (primarily) to anharmonicity in the potential function. The potential function can be written in an expanded form to include higher powers of $(r - r_e)$, resulting in the vibrational energy levels

$$E_v = h\nu[(v + \tfrac{1}{2}) + x(v + \tfrac{1}{2})^2 + y(v + \tfrac{1}{2})^3 + \cdots]$$

Here the anharmonicity constant $x \ll 1$, $y \ll x$, etc., but the effect of anharmonicity is usually sufficient to cause detectable crowding together of the energy levels as the quantum number v increases and relaxation of the selection rule for transitions, such that $v = \pm 2, \pm 3$, etc. are permitted. These are the overtone modes which, together with combination modes in polyatomic molecules, considerably enrich the spectra of real molecules at high frequencies. It will be apparent that overtones will occur at frequencies less than twice the corresponding fundamental frequency and that hot bands no longer will be expected to have the same frequency as the fundamental. This latter point can be important in determining intensities and band shapes in the spectra of high temperature systems, particularly

for low frequency modes. With a molecule at 700°C, for example, a simple Boltzmann distribution calculation shows that even at the fifth vibrational level ($v = 5$) the population is still about half that of the ground level for a 100-cm^{-1} non degenerate fundamental mode.

For polyatomic molecules it is usual to make the approximation that the total vibrational energy can be written as a sum of individual energies associated with each of the vibrational degrees of freedom. With allowance made for anharmonicity, the energy expression incorporates the combination mode possibility as follows:

$$\begin{aligned} E_v = {} & h\nu_1(v_1 + \tfrac{1}{2}) + h\nu_2(v_2 + \tfrac{1}{2}) + \cdots \\ & + hx_1(v_1 + \tfrac{1}{2})^2 + hx_2(v_2 + \tfrac{1}{2})^2 + \cdots \\ & + hx_{12}(v_1 + \tfrac{1}{2})(v_2 + \tfrac{1}{2}) + \ldots \end{aligned}$$

where the anharmonicity constants $x_1, x_2 \ll 1$ as before, and similarly $x_{12} \ll 1$. The nomenclature normally used to describe transitions between

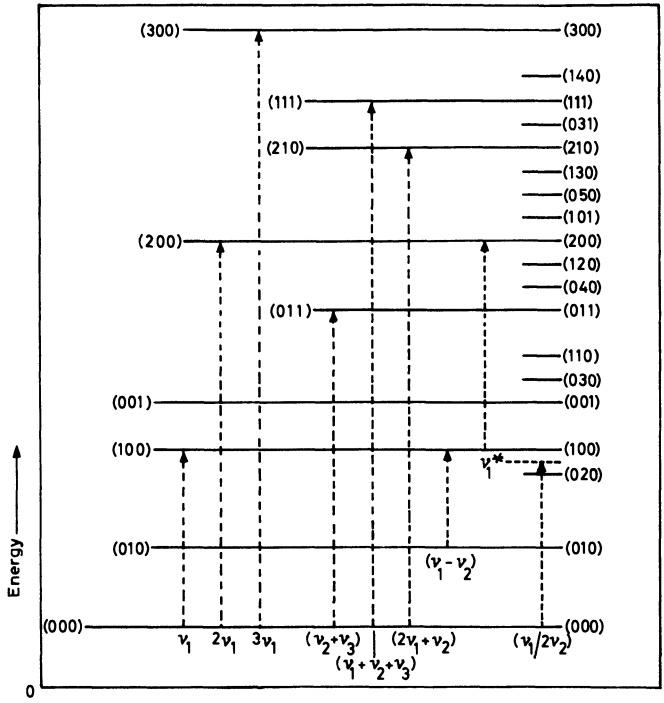

Fig. 1. Energy level diagram (schematic) for a molecule with three modes of vibration. (Adapted from M. J. Ware, in *Physical Methods in Advanced Inorganic Chemistry* (H. A. O. Hill and P. Day, eds.) Wiley-Interscience, New York, 1968, Chap. 6.)

TABLE I. Nomenclature for Some Vibrational Modes

Transition	Name	Symbol
(100) ← (000)	Fundamental	ν_1
(200) ← (000)	First overtone	$2\nu_1$
(300) ← (000)	Second overtone	$3\nu_1$
(011) ← (000)	Binary combination	$\nu_2 + \nu_3$
(111) ← (000)	Ternary combination	$\nu_1 + \nu_2 + \nu_3$
(210) ← (000)	Ternary combination	$2\nu_1 + \nu_2$
(100) ← (010)	Difference tone	$\nu_1 - \nu_2$
(200) ← (100)	Hot band	ν_1*
(100), (020) ← (000)	Fermi resonance	$\nu_1/2\nu_2$

the various energy levels of a polyatomic molecule can be summarized by means of the simple example of a molecule with just three vibrational degrees of freedom (for example, H_2O, CO_2). Three quantum numbers (ν_1, ν_2, ν_3) are needed to specify each of the energy states of such a molecule, and these are the numbers enclosed in parentheses on the illustrative energy level diagram given as Figure 1. Some of the possible transitions in absorption for an anharmonic oscillator are shown as vertically disposed arrows in the diagram, and these are named and symbolized appropriately in Table I.

Although the original harmonic oscillator assumption has been dropped now, it will be noticed that the separation of vibrational energy from the electronic and rotational energy of a molecule has been retained. The cases of vibronic interaction and Coriolis interaction where this further approximation breaks down are treated elsewhere,[2] but they will be neglected here since there are no data on them in molten salt spectroscopy.

1.3. Normal Modes

An n-atomic molecule has $3n$ degrees of freedom arising from the combined motions of the atoms. Of these, three are translations of the molecule as a whole, and for a non linear molecule three more are rotations while for a linear molecule there are just two rotational degrees of freedom. There are thus $3n - 6$ (or $3n - 5$) vibrational degrees of freedom for an n-atomic molecule. There are similarly $3n - 6$ (or $3n - 5$) *normal modes*

of vibration for an n-atomic molecule, these being complicated molecular motions wherein each atom moves with the same frequency (simple harmonic motion almost invariably assumed) and in phase with all the other atoms. Examples of such collective motions are given in Fig. 2 for general AB_2 molecules, both bent and linear. Any other conceivable mode of vibration of these molecules, as indeed for all molecules, can be represented as a superimposition of two or more of the normal vibrations. It is of interest to note that the linear AB_2 system has two equivalent (though not identical) normal modes. These will be equal in energy and are said to be *doubly degenerate.*

The form of the normal modes for any molecule in principle may be determined by solution of the equations of motion appropriate to it. A general form of these equations may be established as follows:

Small displacements of atoms (nuclei, more precisely) from their equilibrium positions may be described in terms of simple Cartesian dis-

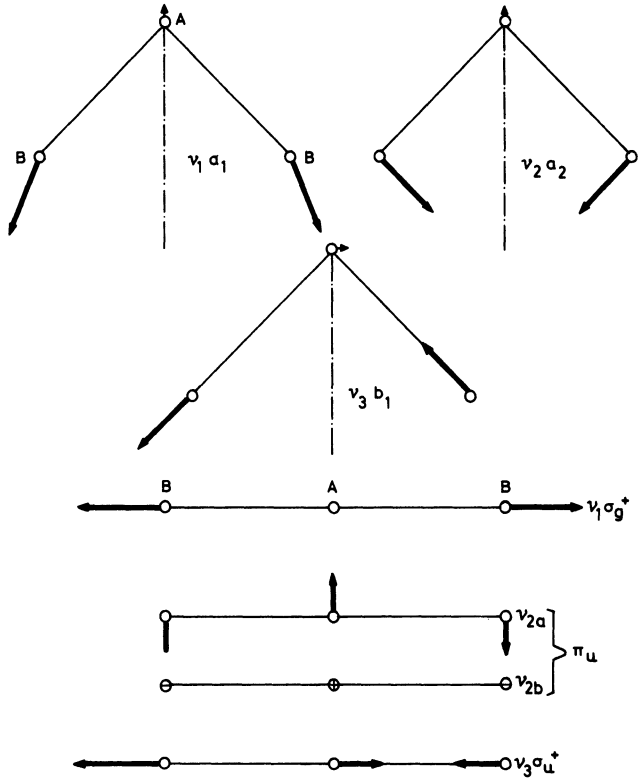

Fig. 2. Normal vibrations of bent and linear AB_2 molecules.

placement coordinates Δx, Δy, Δz or more conveniently by mass-weighted displacement coordinates $q_1 = \sqrt{m_1}\,\Delta x_1$, $q_2 = \sqrt{m_1}\,\Delta y_1$, $q_3 = \sqrt{m_1}\,\Delta z_1$, $q_4 = \sqrt{m_2}\,\Delta x_2$, etc. These coordinates enable the kinetic energy (T) and potential energy (U) to be written in the form

$$T = \frac{1}{2}\sum_{i}^{3n} \dot{q}_i^2$$

and

$$U = U_0 + \sum_{i}^{3n}\left(\frac{\partial U}{\partial q_i}\right)_0 q_i + \frac{1}{2}\sum_{i,j}^{3n}\left(\frac{\partial^2 U}{\partial q_i\,\partial q_j}\right)_0 q_i q_j + \cdots$$

The potential energy expression is normally terminated at the quadratic term, and U_0 is identified with the energy zero. Also, since U reaches a minimum at $q_i = 0$, $(\partial U/\partial q_i)_0 = 0$, and the potential energy expression reduces to

$$U = \frac{1}{2}\sum_{i,j}^{3n} f_{ij} q_i q_j$$

with $f_{ij} = (\partial^2 U/\partial q_i\,\partial q_j)_0$. The cross products in the potential energy expression can be removed by transforming the mass-weighted displacement coordinates q_i into a new set Q_k which are orthogonal, viz.,

$$Q_k = \sum_{i}^{3n} B_{ki} q_i \qquad k = 1, 2, 3, \cdots, 3n$$

These are the normal coordinates. The B_{ki} are chosen such that

$$T = \frac{1}{2}\sum_{k}^{3n} \dot{Q}_k^2 \qquad U = \frac{1}{2}\sum_{k}^{3n} \lambda_k Q_k^2$$

Substitution of these kinetic and potential energy expressions in Newton's equations of motion in the Lagrangian form[3] results in the second-order differential equations

$$\ddot{Q}_k + \lambda_k Q_k = 0 \qquad k = 1, 2, 3, \cdots, 3n$$

which have solutions of the form

$$Q_k = A_k \cos(\sqrt{\lambda_k}\,t + \phi_k) \qquad k = 1, 2, 3, \cdots, 3n$$

where A_k and ϕ_k are constants and λ_k is related to the normal mode frequency ν_k thus

$$\lambda_k = 4\pi^2 \nu_k^2$$

Methods for obtaining values for the λ_k are available through solution of the *secular equation*[4] for the particular molecule, but these require knowledge of the force constants governing the vibrations. It is usual to determine force constants from a knowledge of the vibrational (normal mode) frequencies, though even this procedure is fraught with danger due to the fact that there are almost invariably more force constants than frequencies, so that approximate forms of the molecular force field have to be assumed. If the λ_k can be determined, then the normal coordinates Q_k can be described. We see that these are time-dependent coordinates, the forms sketched in Fig. 2 being instantaneous representations only, with the arrows indicating the relative velocities and amplitudes of motion of the individual nuclei.

1.4. Infrared and Raman Spectra: Selection Rules

Transitions such as those indicated in Fig. 1 can be brought about by direct absorption of energy from electromagnetic radiation in the infrared region of the spectrum. The transition probability is determined by integrals of the form $\int \psi_f^* \boldsymbol{\mu} \psi_i \, d\tau$, where ψ_i and ψ_f are wave functions corresponding to the initial and final energy states, respectively, and $\boldsymbol{\mu}$ is an operator corresponding to the vector sum of the three components of an electric dipole. $\boldsymbol{\mu}$ thus can be replaced by μ_x, μ_y, or μ_z, which have the same symmetry properties as simple displacements of the molecule in the x, y, and z directions. The symmetry of a molecule is of great importance in determining the activities of its normal modes of vibration, since it is necessary for the transition probability integrand to contain a component that is *totally symmetric* with respect to the symmetry operations that comprise the *point group* to which the molecule belongs. The methods of *group theory*[4,5] can be used to show very readily that the wave function for the vibrationally excited state, which has the same symmetry properties as the normal mode, must belong to the same *symmetry species* (*irreducible representation*) as a component of $\boldsymbol{\mu}$ if the transition probability integral is to be non zero. Very simply, this means that a normal mode can be infrared-active only if it has the same symmetry properties (belongs to the same irreducible representation of the molecular point group) as one or more of the three Cartesian coordinates. Point group character tables commonly show the species of the Cartesian coordinates, making this an easy rule to apply.

Classically, the blanket rule for infrared activity of a normal mode is that there should be a finite oscillating dipole associated with the mode. This condition for activity may be expressed $(\partial \boldsymbol{\mu}/\partial Q_k)_0 \neq 0$. The corre-

sponding condition for Raman activity is $(\partial\boldsymbol{\alpha}/\partial Q_k)_0 \neq 0$, where $\boldsymbol{\alpha}$ is the molecular polarizability.

Unlike infrared absorption, Raman scattering[6] is a second-order effect, which is intrinsically much weaker and less readily understood in quantum-mechanical terms. The process of inelastic scattering of high energy (compared with the energy needed to produce vibrational transitions) photons requires the postulation of some "virtual" state[7–9] of the scattering molecule, which can have no simple correspondence with an *actual* or *stationary state* of the molecule. There is thereby a clear distinction from ordinary fluorescence, although the terms Stokes and anti-Stokes are used in both cases to denote shifts of the exciting radiation to long- and short-wavelength, respectively. Typical lifetimes of virtual and actual electronically excited states are of the order 10^{-15} and 10^{-8} sec, respectively, allowing intermolecular collisional deactivation of fluorescence but not of the Raman effect. It must be emphasised that the virtual states of molecules that arise in a discussion of Raman scattering are mere artifacts of mathematical convenience, originating in the perturbation treatment of this problem. For the effective experimental study of Raman scattering, indeed, it is necessary to use exciting radiation that is well-removed from any characteristic absorption frequency of the molecule under study. The special case of resonance Raman scattering[9,10] which arises when the exciting frequency approaches a region of electronic (vibronic) absorption, will not be discussed here.

The vibrational transition probability for the Raman effect is determined by integrals of the form $\int \psi_f^* \boldsymbol{\alpha} \psi_i \, d\tau$, which are similar to those governing infrared absorption. However, while the dipole moment operator $\boldsymbol{\mu}$ can be expressed as a *vector* with components μ_x, μ_y, μ_z, the molecular polarizability $\boldsymbol{\alpha}$ is a *tensor*, since it relates two vectors through the equation $\boldsymbol{\mu}_i = \boldsymbol{\alpha}\mathbf{E}$, where $\mathbf{E}$ represents the electric vector of the incident radiation that perturbs the molecule and $\boldsymbol{\mu}_i$ is an induced dipole. $\boldsymbol{\alpha}$ is a scalar quantity only when the molecule is *isotropic*, so that the vectors $\boldsymbol{\mu}_i$ and $\mathbf{E}$ point in the same direction. More generally, the *polarizability tensor* has nine components and takes the form

$$\begin{bmatrix} \alpha_{xx} & \alpha_{xy} & \alpha_{xz} \\ \alpha_{yx} & \alpha_{yy} & \alpha_{yz} \\ \alpha_{zx} & \alpha_{zy} & \alpha_{zz} \end{bmatrix}$$

though for most cases of interest this tensor in symmetrical, with $\alpha_{xy} = \alpha_{yx}$, $\alpha_{xz} = \alpha_{zx}$, and $\alpha_{yz} = \alpha_{zy}$, so that the number of distinct com-

ponents is six. It is convenient to think of $\boldsymbol{\alpha}$ in terms of a *polarizability ellipsoid* having the form $\alpha_{xx}X^2 + \alpha_{yy}Y^2 + \alpha_{zz}Z^2 + 2\alpha_{xy}XY + 2\alpha_{yz}YZ + 2\alpha_{xz}XZ = 1$, which reduces to $AX^2 + BY^2 + CZ^2 = 1$ if the principal axes X, Y, Z of the ellipsoid are chosen to coincide with the coordinate axes x, y, z. This ellipsoid has the same transformation properties as the polarizability tensor itself. The transformation properties of products of Cartesian coordinates are commonly given in point group character tables, so that, recognizing that these behave in the same way as the corresponding components of the polarizability tensor, it is easy to formulate a useful rule for Raman activity in a similar way to that used for infrared activity. The rule is that a normal mode can be Raman-active only if it has the same symmetry properties (belongs to the same irreducible representation of the molecular point group) as one or more of the products (or combinations of products such as $x^2 - y^2$) of the three Cartesian coordinates.

Since the *selection rules* for activity of a normal mode differ so fundamentally for infrared absorption and Raman scattering it is usually necessary to make both types of measurement if the fullest possible vibrational analysis is to be made. Even where all modes for a given molecule are infrared-active, it still pays to do the Raman work because additional information on the nature of the modes is available from the polarization properties of Raman lines. Referring to the light-scattering diagram given as Fig. 3, if light incident on a molecule is represented by two vectors $\mathbf{E}_x^i$ and $\mathbf{E}_z^i$,

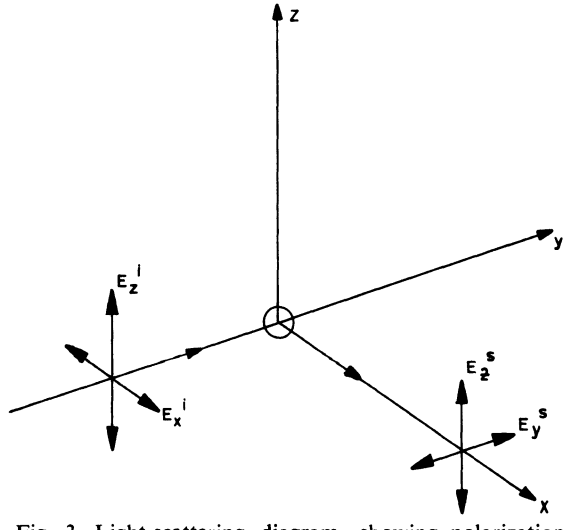

Fig. 3. Light-scattering diagram, showing polarization directions.

and the 90° scattered light by $\mathbf{E}_y^s$ and $\mathbf{E}_z^s$, it is clear that $\mathbf{E}_y^s$ must be zero unless some rotation of the planes of polarization of the incident light is brought about by the scattering process. If no such rotation occurs, the scattered light will be plane polarized in the z-direction. The relative intensities of light scattered in the y- and z-directions are used to define a *depolarization ratio* or *degree of depolarization*. For Raman scattering of natural light this ratio takes the form[7]

$$\varrho_n = \frac{I_y}{I_z} = \frac{6(\gamma')^2}{45(\bar{\alpha}')^2 + 7(\gamma')^2}$$

where $\bar{\alpha}'$ and γ' are independent of the orientation of the scattering molecule with respect to the fixed coordinate system and are given by

$$\bar{\alpha}' = (\tfrac{1}{3})(\alpha'_{xx} + \alpha'_{yy} + \alpha'_{zz}) \qquad \gamma' = (\tfrac{1}{2})[(\alpha'_{xx} - \alpha'_{yy})^2 + (\alpha'_{yy} - \alpha'_{zz})^2 + (\alpha'_{zz} - \alpha'_{xx})^2 + 6(\alpha'^2_{xy} + \alpha'^2_{yz} + \alpha'^2_{xz})]$$

The primes signify derivatives of the polarizability tensor components with respect to the normal coordinate, that is, $\alpha' = (\partial\alpha/\partial Q)_0$, and it is apparent that $\bar{\alpha}$ is a form of *mean molecular polarizability* while γ is the *anisotropy* of the polarizability. We see that for the special case of an isotropic derived polarizability tensor (for example, totally symmetric stretching mode of CH_4) $\varrho_n = 0$ and a completely polarized Raman line results (unless $\bar{\alpha}'$ also is zero, when the mode is Raman-inactive). If $\bar{\alpha}'$ is zero, $\varrho_n = \frac{6}{7}$, and the resulting line is said to be fully depolarized. It can be said quite generally that Raman lines arising from totally symmetric modes will have $0 \leq \varrho_n < \frac{6}{7}$ with the equal sign applying only to molecules belonging to one of the cubic symmetry point groups, while all other lines will have $\varrho_n = \frac{6}{7}$.

If the incident light in Fig. 3 is plane polarized in the z-direction (the usual situation for laser excitation), the degree of depolarization takes the new form

$$\varrho_p = \frac{3(\gamma')^2}{45(\bar{\alpha}')^2 + 4(\gamma')^2}$$

so that in this case totally symmetric modes give $0 \leq \varrho_p < \frac{3}{4}$, while all others give $\varrho_p = \frac{3}{4}$. Again, this formulation is appropriate for scattering at 90° to $\mathbf{E}_z^i$ only, that is, in the x-direction. For scattering in the xz-plane at an angle θ to the x-direction, the degree of depolarization is given[8] by

$$\varrho(\theta) = \frac{\varrho_p}{1 - (1 - \varrho_p)\sin^2\theta}$$

while ϱ_p is invariant in the xy-plane. The validity of this relationship has been checked by recent angular-dependence measurements,[19] and it has been shown that determination of angular variations of intensity in the xy-plane can be used to give very precise ϱ_p values.[19,20]

The reader who is not familiar with the methods of applying group theory to the determination of the symmetry species, degeneracies and activities of normal modes is referred to the several excellent (and lengthy) treatments that have been available in textbook form for several years.[2,4,5,11,12] Since we are concerned here with molten salt spectroscopy, we also must be prepared to consider the consequences of strong interionic/intermolecular interactions that might in extreme cases result in retention of a quasi-lattice structure in the melt. The vibrational modes in this case can be treated by an analysis based on the appropriate crystallographic Bravais unit cell.[13,14] Methods for using this *factor group* analysis have been developed by several authors, and the reader is referred to the original literature for these,[15–17] and for the alternative and somewhat simpler treatment of crystal vibrations by *site group* analysis.[17,18] All these methods are easy to apply if the structure and symmetry of the molecular or crystallographic unit is known. However, it is likely that in many (perhaps most) cases the quasi-crystalline lattice symmetry of a molten salt (even supposing that it is meaningful to discuss this at all) will be different from the solid from which it derives,[21] and the failure to observe all the lattice lines predicted by alternative model structures will make this type of detailed analysis rather pointless.

2. EXPERIMENTAL TECHNIQUES

2.1. Spectrometer Modifications for Molten Salt Work

Most commercial near-infrared and Raman spectrometers need little modification for use with molten salt samples, provided that they have a reasonably spacious sample area which is readily accessible. The problem of direct radiation from a hot sample interfering with the measurement of transmitted infrared radiation or scattered Raman radiation can be serious, however, particularly with long wavelengths and very high temperature samples, and commonly requires instrument modification for its solution. Trouble from localized heating of essential spectrometer components usually is easy to eliminate by judicious use of baffles and water-cooled shields.

Many commercial near infrared double-beam spectrometers use a rotating chopper to recombine reference and sample beams after passage

through the sampling compartment. A phase-sensitive detection system locked to the chopper frequency thus will detect infrared emission from a hot sample just as readily as it will detect radiation from the source. In order to discriminate against the hot sample emission in such a situation it is necessary to replace the standard chopper by a static beam-splitter (for recombination of reference and sample beams) and to introduce a new chopper between the source and the sampling compartment such that both reference and sample beams are chopped before entering the compartment. Some manufactures sell such a prechopper as an accessory, but since the chopping frequency is low (*ca.* 10–15 cps) for use with slow-response infrared detectors, homemade devices of the reciprocating flag type are easily made. A slotted, front-surface-aluminized glass or metal plate serves as a simple and effective beam-splitter.[21,22]

For the far-infrared region (*ca.* 30–400 cm^{-1}), instruments with monochromators can be used and modified if necessary, as above. The Michaelson interferometer type of far-infrared instrument usually has a built-in prechopper, so that no modification other than the construction of a suitable sample cell is necessary. However, difficulties of a different kind are encountered in far-infrared work, since the lens and cell window materials used here are usually polyethylene and polypropylene and neither will withstand much heating. Very little molten salt infrared absorption work has been done in this spectral region, though some experiments using diamond windows have been reported.[23]

Standard Raman spectrometers are in many ways ideally suited for high temperature studies, particularly when blue-end excitation is used (for example, Hg arc or Ar ion laser). There is relatively very little direct emission in the short wavelength end of the visible spectrum from samples at temperatures up to *ca.* 1200°C, and it matters little whether or not presample chopping of the source is used. This assumes that photoelectric detection methods are used, of course, because photographic plates would be blackened by long exposure to emission from a red-hot sample. If red-end excitation (for example, He/Ne laser) is used, however, this necessitates the use of red-sensitive photomultiplier tubes for signal detection, and once again it becomes necessary to prechop the source radiation and avoid chopping the radiation from the sample in order to eliminate interference by the emission from red-hot samples. Unlike most infrared detectors in use in commercial spectrometers, the photomultipliers used in Raman spectrometers have very fast response characteristics, and it is advantageous[24] to use chopping frequencies in the 500–1000 cps range.

Gas lasers as light sources have considerable advantages over the more

traditional arc and discharge lamps for Raman spectroscopy with molten salts, as will be seen from the comparisons made in a following section, but it is not usually possible to change sources without incurring great expense.

2.2. Transmission, Reflectance, and Emission Infrared Methods

Due to the high extinction coefficients of many infrared absorption bands characteristic of polyatomic ions, it is generally necessary to use thin films of molten salts in order to avoid total absorption of the source radiation in the traditional transmission method. For an alkali metal nitrate melt, for example, a path length as low as about 1μ is needed to avoid total absorption by the *ca.* 1400 cm^{-1} $\nu_3 E'$ mode of the nitrate ion. There are obvious problems in holding a high temperature, and often corrosive, molten salt in an infrared beam, and these are discussed in Section 2.4. However, if a suitable holder can be devised, the transmission method offers the possibility of a controlled and variable path length, so that both weak and strong spectral features can be determined.

Recognizing that container problems for corrosive melts are often extremely difficult to solve with materials having good infrared transmission properties, it immediately becomes of interest to explore the possibilities of reflectance spectroscopy. Infrared reflectance methods were used to good effect in investigating molecular and crystal structures and for analytical purposes long before the techniques for transmission measurements had been extensively developed. Nonetheless, reflectance spectroscopy is but rarely used today, largely due to the complicated methods needed for interpretation and the comparative lack of precision afforded by the method.[25] Refractive indices, and hence the dispersion curve of a substance, are in principle available from reflectance measurements, as well as the absorption constants.[26]

Application of the reflectance technique to molten salt studies[27–29] has shown that spectra can be obtained that are essentially identical with those available from direct absorption measurements.[30] Figure 4 shows the essentials of the experimental arrangement due to Wilmshurst and Senderoff.[27] These authors calculated absorption spectra from their reflectance measurements by the method due to Robinson and Price.[31] The figure shows clearly that container problems are minimal with this method, though fairly extensive spectrometer modifications are called for.

A relatively recent[32] development of the reflectance method, which has found some application in molten salt studies, is that of attenuated total

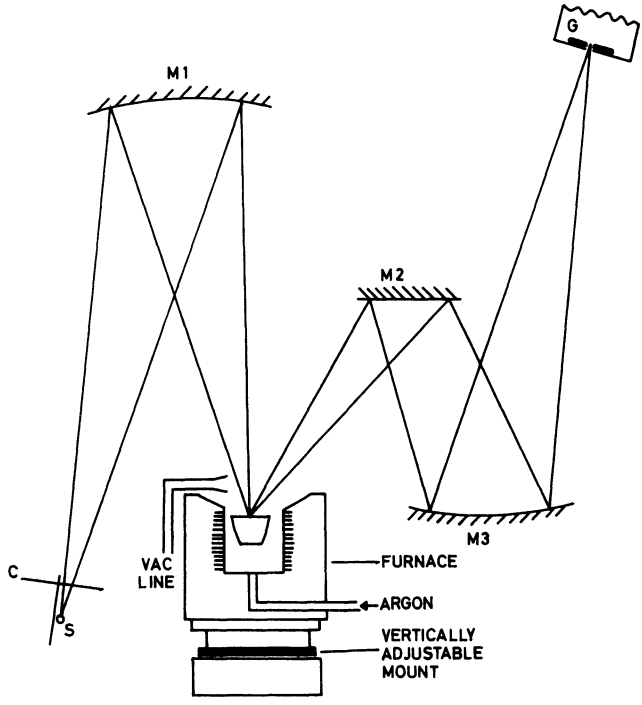

Fig. 4. Schematic diagram of an optical arrangement used to obtain infrared reflectance spectra of molten salts.[26–28] (S = source, C = chopper, M = mirror, and G = monochromator.)

reflectance (ATR) spectroscopy. Crawford and co-workers[33] have demonstrated the utility of the ATR technique for precise intensity measurements at room temperature, and standard units for adapting a conventional spectrometer to this work are now commercially available. No lengthy calculations are necessary if all that is required is the absorption spectrum, since this is obtained directly, the effective path length in the sample being dependent on the refractive indices of the sample and ATR prism, and the number of reflections used. The essential difference from simple reflectance spectroscopy is that in the ATR technique the infrared beam passes from an optically dense medium (the ATR prism) to the less dense (lower refractive index) sample,[34] with total reflection occurring at the interface for wavelengths where the sample is nonabsorbing, provided the angle of incidence θ and the refractive index n at the interface are such that $n \leq \sin\theta$. The reflected energy is reduced by absorption in the surface layers of the second medium (the sample) when this has a nonzero extinction coefficient K for the wavelength used. Thus the reflectance spectrum obtained shows

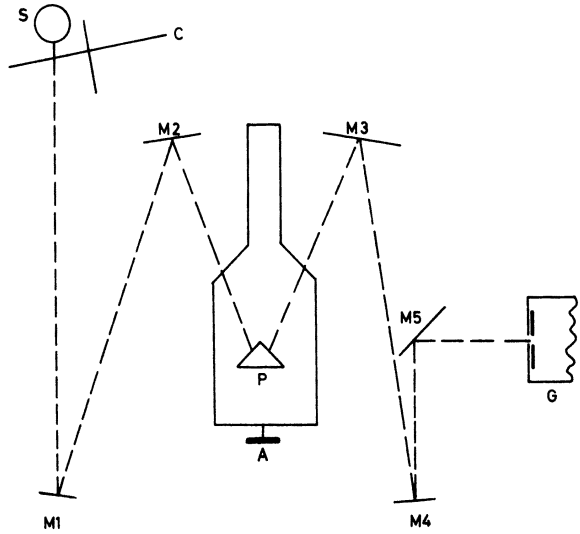

Fig. 5. Optical path for ATR molten salt spectroscopy. (S = source, C = chopper, M = mirror, P = ATR silicon prism, A = sample container, and G = monochromator.)[35]

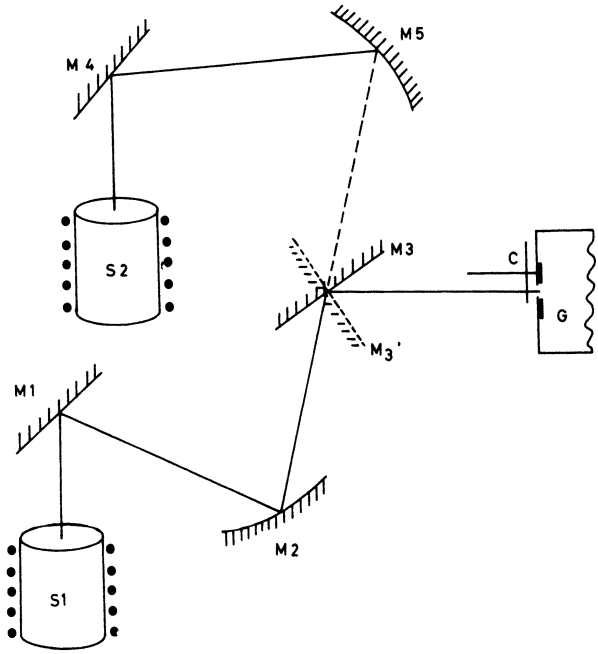

Fig. 6. Optical arrangement used for infrared emission spectroscopy of molten salts. (S1 = sample, S2 = black body emitter, M = mirror, C = chopper, and G = monochromator.)[29]

attenuation at those wavelengths where $K \neq 0$ and is similar in appearance to a straightforward absorption spectrum.

Using an ultrapure silicon ATR prism, Devlin and co-workers[35] have shown that good quality spectra of molten salts can be obtained at temperatures up to *ca.* 400°C. The essential features of their optical arrangement are shown in Fig. 5. Details of the sample cell are given in Section 2.4, together with comments on its performance.

A further method of studying infrared spectra of molten salts is to make use of the radiation *emitted* by the hot sample. Figure 6 shows the optical arrangement used by Wilmshurst[29] for this purpose, where light emitted by the sample is compared with that of a black body at the same temperature. These emissivity studies were compared with reflectivity work, and similar results were obtained for the derived absorption spectra from each method.[29] More recently, Kozlowski[36] also has used the emission technique for molten salt studies, but it remains experimentally difficult and there is evidently scope for further development.

2.3. Arc Lamps, Discharge Lamps, and Lasers as Raman Light Sources

Before the advent of the laser, mercury arc lamps were by far the most common source of light for Raman spectroscopy, and many are still in use today. Hibben[37] has described the early development of the mercury lamp as a Raman source, but the most significant development was made in 1952 by Welsh and co-workers[38] with their design for a helical lamp known as the Toronto arc. This type of source, which typically operates with *ca.* 2.5 kW power consumption, has been very widely used for Raman excitation by the 4358, 4047, and 5461 Å lines, the first of these being the most intense and therefore the most popular. The ultraviolet line at 2536 Å in the mercury arc spectrum has even greater intensity and also has been used extensively for Raman excitation. This 2536-Å line is a resonance line, and its full intensity is only realized if care is taken to avoid self-absorption by surrounding "cool" mercury vapor in a lamp. However, this same self-absorption phenomenon can be used to good effect in selectively filtering out the Rayleigh line from scattered light, allowing measurement of Raman lines at very low frequency. The lamp absorption problem can be solved by magnetically drawing the discharge close to the wall of the lamp.[39]

It is seen that mercury lamps can provide several alternative Raman source frequencies, but the strongest of these are in the ultraviolet and at the blue end of the visible spectrum, where sample fluorescence is most often

a problem. An alternative and rather more versatile type of source was described by Ham and Walsh[40] in 1958. Their lamp employs a range of different fillings, such as helium, mercury, and alkali metals, which are excited by an electrodeless 2450 Mc microwave discharge. Similar annular-shaped lamps have been developed by Powell and co-workers,[41] using a cheaper radio-frequency power supply for excitation. A range of Raman source frequencies is desirable for work with colored or photosensitive samples, as well as for studies of the resonance Raman effect.

A great disadvantage with all the arc and discharge lamps lies in the need to surround the sample with the lamp(s) in order to obtain sufficient illumination intensity for Raman scattering. This is particularly problematical with molten salt samples, where it is necessary to enclose the sample in some type of furnace assembly. The removal of this obstacle represents the most important advantage of laser excitation over all other methods. A laser emits a narrow (typically 1–2 mm in diameter), well-collimated beam of radiation and can be conveniently located well away from the sample. Only a small hole is needed in the sample furnace to allow entry of the laser beam (which can be focused to a diffraction-limited spot of dimensions comparable with its wavelength) and a second small hole to allow exit of the scattered light. Unless stimulated Raman effects are required, the continuous gas lasers are at present more useful than pulsed lasers as Raman sources. Typical frequencies and power levels from commercially available, long-lived (one-year guarantee!) gas lasers are as follows: He/Ne, 6328 Å (80 mW), 6118 Å (8 mW); Ar ion, 4880 Å (1 W), 5145 Å (1 W), 4765 Å (350 mW), 4965 Å (200 mW), 5017 Å (200 mW), 4579 Å (70 mW); Kr ion, 6471 Å (200 mW), 5682 Å (80 mW), 5308 Å (80 mW), 5208 Å (80 mW), 4762 Å (40 mW). An argon laser for blue-end excitation and a krypton laser for red-end excitation are the best Raman sources available today for molten salt work.

2.4. Sample Cells

The problem of attack of cell windows by the sample in infrared spectroscopy of molten salts is one that has no general solution. Refractory materials commonly have only small infrared "windows" and have found but little use.[22] Diamond windows have been used for some far-infrared absorption studies of fused alkali metal nitrates,[23] but even these are useful only up to *ca.* 600°C, and large ones are very expensive. Ultrapure silicon has found some use as a cell material but again is limited to *ca.* 400°C, where kT has the same magnitude as the energy gap between the valence

and conduction bands[35] so that the transmission characteristics deteriorate drastically. Even at normal room temperatures, the high refractive index of silicon causes high reflection losses (*ca.* 30% for normal incidence). However, for melts that "wet" the surface of silicon, infrared absorption spectra of thin films can be obtained using a single platelet as both window and support.[42] A 1-mm platelet of silicon has been found to give acceptable transmission over the frequency range of 200 to 400 cm^{-1} (with 50% reflection loss), and the Irtran materials (4 and 6 particularly) also have been found useful, though they are less chemically inert than silicon.[42]

A clever solution to the window problem was found by Greenberg and Hallgren,[30] who used a 32-mesh platinum screen as the sample holder. This could be heated directly by passage of an electric current through the screen, and molten salt samples were held as thin films on the mesh by surface tension forces. Figure 7 shows the main features of this "windowless" cell. The technique is made more versatile by the use of stainless steel meshes, which can be etched in aqua regia to an optimum wire diameter,[43] and by using the nickel and gold meshes that are commercially available. For controlled atmosphere work the furnace-type cell[22] shown in Fig. 8 is more suitable. With all of these wire mesh sample holders, however, there is great difficulty in achieving a sample thickness below *ca.* 20μ, which already is

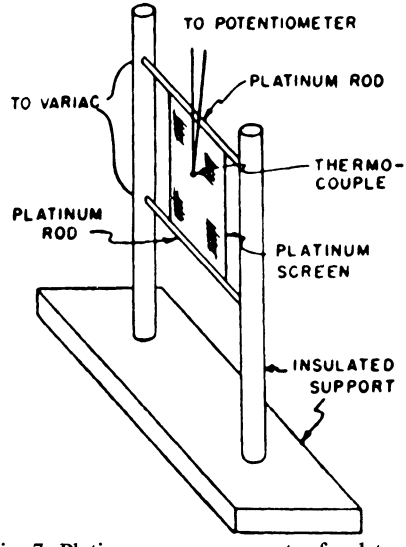

Fig. 7. Platinum screen apparatus for determination of infrared absorption spectra of molten salts.[30]

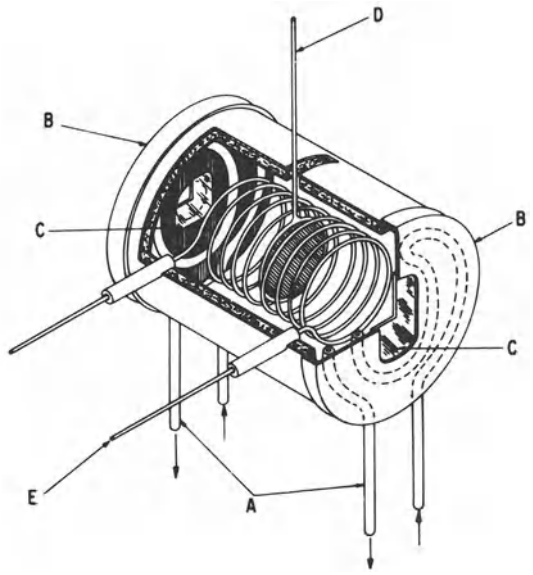

Fig. 8. Wire mesh sample holder in controlled atmosphere furnace.[22]

too great for many samples in regions of high extinction coefficient (for example, a 1400-cm^{-1} region of molten nitrates). In addition, all direct transmission through thin films methods suffer from a tendency to distortion of the most intense bands due to refractive index fluctuations with frequency. However, the ready observation of overtone and combination bands in spectra from relatively thick films compensates somewhat for the occasional total absorption by some fundamentals, and the applicability of the wire mesh method to virtually all molten salts up to temperatures well in excess of 1000°C represents a considerable advantage that this method has over most others.

Cells for use with the reflectance and emission infrared techniques discussed earlier are so simple that they require little comment. A crucible (usually platinum) and furnace are all that is required, with care being taken to keep a clean surface on the melt through the measurement. The cell used by Kozlowski[36] for emission work is shown in Fig. 9, and Fig. 4 shows the essentials of a reflectance cell.

The sample cell used by Devlin and co-workers[35] for ATR measurements with molten salts is shown in Fig. 10. It is used in conjunction with the optical arrangement shown in Fig. 5. The prism angles are cut so as to

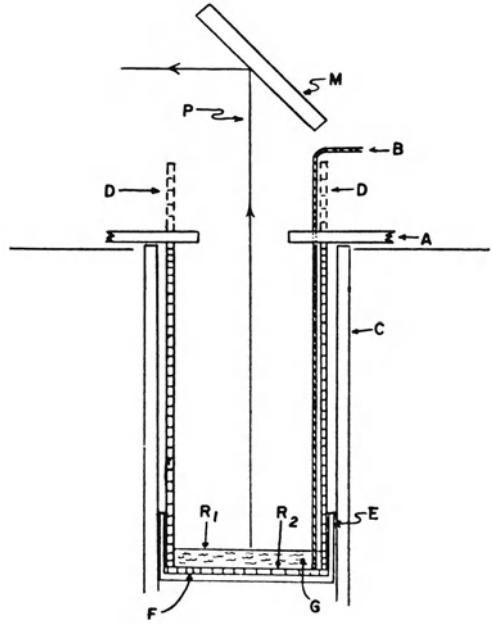

Fig. 9. Sample cell for infrared emission work with molten salts. (M = sample furnace mirror, P = path of emitted radiation, A = aperture plates, B = thermocouple, C = mullite furnace core, D = aluminum core sleeve, E = vycor dish, F = aluminum backplate, G = melt, and R_1 and R_2 = reflectance interfaces.)[36]

give an angle of incidence (θ) at the prism/molten salt interface such that $\theta \gg \theta_{\text{critical}}$ at all wavelengths, ensuring that total internal reflections occur. With this arrangement, effective path lengths in the molten salt of the order of 1μ are obtained, and the problems associated with variable reflectivity with wavelength are virtually eliminated.[42] It is possible that the surface layers investigated by the ATR method may differ from the bulk of the sample in some cases, as has been suggested by Kozlowski,[36] but this problem has not been investigated in any systematic way. The known limitations are mainly those of having to work below *ca.* 400°C with silicon prisms and the corrosion of the prism by some melts.

Since Raman spectra are usually excited by visible light, it has been possible to use regular Pyrex glass (to 550°C) or quartz (to 1400°C) cells for much of the molten salt vibrational spectroscopy that has been done with the method. The cell shown in Fig. 11 has been used to good effect

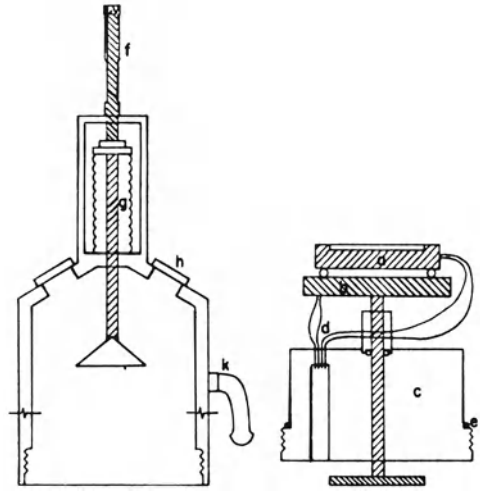

Fig. 10. Sample cell for ATR fused salt spectroscopy. (a = crucible, b = adjustable ceramic crucible platform, c = cell base, d = thermocouple and power leads, e = O-ring seal, f = micrometer screw, g = bellows, h = infrared window, and k = vacuum tap.)[35]

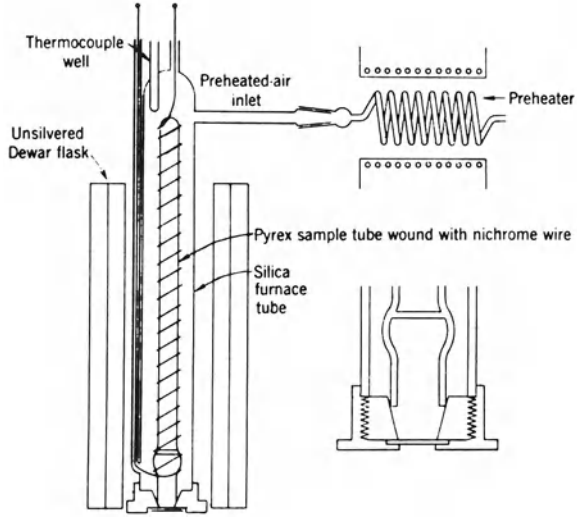

Fig. 11. High temperature Raman cell assembly for use with a Toronto arc.[45]

by Janz and co-workers,[44,45] one of the most active groups in this area, with a mercury lamp of the Toronto arc type providing the exciting radiation. A closely similar nichrome wire heated cell has been described by Young and co-worders[46] for use with a horizontally mounted Toronto arc, and an elaborate further development of these basic designs due to Walrafen[47] is shown in Fig. 12. Radio-frequency induction heating was used to achieve temperature in the region of 1000°C with this cell.

While most pure metal nitrates and halides (except lithium salts)

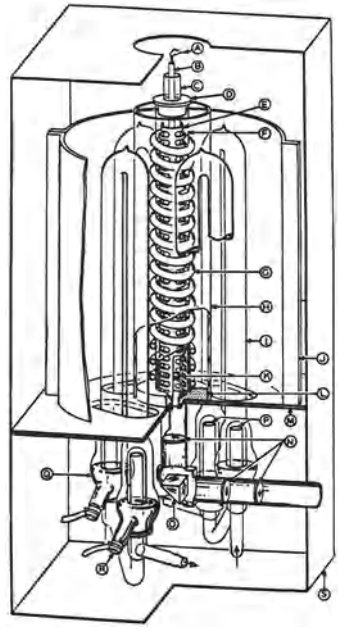

Fig. 12. Schematic diagram of a high temperature accessory for a Raman spectrometer. (A = chromel/alumel thermocouple, B = quartz thermocouple well, C = quartz Raman tube, D = transite spacer, E = Inconel susceptor, F = quartz coil holder and heat shield, G = copper, water-cooled radio frequency heating coil, H = vycor heat shield, I = pyrex Raman lamp, J = brass, MgO-coated reflector, K = quartz optic flat, L = transite spacer, M = transite shelf, N = Cary 81 optics and mask, O = 45° prism, P = cold fingers, Q = mercury, R = kovar-cup electrode, and S = aluminum lamp housing.)[47]

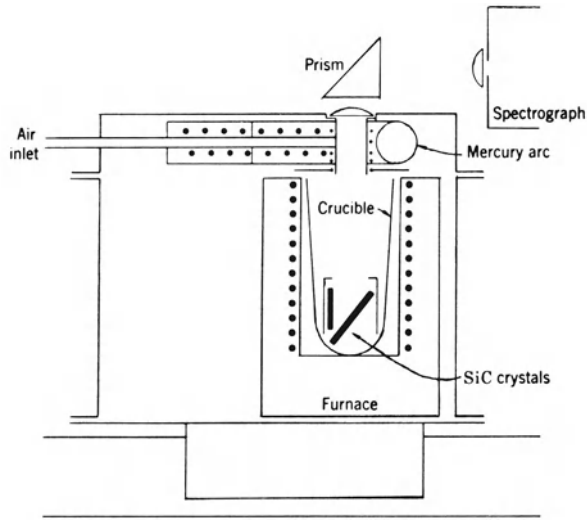

Fig. 13. High temperature Raman cell assembly for use with corrosive melts.[48]

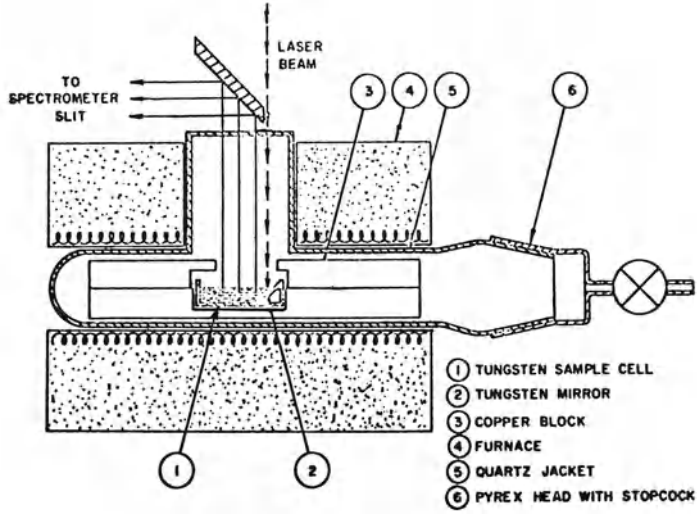

Fig. 14. Raman cell for corrosive fused salts.[86]

do not attack glass or quartz, other molten salts such as fluorides, carbonates, and hydroxides do attack these materials, making the above cells unsuitable. The Raman cell assembly shown in Fig. 13 was designed by Bues[48] so as to overcome this limitation. A platinum crucible can be used to contain the sample in this assembly, which again uses a mercury lamp light source, though it clearly could be easily modified for laser excitation of spectra. Maroni and Cairns have produced such a modification, shown in Fig. 14.[86] Arighi and Evans[49] also designed a cell for use with corrosive systems, using a Monel metal container with sapphire windows sealed by Teflon gaskets located at the side and bottom, as shown in Fig. 15. This cell appears to be ideally suited to laser excitation methods, though it was designed for use with a mercury lamp.

A novel "windowless" Raman cell, specifically built by Solomons and co-workers[50] for use with a laser light source, is shown in Fig. 16. This cell is similar in concept to one used by Young[51] for absorption spec-

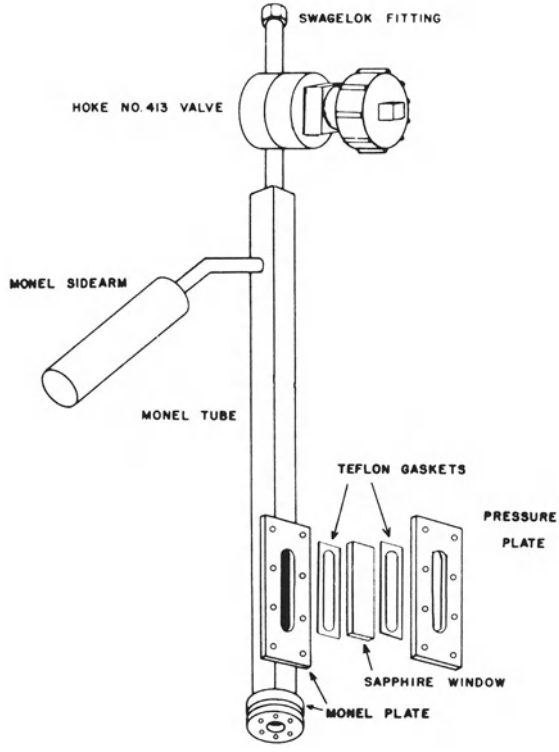

Fig. 15. Raman cell for corrosive liquids.[49]

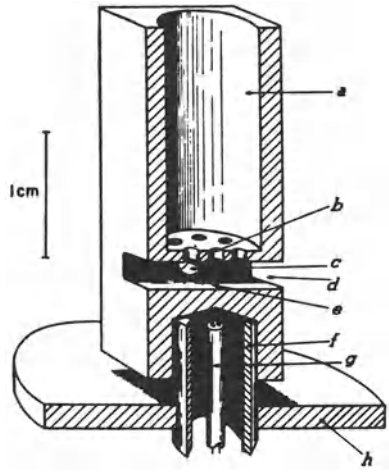

Fig. 16. A section of a windowless Raman cell used for molten cryolite. (a = filling holes, b = retaining holes, c = laser beam entry hole, d = hole for emerging scattered light, e = sample chamber, f = quartz tube support, g = thermocouple leads, and h = boron nitride disk.)[50]

trophotometry and relies on surface tension to retain the liquid sample in the laser beam. It is made entirely from very inert boron nitride and has been used with molten fluoride up to 1030°C. A less chemically resistant, though more convenient, cell design is shown in Fig. 17. This also is from the Pennsylvania laboratory[52] and is used in conjunction with the optical system shown in Fig. 18. Temperatures in the region of 1000°C were recorded with this assembly, with quartz being used as the cell material and a pulsed laser as the light source. A modification of this cell has been described by Clarke and Hester[53] for use with continuous lasers, and this is shown in Fig. 19. This cell is particularly simple to make and convenient to use. The sample tube is made in two concentric sections from silica, the inner tube being closed at its lower end by a fine porosity silica sinter, through which a molten salt can be forced under pressure of dry nitrogen. Since laser excitation with liquids is particularly sensitive to suspended solid particles, this filtration process is an important feature. The design also avoids passage of the laser beam through a liquid meniscus. The furnace is made from a block of silicon resin impregnated asbestos (Syndanyo), eight loops of high

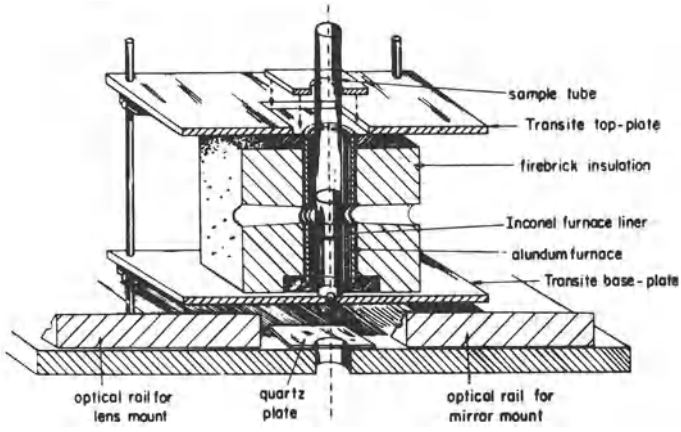

Fig. 17. Section of a molten salt sample furnace for laser-Raman spectroscopy.[52]

current resistance wire being inset into the inner wall of the block and wound parallel to its longitudinal axis to minimize temperature gradients. The furnace power is controlled up to a maximum of 650 W, producing a maximum sample temperature of *ca.* 1200°C. Small holes cut in the block allow passage of the laser beam, and slightly larger cone-shaped holes

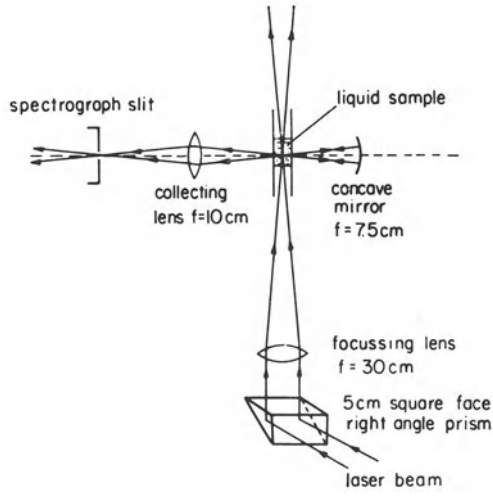

Fig. 18. Optical system for laser excitation of molten salt Raman spectra.[52]

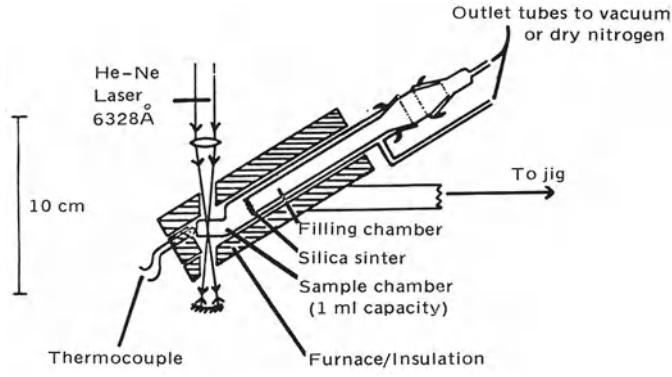

Fig. 19. Molten salt Raman cell and furnace assembly.[53]

cut at right angles to these allow exit of scattered light. The laser beam is focused at the center of the sample by a microscope objective lens, and multipassing of the laser beam is achieved by placing a concave mirror below the cell and furnace assembly. Back-scattered light is collected by a second concave mirror and reflected back through the sample. The scattered light is collected by a large aperture magnifying lens and focused onto the entrance slit of a double monochromator.

The special characteristics of the Cary 81 laser Raman spectrometer sample excitation method, wherein a coaxial optical arrangement is used to produce back-scattered (360°) Raman radiation, have formed the basis for the design of a molten salt cell by Melveger and co-workers.[54] This consists of a simple pyrex U-tube, internally heated with nichrome wire, held close to the Cary hemispherical lens. Good quality spectra have been obtained from molten HgI_2 (m.p. 257°C) in this cell, allowing determination of a band as low as 17.5 cm^{-1}. However, it is apparent that this optical system is generally less useful for high temperature studies than the more conventional 90° scattering system, where the collecting lens can be well removed from the sample cell and furnace assembly.

3. RESULTS

3.1. Monatomic Ions

This section discusses the infrared and Raman spectra obtained from systems composed fundamentally of monatomic ions, such as metal ions and halide ions. For such systems there can be no normal modes of vibra-

tion to interact with infrared radiation or to cause Raman scattering unless the ions cluster together in some way to form distinct polyatomic *complexes* or there exists in the liquid some definite form of *lattice* structure that has its own set of characteristic lattice modes (phonons). It should be recognized that since interionic forces in condensed systems such as molten salts will always be powerful, it must always be an approximation to treat the modes of vibration of a complex species in isolation, that is, without regard to environmental perturbations. However, it also is true that the binding forces within a complex can be, and evidently often are, significantly stronger than the forces of interaction with the environment (neighboring ions), so that it certainly can be considered reasonable to use a complex ion model for a first-order interpretation of spectra. The weaker forces binding a liquid *quasi-lattice* can cause some perturbation of the modes of a polyatomic complex, and cases undoubtedly exist where it no longer is meaningful to talk of complexes at all but rather to interpret spectra in terms of lattice modes. This latter method, unfortunately, will usually be rather vague, due to the equally vague nature of the lattice structures that can be expected to exist in high temperature liquids. Although a structure need only exist for *ca.* 10^{-12} sec in order to be characterized by vibrational modes, it must be recognized that at all times there will exist large regions of disorder in a molten salt, which at least will cause a spread of energies of the quasi-lattice modes, resulting in great width of spectral bands arising from these. Fundamental lattice modes also will usually occur at low frequencies,[55,56] where normal near-infrared techniques are inapplicable, and far-infrared or Raman spectroscopy must be used.

Vibrational spectra of some molten metal halide systems are summarized in Table II. The simple alkali halides have been useful as "solvent" systems for many of the studies reported, since their own characteristic vibrational mode frequencies are lower than those of most of the "solute" species investigated and do not interfere with their measurement. Wilmshurst[28,29] has reported some characteristic "lattice mode" frequencies in his infrared spectra of the fluorides and chlorides of lithium and potassium, though these are but poorly characterized and could equally be attributed to ion pairs. Kozlowski's[36] infrared spectra of the LiCl/KCl eutectic at 550°C do not correspond well with those of Wilmshurst.[28] The alkali halide melt vibrational modes have not been detected in Raman spectra, where they evidently are inactive or at least very weak. However, Raman activity is not expected of modes arising from simple ion pairs, since it is well-established that polarizability derivatives are zero for ionic bonds,[79] and the crystalline alkali halides do not show first-order Raman

TABLE II. Vibrational Spectra of Some Molten Halide Systems

System	Species present	Frequencies (cm^{-1})	References[a]
Group IA			
LiF	Lattice	490, 550	$(29)^{I}$
KF	Lattice	270, 320	$(29)^{I}$
LiCl	Lattice	350	$(28)^{I}$, $(36)^{I}$
KCl	Lattice	220	$(28)^{I}$, $(36)^{I}$
Group IB			
CuCl/LiCl	Lattice	270, 340	$(28)^{I}$
$CuCl_2$/MCl (M = Li, K)	Lattice and $CuCl_4^{2-}$ complex	214, 217, 229, 238, 265, 285, 292, 314, 352	$(28^{I}$
Group IIA			
$MgCl_2$	$MgCl_6^{4-}$	142, 214, 269	$(67)^{R}$
$MgCl_2$/KCl	$MgCl_4^{2-}$, $MgCl_n^{2-n}$, $(MgCl_2)_n$ polymers	163, 221, 233, 255, 282	$(86)^{R}$
$MgBr_2$/KBr	$MgBr_4^{2-}$, $MgBr_n^{2-n}$	90, 125–175	$(86)^{R}$
$BaCl_2$/KCl	$BaCl_3^-$	382, 470, 541	$(68)^{R}$
Group IIB			
$ZnCl_2$	$(ZnCl_2)_n$ polymers, $ZnCl_2$, $ZnCl_n^{2-n}$	75, 95, 110, 226, 230, 250, 266, 285, 305, 360	$(28)^{I}$, $(48)^{R}$, $(57)^{R}$, $(58)^{R}$, $(59)^{R}$
$ZnCl_2$/MCl (M = Li, K, Rb, Cs)	$(ZnCl_2)_n$ polymers, $ZnCl_n^{2-n}$ complexes	80, 125, 218, 230, 265, 292, 317	$(28)^{I}$, $(48)^{R}$, $(58)^{R}$, $(60)^{R}$
$ZnBr_2$/KBr	$(ZnBr_2)_n$ polymers, $ZnBr_3^-$, $ZnBr_4^{2-}$	60, 70, 80, 155, 170, 180, 225	$(59)^{R}$, $(60)^{R}$
$CdCl_2$/KCl	$CdCl_2$, $CdCl_3^-$, $CdCl_4^{2-}$	177, 211, 245, 257	$(48)^{R}$, $(61)^{R}$
$HgCl_2$/MCl (M = K, NH_4)	$HgCl_2$, $HgCl_3^-$, $HgCl_4^{2-}$	180, 192, 210, 267, 276, 282, 287, 313, 376	$(62)^{R}$, $(63)^{R}$, $(64)^{R}$, $(65)^{R}$
$HgBr_2$	$HgBr_2$	195, 271	$(63)^{R}$
HgI_2	HgI_2	41, 146, 138	$(52)^{R}$, $(54)^{R}$, $(66)^{R}$
HgI_2/LiI/KI	HgI_2/HgI_3^-	143, 126, 185	$(86)^{R}$
$HgCl_2/HgBr_2$	HgClBr and dismutation products, $HgBr_2 + HgCl_2$	111, 203, 236, 319, 335	$(63)^{R}$
$HgCl_2/HgI_2$	HgClI	179, 330	$(66)^{R}$
$HgBr_2/HgI_2$	HgBrI	164, 229	$(66)^{R}$
$CdCl_2/AlCl_3$/Cd	Cd_2^{+2}	183	$(71)^{R}$

TABLE II. (*Continued*)

System	Species present	Frequencies (cm^{-1})	References[a]
Group IIIA			
$AlCl_3$/NaCl	$AlCl_4^-(T_d)$	145, 183, 349, 580, 136,	(69)[R], (70)[R],
$AlCl_3$/KCl	$AlCl_4^-(C_{2v})$	155, 168, 182, 196, 353, 505, 562, 597	(71)[R], (69)[R]
Na_3AlF_6	AlF_4^-, AlF_6^{3-}	575, 633	(50)[R]
$GaCl_2$	$GaCl_4^-$	115, 153, 346, 380	(72)[R]
$GaBr_2$	$GaBr_4^-$	79, 107, 209, 288	(73)[R]
$InCl_2$	$InCl_4^-$	91, 116, 317, 349	(74)[R], (75)[R], (76)[R]
$InCl_3$/MCl (M = Li, K, Cs)	$InCl_4^-$, $InCl_6^{3-}$	87, 114, 320, 346, 148, 287	(58)[R], (74)[R], (76)[R]
$InCl_3$/In	In–In bonded species	170	(75)[R]
Group IVA			
$SnCl_2$	$(SnCl_2)_n$ polymer	112, 221	(77)[R]
$SnCl_2$/KCl	$SnCl_3^-$	105, 220, 268	(77)[R]
$PbCl_2$/KCl	$PbCl_3^-$, $PbCl_4^{2-}$	172, 205, 217, 245	(78)[R]
Group IVB			
ZrF_4/KF/MF (M = Li, K)	ZrF_n^{4-n} complexes and lattice	240, 480, 520, 720	(29)[I]

[a] I = reference concerned with infrared spectra and R = reference concerned with Raman spectra.

spectra[55] either. Since there is bound to be some uncertainty in assignments, those given in Table II are uniformly taken from the original publications.

While generally rejecting the existence of complex ions in fused salts, Wilmshurst[28] interpreted his infrared spectra from the $CuCl_2$/KCl system as being at least fully consistent with the existence of the $CuCl_4^{2-}$ species in these melts. However, infrared spectra from the $CuCl_2$/LiCl and CuCl/LiCl systems showed no evidence for distinct complex species and were considered to arise only from lattice-like vibrational modes of the systems. Large variations in band frequencies, and disproportionate intensity variations as the compositions of $ZnCl_2$–alkali chloride systems were varied, were similarly interpreted.[28]

Raman spectra of molten $ZnCl_2$ and $ZnCl_2$–alkali chloride mixtures

have been studied by a large number of authors,[28,48,57–59] and there is much support for the existence of polynuclear aggregates,[57] or polymers, which closely resemble the solid $ZnCl_2$ structure[80]—this being based on $ZnCl_4$ tetrahedral units linked by chlorine bridges. The symmetric Zn–Cl stretching mode of these polymeric species (or this liquid lattice) occurs at *ca.* 230 cm^{-1}, and deformation modes have been identified[60] below 100 cm^{-1}. Depolymerization is caused by raising the temperature[57] of the $ZnCl_2$ melt or by adding an alkali metal chloride,[58] with the symmetrical stretching frequency of the $ZnCl_4^{2-}$ ion shifting to 280 cm^{-1} at high chloride content.[60] Bands characteristic of the species $ZnCl_2$ and $ZnCl_3^-$ also have been identified.[60] A similar interpretation, with polymeric species giving way to complex ions, has been made[59,60] for the Raman spectra from $ZnBr_2$ and $ZnBr_2$/KBr mixtures. Raman spectra from the related $CdCl_2$/KCl system, however, have shown but little evidence for polymers, and bands have been assigned as arising from the species $CdCl_2$, $CdCl_3^-$, and $CdCl_4^{2-}$. Bues[48] favored a planar (D_{3h}) structure for the $CdCl_3^-$ species, while Tanaka and co-workers[61] preferred a pyramidal (C_{3v}) interpretation. Bredig and van Artsdalen[81] interpreted Bues' data as establishing the presence of the tetrahedral (T_d) $CdCl_4^{2-}$ species. It is clear that the spectra in this case are incomplete, and an unambiguous interpretation is not yet possible. The solid-state layer-lattice structure of $CdCl_2$ probably is partially preserved at temperatures little above the melting point, as in the case of $ZnCl_2$.

The data given in Table II show that the mercuric halides have been most thoroughly investigated. The single salt melts appear to be predominantly molecular, though complex ions $HgCl_3^-$ (D_{3h} symmetry) and $HgCl_4^{2-}$ (T_d symmetry) have been identified[63] in $HgCl_2$/KCl mixtures. No evidence for the presence of polymeric species has been reported. $HgCl_2$ and $HgBr_2$ both are linear ($D_{\infty h}$) molecules, with Raman-active Hg–X symmetric stretching frequencies at 313 and 195 cm^{-1}, respectively. These occur as intense, polarized bands in the Raman spectra. Their large widths have been interpreted in terms of increased polar character of the Hg–Cl bonds in molten $HgCl_2$ and $HgBr_2$, with the possibility of halide-atom perturbation due to cooperative molecular rotational interactions.[63] This same interaction is considered responsible for the appearance of the formally forbidden ν_2 modes, at 100 and 90 cm^{-1}, respectively, in the Raman spectra. Figure 20 shows how the simple triatomic molecular species $HgCl_2$ gives way to the complex ions $HgCl_3^-$ and $HgCl_4^{2-}$ as KCl is added to the melt. The data are those of Janz and James.[63] Their conclusions were supported by later Raman studies of the $HgCl_2$/KCl/KNO_3 system.[65]

Raman spectra from mixed mercuric halides also favor a molecular

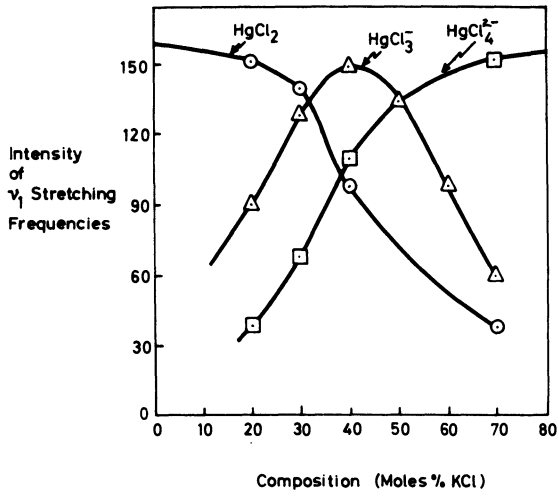

Fig. 20. Composition of $HgCl_2$–KCl molten salt mixtures as indicated by Raman intensity changes.[63]

structure for these melts, in which the mixed halides HgClBr,[63] HgClI,[66] and HgBrI[66] have been identified. These are linear ($C_{\infty v}$) molecules. For HgClBr, the two strongest bands at 335 and 236 cm^{-1} have been assigned as stretching modes and a weak band at 111 cm^{-1} as the bending mode.[63,82] Similarly, for HgClI the assignments ν(Hg-Cl) = 330 cm^{-1} and ν(Hg-I) = 179 cm^{-1} have been made, and for HgBrI, ν(Hg-Br) = 229 cm^{-1} and ν(Hg-I) = 164 cm^{-1}.[66] This latter frequency may be compared with the value of 145 cm^{-1} found for the symmetric ν(Hg–I) stretch of HgI_2 present in mixtures with $HgCl_2$ and $HgBr_2$.[66] The deep color (dark red to black) of a pure HgI_2 melt raises problems for Raman studies, but Melveger and co-workers[54] have obtained these spectra, using red laser excitation, and interpreted them in terms of a linear triatomic HgI_2 molecular structure, with the ν_1, Hg–I stretch, at 138 cm^{-1}. The persistence of a weak band at 41 cm^{-1} in these molten salt spectra indicates a breakdown in the selection rules for a linear molecule similar to that found for $HgCl_2$ and $HgBr_2$,[63] since this has been assigned as the ν_2 bending mode. However, this band clearly shows no signs of the doublet structure that characterizes the corresponding band from solid yellow HgI_2.[54] Comparison of frequencies for the ν_1 symmetric stretching modes of the three HgX_2 compounds when measured in the vapor[83] and liquid states indicates a relatively high covalent character for the Hg–I bond.[66] The complex HgI_3^- has been characterized by Maroni and Cairns[86] in molten HgI_2/LiI/KI mixture.

The next most extensively studied series of halides is that of the Group IIIA metals, and their vibrational spectra appear to be fairly well understood. Raman spectra from molten $AlCl_3$,[69,71,84] $AlBr_3$,[84] and AlI_3[84] all have been interpreted as arising from dimeric Al_2X_6 species. In the presence of excess halide ion, ready conversion to the tetrahedral AlX_4^- species occurs. Molten $AlCl_3 \cdot NaCl$ gave four Raman bands, as listed in Table II, the 349 cm^{-1} band being polarized and more than three times more intense than any other.[69,70] A tetrahedral $AlCl_4^-$ ion offers a ready explanation of this spectrum. However, when KCl was used in place of NaCl in the $AlCl_3$/MCl mixtures, a more complex nine-band spectrum was observed.[69] This was interpreted as arising from a removal of degeneracy from some of the $AlCl_4^-$ ion modes, caused by strong cationic distortion to C_{2v} symmetry, but the spectra were of rather poor quality and might be reinterpreted differently. A four-band Raman spectrum was again recorded by Corbett[71] from $AlCl_4^-$ in $AlCl_3/CdCl_2$ mixtures. Only with the fluoride is there evidence for a 6-coordinate species, and even then only the strongest Raman band has been identified at 575 cm^{-1}.[50] Raman evidence suggests that AlF_6^{3-} dissociates into AlF_4^- and F^- ions to a considerable extent (70–75%) in molten cryolite, though again only one band at 633 cm^{-1} has been observed for the proposed tetrahedral AlF_4^- ion.[50]

The primary purpose of Raman studies performed on liquids of composition $GaCl_2$[72] and $GaBr_2$[73] was to determine whether Ga(II) species were present in the melts. It was found that the observed spectra corresponded closely with those given by the $GaCl_4^-$ and $GaBr_4^-$ species in aqueous solutions, showing that the melt compositions were $Ga^+GaCl_4^-$ and $Ga^+GaBr_4^-$, that is, mixtures of Ga(I) and Ga(III) species in each case. Assignments made[72,73] for these tetrahedral complexes were as follows:

	$\nu_1(A_1)$	$\nu_2(E)$	$\nu_3(F_2)$	$\nu_4(F_2)$
$GaCl_4^-$	346	115	380	153 cm^{-1}
$GaBr_4^-$	209	79	288	209 cm^{-1}

Similar results were obtained from Raman spectral studies of molten $InCl_2$,[74–76] which gave a Raman spectrum essentially identical with that given by $InCl_4^-$ dissolved in ether.[85] This $InCl_4^-$ ion also has been identified in molten $InCl_3$/MCl (M = Li, K, Cs) mixtures, where it gave the four-band spectrum $\nu_1(A_1) = 320$, $\nu_2(E) = 87$, $\nu_3(F_2) = 346$, $\nu_4(F_2) = 114$ cm^{-1} characteristic of a tetrahedral species.[53] The $InCl_2$ and $InCl_3 \cdot KCl$ spectra are shown in Fig. 21. Molten In_2Cl_3 was found to have the structure

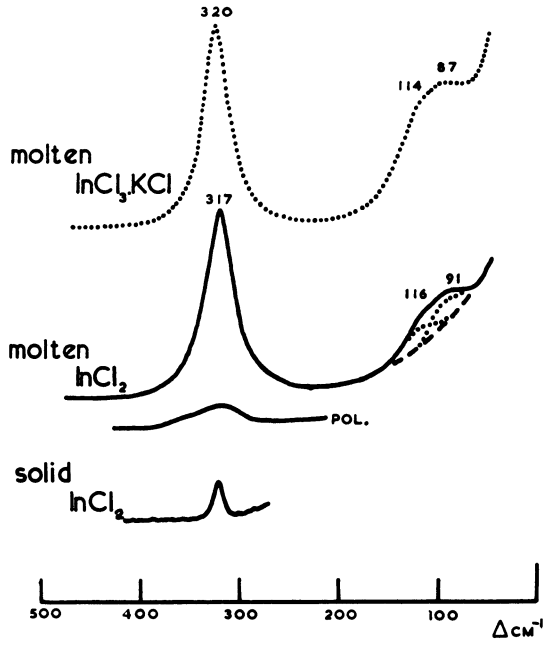

Fig. 21. Raman spectra of molten $InCl_2$ and $InCl_3 \cdot KCl$ and of solid $InCl_2$.[53]

In_3^+ $(In^{III}Cl_6)^{3-}$, though the spectra of this system showed that considerable dissociation of the $InCl_6^{3-}$ species occurs in the melt, and some chloride-induced disproportionation of In(I) to In(0) and In(III) ensues.[53] There is some evidence for important lattice-like interactions in the $InCl_3$/LiCl system, but the complex-ion model appears more satisfactory for the other cases.

Rather little spectroscopic work has been done on the Group IIA metal halides. On the basis of some very feeble Raman spectra, Balasubrahmanyam[67] has proposed the presence of octahedral $MgCl_6^{4-}$ ions in liquid $MgCl_2$ at 730°C and of pyramidal (C_{3v}) $MgCl_3^-$ ions in $MgCl_2$/KCl mixtures at *ca.* 500°C. More intense spectra have been reported by Maroni and Cairns,[86] showing a strong, polarized Raman band at *ca.* 260 cm^{-1} and a weaker depolarized band at *ca.* 160 cm^{-1}. The broad 260-cm^{-1} band was broken down into four components at 282, 255, 233, and 221 cm^{-1} by a Gaussian curve resolution analysis, and these were variously assigned to $MgCl_4^{2-}$ (255 cm^{-1}), an $MgCl_n^{2-n}$ complex (282 cm^{-1}), and $(MgCl_2)_n$ polymers. These authors failed to reproduce the earlier results.[67] Their spectra of $MgBr_2$/KBr mixtures were interpreted similarly, in terms of

$MgCl_4^{2-}$ and $MgCl_n^{2-n}$ complexes.[86] Mixtures of $BaCl_2$ and KCl yielded Raman bands at *ca.* 382, 470, and 541 cm^{-1}, which were assigned by Vallier and Lira[68] to a $BaCl_3^-$ species, but some doubt has been raised[86] about the validity of these investigations. It is apparent that further work is needed on these systems.

On the basis of two Raman bands that were similar to those given by the solid, Clarke and Solomons have assigned the molten $SnCl_2$ spectrum to an $(SnCl_2)_n$ polymeric structure, with the Sn atom being 3-coordinate.[77] Bands at 221 and 112 cm^{-1} were identified as due to Sn–Cl stretching and ClSnCl bending modes. The three new bands that appeared on addition of KCl to the melt were assigned to the pyramidal (C_{3v}) $SnCl_3^-$ ion.[77] Analogous Raman studies of $PbCl_2$ and its mixtures with KCl led Balasubrahmanyam and Nanis[78] to the conclusion that pyramidal (C_{3v}) $PbCl_3^-$ and a distorted tetrahedral (C_{2v}) $PbCl_4^{2-}$ species were present in the mixtures, though no bands at all were found for the pure $PbCl_2$ melt and all their spectra were extremely weak. Finally, Wilmshurst[29] has reported that his infrared spectra from molten mixed ZrF_4–alkali metal fluoride systems are consistent with the assumption of a complex zirconium species of the type ZrF_5^- or ZrF_6^{2-}, characterized by a band around 480 cm^{-1}, though he stresses the fact that a quasi-lattice interpretation is equally acceptable.

3.2. Polyatomic Ions

Spectroscopic studies of molten salts containing stable polyatomic ions such as SCN^-, NO_3^-, CO_3^{2-}, SO_4^{2-}, BF_4^-, and NH_4^+ have an advantage over those in the previous section in that even in the absence of interionic association the characteristic spectrum of the polyatomic ion itself always can be obtained. This can provide valuable information on the nature of the environment in which the polyatomic ion is located in the melt.

3.2.1. Nitrates

Metal nitrates are the most thoroughly investigated class of molten salts. This is due mainly to the fact that they are low-melting and have long, stable liquid ranges compared with most other systems containing polyatomic ions. The D_{3h} symmetry of a free NO_3^- ion dictates that it should have four fundamental modes of vibration, and the widely accepted frequencies of these modes, obtained from dilute aqueous solutions with non-complexing metal ions, are $\nu_1(A_1') = 1050\ cm^{-1}$, $\nu_2(A'') = 830\ cm^{-1}$, $\nu_3(E') = 1400\ cm^{-1}$, and $\nu_4(E') = 720\ cm^{-1}$. Distortion of this trigonal planar

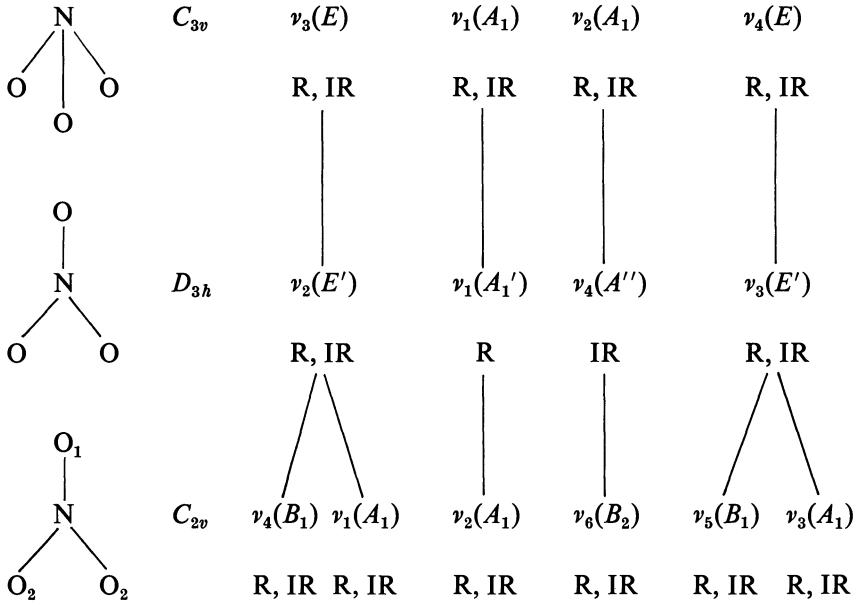

Fig. 22. Correlation diagram for various forms of the nitrate ion.

structure by interaction with neighboring ions in a molten salt, or by straight forward complexation by a metal ion in aqueous solution, can be expected to lower the symmetry according to the scheme shown in Fig. 22. The C_{3v} form of nitrate would result from out-of-plane distortion, while the C_{2v} form arises from in-plane distortion. It is seen that these forms are easily distinguished by the multiplicities and activities (R indicates Raman active, IR infrared active) of the various modes. Further distortion of the C_{3v} form to C_3 or C_s could occur, and this latter case would be vibrationally indistinguishable from the C_{2v} pattern.

Aqueous solutions of metal nitrates give Raman spectra that commonly show features characteristic of the C_{2v} splitting pattern,[86–89] particularly with small and multiply charged metal ions. The detection of low-frequency bands characteristic of metal–oxygen stretching modes[87] has provided further evidence that the nitrate distortion in such systems arises from metal ion complexation, and normal coordinate calculations based on C_{2v} metal–nitrate complex models[90] have been found to reproduce experimental frequencies most effectively. Results obtained from anhydrous and near-anhydrous molten metal nitrates closely resemble those from concentrated aqueous solutions of the salts, and several authors have similarly based their interpretations on a complex ion model.

TABLE III. Fundamental Vibration Frequencies of Nitrate Anion in Condensed Phases[91]

Salt	Phase	Method	Frequencies (cm^{-1})[a]					References
$LiNO_3$	Crystal	Raman	1391	1086		728		(92)
	Crystal	Far Ir					321	(93)
	Crystal	Ir (trans.)			840	733		(30)
	Melt	Ir (trans.)		1053	816	741		(30)
	Melt	Ir (refl.)	1460, 1375	1059	821		343	(27)
	Melt	Raman		1062				(94)
	Melt	Raman	1476, 1366	1061		724		(92)
	Melt	Raman	1452, 1367	1060		722		(93)
	Melt	Raman	1439, 1358	1067		726		(45)
$NaNO_3$	Dilute aqueous	Raman	1390	1050		720		(45)
	Concentrated aqueous	Raman	1410	1052		720		(87)
	Crystal	Far Ir					217	(93)
	Crystal	Raman	1387	1069		728		(92)
	Crystal	Ir (trans.)			833	725		(30)
	Melt	Ir (trans.)		1047	816	714		(30)
	Melt	Ir (refl.)	1412	1053	827		238	(27)
	Melt	Raman	1387	1053		722		(92)
	Melt	Raman	1385	1053		720		(93)
	Melt	Raman	1398	1053		722		(45)
KNO_3	Concentrated aqueous	Raman	1400	1055		725		(87)
	Crystal	Raman	1361, 1343	1050		714		(92)
	Crystal	Far Ir					152	(93)
	Crystal	Ir (trans.)		1042	833	714		(30)
	Melt	Ir (refl.)	1391	1046	829		<220	(27)
	Melt	Ir (trans.)		1042	826	714		(30)
	Melt	Raman		1047		713		(94)
	Melt	Raman	1382	1048		715		(92)
	Melt	Raman	1380	1047		718		(93)
	Melt	Raman	1383	1048		718		(45)
$RbNO_3$	Crystal	Raman	1354	1056		706		(45)
	Crystal	Ir (trans.)		1053	833	719		(30)
	Melt	Ir (trans.)		1042	823	707		(30)
	Melt	Raman	1372	1046		713		(45)
$CsNO_3$	Crystal	Raman	1346	1050		715		(45)
	Crystal	Ir (trans.)		1047	833	714		(30)
	Melt	Ir (trans.)		1036	833	704		(30)
	Melt	Raman	1356	1043		708		(45)

TABLE III. (*Continued*)

Salt	Phase	Method	Frequencies (cm^{-1})[a]					References
$AgNO_3$	Concentrated aqueous	Raman	1420, 1340	1040		720		(87)
	9*M* CH_3CN	Raman	1422, 1275	1043				(97)
	9*M* CH_3CN	Ir (trans.)	1428, 1290		816	730		(97)
	Crystal	Far Ir					170	(93)
	Melt	Raman	1420, 1350	1037,	805	727		
			1290	1015				
	Melt	Ir (refl.)	1395, 1310	1029	800	695	<220	(27)
	Melt	Ir (refl.)	1448, 1390,	1025,	800,	727,		(98)
			1340, 1260	1015	740	713		
	Melt	Raman	1407,1273	1035		733		(45)
$TlNO_3$	Melt	Raman	1383, 1328	1036	813	708		(99)
$Ca(NO_3)_2$	Concentrated aqueous	Raman	1450, 1400, 1360	1053		744,720		(87)
	Crystal	Raman		1054		723		(100)
	Melt	Raman	1415	1050		742,720		(101)
$Sr(NO_3)_2$	3.8*N* aqueous	Raman	1423, 1353	1050		735,718		(102)
	Crystal	Ir (trans.)		1057	815	738		(103)
	Crystal	Raman	1423, 1369	1055		736,715		(104)
$Ba(NO_3)_2$	0.6*N* aqueous	Raman	1370	1047		720		(102)
	Crystal	Raman	1412, 1356	1048		731, 703		(104)

[a] Additional bands at low frequencies are observed in the far-infrared spectra of the crystals.

A thorough survey of vibrational spectroscopic data for alkali metal, alkaline-earth, and thallous nitrates in the solid state, in aqueous and non aqueous solutions, and in the molten state was made by Wait, Ward, and Janz[91] in 1966. Their data are reproduced in Table III. Nitrates also have been treated at length in previous reviews of molten salt spectroscopy.[105–107] The table shows that breakdown of the D_{3h} point group selection rules is common and is shown by spectra arising from solution as well as from solid-state perturbations. Wait and co-workers advanced a *contact* ion pair model to explain their data, with nearest-neighbor pairwise association wherein a metal ion interacts with a nitrate ion at a unidentate oxygen site. Normal coordinate calculations based on their model, using a Urey–Bradley force field, were found to give good agreement between calculated and experimental (from molten salt spectra) frequencies, including those below 400 cm^{-1}, as shown by the comparative figures given in Table IV.

TABLE IV. Comparison of Observed (from Molten Salts) and Calculated (from Ion Pair Models) Frequencies (cm^{-1}) of In-Plane Modes of C_{2v} Metal-Nitrates[91]

	$NaNO_3$		KNO_3		$RbNO_3$		$CsNO_3$		$LiNO_3$		$AgNO_3$		$TlNO_3$	
	Obs.	Calc.	Obs.	Calc.	Obs.	Calc.	Obs.	Calc.	Obs.	Calc.	Obs.	Calc.	Obs.	Calc.
A_1 ν_1	1398	1398	1383	1383	1372	1372	1356	1357	1358	1363	1273	1273	1328	1337
ν_2	1053	1053	1047	1047	1046	1045	1043	1042	1067	1067	1035	1039	1036	1037
ν_3	722	722	718	717	713	712	708	706	726	726	733	731	708	705
ν_4	238	238	170	172		98		90	343	347	190	188		137
B_2 ν_5	1398	1400	1383	1388	1372	1375	1356	1360	1439	1440	1408	1408	1383	1383
ν_6	722	722	718	718	713	714	708	710	725	724	733	733	708	707
ν_7		101		97		94		94		128		93		93

The lowest frequency modes are interpreted here as metal–oxygen bond stretching and MON interbond angle deformation modes.

A contrasting interpretation of the loss of D_{3h} symmetry of nitrate in molten alkali-metal and silver nitrates was earlier advanced by Wilmshurst and Senderoff,[27,28] who attributed the observed effects to a lattice-like structure in which the nitrate is not associated with any particular metal ion but merely is located at a lattice site of C_{2v} or lower symmetry. This point of view has recently been supported by Devlin and co-workers,[98,108] who based their case on the irregular band *shapes* observed in their ATR infrared spectra from molten alkali metal nitrates[108] and silver nitrate.[98] These authors have suggested retention of an orthorhombic lattice structure, such as the D_{2h}^{16} room temperature form of KNO_3,[109] in the melt. This leads to an interpretation in terms of the correlation diagram given in Fig. 23, which has been used to assign the bands (many of them unresolved, however) listed in Table V for molten $LiNO_3$, $NaNO_3$, and KNO_3.[108] It is perhaps surprising to find a full factor-group analysis needed to account for a melt spectrum, when spectra even from low temperature crystalline solids commonly can be accounted for with a simple site-symmetry analysis,[18] but this is perhaps a result of the unusually high resolution claimed for the ATR method.[98,108] Low frequency Raman[110] and far-infrared[23] studies of molten sodium nitrate also have offered support for the lattice model of molten nitrate structures, though while Wegdam and co-workers[23] observed "no special effect" at the point of fusion in their comparative

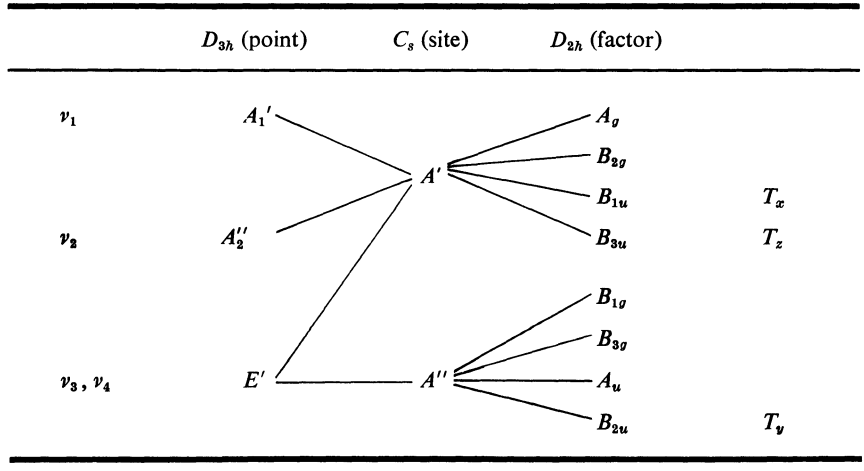

Fig. 23. Correlation diagram for nitrate modes treated under the D_{3h} point group, C_s site group, and D_{2h} factor group symmetries.

TABLE V. ATR Infrared Spectra from Molten Nitrates, (Frequencies in cm^{-1}) Assigned on the Basis of a D_{2h} Factor-Group Analysis[108]

$LiNO_3$	$NaNO_3$	KNO_3	Assignment
1450	1430		$\nu_3(B_{3u})$
1439	1398	1393	$\nu_3(A_g)$
1397	1390	1388	$\nu_3(B_{1u})$
1358			$\nu_3(B_{1g})$
1345	1345	1338	$\nu_3(B_{2u})$
1062	1053	1048	$\nu_1(A_g)$
1053	1047	1045	$\nu_1(B_{1u})$
1030	1032		$\nu_1(B_{3u})$
827	833		$\nu_2(B_{3u})$
818	825	829	$\nu_2(B_{1u})$
742	730	720	$\nu_4(B_{2u})$
726	722	718	$\nu_4(A_g)$

study of crystalline and molten states, James and Leong[110] found a new band appearing in their melt spectra, which "suggests strongly that the quasi-crystalline order in the melt is different from that of the crystal." Surprisingly, still more work on the simple alkali-metal nitrates seems to be needed.

The addition of multiply charged metal ions to alkali-metal nitrate melts produces much greater perturbations of the nitrate ion spectrum than are observed in their absence, and in these circumstances the complex ion or ion pair model again becomes more favorable. The close similarity between spectra of the alkaline-earth metal nitrates in concentrated aqueous solutions and in alkali-metal nitrate melt solutions has further led Hester and Krishnan[43,111] to the assignment of complexed nitrate modes given in Table VI. The band frequencies given in Table VI were obtained from variable concentration studies of mixtures of the nitrates of Mg^{+2}, Ca^{+2}, Sr^{+2}, Ba^{+2}, Cd^{+2}, and Pb^{+2} ions in molten KNO_3 and equimolar KNO_3–$Mg(NO_3)_2$ mixtures. Overtone and combination bands were used as an aid to assign the infrared-active fundamentals, and recent Raman measurements have confirmed their frequencies.[112] Further evidence for complex formation was obtained by the addition of chloride ions (as KCl) to some of the molten nitrate mixtures. Increasing the Cl^- concentration in Ca^{2+}/K^+/NO_3^-/Cl^- mixtures resulted in progressive elimination of the infrared bands believed characteristic of complexed nitrate, with ultimate restoration of the spectrum to a form essentially identical with that given by pure KNO_3, the *solvent* in this study. A similar result was obtained for Cd^{+2},

TABLE VI. Fundamental Frequencies of Complexed Nitrate Ions in Molten Salt Mixtures[111]

Species[a]	Mg^{2+}	Cd^{2+}	Ca^{2+}	Pb^{2+}	Sr^{2+}	Ba^{2+}	Assignments
A_1	1320	1340	1340	1300	1325	1315	ν_1
A_1	1020	1000	1035	1020	1035	1035	ν_2
A_1	760	750	738	722	730	724	ν_3
B_1	1475	1470	1460	1410	1395	1375	ν_4
B_1	750	710	710	722	730	724	ν_5
B_2	805	806	810	815	818	820	ν_6

[a] Assuming monodentate binding, with C_{2v} symmetry for the nitrate ion.

but with Mg^{+2} addition of Cl^- failed to simplify the nitrate spectrum. This result is consistent with nonspectroscopic studies,[113,114] which have shown that chloride complexes of Cd^{+2} are considerably more stable than the corresponding nitrate complexes, though evidently Mg^{+2} has a higher affinity for NO_3^- than for Cl^-. Such mixed molten salt results lend themselves readily to the ligand displacement reaction interpretation so familiar in solution chemistry, but the systems are far too complex for the quasi-lattice mode interpretation to be useful.

The nitrate ion has proved a useful structure "indicator" in infrared and Raman investigations of molten salt hydrates, in addition to its utility in anhydrous molten salt work. Variable-temperature and variable-water-content studies of the zinc nitrate–water system[115,116] provide a good example of what can be done in this area. Figure 24 shows the N–O stretching region of the infrared absorption spectra of liquids of composition $Zn(NO_3)_2 \cdot xH_2O$, with x having values of 1.42, 1.94, 3.42, 5.30, 6.04, 9.63, 36.0, and ∞ (distilled water). Though the systems with high x values simply represent normal aqueous solutions, at low x these are perhaps better considered molten salt hydrates. What is the difference? The spectra suggest that there is essentially no fundamental difference, since there is evidently a steady progression in the extent of complexation of nitrate by zinc ions throughout the range of water content, and a series of ligand displacement equilibria is suggested of the form

$$Zn(H_2O)_6^{2+} \underset{H_2O}{\overset{NO_3^-}{\rightleftharpoons}} Zn(NO_3)(H_2O)_5^+ \underset{H_2O}{\overset{NO_3^-}{\rightleftharpoons}}$$

$$Zn(NO_3)_2(H_2O)_4 \underset{+H_2O}{\overset{-H_2O}{\rightleftharpoons}} Zn(NO_3)_2(H_2O)_{<4}$$

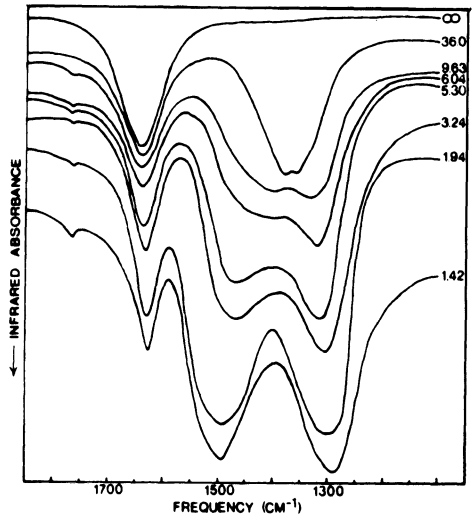

Fig. 24. Composition dependence of infrared bands in the N–O stretching region of liquid $Zn(NO_3)_2 \cdot xH_2O$ (with $x = 1.42$ to ∞) at 90°C.[116]

with the later species becoming progressively more important with decreasing water content. However, these findings are at variance with conclusions drawn by Angell[117] on the basis of solubility and conductance measurements that indicate that the cation hydration shell in such a system should remain intact in the "melt." Figure 25, however, offers still more conclusive spectroscopic evidence for the displacement of innersphere water molecules by nitrate ions in the molten hexahydrate of zinc nitrate. The symmetrical singlet structure of the $\nu_3(E')$ band of NO_3^- in the solid, where it is known to be separated from the nearest Zn^{2+} by a layer of water molecules,[118] splits into a widely spaced doublet in the melt, consistent with the proposed ligand-exchange process occurring in the liquid. Proton magnetic resonance results from a wide range of molten salt hydrates provide further evidence for some anion displacement of water molecules from metal innersphere coordination sites.[119]

Molten mixtures of alkali-metal nitrates and nitrates of multiply changed metal ions are of further interest in that they commonly form clear glasses on cooling[120] and therefore can be studied effectively by spectroscopic methods without the experimental complications of high temperature assemblies. Raman and infrared spectra of a wide range of such glasses have been obtained.[121] For the $Mg(NO_3)_2/KNO_3$ system it was found that the

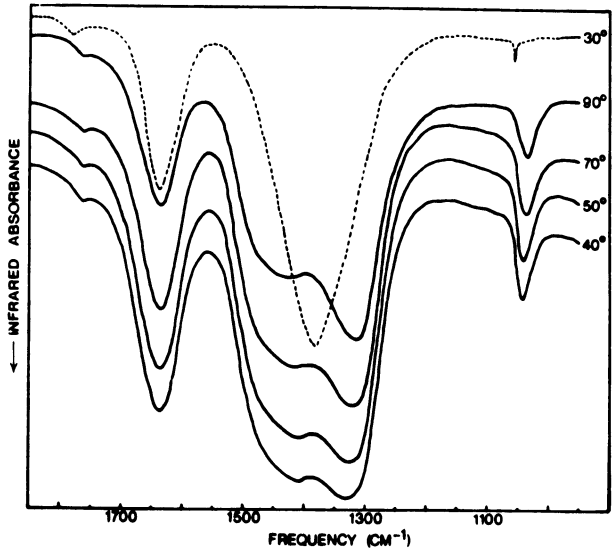

Fig. 25. Temperature dependence of infrared bands in the N–O stretching region of $Zn(NO_3)_2 \cdot 6.04H_2O$; (——) liquid, (– – – –) solid.[116]

ca. 1050 cm^{-1} ($\nu_1 A_1$ of D_{3h} nitrate) band had a doublet structure, with component frequencies at 1064 and 1045 cm^{-1}. The 1064-cm^{-1} component was found to increase in relative intensity as the Mg^{+2} content of the system was increased, while all band frequencies were found independent of composition over a wide range. The effect on the *ca.* 1050 cm^{-1} band of changing the alkali metal (M) in $Mg(NO_3)_2/MNO_3$ glassy mixtures was to shift the lower frequency component from 1049 cm^{-1} with Na to 1037 cm^{-1} with Cs without shifting the higher component frequency from 1064 cm^{-1}. These facts were interpreted as indicating the presence of distinct magnesium–nitrate complexes in the glasses, though secondary effects of a form attributable to less specific environmental perturbations of the nitrate component were also apparent. The designation of vibrational modes from glassy solids as lattice modes would not be useful, since such systems have no regular, ordered structure. Vibration spectra from mixed nitrate glasses with variable water content and from alkali metal nitrate–zinc chloride glassy mixtures also have been reported.[121]

3.2.2. Oxyanions Other than Nitrate

A large range of other metal–oxyanion systems have been investigated, though none as thoroughly as the nitrates. Table VII contains vibrational

TABLE VII. Vibrational Spectra of Molten Metal–Oxyanion Systems

Compounds	Fundamentals (cm^{-1})	References[a]
Hydroxides		
LiOH	3652, 440	(122)[I], (28)[I], (123)[I]
NaOH	3295, 265	(122)[I], (28)[I]
KOH	3300, 233	(122)[I]
Nitrites		
$NaNO_2$	1331, 1220, 813	(30)[I]
KNO_2	1333, 1220, 806	(30)[I]
Sulfates and Bisulfates		
Li_2SO_4	1115, 987, 625, 460	(47)[R], (123)[I]
Na_2SO_4	1095, 972, 625, 460	(47)[R], (123)[I]
K_2SO_4	1075, 960, ~620	(47)[R], (123)[I]
Rb_2SO_4	1060, 940	(123)[I]
$ZnSO_4/K_2SO_4$	1155, 1030, 970, 630, 615, 475	(123)[I,R]
$CuSO_4/K_2SO_4$	1145, 1025, 945, 640, 610, 495	(123)[I]
$CoSO_4/K_2SO_4$	1155, 1030, 950, 625, 615, 475	(123)[I]
$NiSO_4/K_2SO_4$	1145, 1030, 945, 630, 616, 490	(123)[I]
$KHSO_4$	~1380, 1230, 1050, 840, 590, 420	(46)[R]
Selenates		
H_2SeO_3	930, 880, 670, 600, 535, 385, 350, 320, 280, 230	(124)[R]
Chlorates and perchlorates		
$LiClO_3$	1018, 977, 938, 620, 478, 338	(125)[I]
$NaClO_3$	988, 932, 611, 482, <200	(125)[I]
$KClO_3$	981, 931, 603, 489, <200	(125)[I]
$AgClO_3$	969, 931, 895, 720, 595, 477, 440, <200	(125)[I]
$LiClO_4$	1139, 948, 627, 470, 315, 260	(125)[I]
Molybdates and tungstates		
Na_2MoO_4	894, 833, 314	(126)[R]
Na_2WO_4	928, 838, 316	(126)[R]
Borates		
$3Li_2O \cdot B_2O_3$	1255, 910, 600	(127)[R]
$2LiO \cdot B_2O_3$	1481, 1383, 1218, 1123, 1021, 910, 824, 750, 720, 630	(127)[R]
$5Li_2O \cdot 3B_2O_3$	1500, 1400, 1210, 910, 750–850, 720, 600	(127)[R]
$LiKO \cdot B_2O_3$	1400–1500, 1200, 700–800, 600	(127)[R]

TABLE VII. (*Continued*)

Compounds	Fundamentals (cm^{-1})	References
Phosphates and Arsenates		
$(Na, Li)_4P_2O_7$	1124, 1030, 980, 910, 730, 565, 500–300	(128)[R]
$(Na, Li)_4As_2O_7$	880, 838, 547, 340, 245	(128)[R]
$P_2O_7^{4-}/As_2O_7^{4-}$ mixture	1112, 1010, 988, 854, 717, 649, 566, 478, 373, 320, 276, 239	(128)[R]
Carbonates		
$Na_2CO_3-K_2CO_3$ eutetic	1575–1250, 1040, 870, 690	(129)[I]
$CaCO_3/(Na/K)_2CO_3$	As for $Na_2CO_3-K_2CO_3$ eutectic, but bands broadened asymmetrically	(129)[I]
$BaCO_3/(Na/K)_2CO_3$		(129)[I]

[a] I indicates references concerned with infrared spectra, while R indicates those for Raman spectra.

spectroscopic data obtained from molten metal hydroxides, nitrites, sulfates, bisulfates, selenates, chlorates, perchlorates, molybdates, tungstates, borates, phosphates, arsenates, and carbonates. The alkali-metal hydroxide spectra reported by Wilmshurst[122] are considerably more complex than is indicated by the most intense band frequencies listed in Table VII, and he again has drawn on a lattice-like model to account for the complexity, though the published spectra suggest that some of the weaker recorded bands may be spectral artifacts. It is clear, however, that these spectra contain more than a single O–H stretching mode, and the evidence for coupling of vibrations between two or more OH^- ions and for distinct metal–hydroxide stretching (lattice) modes is undeniable. The further work by Buchanan and coworkers[139] on infrared spectra of evaporated LiOH films produced good evidence for solid-state coupling of OH^- motions in the LiOH lattice, though Wilmshurst's solid state spectra evidently failed to produce this evidence. James[106] has questioned the interpretation of the molten hydroxide spectra on the basis of possible influence of water, which is likely to have been presented in the melts.

Raman spectra of molten lithium and sodium sulfate, obtained at 950°C, showed only small differences from the corresponding concentrated aqueous spectra.[123] No signs of loss of degeneracy in the E or F_2 modes of the tetrahedral (T_d) SO_4^{2-} ion were observed, though changes in relative band intensities and systematic frequency shifts were interpreted in terms of weak but specific cation–sulfate interactions. More recent work has con-

firmed these earlier results for the alkali-metal sulfate melts and has provided more evidence for small cation perturbation effects in the appearance in the infrared spectra of the formally forbidden (for a T_d molecule) $\nu_2(E)$ mode at *ca.* 450 cm^{-1}.[123] In contrast to these results, mixtures of divalent metal sulfates with K_2SO_4 (acting as a solvent system) show gross perturbations of the SO_4^{2-} ion structure. Raman and infrared studies have revealed splitting of the $\nu_3(F_2)$ and $\nu_4(F_2)$ bands into doublets, consistent with the lowering of SO_4^{2-} symmetry from T_d to C_{3v}, in spectra obtained from 40 mole % solutions of Ag(I), Mg(II), Ca(II), Sr(II), Ba(II), Zn(II), Cd(II), Pb(II), Cn(II), Co(II), and Ni(II) sulfates in molten K_2SO_4.[123] Frequency differences between corresponding infrared and Raman bands exclude the possibility of simple 1 : 1 metal–sulfate complex formation in these systems but do not distinguish between the possibilities of 1 : 2 complexes and a more general correlation field splitting arising in a quasi-lattice structure. Failure to observe splitting of the *ca.* 450 cm^{-1} $\nu_2(E)$ band, or triplet structure in the F_2 bands, indicates that the sulfate symmetry is not lower than C_{3v} in these melts, though a lower symmetry is common in the corresponding solid-state structures of the divalent metal sulfates.[13] Infrared-active overtone and combination bands were used to confirm assignments in the foregoing work,[123] which was done at temperatures in the range of 610 to 1100°C.

Related work on $KHSO_4$ has been reported,[46] with Raman spectra indicating reactions in the temperature range 300 to 700°C to form species $S_2O_7^{2-}$ and SO_4^{2-}. Figure 26 shows correlations between modes of the three species SO_4^{2-} (T_d symmetry), H_2SO_3 (C_{2v}), and HSO_4^- (C_s), which demonstrate the complexity of the task of spectral analysis when several species are simultaneously present. Selenious acid, though not a salt at all, has been studied in the molten state by Raman spectroscopy[124] and is included in Table VII. As with the HSO_4^- results, Walrafen[124] has interpreted his spectra in terms of reactions taking place to form such complex species as $H_2Se_2O_5$, $(H_2SeO_3)_2$, and $(SeO_2)_n$ polymers. Even with the ionic species, no account was taken in these interpretations of possible interionic correlations that might be responsible for some of the spectral features.

The data obtained from reflectance spectra of the molten chlorates listed in Table VII show a lowering of the C_{3v} symmetry of the ClO_3^- ion in the cases of the Li and Ag salts, resulting in loss of degeneracy in the $\nu_3(E)$ modes (*ca.* 980 cm^{-1}). Wilmshurst[125] has suggested that this is caused by removal of the threefold axis of symmetry of the chlorate ion, such that the greatest element of symmetry common to the surrounding cation field and the chlorate ion is probably C_s, and also by inhibition of free rotation about

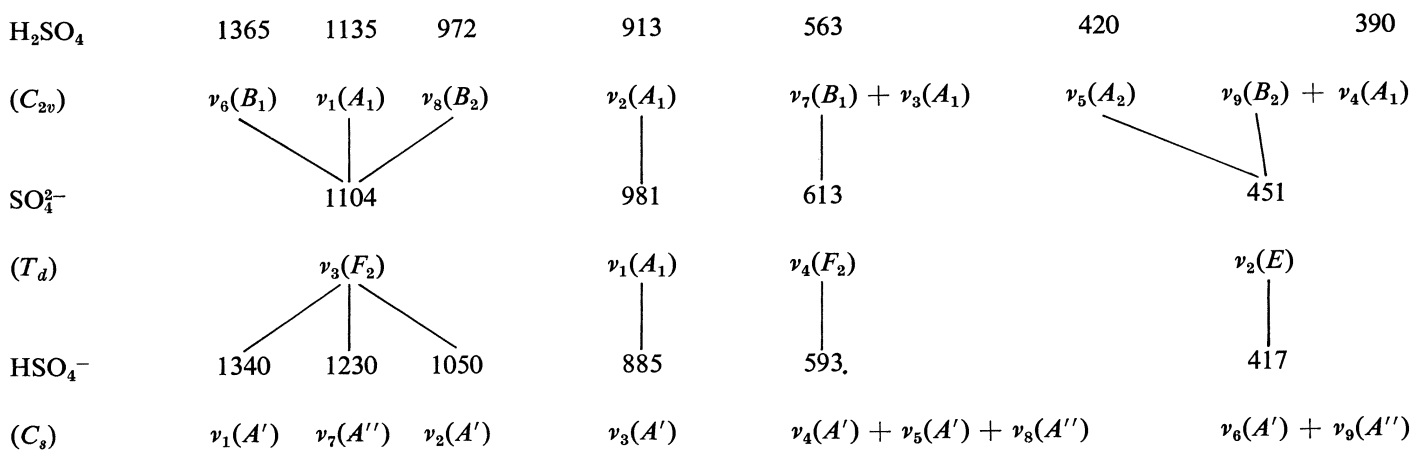

Fig. 26. Correlations of modes from SO_4^{2-}, HSO_4^-, and H_2SO_4.[46]

this axis. Infrared activity of the $\nu_1(A_1)$ and $\nu_2(E)$ modes, at 948 and 470 cm^{-1}, respectively, was observed for molten $LiClO_4$, though no splitting of the E or of the F_2 bands of the tetrahedral ClO_4^- ion was detectable.[125] Evidently the ClO_4^- retains its T_d symmetry in the melt and rotates freely,[125] though the relaxation of selection rules and the appearance of low-frequency "lattice" modes are evidence of weak environmental interactions.

Raman spectra of sodium molybdate and sodium tungstate have been obtained by Vallier.[126] These show only bands expected of the simple tetrahedral ions MoO_4^{2-} and WO_4^{2-}, though in acid media, achieved by adding excess MoO_3 or WO_3, several new bands arise. Vallier has speculated that these might be due to formation of bimolybdate and bitungstate species, though more complex species could be present.

Bues and co-workers[127] have shown that it is possible to characterize planar BO_3^{3-} ions of D_{3h} symmetry in molten lithium orthoborate by Raman spectroscopy. A melt of composition $3Li_2O \cdot B_2O_3$ at 750°C gave three bands, the higher frequency pair of which were assigned as B–O stretching modes, the low frequency band arising from a BO_3 deformation mode. Changes in the Raman spectrum as the Li_2O B_2O_3 ratio was varied were accounted for by formation of the ions $B_2O_5^{4-}$, BO_3^{3-}, and $B_3O_7^{5-}$, and evidence was found for the presence of polymeric anions in metaborate melts.

Analogous work by Bues and co-workers[128] on molten alkali-metal diphosphates, diarsenates, and their mixtures produced evidence for retention of a network polymeric structure in the melts in the 800–850°C temperature range. Closely similar vibrational frequencies were obtained from an infrared study of a glassy solid of composition $Na_4P_2O_7 + Li_4P_2O_7$, from crystalline $Na_4P_2O_7$, and from a Raman study of the molten salt mixture. Diarsenate mixtures similarly resembled the crystalline solids, but distinct new bands were found for diphosphate–diarsenate mixtures, believed to arise from the $PAsO_7^{4-}$ species formed in the simple exchange reaction $P_2O_7^{4-} + As_2O_7^{4-} \rightleftharpoons 2AsPO_7^{4-}$.

No spectroscopic work has been reported on molten metal carbonates. Infrared spectra of the alkali-metal carbonate melts and of mixtures containing doubly charged metal ions have recently been recorded by the author but are of rather poor quality due to attack of container materials and supports by the highly corrosive liquids, coupled with a strong tendency to thermal decomposition, with loss of CO_2. Corrosion problems also have foiled most of the attempts to record Raman spectra of molten carbonates, though it is anticipated that these problems will soon be overcome by use of one of the special cells described earlier. From controlled atmosphere (pressurized CO_2) infrared experiments, using platinum, nickel, and gold

wire mesh supports, the frequencies given in Table VI have been reliably recorded. The frequencies listed are of carbonate fundamentals only, though overtone and combination bands also were recorded and support the assignment of the very strong band in the 1575–1250-cm^{-1} region as $\nu_3(E')$ of a D_{3h} ion, of the 1040-cm^{-1}–band as $\nu_1(A_1')$, of the 870-cm^{-1} band as $\nu_2(A'')$, and of the 690-cm^{-1} band as $\nu_4(E')$. These frequencies differ significantly from those reported as characterizing the free CO_3^{2-} ion[2] (ν_1, 1063; ν_2, 879; ν_3, 1415; ν_4, 680 cm^{-1}) but no structure was discernible in the bands. Some asymmetric band broadening resulted from addition of alkaline-earth metal carbonates to the sodium–potassium carbonate eutectic, though it was not possible to resolve new bands. The melts were held at *ca.* 900°C while their spectra were obtained.

3.2.3. Thiocyanates

The low melting points of alkali-metal thiocyanates (*ca.* 170–290°C) would appear to make them convenient systems for molten salt studies, but they all have very short ranges of stability as liquids, decomposition usually setting in at *ca.* 30° above the melting point. Baddiel and Janz[130] obtained the frequencies listed in Table VIII for the alkali-metal salts from Raman spectroscopic measurements. Their values are significantly higher than the infrared frequencies previously reported by Greenberg[131] but are in good agreement with more recent infrared data obtained by Hester and Krishnan.[132] These latter authors also obtained the data listed for the molten thiocyanates of doubly charged metal ions, using 30 mole % solutions in KSCN in each case.

TABLE VIII. Vibrational Spectra of Molten Thiocyanates

Salt	Fundamentals (cm^{-1})	References
LiSCN	2083, 764, 499	$(130)^R$, $(131)^I$
NaSCN	2074, 745, 490	$(130)^R$, $(131)^I$
KSCN	2068, 745, 478	$(130)^R$, $(131)^I$
$Mg(SCN)_2$/KSCN	2075, 775, 480	$(132)^I$
$Ca(SCN)_2$/KSCN	2062, 768, 485	$(132)^I$
$Ba(SCN)_2$/KSCN	2065, 745, 472	$(132)^I$
$Zn(SCN)_2$/KSCN	2077, 818, 475	$(132)^I$
$Hg(SCN)_2$/KSCN	2108, 712, 445	$(132)^I$
$Pb(SCN)_2$/KSCN	2085, 725, 452	$(132)^I$

The alkali-metal thiocyanate spectra indicate that these are fully ionized melts, containing linear SCN^- ions of $C_{\infty v}$ symmetry. The frequencies correspond only roughly to C–N stretching (*ca.* 2070 cm^{-1}), C–S stretching (*ca.* 740 cm^{-1}), and NCS deformation (*ca.* 470 cm^{-1}) modes, since normal coordinate calculations have shown[130,132] that there is considerable mixing of the simple stretching coordinates in the two Σ^+ type normal modes. Baddiel and Janz[130] showed that concentrated aqueous solutions of alkali-metal thiocyanates gave Raman spectra little different from those given by the anhydrous molten salts, but the results from the molten salt systems containing multiply charged metal ions were distinctly different.[132] Distinct new bands appeared in spectra from these mixed thiocyanates, as shown in Fig. 27, which reproduces the C–S stretching regions of spectra from several of the systems studied. The new bands are believed to arise from complexed thiocyanate, which exists in a normal thermodynamic equilibrium with kinetically free (non complexed) thiocyanate ions. Intensity variations with melt composition support this interpretation, and there is evidence for binding of the SCN^- ion through the nitrogen end with Mg^{2+}, Ca^{2+}, Ba^{2+}, Zn^{2+}, Co^{2+}, Ni^{2+}, and Cr^{3+}, but through the sulfur end with Hg^{2+} and Pb^{2+} ions.[132]

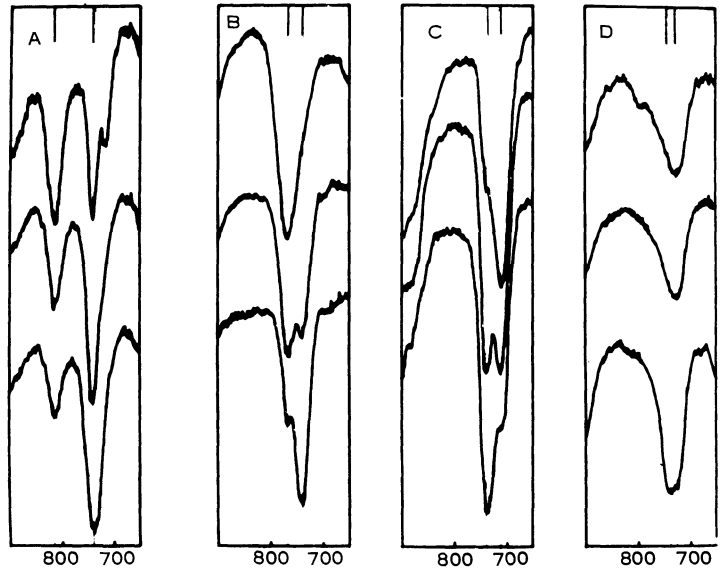

Fig. 27. The C–S stretching region of the infrared spectra of molten thiocyanates. (A) KSCN–$Zn(SCN)_2$; (B) KSCN–$Ca(SCN)_2$; (C) KSCN–$Hg(SCN)_2$; and (D) KSCN–$Pb(SCN)_2$. In each case curves represent KSCN contents of 90, 80, and 70 mole %. respectively, from bottom to top.[132]

3.3. Covalent Melts

Most of the discussion in the preceding section was concerned with ionic melts, though a number of salts have been included that are known to be essentially covalent even in the solid state. Covalent systems can be classified as molecular (for example, $HgCl_2$, $HgBr_2$, HgI_2) or polymeric (for example, $ZnCl_2$, $ZnBr_2$), though the chemical bonds in essentially all of them retain significant polarity, and it is sometimes convenient to treat them simply as intermediate states in stepwise interionic associative schemes of the general form $M^{n+} + X^{m-}$, giving successively cationic, neutral, and finally anionic species.

Operational criteria for the designation of molten salts as covalent or ionic are based primarily upon physico-chemical properties such as electrical conductivity and viscosity,[133] but vibrational spectra also are useful, particularly if used for comparisons between the solid, liquid (molten salt), and vapor states. Such comparisons have been made, for example, with the mercuric halides discussed in the previous section. However, use of the words "covalent" and "ionic" in the context of molten salts is in itself rather limiting, because in none of the cases discussed is it entirely satisfactory to formulate interactions as wholly electrostatic, and bond polarity can cause electrostatic-type interactions even between molecules that are individually electrically neutral. Molten salt vibrational spectroscopy clearly does not represent the simplest or best method of examining the nature of the chemical bond, and it probably would be unprofitable to treat "covalent melts" further as a distinct category here. The difficulties with bonding concepts raised here are expanded upon in the following section.

4. THEORETICAL PROBLEMS

Problems of interpretation of spectra have arisen at frequent intervals throughout this survey, and the views of various research workers have been outlined in the context of their experimental findings. Apart from the covalent/ionic difficulties raised in the previous section, the major conflict of views has been over the question of whether it is at all meaningful to use the concept of a "complex ion" to account for vibrational spectra of molten salts. As has been seen, this is a concept much favored by chemists who have seen close similarities between spectra from molten salts and spectra from aqueous and non aqueous solutions that are known to contain distinct complexes (for example, see Moyer *et al.*[58] Janz and James,[63] and Clarke and Hester[75]). However, the anhydrous molten salt environment is so

markedly different from that of a neutral solvent that perturbations of a polyatomic complex can be expected to be so severe, in some cases, that the complex loses its identity as such, and what vibrational modes there are must be thought of as involving a significantly larger unit of the structure. When the larger unit is the whole system, the model is that advocated by Wilmshurst.[28] Wilmshurst has pointed out that the lifetime of a single configuration of a molten salt must be long compared with the time needed for vibrations, so that it is the bulk "structure" of the liquid that determines the vibrational spectrum. This statement holds equally for aqueous salt solutions, however, and it is hardly questioned that complex species can be characterized by their vibrational spectra in these circumstances.

Vibrational spectra of crystalline solids that are known (from X-ray crystallographic analysis) to contain molecular or polyatomic ionic species commonly show features characteristic of their particular lattice structures.[15] Coupling of vibrational modes between neighboring polyatomic units is responsible for some of these features, while others, usually at much lower frequencies, arise from vibration of one part of the lattice against another or from organized, restricted rotational modes of the polyatomic species. These latter types are the *lattice modes*. All of these features are easily calculated on the basis of a single primitive unit cell of the crystal structure by factor group analysis[16,17] although, as mentioned earlier, a simpler site symmetry analysis is usually adequate to account for observed spectra.[18] But it is well known that positional disorder introduced in solids by raising their temperatures (much above that of liquid nitrogen) causes considerable line broadening and loss of fine structure in their vibrational spectra, so that it would be surprising if spectra from high temperature molten salt, in general, could be interpreted satisfactorily on the basis of well-defined crystal lattice structures. The concept of unit cell oscillations propagating in an organized manner throughout an extended lattice structure (phonons) in particular cannot have much validity for molten salt systems. The fact that significant structural changes probably are common on melting ionic solids[133] further limits the utility of the lattice model, since although local order may be preserved in a molten salt, this local order may well be of a different symmetry from that present in bulk in the crystalline solid.

As an example of the type of analysis that is possible for crystal lattice structures and to see how far the analysis is useful for determining structure after melting, it is instructive to consider the case of mercuric iodide. Even in the solid state this compound exists in two different structural forms. The red form of HgI_2 is stable at temperatures below 126°C and consists

of a tetragonal layer like polymeric lattice of linked tetrahedral HgI_4 units.[135] However, the long Hg–I distances of 2.783 Å indicate that this is a predominantly ionic lattice, based on a distorted cubic close-packed arrangement. The unit cell, given in Fig. 28, shows the I atoms located on sites having $4d(C_{2v})$ symmetry and Hg atoms on sites of $2a$ (D_{2d}) symmetry. A summary of a factor group analysis for this structure is reproduced[136] in Table IX, showing how the normal modes are distributed between the various symmetry species; how they are classified as acoustic, lattice translational, librational, and internal (within the linked HgI_4 layers) modes; and which of them are Raman and/or infrared active. It will be seen that the presence of a center of symmetry in the D_{4h}^{15} structure leads to operation of the mutual exclusion rule for Raman and infrared activities.

Yellow HgI_2, the stable form above 126°C, exists as orthorhombic crystals with space group $Cmc2_1(C_{2v}^{12})$ symmetry. The unit cell has four molecules arranged as shown in Fig. 29. The structure is based on a severely distorted hexagonal close-packed arrangement, within which the HgI_6 octahedra have two Hg–I distances of 2.617 Å (approximately the sum of Hg and I covalent radii), while the other four are 3.508 Å (only 0.1 Å shorter than the van der Waals radii). Thus the structure may be considered essentially molecular. Two HgI_2 molecules of the unit cell are located in the *bc* plane (see Fig. 29), and the other two are a half-unit above or below this plane. Only two molecules need be considered for determination of the optically active modes,[138] since they are related to the other two by a simple

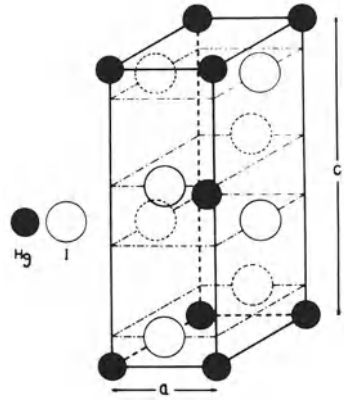

Fig. 28. Tetragonal unit cell of red HgI_2 in the space group $P4_2/nmc(D_{4h}^{15})$, containing two molecules of HgI_2.[54]

TABLE IX. Character Table and Distribution of Modes for Red Mercury(II) Iodide[136] [a]

D_{4h}^{15}	E	$2C_4$	C_2	$2C_2'$	$2C_2''$	i	$2S_4$	σ_h	$2\sigma_v$	$2\sigma_d$	n_i	T	T'	n_i'	Activity
A_{1g}	1	1	1	1	1	1	1	1	1	1	1	0	0	1	R
A_{2g}	1	1	1	−1	−1	1	1	1	−1	−1	0	0	0	0	
B_{1g}	1	−1	1	1	−1	1	−1	1	1	−1	0	0	0	0	R
B_{2g}	1	−1	1	−1	1	1	−1	1	−1	1	2	0	1	1	R
E_g	2	0	−2	0	0	2	0	−2	0	0	3	0	1	2	R
A_{1u}	1	1	1	1	1	−1	−1	−1	−1	−1	0	0	0	0	
A_{2u}	1	1	1	−1	−1	−1	−1	−1	1	1	2	1	0	1	I
B_{1u}	1	−1	1	1	−1	−1	1	−1	−1	1	1	0	0	1	
B_{2u}	1	−1	1	−1	1	−1	1	−1	1	−1	0	0	0	0	
E_u	2	0	−2	0	0	−2	0	2	0	0	3	1	0	2	I
ω_R [b]	6	0	6	2	0	0	2	0	0	6					
$2\cos\phi_R \pm 1$	3	1	−1	−1	−1	−3	−1	1	1	1					
$\chi_j'(n_i)$	18	0	−6	−2	0	0	−2	0	0	6					
$\omega_R(s)$	2	0	2	2	0	0	2	0	0	2					
$\omega_R(s) - 1$	1	−1	1	1	−1	−1	1	−1	−1	1					
$\chi_j'(T')$	3	−1	−1	−1	1	3	−1	−1	−1	1					

[a] n_i is total number of modes; T, T', R', n_i' are the numbers of acoustic, lattice translational, librational, and internal modes of vibration, respectively.
[b] Notation as in reference 56.

translation. A factor group analysis based on this structure is summarized in Table X, and the results of this are compared with site group[18] and point group[11] analyses in Table XI. From this it is clear that in the limit of no intermolecular interaction (dilute gas phase HgI_2) the eight internal modes predicted by the C_{2v} factor group analysis will reduce to the three normal modes of the free HgI_2 molecule. Even with moderate interaction, the frequencies $\nu_1(A_1)$ and $\nu_3(A_1)$ should be very similar to $\nu_1(B_2)$ and $\nu_3(B_2)$, respectively, since the corresponding modes differ only in phase. It can be anticipated, therefore, that these modes will appear as doublets (perhaps unresolved) at frequencies close to those of the free (gaseous) molecule. However, the doubly degenerate bending mode of the free molecule, $\nu_2(\pi_u)$, should be, and in fact is, more strongly split in the crystal spectrum, since the large separation between the HgI_2 molecular layers will distinguish the in-layer-plane mode ν_2, from the out-of-layer-plane mode ν_2.

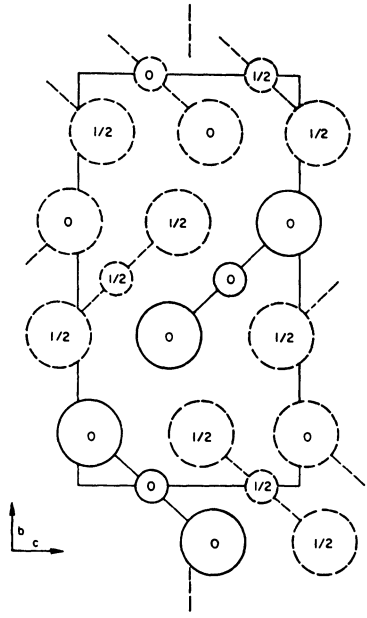

Fig. 29. Crystal structure of yellow HgI_2. Large circles represent I atoms. The figures in the circles indicate coordinates in the *a* direction.[137]

TABLE X. Character Table and Distribution of Modes for Yellow Mercury(II) Iodide[136]

C_{2v}^{12}	E	C_2	σ_v	σ_v'	n_i	T	T'	R'	n_i'	Activity
A_1	1	1	1	1	6	1	1	1	3	R, I
A_2	1	1	−1	−1	3	0	1	1	1	R
B_1	1	−1	1	−1	3	1	0	1	1	R, I
B_2	1	−1	−1	1	6	1	1	1	3	R, I
ω_R	6	0	0	6						
$2\cos\phi_R \pm 1$	3	−1	1	1						
$\chi_j'(n_i)$	18	0	0	6						
$\omega_R(s)$	2	0	0	2						
$\omega_R(s) - 1$	1	−1	−1	−1						
$\chi_j'(T')$	3	1	−1	1						
$\chi_j'(P)$	2	0	0	0						
$\omega_R(s-p)$	2	0	0	2						
$\chi_j'(R')$	4	0	0	0						

TABLE XI. Correlation Table for the Factor Group, Site Group, and Point Group of the HgI_2 (Yellow) Crystal[a]

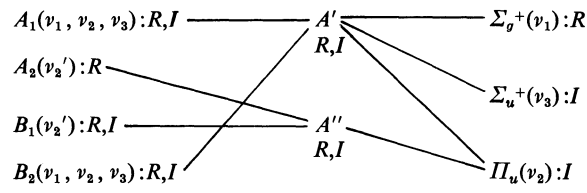

[a] R indicates Raman-active; I, infrared-active.

The Raman spectrum of molten HgI_2, as stated earlier, shows that the liquid is molecular,[54] with restoration of the degeneracy of the π-type deformation modes (a 41 + 37-cm^{-1} doublet in the yellow solid spectrum)[54] indicating break up of the layer-lattice structure of yellow HgI_2 on melting. Only the weak Raman activity of the 41-cm^{-1} band in the melt spectrum remains as evidence of intermolecular interactions, and the detailed analyses of crystal vibrations that are so useful for understanding solid-state vibrational spectra are barely relevant for this molten salt. Of course, it is possible that for molten salts that are more ionic in nature the predictions of factor-group analyses will be more useful, as some of the results discussed earlier from nitrate melts[108] already have indicated, but experimental spectra are likely to be insufficiently resolved from most high temperature molten salts, so that considerable uncertainty is likely to characterize most attempts to apply such analytical methods in detail.

REFERENCES

1. J. K. Wilmshurst and J. M. Bracker, paper read at the American Chemical Society Symposium on Molten Salts, September 1968.
2. G. Hertzberg, *Molecular Spectra and Molecular Structure* Vol. II and III, Van Nostrand Reinhold, New York (1945 and 1966).
3. L. Pauling and E. B. Wilson, *Introduction to Quantum Mechanics*, McGraw-Hill, New York (1935).
4. F. A. Cotton, *Chemical Applications of Group Theory*, John Wiley (Interscience), New York (1963).
5. D. Schonland, *Molecular Symmetry*, Van Nostrand Reinhold, New York (1965).
6. C. V. Raman, *Indian J. Phys.* **2**: 387 (1928).

7. L. A. Woodward, in: *Raman Spectroscopy* (H. A. Szymanski, ed.), Chap. 1, Plenum Press, New York (1967).
8. G. Placzek, in: *Handbuch der Radiologie*, (E. Marx, ed.), Vol. 6, Pt. 2, Akademische Verlagsgesellschaft, Leipzig (1934).
9. A. C. Albrecht, *J. Chem. Phys.* **34**: 1476 (1961).
10. J. Brandmüller and H. Moser, *Einführung in die Ramanspektroskopie*, D. Steinkopff Verlag, Darmstadt (1962).
11. E. B. Wilson, Jr., J. C. Decius, and P. C. Cross, *Molecular Vibrations*, McGraw-Hill, New York (1955).
12. S. Bhagavantam, *Scattering of Light and the Raman Effect*, Andhra University Waltair, India (1940).
13. W. G. Wyckoff, *Crystal Structures*, Vol. 1, 2nd ed., John Wiley (Interscience) New York, (1963).
14. *International Tables for X-Ray Crystallography*, Vol. I, Kynock Press, Birmingham, England (1962).
15. S. Bhagavantam and T. Venkatarayudu, *Proc. Indian Acad. Sci.* **A9**:224 (1939); S. Bhagavantam, *Proc. Indian Acad. Sci.* **A13**, 543 (1941).
16. S. Bhagavantam and T. Venkatarayudu, *Theory of Groups and Its Application to Physical Problems*, Andhra University, Waltair, India (1951).
17. S. S. Mitra, *Z. Kristallogr.* **116**:149 (1961); *Solid State Physics*, **13**:1 (1962).
18. R. S. Halford, *J. Chem. Phys.* **14**:8 (1946).
19. M. C. Hutley and D. J. Jacobs, personal communication.
20. S. P. S. Porto, *J. Opt. Soc. Amer.* **56**:1585 (1966).
21. R. E. Hester and K. Krishnan, *J. Chem. Phys.* **49**:4356 (1968).
22. J. D. Mackenzie, *Rev. Sci. Instrum.* **32**:118 (1961).
23. G. H. Wegdam, R. Bonn, and J. van der Elsken, *Chem. Phys. Lett.* **2**:182 (1968).
24. F. N. H. Robinson, *Noise in Electrical Circuits*, Chap. 6, Oxford University Press, New York (1962).
25. W. Brügel, *Infrared Spectroscopy*, Pt. III, Chap. 4, Methuen, London, (1962).
26. W. W. Wendlandt and H. G. Hecht, *Reflectance Spectroscopy*, John Wiley (Interscience), New York (1966); W. W. Wendlandt, *Modern Aspects of Reflectance Spectroscopy*, Plenum Press, New York (1964).
27. J. K. Wilmshurst and S. Senderoff, *J. Chem. Phys.* **35**:1078 (1961).
28. J. K. Wilmshurst, *J. Chem. Phys.* **39**:1779 (1963).
29. J. K. Wilmshurst, *J. Chem. Phys.* **39**:2545 (1963).
30. J. Greenberg and L. J. Hallgren, *J. Chem. Phys.* **33**:900 (1960).
31. T. S. Robinson and W. C. Price, *Molecular Spectroscopy*, p. 211 (G. Sell, ed.), Institute of Petroleum (1955).
32. J. Fahrenfort, *Spectrochim. Acta* **17**:698 (1961); J. Fahrenfort and W. M. Vissar, *Spectrochim. Acta* **18**:1103 (1962).
33. A. C. Gilby, J. Burr, Jr., and B. Crawford, Jr., *J. Phys. Chem.* **70**:1520 (1966); A. C. Gilby, J. Burr, Jr., W. Krueger, and B. Crawford, Jr., *J. Phys. Chem.* **70**:1525 (1966); A. A. Clifford and B. Crawford, Jr., *J. Phys. Chem.* **70**:1536 (1966).
34. N. J. Harrick, *Internal Reflection Spectroscopy*, John Wiley (Interscience), New York (1967).
35. A. Bandy, J. P. Devlin, R. Burger, and B. McCoy, *Rev. Sci. Instrum* **35**:1206 (1964).
36. T. R. Kozlowski, *Appl. Opt.* **7**:795 (1968).

37. J. H. Hibben, *The Raman Effect and Its Chemical Applications*, Van Nostrand Reinhold, New York (1939).
38. H. L. Welsh, M. F. Crawford, T. R. Thomas, and G. R. Love, *Can. J. Phys.* **30**:577 (1952).
39. R. S. Krishnan, technique used routinely at the Indian Institute of Science, Bangalore, India.
40. N. S. Ham and A. Walsh, *Spectrochim. Acta* **12**:88 (1958).
41. F. X. Powell, O. Fletcher, and E. R. Lippincott, *Rev. Sci. Instrum.* **34**:36 (1963); F. X. Powell, E. R. Lippincott, and D. Steele, *Spectrochim. Acta* **17**:880 (1961).
42. J. P. Devlin, P. C. Li, and R. P. J. Cooney, paper read at the American Chemical Society Symposium on Molten Salts, September, 1968.
43. R. E. Hester and K. Krishnan, *J. Chem. Phys.* **46**:3405 (1967).
44. G. J. Janz, Y. Mikawa, and D. W. James, *Appl. Spectrosc.* **15**:47 (1961).
45. G. J. Janz and D. W. James, *J. Chem. Phys.* **35**:739 (1961).
46. G. Walrafen, D. E. Irish, and T. F. Young, *J. Chem. Phys.* **37**:662 (1962).
47. G. E. Walrafen, *J. Chem. Phys.* **43**:479 (1965).
48. W. Bues, *Z. Anorg. Chem.* **279**:104 (1955).
49. L. S. Arighi and M. V. Evans, *Appl. Spectrosc.* **21**:43 (1967).
50. C. Solomons, J. H. R. Clarke, and J. O'M. Bockris, *J. Chem. Phys.* **49**:445 (1968).
51. J. P. Young, *Anal. Chem.* **36**:390 (1964).
52. J. H. R. Clarke, C. Solomons, and K. Balasubrahmanyam, *Rev. Sci. Instrum.* **38**:665 (1967).
53. J. H. R. Clarke and R. E. Hester, *J. Chem. Phys.* **50**:3106 (1969).
54. A. J. Melveger, R. K. Khanna, B. R. Guscott, and E. R. Lippincott, *Inorg. Chem.* **7**:1630 (1968).
55. S. S. Mitra and P. J. Gielisse, in: *Progress in Infrared Spectroscopy*, Vol. 2 (H. A. Szymanski, ed.), Plenum Press, New York (1964).
56. S. S. Mitra, *Solid State Phys.* **13**:1 (1962).
57. D. E. Irish and T. F. Young, *J. Chem. Phys.* **43**:1765 (1965).
58. J. R. Moyer, J. C. Evans, and G. Y-S. Lo, *J. Electrochem. Soc.* **113**:158 (1966).
59. E. J. Salstrom and L. Harris, *J. Chem. Phys.* **3**:241 (1935).
60. R. B. Ellis, *J. Electrochem. Soc.* **113**:485 (1966).
61. M. Tanaka, K. Balasubrahmanyam, and J. O'M. Bockris, *Electrochim. Acta* **8**:621 (1963).
62. G. J. Janz and J. D. E. McIntyre, *J. Electrochem. Soc.* **109**:842 (1962).
63. G. J. Janz and D. W. James, *J. Chem. Phys.* **38**:902 (1962); **38**:905 (1963).
64. G. J. Janz and T. R. Kozlowski, *J. Chem. Phys.* **39**:843 (1963).
65. G. J. Janz, C. Baddiel, and T. R. Kozlowski, *J. Chem. Phys.* **40**:2055 (1964).
66. J. H. R. Clarke and C. Solomons, *J. Chem. Phys.* **48**:528 (1968).
67. K. Balasubrahmanyam, *J. Chem. Phys.* **44**:3270 (1966).
68. J. Vallier and R. Lira, *C. R. Acad. Sci. (Paris)* **259**:4579 (1964).
69. K. Balasubrahmanyam and L. Nanis, *J. Chem. Phys.* **42**:676 (1965).
70. H. Gerding and H. Hontgraaf, *Rec. Trav. Chim.* **72**:21 (1953).
71. J. D. Corbett, *Inorg. Chem.* **1**:700 (1962).
72. L. A. Woodward, G. Garton, and H. L. Roberts, *J. Chem. Soc.* 3723 (1956).
73. L. A. Woodward, N. N. Greenwood, J. R. Hall, and I. J. Worrall, *J. Chem. Soc.* 1505 (1958).
74. J. H. R. Clarke and R. E. Hester, *Chem. Commun.* 1042 (1968).

75. J. H. R. Clarke and R. E. Hester, *Inorg. Chem.* **8**:1113 (1969).
76. J. T. Kenney and F. X. Powell, *J. Phys. Chem.* **72**:3094 (1968).
77. J. H. R. Clarke and C. Solomons, *J. Chem. Phys.* **47**:1823 (1967).
78. K. Balasubrahmanyam and L. Nanis, *J. Chem. Phys.* **40**:2657 (1964).
79. R. E. Hester, in: *Raman Spectroscopy*, Chap. 4 (H. A. Szymanski, ed.), Plenum Press, New York (1967).
80. B. Brehler, *Z. Kristallogr.* **115**:375 (1961).
81. M. A. Bredig and E. R. van Artsdalen, *J. Chem. Phys.* **24**:478 (1956).
82. M. Delwaulle, *Compt. Rend.* (*Paris*) **206**:1965 (1938).
83. W. Klemperer, *J. Chem. Phys.* **25**:1066 (1956).
84. H. Gerding and E. Smit, *Z. Phys. Chem.* (*Leipzig*) **B50**:171 (1941).
85. L. A. Woodward and M. J. Taylor, *J. Chem. Soc.* 4473 (1960).
86. V. A. Maroni and E. J. Cairns, paper read at the American Chemical Society Symposium on Molten Salts, September 1968.
87. R. E. Hester, R. A. Plane, and G. E. Walrafen, *J. Chem. Phys.* **38**:249 (1963); R. E. Hester and R. A. Plane, *J. Chem. Phys.* **40**:411 (1964); **45**:4588 (1966); *Inorg. Chem.* **3**:769 (1964).
88. J. T. Miller and D. E. Irish, *Can. J. Chem.* **45**:147 (1967).
89. P. M. Vollmar, *J. Chem. Phys.* **39**:2236 (1963).
90. H. Brintzinger and R. E. Hester, *Inorg. Chem.* **5**:980 (1966); R. E. Hester and W. E. L. Grossman, *Inorg. Chem.* **5**:1308 (1966).
91. S. C. Wait, Jr., A. T. Ward, and G. J. Janz, *J. Chem. Phys.* **45**:133 (1966).
92. W. Bues, *Z. Phys. Chem.* (*Frankfurt*) **10**:1 (1957).
93. J. R. Ferraro and A. Walker, *J. Chem. Phys.* **42**:1273 (1965).
94. P. Grassman, *Z. Phys.* **77**:616 (1932).
95. Y. Doucet and J. Vallier, *Compt. Rend.* (*Paris*) **225**:2935 (1962).
96. C. B. Baddiel, M. J. Tait, and G. J. Janz, *J. Phys. Chem.* **69**:3634 (1965).
97. G. E. Walrafen and D. E. Irish, *J. Chem. Phys.* **40**:911 (1964).
98. J. P. Devlin, K. Williamson, and G. Austin, *J. Chem. Phys.* **44**:2203 (1966).
99. G. J. Janz, T. R. Kozlowski, and S. C. Wait, Jr., *J. Chem. Phys.* **39**:1809 (1963).
100. R. Bar, *Nature* **124**:692 (1929).
101. E. F. Gross and V.A. Koksova, *Akad. Nauk. SSSR* 231 (1952).
102. J. P. Mathieu and M. Lounsbury, *Discuss. Faraday Soc.* **9**:196 (1950).
103. R. A. Schroeder, C. E. Weir, and E. R. Lippincott, *J. Chem. Phys.* **36**:2803 (1962).
104. L. Couture and J. P. Mathieu, *Ann. Phys.* (*Paris*) **3**:521 (1948).
105. G. J. Janz and S. C. Wait, Jr., *Quart. Rev.* (*London*) **17**:225 (1963).
106. D. W. James, in: *Molten Salt Chemistry* (M. Blander, ed.), John Wiley (Interscience), New York (1964).
107. G. J. Janz and S. C. Wait, Jr., in: *Raman Spectroscopy*, Chap. 5 (H. A. Szymanski, ed.), Plenum Press, New York (1967).
108. K. Williamson, P. Li, and J. P. Devlin, *J. Chem. Phys.* **48**:3891 (1968).
109. J. C. Decius, *J. Chem. Phys.* **23**:1290 (1955).
110. D. W. James and W. H. Leong, *Chem. Commum.* 1415 (1968).
111. R. E. Hester and K. Krishnan, *J. Chem. Phys.* **47**:1747 (1967).
112. R. E. Hester and K. Krishnan, unpublished results.
113. D. Inman, *Electrochim. Acta* **10**:11 (1965).
114. G. G. Bombi, G. A. Mazzocchin, and M. Fiorani, *Ric. Sci.* **36**:573 (1966).
115. R. E. Hester and C. W. J. Scaife, *J. Chem. Phys.* **47**:5253 (1967).

116. R. E. Hester, K. Krishnan, and C. W. J. Scaife, *J. Chem. Phys.* **49**:1100 (1968).
117. C. A. Angell, *J. Electrochem. Soc.* **112**:1224 (1965).
118. A. Ferrari, A. Briabanti, A. M. M. Lanfredi, and A. Tiripicchio, *Acta Crystallogr.* **22**:240 (1967).
119. V. S. Ellis and R. E. Hester, *J. Chem. Soc.* (*A*) 411 (1969).
120. E. Thilo, C. Wieker, and W. Wieker, *Silikattechn.* **15**:109 (1964).
121. R. E. Hester and K. Krishnan, *J. Chem. Soc.* (*A*), 1955 (1968).
122. J. K. Wilmshurst, *J. Chem. Phys.* **35**:1800 (1961).
123. R. E. Hester and K. Krishnan, *J. Chem. Phys.* **49**:4356 (1968).
124. G. E. Walrafen, *J. Chem. Phys.* **37**:1468 (1962).
125. J. K. Wilmshurst, *J. Chem. Phys.* **36**:2415 (1962).
126. J. Vallier, *J. Chem. Phys.* **63**:1530 (1966).
127. W. Bues, G. Förster, and R. Schmitt, *Z. Anorg. Allg. Chem.* **344**:148 (1966).
128. W. Bues, K. Bühler, and P. Kuhnle, *Z. Anorg. Allg. Chem.* **325**:8 (1963).
129. R. E. Hester, previously unpublished results.
130. C. B. Baddiel and G. J. Janz, *Trans. Faraday Soc.* **60**:2009 (1964).
131. J. Greenberg, *J. Chem. Phys.* **39**:3158 (1963).
132. R. E. Hester and K. Krishnan, *J. Chem. Phys.* **48**:825 (1968).
133. G. J. Janz and R. D. Reeves, in: *Advances in Electrochemistry and Electrochemical Engineering*, Vol. V (C. Tobias and P. Delahay, eds.), John Wiley (Interscience), New York (1965).
134. A. R. Ubbelohde, *Melting and Crystal Structure*, Chap. 7 Clarendon Press, Oxford, England (1965).
135. G. A. Jeffrey and M. Vlasse, *Inorg. Chem.* **6**:396 (1967).
136. R. P. J. Cooney, J. R. Hall, and M. A. Hooper, *Aust. J. Chem.* **21**:2145 (1968).
137. Y. Mikawa, R. J. Jakobsen, and J. W. Brasch, *J. Chem. Phys.* **45**:4528 (1966).
138. T. Shimanouchi, M. Tsuboi, and T. Miyazewa, *J. Chem. Phys.* **35**:1597 (1961).
139. R. Buchanan, H. H. Caspers, and H. R. Martin, *J. Chem. Phys.* **40**:1125 (1964).

Chapter 2

LIQUID EXTRACTION FROM MOLTEN SALTS

Yizhak Marcus
Department of Inorganic and Analytical Chemistry
The Hebrew University of Jerusalem
Jerusalem, Israel

1. INTRODUCTION

1.1. The Scope of the Survey

Several technologies use molten salts as reaction media or as solvents for valuable solutes, and it is necessary to remove the solute into another phase at a certain stage. This can be done by volatilization, by electrodeposition, by precipitation, or finally by extraction into another liquid phase. Because of the properties of molten salts, their being ionic liquids with predominantly Coulombic forces between the ions, and the circumstances of their use, that is, relatively high temperatures, only a limited number of materials is suitable as the second liquid phase. These are certain metals with appropriate melting points (such as bismuth), certain molten salts with predominantly covalent forces between their ions, making them immiscible with ionic melts (such as silver bromide or boron oxide), and certain organic materials that are thermally stable and have high boiling points (such as terphenyls). Only the first category has as yet found practical use in technology.[1]

From a quite different standpoint, extraction from molten salts has been used as a tool for studying interactions in these melts[2] in a way analogous to the use of extraction from aqueous solutions.[3] It is generally assumed for the latter case, and is indeed sometimes true, that the species in the organic solvent used for extraction are well defined and specifically

known and that they interact little with the solvent. If this is so, distribution data should be easy to interpret in terms of the complexes formed in the aqueous phase and their (non stoichiometric) interactions with the aqueous solvent and other solutes present. This argument has been applied to extraction from molten salts. It so happens that the circumstances of employing extraction methods with molten salts make the above assumptions concerning the species in the immiscible second liquid much more valid than for extraction from aqueous solutions.[2] Thus, in such systems as tri-*n*-butyl phosphate (TBP) extracting metal ions from chloride or nitrate melts, the absence of water and acid in the molten salt precludes the competition of acido-complexes and hydrated protons or metal cations ion-paired with large anions, with the metal salt TBP solvates. Such organic solvents as the hydrocarbon mixtures of polyphenyls that have been used for extraction from molten salts also ensure a minimum of interaction. It also could be argued that, since the aggregation of long-chain amine salts in hydrocarbon solvents decreases with increasing temperatures,[4] extraction systems involving these reagents with molten salts should be simpler than when they are used with aqueous solutions at room temperature.† Whatever the validity of these arguments, it is true that with auxiliary information concerning the second liquid phase, which is in equilibrium with the molten salt, obtainable independently from the distribution measurements, the latter can throw much light on species and interactions in the molten salt.

In order to refer to the two phases in the distribution systems, it is expedient in the following to regard the molten salt, or the more ionic one of two immiscible molten salts, as the "ionic" phase. The second liquid is referred to as the "covalent" phase, without trying to justify this name by actually examining the bonding between the atoms in this liquid. Quantities, such as extrinsic or intrinsic thermodynamic functions, concentrations, etc., relating to this so-called "covalent" phase are designated by a bar above the symbols, while those relating to the (ionic) molten salt will have no bar. This usage is in line with established practices.[2,3,5]

1.1.1. Molten Salt–Molten Metal Systems

In many metallurgical processes there exists a molten metal and a molten slag in contact, possibly at equilibrium. Minor constituents distribute between these two liquid phases, so that an extraction system could be

† This argument cannot be pushed very far, since there is no evidence that the amine salts are completely monomeric at the higher temperatures involved, so that complications due to aggregation must still be taken into account.

defined. However, such systems have not been considered from this point of view and will not be treated here. The systems discussed in this chapter therefore will comprise only those where a molten salt and a molten metal are deliberately equilibrated with each other, in order to extract a solute from one phase into the other. Such systems have been studied in great detail in connection with liquid-metal-fueled nuclear reactors[6–10] and to some extent also with molten-salt-cooled and fueled nuclear reactors[11,12] and other systems.[13–20]

There is a fundamental difference between the reaction that leads to the distribution of a solute in liquid metal–molten salt systems and those involved in molten salt–molten salt or molten salt–organic solvent distribution systems. In the former system there is always an oxidation–reduction reaction, for example,

$$\overline{\text{La}}[\text{in Bi}(l)] + \tfrac{3}{2}\text{MgCl}_2\ (\text{in salt eutectic}) \rightleftharpoons \text{LaCl}_3\ (\text{in salt eutectic}) + \tfrac{3}{2}\overline{\text{Mg}}[\text{in Bi}(l)] \quad (1)$$

Since the molten metal (bismuth) is dictated by the nuclear properties of the reactor fuel, it is fortunate that it is sufficiently noble not to be attacked by the oxidizing agent preferably used, which is magnesium chloride. Thus an extraction process can be set up in which metals that form chlorides thermodynamically more stable than that of magnesium are transferred from the liquid metal to the molten salt.

Some of the molten metal–molten salt systems that have been examined are summarized in Table I. It is seen that the liquid metal need not be at all noble, provided it does not react with the molten salt and has a low solubility in it. This is the case with some metals with their own salts, such as the Na–NaCl, Mg–$MgCl_2$, or Al–$AlCl_3$ systems, and furthermore, the metal salt may be diluted with salts of less noble metals, such as the Mg–$MgCl_2$, NaCl, KCl, or Al–$AlCl_3$, KCl systems.

In addition to the nonsolubility requirement, the metal and salt must also have compatible liquid ranges, and they should not be excessively volatile. Halides have been used as the salts, since these ions cannot be reduced by the metals. The use of other nonreducible anions is of course conceivable, and considerations of melting temperatures (use of eutectics), ease of purification (removal of water), and avoidance of corrosion of containers are the prime considerations, after the chemical nature of the salt has been decided on.

The system used for reprocessing the fuel of the liquid metal fuel reactor (LMFR), consisting of liquid bismuth and molten magnesium and alkali metal chlorides, is discussed in detail in Section 5.

TABLE I. Some Molten Metal-Molten Salt Extraction Systems

Metal Phase	Salt Phase	Distribuends	Temperature, °C	References
Bi	$MgCl_2$ 50 mole % NaCl 30 mole % KCl 20 mole %	Cs, Ba, rare earth metals	500	(6–10)
Bi	NaCl–KCl eutetic	Zn, Cd, Pb	450	(13)
Bi	LiCl–NaCl eutetic	Cu, Po, and many other metals	550	(17–19)
Al	$AlCl_3$–KCl	U	725	(13)
Mg–40% Th or Zn–7% Mg	$MgCl_2$ 25 mole % KCl, LiCl	Y, Ce, Nd	600	(15)
Bi–Li–Th	LiF 72 mole % BeF_2 16 mole % ThF_4 12 mole %	Pa	500–700	(12)
Na	$CaCl_2$, LiCl, NaCl or CsCl, LiCl, NaCl	Li, Ca Li, Cs	540–600 380	(16)
Pu	$PuCl_3$	Am	700–780	(20)

1.1.2. Molten Salt–Molten Salt Systems

In order for a distribution system involving two molten salt phases to be set up, these must be reasonably immiscible at the temperature of operation. However, since ionic melts usually show high mutual solubility, special circumstances must be sought to obtain immiscibility. This point is discussed in Section 3, and here reference is made only to a number of recent compilations of salt mixtures showing a miscibility gap.[2,21–23] The common feature of these systems is that one salt is more "covalent," consisting of large, polarizable or "soft" ions, whereas the other is more "ionic," consisting of small, "hard" ions. Solutes thus distribute between the two phases according to their preferring a "soft" or a "hard" environment. As "covalent" molten salts in such distribution systems have served mercury bromide,[24] silver halides,[25] potassium chloroaluminate,[26] sodium borate,[27] and some others.

1.1.3. Molten Salt–Organic Solvent Systems

Whereas the previous two distribution systems permit—or require—rather high temperatures to be used, organic solvents make fairly low temperatures necessary. It is difficult to find organic solvents that are therma-

lly stable and have low vapor pressures above 350°C.[2] On the other hand, there is a considerable number of eutectic salt mixtures, and a few pure salts that melt below 350°C[2,28] and can be employed in conjunction with suitable organic solvents.

Two approaches have been used as regards the organic solvents. In one a nonpolar solvent is used, into which the more "covalent" solutes extract from a molten salt. Aromatic hydrocarbons, and in particular terphenyls or their mixture with biphenyl, have been used in this capacity, and as solutes, mercury halides can be cited as an example.[29] Such distribution systems are discussed in Section 5.3. In the other approach, a polar extracting agent is used, which may be a solid or a liquid and, when undiluted, may even be thermally unstable at the operating temperatures. It is usually employed diluted with a suitable diluent, such as the polyphenyls mentioned above. Tributyl phosphate has been an extractant of choice, and results obtained with it have been reviewed.[2] Triphenyl phosphine and arsine oxide have recently been tried for extraction of cobalt and nickel from chloride-containing alkali metal nitrate melts,[30] with results similar to those obtained with tributyl phosphate.[31,32] Of the other organic extractants that can be used, long-chain amine salts have come to prominence in recent years, and are discussed in detail in Section 5.4.

1.2. Experimental Techniques

The procedure for obtaining distribution data, for the distribution of a solute between a molten salt and an immiscible liquid, is quite simple. The molten salt (purified and dried, if necessary, and homogenized if it is a mixture, eutectic or otherwise), the second liquid (again appropriately treated to ensure purity and homogenity), and the solute, dissolved in either the one or the other, are brought into contact. The system is equilibrated at a definite temperature, some mixing or agitation for a length of time being necessary to ensure equilibrium. The phases are permitted to separate at the temperature of equilibration and are then analyzed, usually by sampling after quenching to a lower temperature. The quantities that are determined are the following.

The quantity of the molten salt, expressed usually as the number of moles present n or its weight w and seldom as its volume, and the quantity ot the second liquid, expressed accordingly, should be known. The quantities weighed in are usually an adequate estimate for these values, but in cases where miscibility of the two phases is considerable, the equilibrium values should be used.

It is useful to know the concentration of the solute in each phase separately, in terms of moles of solute per mole of solvent (mole ratio r) or per unit weight of solvent (molality m) or in terms of the mole fraction N. In very dilute solutions the mole ratio and mole fraction are equivalent. Volume concentrations (molarity c) are less useful. In all cases the stoichiometric concentration is meant, so that formula weights are understood for moles of solute, the total, analytical concentration is used irrespective of the species it forms, and any interactions between the solute and solvent, such as solvation, are disregarded. In some cases it is impossible to obtain the absolute concentration of a solute; rather a number proportional to it is obtained, with a proportionality factor for each phase independent of the concentration. In such cases only the distribution ratio between the phases can be determined.

The distribution ratio of a solute k thus is defined on the various concentration scales as

$$D_{k(r)} = \frac{\bar{r}_k}{r_k} \qquad D_{k(m)} = \frac{\bar{m}_k}{m_k} \qquad D_{k(N)} = \frac{\bar{N}_k}{N_k} \tag{2}$$

All these quantities are pure numbers, and mixed concentration scales should be avoided. For the purpose of calculating material balance, however, it is necessary to know the relative quantities of the two phases, thus

$$\bar{m}_{k(\text{initial})} = \bar{m}_{k(\text{equil.})} + q m_{k(\text{equil.})} \tag{3}$$

where $q = w/\bar{w}$ is the weight of the molten salt divided by the weight of the "covalent" liquid.

1.2.1. Equilibration Methods

There is nothing extraordinary in the equilibration methods that have been used for the molten salt and the other liquid phases at elevated temperatures. Two general methods are used: in one the two phases are stirred together in a suitable thermostated vessel open to the atmosphere, or with a protective gas flowing through or over the liquids, and in the other they are mixed in closed tubes tumbled in a thermostated bath. Several authors thought it sufficiently important to describe and depict the arrangements they have used for the stirring[25,30,31,33,34] or tumbling[24,29,35] methods (Fig. 1). In particular cases special techniques must be used, such as employing graphite or platinum crucibles for equilibrating the phases at high temperatures (830°C),[36,37] or sealed glass tubes when a component of the

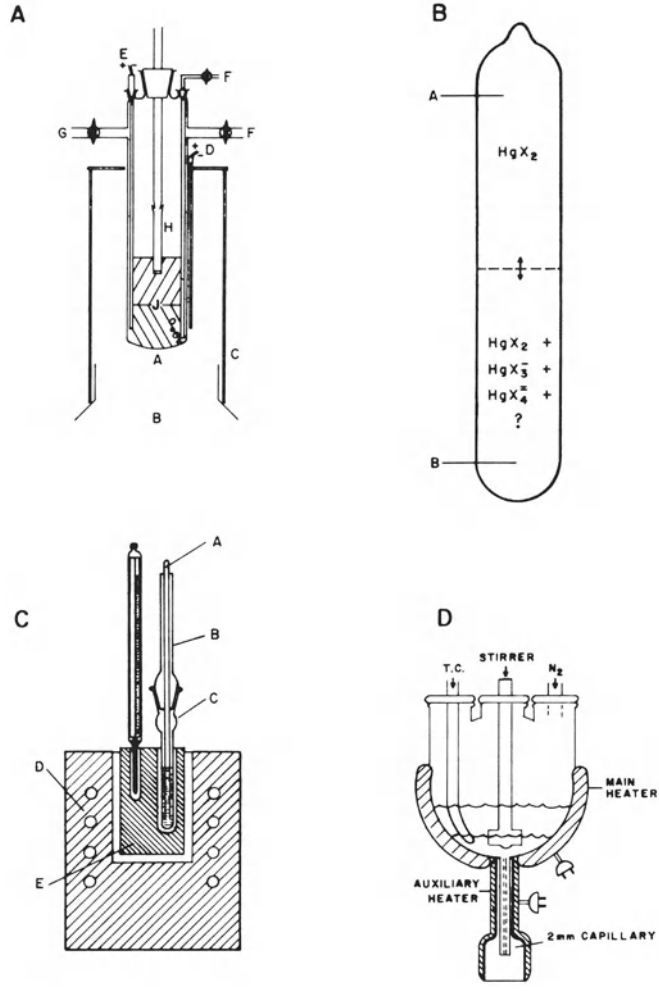

Fig. 1. Experimental set ups used for equilibrating molten salts with a second liquid. A: Apparatus for contacting two immiscible melts, from Ammon[34] (by permission of Pergamon Press, Ltd., London), A, vessel of Pyrex-glass; B, air oven; C, isolating mantle; D, controlling thermocouple; E, measuring thermocouple; F, gas inlet; G, gas outlet; H, sampling tube with sinter; and I, salt melts. B: Sealed tube for tumbling together a salt melt and a polyphenyl solvent, from the author's and Dr. M. Zangen's laboratory, A, polyphenyl phase; B, nitrate melt. C: Apparatus for contacting a molten salt with an organic solvent, from Borkowska[33] (by permission of Pergamon Press, Ltd., London), A, glass stirring rod; B, air cooler; C, extraction tube; D, electric furnace; and E, brass heating mantle. D: Apparatus for contacting two molten salts in a three-necked flask, reprinted from Kennedy[25] (Copyright 1961 by The American Chemical Society, reprinted by permission of the copyright owner). The lower heater is off during equilibration and is used to release the frozen salt plug in the capillary for sampling.

system is volatile, such as a mercury halide.[29] Equilibration times are those habitually employed in liquid–liquid distribution studies, from several minutes to a few hours. Kinetic problems involved in the distribution reactions are discussed in Section 4.

1.2.2. Phase Separation and Sampling

Molten salts generally have low viscosities, with the exception of the highly structured melts such as boron oxide. They have the advantage over aqueous extraction systems that generally there is a considerable difference in the density of the two phases. The "covalent" phase is either much lighter or much heavier than the "ionic" phase. Thus the organic solvents used have densities near 1 g cm^{-3} and molten silver chloride and mercury bromide have densities of 4.8 and 5.1 g cm^{-3}, respectively, compared with 1.9–2.2 for many molten nitrate salts and eutectics from which extraction has been effected. Finally, surface effects, leading to emulsion formation, have not been encountered in molten salt extraction systems. Therefore, phase separation is generally no problem and the phases separate rapidly and clearly when left to rest at the equilibration temperature.

The mechanical separation between the phases can take advantage of the freezing of the molten salt as the temperature decreases. It is then generally assumed that the rapid lowering of the temperature of the separated phases quenches the equilibrium reached at the higher temperature and that no changes in the distribution ratio are thereby caused. In a molten salt–organic solvent system it is then easy to sample the still-liquid organic phase (organic eutectics melting near room temperature, such as 37 mole % biphenyl, 48% orthoterphenyl, and 15% metaterphenyl, m.p. 22°C[2], are more convenient in this respect than a solvent such as pure metaterphenyl, m.p. 87°C). If necessary it is possible to rinse the solidified salt with a cold organic solvent to remove traces of the equilibrated solvent phase before the salt phase is analyzed. The latter, of course, can be dissolved in water for the purpose of analysis.

A different approach to sampling utilizes preheated pipettes to remove aliquots of the separated phases at the equilibration temperature. These aliquots are then normally weighed and analyzed on a weight basis. Alternatively, the two liquids are permitted to run out of the equilibration vessel sequentially through a plug in the bottom (conveniently made of a solidified portion of the heavier molten salt, melted at the appropriate moment with a small auxiliary heater),[25] and aliquot fractions of each phase are weighed and analyzed. This method is often utilized in distribution systems involving two immiscible molten salts (Fig. 1D).

2. THERMODYNAMICS OF THE DISTRIBUTION

Distribution of a solute between a molten salt phase and another, immiscible liquid phase is a reversible process leading to equilibrium. The methods of chemical thermodynamics are therefore most suitable for dealing with the relationships between the measured quantities: the composition of the phases and the distribution ratio. Furthermore, certain conclusions about the species present and structural aspects of the molten salt also can result from thermodynamic arguments.

2.1. Activities in Molten Salt Mixtures

A short description of the systems dealt with in this chapter and the main thermodynamic relationships used are in place here. Consider a mixture containing cations A, B,... and anions X, Y,.... It is customary to use the Temkin model[38] for defining the ideal entropy of mixing, which is

$$S_{\mathrm{id}}^{\mathrm{M}} = -R(n_{\mathrm{A}} \ln N_{\mathrm{A}} + n_{\mathrm{B}} \ln N_{\mathrm{B}} + \cdots + n_{\mathrm{X}} \ln N_{\mathrm{X}} + n_{\mathrm{Y}} \ln N_{\mathrm{Y}} + \cdots) \quad (4)$$

where n_i is the number of moles of ion i present and N_i is the ion fraction $N_i = n_i/\Sigma_j n_j$, summed over all ions j of the same sign as i.

Since, by definition, $H_{\mathrm{id}}^{\mathrm{M}} = 0$, the ideal free energy of mixing is $G_{\mathrm{id}}^{\mathrm{M}} = -TS_{\mathrm{id}}^{\mathrm{M}}$, and the total free energy of the system is

$$G = \sum_k n_k G_k^0 - TS_{\mathrm{id}}^{\mathrm{M}} + G^{\mathrm{E}} \quad (5)$$

where the summation is over all the components k of the system, G_k^0 is the standard molar free energy of component k and G^{E} is the excess free energy of mixing. Consider now the component $k = \mathrm{AX}$ of the system. Its chemical potential, that is, its partial molar free energy, is

$$\begin{aligned} \mu_k &= \left(\frac{\partial G}{\partial n_k}\right)_{T,P,n_{i\neq k}} = \left(\frac{\partial G}{\partial n_{\mathrm{A}}}\right)_{T,P,n_{i\neq \mathrm{A}}} + \left(\frac{\partial G}{\partial n_{\mathrm{X}}}\right)_{T,P,n_{i\neq \mathrm{X}}} \\ &= G_k^0 + RT \ln N_{\mathrm{A}} N_{\mathrm{X}} + \left(\frac{\partial G^{\mathrm{E}}}{\partial n_k}\right)_{T,P,n_{i\neq k}} \\ &= G_k^0 + RT \ln N_{\mathrm{A}} N_{\mathrm{X}} + RT \ln f_k = G_k^0 + RT \ln a_k \end{aligned} \quad (6)$$

The last line of equation (6) contains the definitions of the activity coefficients $f_k = f_{\mathrm{A}} f_{\mathrm{X}}$ of the component k and its activity a_k. As usual, the activity is defined only when the component k and the standard state have been specified. Suppose one is interested in the ionic species A and the system is

a binary mixture with common anion of AX and BX. Then the A-containing component is unambiguously determined. However, if the system is a reciprocal mixture of AX and BY, either AX or AY may be chosen as components and the choice of $k = \mathrm{AX}$ is arbitrary, although it is expedient in cases where AX is a minor component (a solute in solvent BY) or is highly associated. The choice of the standard state is also arbitrary, and two approaches are common. The pure liquid AX may be chosen as the standard state and is designated by the superscript^0. This state is often hypothetical, since mixtures are commonly studied at temperatures below the melting points of the pure components. When dilute solutions are involved, either a given low concentration or infinite dilution may be chosen as standard states and are designated by the superscript*. The standard chemical potential is identical with the standard molar free energy, so that equation (6) becomes

$$\mu_k = \mu_k^0 + RT \ln a_k = \mu_k^* + RT \ln a_k^* \tag{7}$$

Since $\mu_k^0 - \mu_k^*$, the molar free energy change on transfer of component k from tis pure liquid (hypothetical supercooled) state to its dilute solution state, is generally not zero, the activities a_k and a_k^* will be different.

In those cases where the solute $k = \mathrm{AX}$ has no common ion with the solvent BY, the right-hand side equality of equation (7) can be rewritten as

$$\begin{aligned} \mu_k &= \mu_k^* + RT \ln N_\mathrm{A} N_\mathrm{X} + RT \ln f_\mathrm{A}^* f_\mathrm{X}^* \\ &= \mu_k^* + 2RT \ln N_\mathrm{AX} + RT \ln f_k^* \end{aligned} \tag{8}$$

which leads to

$$\frac{f_k^*}{f_k} = \frac{\exp(\mu_k^0 - \mu_k^*)}{RT} \tag{9}$$

Now, if the minor component $k = \mathrm{AX}$ does have a common ion with the solvent, for example, X, then in the binary mixture $N_\mathrm{X} = 1$ and

$$\mu_k = \mu_k^* + RT \ln N_\mathrm{A} + RT \ln f_k^* \tag{10}$$

But if in a reciprocal system, excess of either X or A, exists, so that $\ln N_\mathrm{A} N_\mathrm{X} \neq 2 \ln N_\mathrm{AX}$, then only the first line of equation (8) is valid.

2.2. Activities from Distribution Measurements

There are certain advantages to obtaining activities of components in molten salt mixtures from distribution measurements over certain other methods, particularly those involving phase equilibria. Activities may be

obtained from phase diagrams, but only at the melting temperatures of the mixtures and at the particular compositions pertaining to these temperatures. The solubility method is not restricted as to temperature, but it is limited as to the composition of the saturated solution

$$\begin{aligned} RT \ln a_{\mathrm{AX(saturated)}} &= \mu_{\mathrm{AX}} - G^0_{\mathrm{AX(supercooled\ liquid)}} \\ &= G^0_{\mathrm{AX(solid)}} - G^0_{\mathrm{AX(supercooled\ liquid)}} \end{aligned} \tag{11}$$

The cryoscopic method, on the other hand, is not limited as to the composition and is applicable over a range of concentration in dilute solutions but is limited as to the temperature interval immediately below the melting point of the solvent salt.

The distribution method described in the following, in contrast, can be applied over both a wide range of temperatures and a wide range of concentrations.[39] Consider, as an illustration, a system having three components: the solute $k = \mathrm{AX}$, the solvent $j = \mathrm{BY}$ (which is a molten salt with no ion in common with the solute), and the immiscible solvent S. At equilibrium there will be two liquid phases, with the solute distributed between them. The distribution ratio D, which is the ratio of the total concentration of k in the solvent S, $\bar{N}_k$, to its total concentration in the molten salt, N_k, is measured by suitable analytical methods. One advantage of the distribution method is that since only the ratio of the concentrations is required, methods can be used giving values proportional to the concentrations (such as radioactivity per unit amount of liquid) rather than the absolute concentrations themselves, provided the proportionality factor is independent of the concentration.

Equating the chemical potential of the solute in the two phases at equilibrium leads at a given temperature T to

$$\begin{aligned} \bar{\mu}_k &= \bar{\mu}_k^0(T) + RT \ln \bar{N}_k + RT \ln \bar{f}_k(\bar{N}_k, T) \\ &= \mu_k^0(T) + RT \ln N_k + RT \ln f_k(N_k, T) = \mu_k \end{aligned} \tag{12}$$

and since $D = D_{k(N)} = \bar{N}_k / N_k$, this becomes

$$\ln f_k = \frac{(\bar{\mu}_k^0 - \mu_k^0)}{RT} + \ln D + \ln \bar{f}_k(\bar{N}_k, T) \tag{13}$$

The first term on the right-hand side is obviously equal to zero, since the same standard state, the pure liquid k, applies to both phases. The last term on the right-hand side can be determined independently, and this is particularly convenient if the solvent S is volatile, which is commonly the

case with organic solvents. Thus

$$\ln \bar{f}_k = -\ln \bar{N}_k - \int_0^{\bar{N}_S} \left(\frac{\bar{N}_S}{\bar{N}_k}\right) d \ln\left(\frac{p_S}{p_S{}^0}\right) \tag{14}$$

according to the Gibbs–Duhem relationship, where p_S is the vapor pressure of the solvent S. Hence the activity coefficient of the solute in the molten salt can be determined from

$$\ln f_k = \ln D + \ln \bar{f}_k \tag{15}$$

or, if the standard state is selected as a dilute solution, equation (12) is rewritten as

$$\ln f_k^* = \frac{(\bar{\mu}_k^* - \mu_k^*)}{RT} + \ln D + \ln \bar{f}_k^* \tag{16}$$

Furthermore, if D is measured in such a way that $\bar{N}_k$ remains constant, while different molten salts j : BY, CY,... or BY, BZ,... are compared,

$$\mu_k^*(j) + RT \ln f_k^*(j) - RT \ln D(j) = \bar{\mu}_k - RT \ln \bar{N}_k = \text{const} \tag{17}$$

even in nondilute concentration ranges, where Henry's law cannot be expected to hold. The comparison thus is made at a constant chemical potential, and if f_k^* is assumed to be approximately unity, values of μ_k^* for different solvents can be compared. A constant composition of the solvent phase, that is, of $\bar{N}_k$, is easily attained if D is high, since if a constant initial amount of solute k is mixed with a constant amount of solvent S, the ratio D can vary widely with still practically all of k remaining in the solvent S. When several close values of $\bar{N}_k$ are used, a short interpolation will normalize the data to a definite constant $\bar{N}_k^*$.

2.3. Thermodynamic Functions of Transfer

The transfer of the solute k between the solvent S and the molten salt j, or between several molten salts j via the solvent, is best described through the molar free energy, enthalpy, entropy of transfer, and partial molar heat capacity difference. Using dilute solutions as the standard state, applying equations (12) and (16), and since

$$\lim_{N_k \to 0} \ln f_k^* = \lim_{\bar{N}_k \to 0} \ln \bar{f}_k^* = 0$$

according to Henry's law, we get the molar free energy of transfer of the

solute from a dilute solution in the solvent S as

$$\Delta G_k^* = \mu_k^* - \bar{\mu}_k^* = RT \lim_{N_k, \bar{N}_k \to 0} \ln D \simeq RT \ln D \tag{18}$$

The last approximate equality holds since in dilute solutions ln $(\bar{f}_k^*/f_k^*)$ approaches zero more rapidly than the activity coefficients themselves approach unity.

Further information on the system can be obtained from studying the variation of D with temperature. From the partial molar enthalpy change on transferring the solute from its standard state to a solution of concentration N_k,

$$\frac{d \ln f_k}{dT} = \frac{-L_k}{RT^2} \tag{19}$$

where $L_k = (H_k - H_k^0)$, and similarly for asterisked or barred quantities (f_k^* and L_k^*, $\bar{f}_k$ and $\bar{L}_k$, $\bar{f}_k^*$ and $\bar{L}_k^*$, noting that $\bar{H}^0 = H^0$) the relationships

$$\frac{d \ln D}{dT} = \frac{-(L_k - \bar{L}_k)}{RT^2} = \frac{-(L_k^* - \bar{L}_k^* - \Delta H^*)}{RT^2} \tag{20}$$

are obtained. If a constant composition of the solvent phase is used, $\bar{N}_k$ = const, the difference $(\bar{L}_k - \bar{L}_k^*)$ will depend only on the temperature,

$$\frac{d(\bar{L}_k - \bar{L}_k^*)}{dT} = \bar{C}_{p(k)} - \bar{C}_{p(k)}^* = J_k \tag{21}$$

where $C_{p(k)}$ is the partial molal heat capacity of k. Integration then leads to the equation

$$\log D = A + \frac{1000\, B}{T} + C \log T \tag{22}$$

where $B = (L_k^* - \bar{L}_k^*)/2.303R + \Delta H^*/2.303R$, ΔH^* being the enthalpy change on transfer from a dilute solution in the molten salt to a dilute solution in the solvent, and $C = \Delta J_k/R$, giving the corresponding heat capacity change. Also

$$\lim_{N_k \to N_k^*} B = \frac{\Delta H^*}{2.303R}$$

Finally, the entropy change of transfer is obtained from

$$\Delta S^* = \frac{\Delta H^* - \Delta G^*}{T} \tag{23}$$

These thermodynamic functions, for the transfer of the solute from the

molten salt phase to the solvent phase, can be related to interactions in either one. In particular, if the composition of the solvent phase is held constant and transfer from different molten salts is studied, information on these interactions in the molten salts is obtained. Thus the reciprocal Coulomb effect[40] should be observed for a solute AX in a series of molten salts BY, CY, ... so that

$$\Delta(\Delta H^*) = Ne^2\left(\frac{1}{d_{CX}} - \frac{1}{d_{CY}} + \frac{1}{d_{BY}} - \frac{1}{d_{BX}}\right) \tag{24}$$

provided that polarization effects are absent and that no covalent bonding occurs.

3. IMMISCIBLE MOLTEN SALTS

Binary, ternary, or reciprocal ternary molten salt mixtures as a rule show complete miscibility. The general structure of such mixtures can be described in terms of two interpenetrating subquasi-lattices, one for the cations and one for the anions. The ions on each sublattice are distributed randomly, except when strong interactions prevail. Coulombic forces alone do not suffice to cause unmixing,[41] but if polarization forces are added, not to speak of covalent bond formation, demixing may occur. Several hundreds of systems are now known that have miscibility gaps[23] that could be used, in principle, for distribution studies of an added minor component.

3.1. Thermodynamics of Immiscible Molten Salts

The condition for immiscibility for two liquids i and j is that the plot of the free energy of mixing G_M against the composition has a region where it is convex upward, so that

$$\left(\frac{\partial^2 G^M}{\partial N_i^2}\right)_{T,P} = 0 \tag{25}$$

at two points, the inflection points. When the overall composition is in the miscibility gap there result two liquid layers at equilibrium, each at a constant composition at a given temperature (according to the phase rule). The following discussion of the occurrence of a miscibility gap is in terms of the treatment proposed by Blander and Topol.[42]

Consider a ternary reciprocal salt system, made up of the components AX, BX, and AY. According to the theory of conformal ionic solutions,[42,43]

the excess free energy of mixing is given as

$$G^{E} = N_B N_Y \Delta G^0 + N_A G^{E}_{A(X,Y)} + N_B G^{E}_{B(X,Y)} + N_X G^{E}_{(A,B)X} + N_Y G^{E}_{(A,B)Y} + N_A N_B N_X N_Y \Lambda \tag{26}$$

where ΔG^0 is the standard free energy change for the metathesis reaction forming BY:

$$AY(l) + BX(l) \rightleftharpoons AX(l) + BY(l) \tag{27}$$

$G^{E}_{A(X,Y)} = N_X N_Y \lambda_{A(X,Y)}$ etc., $\lambda_{A(X,Y)}$ being the interaction energy for the binary system AX + AY, and Λ being the ternary interaction energy, which can be approximated by $\Lambda = -(\Delta G^0)^2/12RT$, where $12 = 2Z$, with $Z = 6$ as the coordination number, is used in the denominator.[42] From relationship (26) it follows for the activity coefficient of the component BY that

$$\begin{aligned} RT \ln f_{BY} = N_A N_X \{ &\Delta G^0 + (N_X - N_Y)\lambda_{A(X,Y)} + (N_A - N_B)\lambda_{(A,B)X} \\ &+ (N_A N_Y + N_B N_X)[(1/N_A)\lambda_{B(X,Y)} + (1/N_X)\lambda_{(A,B)Y}] \\ &+ (N_A N_Y + N_B N_X - N_B N_Y)\Lambda \} \end{aligned} \tag{28}$$

If we restrict ourselves to the quasi-binary compositions along the diagonal AX + BY, so that $N_A = N_X = N_{AX}$ and $N_B = N_Y = N_{BY}$, this equation is simplified to

$$\begin{aligned} RT \ln f_{BY} = N^2_{AX} [&\Delta G^0 + \lambda_{A(X,Y)} + \lambda_{(A,B)X} + 2(1 - N_{AX})(\lambda_{B(X,Y)} \\ &+ \lambda_{(A,B)Y} - \lambda_{A(X,Y)} - \lambda_{(A,B)X}) - (3N^2_{AX} - 4N_{AX} + 1)\Lambda] \end{aligned} \tag{29}$$

Returning now to the condition for phase separation, it is seen that equation (25) leads to

$$\left(\frac{\partial a_{BY}}{\partial N_{BY}} \right)_T = 0 \tag{30}$$

so that for the system described by (27), and since at the critical consolute temperature also $(\partial^3 G^M / \partial N_i^3)_{T_c} = 0$,

$$\left(\frac{\partial N^2_{BY} f_{BY}}{\partial N_{BY}} \right)_{T_c} = 2N_{BY} f_{BY} - N^2_{BY} \left(\frac{\partial f_{BY}}{\partial N_{AX}} \right)_{T_c} = 0$$

or

$$\left(\frac{\partial \ln f_{BY}}{\partial N_{AX}} \right)_{T_c} = \frac{2}{N_{BY}} \tag{31}$$

On differentiation of equation (29) with respect to N_{AX} and utilization of equation (31) the following relationship is obtained:

$$\frac{RT_c}{N_{AX}N_{BY}} = \Delta G^0 + \frac{1}{2}\Sigma\lambda + 3\left(N_{BY} - \frac{1}{2}\right) \times (\lambda_{(A,B)Y} + \lambda_{B(X,Y)} - \lambda_{A(X,Y)} - \lambda_{(A,B)X}) + (6N_{AX}N_{BY} - 1)\Lambda \tag{32}$$

where $\Sigma\lambda$ is the sum over the four binary interaction energies. Now if ΔG_c^0, that is, ΔG^0 at the critical consolute temperature, is sufficiently large, Λ in the last term can be approximated by $-3RT_c$,[42] and for a symmetrical system $N_{BY_c} \approx N_{AX_c} \approx \frac{1}{2}$, so that the third term on the right-hand side becomes negligible, and

$$T_c = \frac{\Delta G_c^0}{5.5R} + \frac{\Sigma\lambda}{11R} \tag{33}$$

Finally, if T_c calculated in this manner is sufficiently high, that is, above the melting point of the higher melting component, this derivation shows that there is a temperature region where a miscibility gap exists, between the monotectic point of the system (the invariant temperature at which a solid and two liquids are at equilibrium) and the critical consolute temperature T_c.

In order to have a high T_c, and thus a miscibility gap, it is necessary for a system to have both a large positive ΔG_c^0 and a not very negative $\Sigma\lambda$. Values of ΔG_c^0 are usually approximated from the values of the free energy of formation reported in tables, usually for 298°K. A large positive ΔG^0 means that AY and BX are by far the more stable pair of the reciprocal system, so that the two liquid phases will approach these two components as ΔG^0 increases. Values of the λ parameters must be obtained from the binary systems and may be estimated from the eutectic temperatures, assuming regular solution behavior.[42] Thus, for the binary system AX + BX, for instance,

$$T_{\text{eutectic}} = \frac{\lambda_{(A,B)X}(1 - N_A)^2 + L_{AX}}{(L_{AX}/T_{0AX}) - R \ln N_A} = \frac{\lambda_{(A,B)X}N_A^2 + L_{BX}}{(L_{BX}/T_{0BX}) - R \ln(1 - N_A)} \tag{34}$$

where L is the heat of fusion and T_0 is the melting point of the indicated component, L being assumed to be independent of temperature for the purpose of this approximation. The value of λ can be obtained more directly from G^E when activity data for the binary system are available.

3.2. Criteria for Immiscible Salt Systems

The question now arises what chemical factors are responsible for the values of ΔG^0 and $\Sigma\lambda$ required for obtaining demixing. Certain empirical correlations were advanced by the Russian Kablukov,[44] who was among the first to note the formation of two liquid layers in molten salt systems. Since then the Russian school has published extensively on this subject, as can be seen in several recent reviews.[21,23,45] It is difficult to decide which effects are primary causes for phase separation and which are results, and usually several factors operate simultaneously. Following Belyaev,[21] we shall discuss binary systems and ternary-reciprocal systems separately.

3.2.1. Binary Systems

One cause for unmixing in a binary molten salt mixture, that is, one with a common ion, is the occurrence of a large difference in the cohesive energy densities of the two components. For nonpolar liquids the cohesive energy density is usually expressed in terms of the solubility parameter. For molten salts this is probably inappropriate, because of the nonvanishing entropy of mixing of the polar salts. The concept of internal pressure[46] $(\partial E/\partial V)_T$ has been used instead,[21,47] this quantity being proportional to the product of the boiling point and the molar volume. Immiscibility in the system antimony trichloride–tin tetrachloride has been ascribed to this effect,[21] although both salts have relatively low internal pressures (3000–4000 atm). Immiscibility of such salts with the highly ionic alkali metal chlorides, with internal pressures of from 9000 to 37,000 atm, would have been more understandable. Here, however, enters the complication of compound formation, and it is the compound, such as sodium tetrabromoaluminate, that forms an immiscible pair with the much less polar aluminum tribromide. For such AX–BX systems to show immiscibility, ion A should be a mono- or bivalent cation and B a ter- or higher valent one,[21] but exceptions have been noted, such as the binary K_2TiO_3–K_2SO_4 system.[48]

3.2.2. Reciprocal Ternary Systems

With these more complicated systems, where phase separation is indeed more common than with the binary systems, essentially the same factors have been held responsible. The ratio between the polarities of the salts constituting the stable pair,[49,50] the ratio between the nominal field strengths of the ions z/r, and the ratio between their corrected field strengths *effective charge*/r have been cited[21] as the major factors. The qualitative

description of two components AX and BY that would form two liquid layers is[21]

AX: a typical salt, such as halide, nitrate, sulfate, or carbonate of an alkali metal or alkaline earth cation.

BY: a simple compound of low polarity, an acid anhydride such as B_2O_3, V_2O_5, or TiO_2 or a halide, oxide, or sulfide of a nonrare-gas type cation (that is, one with ≥ 18 electrons in the outer shell, a post transition-metal cation).

A still different way to express these differences is to require the ions to differ markedly in their field strengths, the cations also to differ in their polarities[50] and electronic structure, and the anions to differ in their electronegativities. In more modern usage, on would say that if A and X are hard ions and B and Y are soft ions, the liquid system AX + BY would show a miscibility gap.

Beyond these qualitative terms stand the estimated values of ΔG^0 for the metathetical reaction[27] at the temperature of the liquid mixture. They are approximated by the values of ΔG^0 for the corresponding reaction between the solids at 298°K. The width of the miscibility gap, and the flatness of the "S" shape of the liquidus curve along a diagonal of the reciprocal system, are related to the magnitude of ΔG^0 in a homologous series.

TABLE II. Correlation of Miscibility Gaps in Reciprocal Systems with ΔG^0

AX	BY	ΔG^0 (kcal/equiv.)	Temperature (°C)	Miscibility gap size		
				Stable diagonal	Unstable diagonal	% Area
NaF	CsCl	14.6		S-shaped curve, no gap		
LiF	CsCl	25.0	824	33–94% LiF	42–54% CsF	14
LiF	CsBr	30.5	838	9–94% LiF		
LiF	KBr	21.6	804	20–97% LiF	43–54% KF	15
$NaNO_3$	AgCl	14.2		~0–100% AgCl		
$NaNO_3$	AgBr	19.6	507	~0–100% AgBr	30–72% NaBr	61.2
$NaNO_3$	AgI	29.0	554	~0–100% AgI	30–72% NaI	64.3
Li_2SO_4	$SrCl_2$	−0.5		No miscibility gap		
Li_2SO_4	$ZnCl_2$	6.5		Marked S-shaped curve, no gap		
Li_2SO_4	$PbCl_2$	7.2	650	7–88% Li_2SO_4	38–63% $PbSO_4$	43.5
Li_2SO_4	$CdCl_2$	9.5	650	8–80% Li_2SO_4	35–62% $CdSO_4$	29.3
Li_2SO_4	TlCl	12.4	654	4–92% Li_2SO_4	30–59% Tl_2SO_4	51.7
Li_2SO_4	AgCl	19.2	818	2–99% Li_2SO_4	23–72% Ag_2SO_4	65.2

TABLE III. Miscibility Gaps in Binary Systems

Number	AX	BX	Monotectic (consolute) temperature (°C)	Gap width, % BX	Reference
1	$AlCl_3$	(Li, K)Cl	450 (775)	1–25	(51)
2	$AlCl_3$	NaCl	193.5	0.2–18	(47)
3	$AlCl_3$	KCl	193.0	0.4–18.2	(47)
4	$AlCl_3$	NH_4Cl	192.5	0.2–20.5	(47)
5	$AlCl_3$	TlCl	192.0	1.2–14.7	(47)
6	$AlCl_3$	AgCl	192.9	0.7–17.6	(47)
7	$AlCl_3$	$BaCl_2$	191.5	2.0–13.0	(47)
8	$AlCl_3$	$SnCl_2$	192.0	1.5–14.3	(47)
9	$AlBr_3$	NaBr	95.4 (232)	2.6–16.3	(47)
10	$AlBr_3$	KBr	98.1	0.4–22.1	(47)
11	$AlBr_3$	NH_4Br	98	0.5–20.8	(47)
12	$AlBr_3$	TlBr	103.9	0.6–22.8	(47)
13	$AlBr_3$	AgBr	105.9 (186)	2.2–17.0	(47)
14	$AlBr_3$	$CaBr_2$	208.8	0.8–14	(47)
15	$AlBr_3$	$BaBr_2$	269.4	0.9–16	(47)
16	$AlBr_3$	$SnBr_2$	161.1 (205)	1.8–14.2	(47)
17	$AlBr_3$	$PbBr_2$	210.4	0.8–16.2	(47)
18	$AlBr_3$	Hg_2Br_2	238.1	1.8–30.8	(47)
19	BeF_2	SrF_2	774	7.5–25	(52)
20	BeF_2	BaF_2	775 (838)	7–20	(53)
21	$NbCl_5$	NaCl	378	2.2–8.3	(54)
			392	~0–34	(55)
22	$NbCl_5$	KCl	285	0.3–14.7	(54)
23	$NbCl_5$	RbCl	324	~0–41	(55)
24	$NbCl_5$	CsCl	475	~0–39	(55)
25	$TaCl_5$	NaCl	404	~0–39	(55)
26	$TaCl_5$	KCl	303	~0–50	(55)
27	$TaCl_5$	RbCl	370	~0–43	(55)
28	AgI	InI_3	250	25–67	(56)
29	$BiCl_3$	$ZnCl_2$	280	12–97	(57)
30	$SbCl_3$	$SnCl_2$	243.1	1.4–41.2	(47)
31	$SbCl_3$	$SnCl_4$		36–73	(47)
32	B_2O_3	MgO	1142	0.6–36.0	(58)
33	B_2O_3	CaO	971	0.2–23	(59)
34	B_2O_3	BaO	878 (1225)	1.6–30.2	(60)
35	B_2O_3	CoO	1050	4.7–45	(61, 62)
36	B_2O_3	ZnO	982	~0–53.5	(63, 64)
37	B_2O_3	CdO	980	~0–53.6	(65)
38	B_2O_3	PbO	747 (785)	9–43	(66)

TABLE III. (*Continued*)

Number	AX	BX	Monotectic (consolute) temperature (°C)	Gap width, % BX	Reference
39	B_2O_3	La_2O_3	1136	~0–21.5	(67)
40	B_2O_3	Bi_2O_3	709	~0–19.0	(68)
41	B_2O_3	ThO_2	1483	10–80	(69)
42	SiO_2	MgO	1695	0.8–31	(70)
43	SiO_2	CaO	1698	0.6–28	(70)
44	SiO_2	SrO	1693	24–30	(70)
45	SiO_2	MnO	1705	~0–45	(71)
46	SiO_2	FeO	1690	3–42	(72)
47	SiO_2	CuO	1690	6–65	(73)
48	SiO_2	ZnO	1695	2–35	(74)
49	SiO_2	Cr_2O_3	2200	~5–95	(75)
50	SiO_2	Ga_2O_3	1652	~8–65	(76)
51	SiO_2	ZrO_2	2250 (2430)	38–59	(77)
52	SiO_2	Mo_2O_5	1695	5–80	(78)
53	GeO_2	MgO	1480	8–34	(79)
54	CaF_2	CaO	1380 (1485)	6.8–10	(80)
55	Na_2TiO_3	NaCl	964	25–97.5	(21, 81)
56	K_2TiO_3	KCl	Evidence for gap		(21)
57	$LiVO_3$	Li_2SO_4	Evidence for gap		(21)
58	$NaNO_3$	$NaC_5H_{11}CO_2$	300	60–99.8	(82)

Illustrative examples for this statement are shown in Table II. It is seen that the correlation is not perfect (for example, the Na, Ag/NO_3, Cl and Na, Ag/NO_3, Br systems with different ΔG^0 and similar gaps, or the reversal of Cd and Pb in the series Li(Pb, Cd, Tl, Ag)/Cl, SO_4), but in view of the $\Sigma\lambda$ term in equation (33) it should not be expected to be so. If nonhomologous series are compared, it is found that a lower ΔG^0 suffices for phase separation, the greater the difference between the "hardness" of the hard pair of ions and the "softness" of the soft pair (compare at $\Delta G^0 = 14$ kcal/mole Na, Cs/F, Cl and Na, Ag/Cl, NO_3).

3.3. Survey of Systems with Miscibility Gaps

The recent surveys of molten salt systems in which miscibility gaps have been observed, those of Belyaev,[21] Ricci,[45] and especially the very complete one of Sinistri *et al.*,[23] include several hundreds of systems. Not

in every case has complete information been given in the literature available to the compilers, so that about numerable systems only the qualitative information, that a miscibility gap has been observed, is known. About most of the systems, fortunately, rather complete information is available. It has been attempted to include in the following as complete information as can be shown in tabulated material, without trying to present the actual phase diagrams. (These are available in the work of Sinistri *et al.*[23]). Binary systems are shown in Table III, where the monotectic and critical consolute temperatures are given, where available, together with the gap width. The more "covalent" or "soft" salt is designated as AX and the more "ionic" or "hard" one as BX. Ternary oxide systems, that is, with a common anion, where one of the components is silica and in which miscibility gaps were observed, are collected in Table IV. Since the data for such systems are given in composition triangles with nonisothermal outlines of the gap, only the limits of composition for BX and CX (AX = SiO_2) below which stratification is observed are given, except in the cases where closed curves are formed, that is, that the binaries do not show gaps. Finally, the data for reciprocal ternary systems are shown in Table V. For the purpose of this table, the salt pair AX and BY is considered the stable one, and AX is the more "covalent" of the two. Estimates of the free energy change per

TABLE IV. Miscibility Gaps in Ternary Systems with a Common Ion[a]

Number	AX	BX	CX	Temperature range (°C)	Gap width, (wt %)		Reference
					BX	CX	
1	SiO_2	MgO	Na_2O		–31	–1.8	(70)
2	SiO_2	MgO	K_2O		–31	–1.8	(83)
3	SiO_2	MgO	FeO		–31	–40	(72)
4	SiO_2	MgO	Al_2O_3		–31	–4.5	(70)
5	SiO_2	CaO	Na_2O		4–28	–2	(84)
6	SiO_2	CaO	K_2O		4–28	–2	(85)
7	SiO_2	CaO	MgO		–28	–31	(72)
8	SiO_2	CaO	FeO	1698–1707	3–27	5–42	(86)
9	SiO_2	B_2O_3	CaO			2–38	(87)
10	SiO_2	B_2O_3	BaO	900–1400	10–100	1–45	(60)
11	SiO_2	B_2O_3	ZnO			2.5–62	(63)
12	SiO_2	B_2O_3	PbO		5–92	4–60	(88)
13	SiO_2	FeO	K_2O		–40	–2	(89, 90)
14	SiO_2	FeO	Fe_2O_3	>1670		5–68 (B : C = 1 : 1)	(91)

[a] Some nonoxide ternary systems also show miscibility gaps, e.g., LiF–BeF_2–ZnF_4.[86, 229]

TABLE V. Reciprocal Ternary Systems with Miscibility Gaps

Number	AX	BY	$\Delta G°(\Delta H°)$	Monotectic (consolute) temperature (°C)	Gap width of diagonals (mole %)		Reference
					Stable	Unstable	
1	AgCl	$LiNO_3$	19.8 (18.6)	455	~0–100 AgCl	28–77 LiCl	(92)
2	AgCl	$NaNO_3$	14.2		~0–100 AgCl		(93)
3	AgCl	KNO_3	14.9 (14.5)	452	~0–100 AgCl	30–65 KCl	(94)
				(480)	1.8–99.4 AgCl		(25)
4	AgCl	$CsNO_3$	(15.5)	444	1.5–97.0 AgCl	32–62 CsCl	(95)
5	AgCl	$TlNO_3$		Evidence for gap			(96)
6	AgCl	$Ca(NO_3)_2$	17.6 (17.9)	546	~0–100 AgCl	31–70 $\frac{1}{2}CaCl_2$	(97)
7	AgCl	$LiVO_3$		588	5–98 AgCl		(98)
8	AgCl	$NaVO_3$		570	5–98 AgCl		(98)
9	AgCl	KVO_3		570	13–96.5 AgCl		(98)
10	AgCl	Li_2SO_4	19.2 (19.0)	818	1.2–98 AgCl	28–77.5 LiCl	(99)
11	AgCl	Na_2SO_4	12.2	Evidence for gap			(100)
12	AgCl	$KHSO_4$		(480)	0.7–99.2 AgCl		(25)
13	AgCl	$K_2S_2O_7$		(480)	0.9–99.2 AgCl		(25)
14	AgCl	Tl_2SO_4		Evidence for gap			(100)
15	AgCl	Li_2CrO_4		472	20–30 AgCl	36–58 LiCl	(101)
16	AgCl	Na_2CrO_4		618	18–55 Na_2CrO_4		(98)
17	AgCl	Li_2MoO_4		Evidence for gap, 57.3 % of area of square			(101)
18	AgCl	Na_2MoO_4		550	12.5–50 Na_2MoO_4		(98)
19	AgCl	Li_2WO_4		702	6–100 AgCl	14–74 LiCl	(102)
				734	1.5–95 Li_2WO_4		(98)
20	AgCl	Na_2WO_4		610	20–68 Na_2WO_4		(98)
21	AgCl	$(Na, K)BF_4$			~1–99 AgCl		(103)

22	AgBr	$NaNO_3$	19.2	(19.5)		419	~0–100	AgBr	26–72	NaBr	(104)
23	AgBr	KNO_3	18.6	(18.4)		419	~0–100	AgBr	30–66	KBr	(94)
24	AgBr	$LiVO_3$				588	2.5–95	AgBr			(98)
25	AgBr	$NaVO_3$				571	6–99	AgBr			(98)
26	AgBr	KVO_3				500	7.5–97	AgBr			(98)
27	AgBr	Li_2SO_4	26.5	(26.2)		885	1–98	Li_2SO_4			(98)
28	AgBr	Na_2SO_4	17.7	(17.6)		877	1–99	Na_2SO_4			(98)
29	AgBr	Li_2CrO_4				478	4–99	Li_2CrO_4			(98)
30	AgBr	Na_2CrO_4				737	8–90	Na_2CrO_4			(98)
31	AgBr	Li_2MoO_4				670	1.5–97.5	Li_2MoO_4			(98)
32	AgBr	Na_2MoO_4				650	7–92	Na_2MoO_4			(98)
						666	7.3–95.3	AgBr	36.5–66.4	NaBr	(105)
33	AgBr	Li_2WO_4				734	1.5–97.5	Li_2WO_4			(98)
34	AgBr	Na_2WO_4				672	1–90	Na_2WO_4			(98)
35	AgBr	LiCl	7.5	(7.3)	at	540	31.5–92.5	AgBr	45–52.5	LiBr	(106)
36	AgI	$NaNO_3$	29.0	(28.2)		554	~0–100	AgI	30–72	NaI	(97)
37	AgI	KNO_3	25.1	(24.9)		552	~0–100	AgI	29–65	KI	(107)
38	AgI	$TlNO_3$				Evidence for gap					(21)
39	AgI	Tl_2SO_4	11.0	(10.8)		598 (730)	11–86	AgI	47–55	TlI	(108)
40	AgI	LiCl	17.3			Evidence for gap					(109)
41	AgI	NaCl	14.7			Evidence for gap					(21)
42	$HgCl_2$	$LiNO_3$				281	~0–100	$HgCl_2$			(110)
43	$HgCl_2$	$NaNO_3$				304 (580)	~0–100	$HgCl_2$			(110)
44	$HgBr_2$	$LiNO_3$				252	~0–100	$HgBr_2$			(110)
45	$HgBr_2$	$NaNO_3$				306	~0–100	$HgBr_2$			(110)
46	$HgBr_2$	KNO_3				328 (586)	~0–100	$HgBr_2$			(110)
47	$HgBr_2$	$RbNO_3$				264 (350)	27–97	$HgBr_2$			(110)
48	HgI_2	$LiNO_3$				258	~0–100	HgI_2			(110)
49	HgI_2	$NaNO_3$				306	~0–100	HgI_2			(110)
50	HgI_2	KNO_3				334	~0–100	HgI_2			(110)

TABLE V. (*Continued*)

Number	AX	BY	$\Delta G°(\Delta H°)$	Monotectic (consolute) temperature (°C)	Gap width of diagonals (mole %)		Reference
					Stable	Unstable	
51	HgI_2	$RbNO_3$		310	1–100 HgI_2		(110)
52	HgI_2	$CsNO_3$		401	7.5–100 HgI_2		(110)
53	TlCl	Li_2SO_4	12.4 (12.0)	654	7.5–96 TlCl	35–75 LiCl	(111)
54	TlBr	$LiNO_3$	(14.8)	460 (642)			(112)
55	TlBr	(Li, Na)NO_3		446 (625)	11–95 TlBr		(112)
56	TlBr	(Li, K)NO_3		450 (630)	11–95 TlBr		(112)
57	TlBr	$NaNO_3$	7.6 (8.4)	445 (588)	10–95 TlBr	33.5–66.5 NaBr	(113)
58	TlBr	(Na, K)NO_3		446 (574)	11–95 TlBr		(112)
59	TlBr	(Na, Rb)NO_3		445 (554)	15–93 TlBr		(112)
60	TlBr	(Na, Cs)NO_3		439 (527)	18–92 TlBr		(112)
61	TlBr	KNO_3		444 (543)	15.5–92.5 TlBr		(112)
			7.0 (7.2)	435 (535)	14–92.5 TlBr	34–61 KBr	(114)
62	TlBr	(K, Rb)NO_3		444 (520)	11–90 TlBr		(112)
63	TlBr	(K, Cs)NO_3		438 (488)	23–90 TlBr		(112)
64	TlBr	$RbNO_3$		443 (500)	20–90 TlBr		(115)
			(7.2)	441 (494)	23–88 TlBr	38.5–59 RbBr	(113)
65	TlBr	(Rb, Cs)NO_3		434 (460)	31–85.3 TlBr		(112)
66	TlBr	Li_2SO_4	(18.1)	764	2.5–95 TlBr		(116)
67	TlBr	Na_2SO_4	9.6 (9.4)	800	5–94 TlBr		(117)
				800	9–94 TlBr		(118)
68	TlI	$NaNO_3$	13.1 (14.4)	427	1.5–99 TlI		(112)
69	TlI	KNO_3	10.6 (11.1)	438	3–98.5 TlI		(112)
70	TlI	$RbNO_3$	(10.2)	422	6–98 TlI		(112)

71	TlI	$CsNO_3$		(9.3)	424 (599)	8.5–96	TlI				(112)
72	Tl(Cl, Br)	$NaNO_3$			410 (495)	10–90	Tl(Cl, Br)				(112)
73	Tl(Cl, Br)	$(Na, Rb)NO_3$			Evidence for gap at 443						(115)
74	Tl(Cl, Br)	$(Li, Na)_2SO_4$			Evidence for gap at 764						(116)
75	Tl(Cl, Br)	Na_2SO_4			Evidence for gap at 800						(119)
76	Tl(Cl, I)	$NaNO_3$			Gaps when TlI/TlCl > 3						(112)
77	$CdCl_2$	Li_2SO_4	9.5	(9.7)	650	20–92	$CdCl_2$	35–62	$CdSO_4$		(120)
78	$CdBr_2$	Li_2CrO_4			530	3–70	Li_2CrO_4				(98)
79	$PbCl_2$	Li_2SO_4	7.2	(7.0)	650	12–93	$PbCl_2$	28–64	$PbSO_4$		(121)
80	$PbCl_2$	$(Na, K)BF_4$			Evidence for gap						(103)
81	Ag_2S	$PbCl_2$	5.0		Evidence for gap						(122)
82	KBr	LiF	21.8	(21.9)	804	3–80	KBr	46–57	LiBr		(123)
83	CsBr	LiF	30.5	(30.0)	838	6–91	CsBr				(122)
84	CsCl	LiF	25.0		820	10–70	CsCl				(122)
85	CsCl	CaF_2	26.3		Evidence for gap						(122)
86	Ag_2CrO_4	Li_2SO_4			669	30–60	Ag_2CrO_4	43–59	Li_2CrO_4		(101)
87	Sb_2S_3	Na_2SO_4			875	~14–93	Na_2SO_4				(124)
88	B_2O_3	(Li, K)Cl			Evidence for gap						(125)
89	B_2O_3	NaCl			Evidence for gap						(128–130)
90	B_2O_3	NaBr			Evidence for gap						(128, 131)
91	B_2O_3	NaI			Evidence for gap						(128, 132)
92	B_2O_3	KCl			Evidence for gap						(21)
93	B_2O_3	(Na, K)Cl			Above 830	<5–39	(wt)(Na, K)Cl				(129)
94	B_2O_3	K(F, Cl)			Near 800–900	Evidence for gap					(133)
95	B_2O_3	Na_2SO_4			Evidence for gap						(21)
96	SiO_2	CaF_2			Evidence for gap						(140)
97	SiO_2	SrF_2			Evidence for gap						(140)
98	SiO_2	BaF_2			Evidence for gap						(140)
99	SiO_2	CaS			Evidence for gap						(21)
100	SiO_2	FeS			1713	2–95	SiO_2				(141)

TABLE V. (*Continued*)

Number	AX	BY	$\Delta G°(\Delta H°)$	Monotectic (consolute) temperature (°C)	Gap width of diagonals (mole %)		Reference
					Stable	Unstable	
101	SiO_2	Na_2SO_4		Evidence for gap			(142)
102	TiO_2	CaF_2		1365	6–55 (wt)TiO_2		(143)
103	PbO	LiF		Evidence for gap			(21)
104	PbO	NaF	32.9 (33.3)	880	1.4–99.4 NaF		(98)
105	PbO	KF	37.0 (38.0)	870	1–99 PbO		(98)
106	PbO	NaCl	31.9 (31.8)	841	0.7–99 PbO		(98)
107	PbO	KCl	44.2 (44.0)	860	1.4–99 PbO		(98)
108	PbO	RbCl	(46.7)	717	1.4–99 PbO		(98)
109	PbO	NaBr	30.0 (29.8)	830	1.4–99 PbO		(98)
110	PbO	KBr	43.6 (43.4)	860	1.0–99 PbO		(98)
111	PbO	KI	40.4 (40.2)	850	1–99 PbO		(98)
112	PbO	Li_2CO_3	31.9 (32.5)	870	1.4–99 PbO		(98)
113	PbO	Na_2CO_3	60.0 (56.0)	860	1–99 PbO		(98)
114	PbO	K_2CO_3	72.1 (72.2)	878	0.5–98 PbO		(98)
115	PbO	Li_2SO_4	(32.6)	847	1–99 PbO		(98)
116	PbO	Na_2SO_4	64.1 (64.4)	860	1–99 PbO		(98)
117	PbO	K_2SO_4	89.0 (88.8)	1020	1–99 PbO		(98)
118	PbO	Na_2CrO_4		726	1–99 PbO		(98)
119	PbO	K_2CrO_4		940	1–99 PbO		(98)
120	PbO	Na_2MoO_4		685	0.5–99.5 PbO		(98)
121	PbO	K_2MoO_4		920	0.5–99.5 PbO		(98)
122	PbO	Li_2WO_4		880	0.5–99.5 PbO		(98)
123	PbO	Na_2WO_4		680	0.5–99.7 PbO		(98)

124	PbO	K_2WO_4			885	0.5–99	PbO		(98)
125	PbO	Na_2TiO_3			880	1–98	PbO		(98)
126	PbO	K_2TiO_3				Evidence for gap			(21)
127	$NaNO_3$	$LiC_2H_5CO_2$				27–87	$NaNO_3$	37–60 $LiNO_3$	(144)
128	$NaNO_3$	$LiC_3H_7CO_2$			300	10–97.5	$NaNO_3$	21–75 $LiNO_3$	(144, 145)
129	$NaNO_3$	$LiC_4H_9CO_2$				10–95	$NaNO_3$	24–89 $LiNO_3$	(144)
130	$NaNO_3$	$LiC_5H_{11}CO_2$				Evidence for gap			(144)
131	KNO_3	LiOH	17.3	(17.2)	465	5–95	KNO_3	44–59 $LiNO_3$	(146)
132	KNO_3	$LiCH_3CO_2$				11–87	KNO_3	26–69 $LiNO_3$	(144)
133	KNO_3	$LiC_2H_5CO_2$				Evidence for gap			(144)
134	KNO_3	$LiC_3H_7CO_2$				Evidence for gap			(144)
135	KNO_3	$LiC_4H_9CO_2$				Evidence for gap			(144)
136	KNO_3	$LiC_5H_{11}CO_2$				Evidence for gap			(144)
137	KNO_3	$NaC_4H_9CO_2$				Gap 52.5% of diagonal			(144)
138	KNO_3	$NaC_5H_{11}CO_2$				Gap 74 % of diagonal			(144)
139	$RbNO_3$	LiOH	19.0	(19.3)	458	~4–87	$RbNO_3$		(147)
140	$RbNO_3$	NaOH	8.8	(8.6)	285	~7–93	$RbNO_3$		(147)
141	$CsNO_3$	LiOH	21.9			Evidence for gap			(147)
142	$CsNO_3$	NaOH	11.7			Evidence for gap			(147)
143	NaSCN	$LiC_2H_5CO_2$				Gap 17.5% of diagonal			(144)
144	NaSCN	$LiC_3H_7CO_2$				Evidence for gap			(144)
145	NaSCN	$LiC_4H_9CO_2$				Evidence for gap			(144)
146	NaSCN	$LiC_5H_{11}CO_2$				Evidence for gap			(144)
147	KSCN	$LiCH_3CO_2$				Gap 55% of diagonal			(144)
148	KSCN	$LiC_2H_5CO_2$				Evidence for gap			(144)
149	KSCN	$LiC_3H_7CO_2$				Evidence for gap			(144)
150	KSCN	$LiC_4H_9CO_2$				Evidence for gap			(144)
151	KSCN	$LiC_5H_9CO_2$				Evidence for gap			(144)
152	KSCN	Na *i*–$C_4H_9CO_2$				39–55	KSCN	44–66 NaSCN	(144)
153	KSCN	$NaC_6H_{13}CO_2$				Evidence for gap			(144)

equivalent of the metathetical reaction[27] (or the enthalpy change, in parenthesis) are given, obtained from the data for the solids. The monotectic temperature (and the upper critical consolute temperature, in parenthesis) are given, as well as the extent of the miscibility gap along the stable and the unstable diagonals. This extent is given in mole % of the listed salts (except where otherwise indicated), usually of AX for the stable pair and BX for the unstable one.

Only a very small fraction of the systems that show miscibility gaps has been utilized for distribution studies. In view of the wealth of information on such systems obtainable from the study of the distribution of a minor component between the liquid phases, it is hoped that placing these tables in the present context will stimulate further research along those lines.

4. THE KINETICS OF THE DISTRIBUTION

The kinetics of liquid–liquid distribution have been the subject of only a few studies.[148] In these investigations, diffusion, phase boundary crossing, and slow chemical reactions were recognized as rate determining under suitable circumstances.

4.1. Diffusion-Controlled Rates

The most common limiting factor for the rate of distribution is diffusion in the bulk of one of the liquid phases (if they are unstirred, so that convection cannot assist in bringing the relevant species to the interface or removing it from this) or diffusion in a diffusion layer near the interface, in the more common case of stirred liquids. In molten salt systems, at the higher temperatures involved compared to the aqueous–organic liquid systems studied heretofore, this step is not expected to be rate determining. However, with highly structured molten salts, such as certain oxide melts, diffusion in the viscous molten salt may become the rate-limiting step. Preliminary results show that diffusion in the borate phase in the two-phase boron oxide–sodium oxide–sodium chloride system becomes rate determining, especially at low sodium oxide–boron oxide ratios.[149] The distribution of rare earths took considerably longer than that of sodium ions (labeled with ^{22}Na) to reach equilibrium in this system.

4.2. Rates Controlled by Boundary Crossing

In particular cases, where surface active agents are involved either as the distributing solutes or as sorbed interferences that block the pathway

of the distributing species, crossing of phase boundary may control the rate of distribution. As yet, in no distribution system involving molten salts has this step been shown to be rate determining.

4.3. Rates Controlled by Slow Chemical Reactions

The rate of a chemical reaction, in which bonds between the distributing species and other molecules or ions must be broken or must be formed, and which involves a sufficiently high activation energy, may in certain cases be overall rate determining for the distribution. A detailed investigation of this case has been made for two systems, involving the distribution of mercury[150] and zinc[151] bromides between an alkali nitrate melt and a liquid polyphenyl mixture. Following is a discussion of the results and conclusions of these studies.

The molten salt phase consisted of the lithium nitrate–potassium nitrate eutectic mixture, and the organic phase consisted of 37 mole % biphenyl, 48 mole % orthoterphenyl, and 15 mole % metaterphenyl. Both the metal and the bromine were labeled radioactively for the two systems, and the distribution between the two liquid phases of each radioisotope was measured as a function of time. It was observed that the time required to reach equilibrium was different when measured by following the distribution of the metal and when measured by the bromine distribution, provided that excess bromide, as potassium bromide, over the mercury or zinc bromide, was present. This was explained by a sequence of reactions, such as

$$\begin{aligned} HgBr_2(NO_3)_2^{2-} + Br^{-*} &\rightleftarrows HgBr_2Br^*(NO_3)^{2-} \\ + NO_3^- &\rightleftarrows HgBrBr^*(NO_3)_2^{2-} + Br^- \end{aligned} \tag{35}$$

which constitutes a net exchange of inactive and radioactive bromide. This exchange superimposes on a set of reactions in which different bromo complexes of the metals are involved:

$$Zn(NO_3)_n^{2-n} + Br^- \underset{k_1^-}{\overset{k_1}{\rightleftharpoons}} ZnBr(NO_3)_{n-1}^{2-n} + NO_3^- \tag{36}$$

$$ZnBr(NO_3)_{n-1}^{2-n} + Br^- \underset{k_2^-}{\overset{k_2}{\rightleftharpoons}} ZnBr_2(NO_3)_2^{2-} + (n-3)NO_3^- \tag{37}$$

$$MBr_2(NO_3)_2^{2-} \underset{k_d^-}{\overset{k_d}{\rightleftharpoons}} \overline{MBr_2} + 2\,NO_3^- \tag{38}$$

$$MBr_2(NO_3)_2^{2-} + Br^- \underset{k_3^-}{\overset{k_3}{\rightleftharpoons}} MBr_3(NO_3)^{2-} + NO_3^- \tag{39}$$

$$HgBr_3(NO_3)^{2-} + Br^- \underset{k_4^-}{\overset{k_4}{\rightleftharpoons}} HgBr_4^{2-} + NO_3^- \tag{40}$$

where M is either zinc or mercury and n is assumed to equal four. It could be shown from equilibrium measurements that the species $Hg(NO_3)_n^{2-n}$, $HgBr(NO_3)_{n-1}^{2-n}$, and $ZnBr_4^{2-}$ can be ignored under the experimental conditions. The forward reaction on the left-hand side of equation (35) proceeds, of course, with the rate constant k_3, while that on the right-hand side proceeds with a rate constant of $\frac{2}{3}k_3^-$, since statistically only two out of three exchanges result in retention of radioactive bromide in the complex.

Rate equations involving the rate constants k and concentrations of species were set up, and were solved, using the known equilibrium constants for reactions (36) to (40)[29,152] and the known free bromide ion concentration (the nitrate ion, being a part of the solvent, has a practically constant concentration). The rate constants found are summarized in Table VI. The values of k_d and k_d^- are relatively low and much faster distribution reactions were observed with the same solvent and aqueous solutions under similar conditions. Thus it must be some chemical reaction (perhaps bending of the linear $HgBr_2$ molecules into the tetrahedral angle and taking on two nitrate ions from the solvent) that is rate determining. The very small values of k_1^- and k_2^- for zinc (those for mercury are apparently too small to measure) and their high activation energies (*ca.* 50 kcal/mole) reflect the difficulty of breaking the Zn–bromide bonds in $ZnBr_2$, relative to the ease of breaking the metal–nitrate bonds involved in the other reactions. It

TABLE VI. Rate Constants for Distribution and Complexation Reactions[a]

Constant	Hg (150°C)	Zn (150°C)	Zn (200°C)
k_d	$(2.5 \pm 0.2) \times 10^{-2}$	$(4.0 \pm 0.4) \times 10^{-3}$	$(1.2 \pm 0.1) \times 10^{-2}$
k_d^-	$(2.7 \pm 0.1) \times 10^{-3}$	$(1.7 \pm 0.2) \times 10^{-4}$	$(1.0 \pm 0.1) \times 10^{-3}$
k_1		$(2.7 \pm 0.4) \times 10^{-1}$	$(4.5 \pm 0.7) \times 10^{-1}$
k_1^-		$(9 \pm 3) \times 10^{-9}$	$(3.5 \pm 1.0) \times 10^{-6}$
k_2		$(2.5 \pm 0.4) \times 10^{-1}$	$(4.2 \pm 0.6) \times 10^{-1}$
k_2^-		$(1.4 \pm 0.5) \times 10^{-8}$	$(6 \pm 2) \times 10^{-6}$
k_3	$(1.3 \pm 0.2) \times 10^{-1}$	$(2.2 \pm 0.3) \times 10^{-1}$	$(3.7 \pm 0.5) \times 10^{-1}$
k_3^-	$(1.6 \pm 0.2) \times 10^{-2}$	$(8.5 \pm 2.0) \times 10^{-2}$	$(2.0 \pm 0.4) \times 10^{-1}$
k_4	$(6.2 \pm 1.0) \times 10^{-2}$		
k_4^-	$(6.9 \pm 0.1) \times 10^{-3}$		

[a] The units are sec^{-1} for all constants, except for k_1, k_2, k_3, and k_4, where they are kg $mole^{-1}$ sec^{-1}, disregarding the constant nitrate ion concentration.

should be noted that the ratio k_3/k_4 for mercury is two to one, the same as that between the number of nitrate groups in the reacting species, available for exchange for bromide. For zinc $k_1 : k_2 : k_3$ are not in the ratio 4 : 3 : 2 but do decrease somewhat in the expected order for hexacoordination 6 : 5 : 4. The rate constants listed in Table VI are able to account quantitatively for the rate of distribution of both the mercury or the zinc and the bromine radioactivities at 150°. At 200°, on the other hand, only the rate of zinc activity distribution is accounted for by them, while it is necessary to invoke direct exchange, such as

$$ZnBr_2(NO_3)_2^{2-} + Br^{-*} \rightleftarrows ZnBrBr^*(NO_3)^{2-} + Br^- \tag{41}$$

which becomes important, contrary to reaction (35), to explain the bromine distribution rate. The higher temperature permits a reaction path through the tricoordinated $ZnBr(NO_3)_2^-$ transition state, whereas only the tricoordinated $ZnBr_2(NO_3)^-$ transition state is available at the lower temperature, again reflecting the great strength of the zinc–bromide bond in $ZnBr_2$.

5. SURVEY OF SELECTED DISTRIBUTION SYSTEMS

5.1. Distribution of Solutes Between Molten Salts and Liquid Bismuth

5.1.1. Chloride Melts

As mentioned in the introduction, an important fraction of the studies related to the distribution of minor constituents between a molten metal and a molten salt has been done in connection with the reprocessing of the LMFR (liquid metal fueled reactor) fuel. The reactor experiment was conducted at the Brookhaven National Laboratory, but other American laboratories, and even Japanese ones, contributed to our knowledge of this process.

One of the earliest publications on this subject[6] presented the thermodynamic basis for the process. Consider the LMFR fuel, which consists of liquid bismuth in which are dissolved 1000–2000 ppm uranium ($\bar{N}_U = (8.7 \text{ to } 17.4) \times 10^{-4}$), 250 ppm zirconium ($\bar{N}_{Zr} = 5.5 \times 10^{-4}$), and 350 ppm magnesium ($\bar{N}_{Mg} = 3 \times 10^{-3}$) in addition to a much smaller concentration of fission products (at the envisioned fuel burnups this would be $\leq 10^{-4}$ mole fraction).[7] Consider also the molten salt to be used for the extraction of certain fission products: it is a eutectic of the chlorides

of magnesium (50 mole %), sodium (30 mole %), and potassium (20 mole %), having a melting point of 396°C. The magnesium chloride in this melt can chlorinate (oxidize) those metals present in the liquid bismuth that form chlorides thermodynamically more stable than it. Table VII contains some standard free energies of formation of relevant chlorides. Now for a reaction such as

$$\overline{\text{La}}[\text{in Bi}(l)] + \tfrac{3}{2}\text{MgCl}_2(\text{in melt}) \rightleftharpoons \text{LaCl}_3(\text{in melt}) + \tfrac{3}{2}\overline{\text{Mg}}[\text{in Bi}(l)] \quad (42)$$

the equilibrium constant is

$$K = a_{\text{LaCl}_3}\,\bar{a}_{\text{Mg}}^{\frac{3}{2}}\,\bar{a}_{\text{La}}^{-1}\,a_{\text{MgCl}_2}^{-\frac{3}{2}} = \exp\left(\frac{-\Delta G^0}{RT}\right) \quad (43)$$

where ΔG^0 should be calculable from the difference of the free energies of formation of the chlorides from the elements, obtainable from Table VII. Thus for 773°K, ΔG^0 would be $3(62.3 - 70.0) = -23.1$ kcal/mole La, or $K = 3 \times 10^6$. However, it is still necessary to relate the activities appearing in equation (43) to the concentrations. It has been found that some of the activity coefficients are far from unity.[10] These have been evaluated[153] in emf cells of the type

$$\text{M}/\text{M}^{m+} \text{ in molten salt}/\overline{\text{M}} \text{ in Bi}(l) \quad (44)$$

TABLE VII. Standard Free Energies of Formation of Some Metal Chlorides

Salt	$-\Delta G_f^0$ (kcal/g atom Cl)	
	500°K[a]	773°K[b]
CsCl		88.3
$BaCl_2$		87.4
$SrCl_2$	89.0	
NaCl	87.4	
$LaCl_3$	76.0	70.0
$CeCl_3$		68.9
YCl_3	69.5	
$PuCl_3$	67.4	
$MgCl_2$	66.8	62.3
UCl_3	62.2	
$BiCl_3$	22.2	

[a] From Bareis *et al.*[6]
[b] From Wiswall and Egan.[10]

for the metal phase. In cell (44) the metal ion concentration in the salt melt is kept constant, and in the liquid bismuth the metal concentration is permitted to vary, so that

$$E = E^0 + \frac{RT}{mF} \ln \bar{N}_M \bar{f}_M \tag{45}$$

The following equation[6] should thus relate the activities and the concentrations:

$$D_{La} = \frac{\bar{N}_{La}}{N_{LaCl_3}} = N_{MgCl_2}^{-\frac{3}{2}} \frac{f_{LaCl_3} \bar{f}_{Mg}^{\frac{3}{2}}}{\bar{f}_{La} f_{MgCl_2}^{\frac{3}{2}}} \exp \frac{\Delta G^0}{RT} \times \bar{N}_{Mg}^{\frac{3}{2}} = \text{const} \times \bar{N}_{Mg}^{\frac{3}{2}} \tag{46}$$

In the quantity $N_{LaCl_3} = N_{La^{3+}} N_{Cl^-}^3 = N_{La^{3+}}$, the chloride fraction in the molten salt phase can be neglected, since chloride is the only and the common ion, so that $N_{Cl^-} = 1$. In the same manner $N_{MgCl_2} = N_{Mg^{2+}}$ in the square brackets. Since lanthanum is present only at low concentrations, the extent of reaction (42) is very small and $N_{Mg^{2+}}$ is essentially constant at its initial value of 0.50. The same holds for f_{MgCl_2}, which has been estimated at 0.21, and f_{LaCl_3}, which has been estimated at 0.01.[153] The former value can be confirmed from measurements independent of the distribution data, while the latter could be treated as a parameter to be obtained from the distribution measurements and equation (46). In any case, since the salt melt phase is essentially of constant composition, both activity coefficients should be constant. Since the concentrations of all the solutes in the liquid bismuth also are very low, the activity coefficients in this phase, $\bar{f}_{La}$ and $\bar{f}_{Mg}$, are also constant. Their values have been obtained from equation (45) as 2.3×10^{-15} and 1.5×10^{-3}, respectively, at 500°C.† Thus in equation (46) the whole expression in the parenthesis is independent of $\bar{N}_{Mg}$, so that a plot of log D_{La} against log $\bar{N}_{Mg}$ should be a straight line of slope $\frac{2}{3}$. This is indeed what has been found experimentally. The value of the constant in equation (46) is about 450, and with the concentration of magnesium in the bismuth, $\bar{N}_{Mg} = 3 \times 10^{-3}$, the distribution coefficient of lanthanum on a mole fraction basis comes out to be 0.075. It is seen that the lanthanum is removed from the liquid metal, that is, from the fuel, into the molten salt. The extent of removal depends, of course, on the relative amounts of the two phases. The same arguments apply to other fission products, and the corresponding relationships between D_M and $\bar{N}_{Mg}$ have been

† The values of $G_M^E = RT \ln \bar{f}_M$ at 500°C that have been obtained are La −52, Ce −50, Nd −44, Sm −63, Ba −63, Cs −27, U −18, Li −18, Na −14.6, and Mg −8.2 (9.0 at 450°C) kcal/mol.[10,153]

obtained both in laboratory experiments[6,8,10,153] and in pilot plant experiments on the kilogram scale.[9,154] Not only are fission products that give chlorides more stable than magnesium extracted into the molten salt, but also those of comparable or slightly lower stability because of the mass action effect of the high concentration of the magnesium chloride in the molten salt. Uranium, on the other hand, is held back in the liquid bismuth (here $\bar{f}_U$ seems to play a not less important role than ΔG^0), and the separation factor $\alpha_{Ce}^{U} = D_U/D_{Ce}$ is a few hundreds.[154] The industrial extraction process for the LMFR has been described in a number of publications.[7, 155–160]

Further information relevant to the distribution of solutes between molten chlorides and liquid bismuth has been published outside of the LMFR program. For example, it was found[161] that liquid bismuth reduces uranium tetrachloride, dissolved in molten lithium, sodium, potassium, or calcium chlorides at 700–850°C, forming uranium(III), with three moles of bismuth dissolving in the salt melt for every eight moles of uranium reduced. It requires a much more electropositive metal (see Table VII) to reduce the uranium further to the metal. In a series of papers, Yamagishi and Kamemoto studied the distribution of numerous metals at 550°C between liquid bismuth and molten lithium chloride–potassium chloride eutectic.[17–19] Their data are shown in Table VIII, and although their precision is low, the authors showed that distribution equilibrium has been achieved by sampling at various times between 1 hr and 4 days and by starting with the distribuend initially in either of the phases.[17] They showed that air oxidation stabilizes copper(II) in the salt melt, as does oxidation with bismuth trichloride in an argon atmosphere ($D < 0.01$), while reduction with 0.2% magnesium in the bismuth leads to a species [copper(I)?] that strongly favors the molten bismuth ($D \sim 500$).

5.1.2. Polarography with the Dropping Bismuth Electrode

The distribution of metals between a polarized liquid bismuth electrode and a molten salt is another item of information relevant to the above topic, but its use has not been widespread. It has been observed that the chronopotentiometric reduction of copper(I) in the LiCl–KCl eutectic at 450°C is more accurate when the platinum electrode has been precovered with a layer of liquid bismuth, in which copper is reasonably soluble, than without this layer,[162] but polarography gives more detailed information.

Polarographic studies in molten salts have been conducted mainly with

TABLE VIII. Distribution Coefficients of Trace Metals between Liquid Bismuth and Molten Lithium-Potassium Chloride Eutectic at 550°C[17]

Metals favoring the bismuth phase		Metals favoring the chloride phase	
Metal	Lower limit of D	Metal	Upper limit of D
Pt	300	Cu[a]	0.12
Sb	300	In	0.10
Ag	200	Fe	0.05
Te	20	Sc	0.005
Tc	13	Co	0.003
Po	10	Mg	0.0025
Sn	1.6	Sr	0.0012
		Cd	6×10^{-4}
		Zn	5×10^{-4}
		Cr	5×10^{-4}
		Gd	5×10^{-4}
		Mo	8×10^{-5}
		W	6×10^{-5}
		Mn	1×10^{-5}
		La	1×10^{-5}

[a] Average number; when air is present, $D \sim 0.01$, and when argon atmosphere is used, $D \sim 0.3$.[18]

solid microelectrodes,[163] but the dropping mercury electrode has been used in a number of investigations.[164–172] Delimarskii and Markov stated in their book[163] that the dropping mercury electrode is not useful above 215°C and that attempts to use electrodes of other liquid metals (bismuth, tin, and antimony) have been unsuccessful. Both statements have been challenged: the first with studies at 250°[171] and 260°[169] with the dropping mercury electrode and the second with voltammetric studies with liquid lead[173] (at 400°C), lead–gold alloy[174] (at 518°C) electrodes, and a polarographic study at 450°C with the dropping bismuth electrode.[13] These electrodes have been used with the lithium chloride–potassium chloride eutectic. The lead electrodes are useful if lead chloride is present in the molten salt; otherwise lead is oxidized enough to provide some, but bismuth seems to be sufficiently noble and not to be oxidized appreciably (lead chloride has caused some trouble, being slightly reduced by the bismuth pool reference electrode in the absence of polarization).[13] Metal ions such as lead, cadmium, and zinc have been successfully reduced polarographically, the diffusion current being proportional to the concentration in the con-

centration range 0.5–5.0 mM. Indeed, all metal ions forming in the eutectic melt chlorides more stable than that of gallium and less stable than that of manganese could be studied. The practical limit occurs at -0.8 V against the bismuth pool reference because of reduction of the lithium chloride of the solvent.

The polarographic method can be viewed as a variant of the extraction reaction, illustrated by equation (42), for example, for cadmium:

$$Cd^{2+}(\text{in melt}) + 2\bar{e}^{-}[\text{in Bi}(l)] \rightleftarrows \overline{Cd}[\text{in Bi}(l)] \tag{47}$$

The half-wave potential is thus related to the equilibrium constant for the distribution of cadmium, since the waves are reversible. Since the activity coefficients of the metals in bismuth are very small (see footnote on p. 95), their deposition potentials are shifted to relatively positive values.

5.1.3. Fluoride Melts

Whereas with the LMFR (Section 5.1.1) the fuel is a solution of the fissile material in a liquid metal and the molten salt is used for the reprocessing, that is, for the removal of certain fission products, the opposite is true for the MSRE (molten salt reactor experiment) and MSBR (molten salt breeder reactor). Here the fuel is a solution of the fissile (and fertile) material in a suitable molten salt, whereas a liquid metal can be used for reprocessing.[175] Two versions of the molten salt have been used: one consisting of lithium fluoride (66 mole %) and beryllium fluoride (34 mole %) with a small concentration of uranium tetrafluoride (0.83 mole %) and the other, used for the single fluid breeder reactor, consisting of lithium fluoride, beryllium fluoride, and thorium fluoride (for example 72, 16, and 12 mole %, respectively) and again some uranium or plutonium fluoride. Bismuth, again, has been chosen as the liquid metal, and because of the presence of lithium fluoride in the molten salt, lithium, dissolved in the bismuth, has been used as the reductive extractant.[176,177] Just as described in equation (46) for the chloride melts, there is a definite relationship between D_M for a m-valent metal and the lithium concentration in the liquid metal:

$$\log D_M = \text{const.} + m \log \bar{N}_{Li} \tag{48}$$

Values of ΔG^0 for the extractive reaction can be calculated from $\Delta G^0 = -mF\,\Delta E_0'$ [where F is the Faraday constant and $\Delta E_0'$ is a formal potential, obtained from $\Delta E_0' = (RT/mF)(\ln D_M - m \ln D_{Li}]$: U -57, Th -35, La -30, Eu (with $m = 2$) -14, and Na -5, all in kilocalories per mole.[175] The values of $\Delta E_0'$ were found to be independent of the

temperature in the range 500–700°C. However, another set of experiments for the lithium–beryllium fluoride (of composition Li_2BeF_4) salt melt and lithium in liquid bismuth metal system at 600°C gave nonintegral m values [2.7 for La, 2.3 for Ce, 2.5 for Nd (instead of 3), and 1.6 for Sm, 1.9 for Eu instead of 2], which could not be explained. It also was found necessary to consider the reaction[177]

$$2\overline{Li}(\text{in Bi}) + BeF_2(\text{in salt}) \rightleftarrows 2LiF(\text{in salt}) + Be(\text{solid}) \qquad (49)$$

At higher concentrations of reducible metal fluorides, such as thorium in the breeder reactor fuel, equation (48) breaks down when the metal saturates the liquid bismuth (excess thorium is precipitated as Th_3Bi_4). Until this point, however, good agreement of the quantity of lithium consumed and the quantities of metal extracted is obtained.

Of special importance is the possibility to isolate protactinium from the thorium and uranium containing breeder reactor fuel.[1,12,178] From distribution experiments using solutions of thorium and lithium in liquid bismuth at 500–700°C, and employing equation (48), it was found that protactinium(IV) and uranium(III) are the stable oxidation states of these elements in the fluoride melt.[12] The role of the thorium in this system is to poise (buffer) the redox system: Since it is present together with the lithium at a great excess over the other metal ions, their distribution will be determined uniquely by the ratio of lithium to thorium. The separation factors attained were $\alpha_{Th}^{Pa} = 2000$, $\alpha_{Pa}^{U} = 28$, and $\alpha_{Pa}^{Pu} = 2.5$, so that by careful control of the system protactinium could be isolated.[12] One way to control the system is to vary the "free fluoride equivalence" in the molten salt, defined as $N_{LiF} - 2N_{BeF_2} - 3N_{ThF_4}$; increasing this increases the separation factor relative to thorium.[175]

Of the transuranium elements, plutonium, californium, and americium are extracted well into bismuth, separable as a group from curium ($\alpha_{Cm}^{Am} = 7$), which in turn is separable from the lanthanides ($\alpha_{Nd}^{Cm} \simeq 200$).[175]

5.2. Distribution of Solutes Between Molten Borates and Molten Halides

As an illustration for the distribution of solutes between two immiscible molten salts, the molten alkali borate–halide system is of particular interest. It shows a high temperature (>800°C) application of solvent extraction and involves an ion exchange reaction, so that the molten borates can be classed as liquid cation exchangers.[179] Before discussing the distribution equilibria, it is expedient to complement here the data given in Table V on miscibility gaps in alkali oxide–boron oxide–alkali halide systems.

5.2.1. Alkali Oxide–Boron Oxide–Alkali Halide Systems

Alkali metal oxides are miscible with boron oxide and so are alkali metal fluorides, but the heavier halides are not, and it requires an appreciable concentration of alkali metal oxide in the boron oxide to bring about miscibility. The binary alkali metal (and alkaline earth) chloride–boron oxide systems have been studied by Kotlova, Olshanskii, and Tsvetkov.[180] The system is considered a binary since metathesis to give boron chloride and alkali metal oxide can be completely neglected. In the temperature range of study, 700–1000°C, the two reactions

$$2MCl + \tfrac{1}{2}O_2 \rightarrow M_2O + Cl_2 \qquad (50)$$

$$2MCl + H_2O \rightarrow M_2O + 2HCl \qquad (51)$$

with the atmosphere can cause a loss of chloride and contamination of the melt with alkali,[130,133] so that it seems to require special precautions to obtain valid data for alkali-free B_2O_3–MCl systems. The ternary systems $B_2O_3 - M_2O - MX$ were studied first by Stalhane (with M = Na and K for X = Cl at 850°C and M = Na for X = Br at 830°C)[181] and more recently by Dunicz and Scheidt (with M = Na and X = Cl at 800 and 980°C,[130] X = Br at 810 and 980°C,[131] and X = I at 980°C)[128] and less completely by Scheidt and Freiling (with M = Na + K and X = Cl at 830°C)[132] and by Rowell (with M = Na and X = Cl at 830°C).[37] A simplified diagram for the system B_2O_3–Na_2O–NaCl is shown in Fig. 2, where a two-liquid-phase region is seen, one being rich in borate and the other in chloride. The solubility of boron oxide in sodium chloride at 830°C is only 4×10^{-4} mole fraction.[37] In the following it will be convenient to use the mole fraction of sodium oxide referred to the oxides only in the borate-rich phase, $\bar{N}'_{Na_2O} = \bar{n}_{Na_2O}/(\bar{n}_{Na_2O} + \bar{n}_{B_2O_3})$, as the independent variable. As $\bar{N}'_{Na_2O}$ increases, the solubility of both boron oxide and sodium oxide in the sodium chloride melt remains negligible† in what may be called the "acid" region A up to $\bar{N}'_{Na_2O} \approx 0.17$, corresponding to $Na_2O: 5B_2O_3$. Above this point, in the "basic" region B, they increase parallely up to $\bar{N}'_{Na_2O} \approx 0.25$, that is, $Na_2O : 3B_2O_3$, so that the composition of the dissolving solute is $Na_2O : B_2O_3$ or that of the metaborate $NaBO_2$.[182] It is interesting to note at this context that the vapor pressure

† The fine structure of the solubility curve near the sodium chloride corner of the composition triangle cannot be seen in Fig. 2. The detailed study[130] shows a sharp maximum in the solubility at a composition corresponding to the octaborate, a compound with m.p. 816°C ($Na_2B_8O_{13}$ or $Na_2O \cdot 4B_2O_3$).

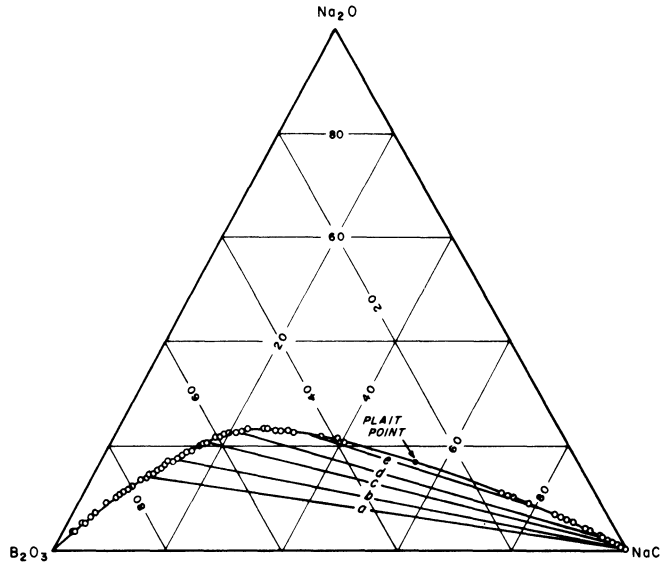

Fig. 2. The phase diagram of the sodium oxide–boron oxide–sodium chloride system at 830°C, in terms of mole fractions. Compositions along the tielines *a* to *e* separate into two liquid phases at the indicated compositions. Reprinted from Rowell[37] (Copyright 1964 by The American Chemical Society, reprinted by permission of the copyright owner).

of $RbBO_2$ above Rb_2O–B_2O_3 melts increases abruptly at the same composition[183] and the ultraviolet absorption edge shifts sharply to longer wavelengths as the Na_2O content in $Na_2O - B_2O_3$ melts passes through 15 mole %.[184] It should not be concluded from this that in region B, that is, above the ratio $Na_2O : 5B_2O_3$, the species $NaBO_2$ become important in borate melts (infrared spectra do not support the formation of new species at this point[185]) but that the pentaborate, which was a major constituent in region A, that is, up to this point, breaks down. Above $\bar{N}'_{Na_2O} \approx 0.25$ more boron oxide than sodium oxide enters the chloride phase, up to the plait point $\bar{N}'_{Na_2O} \approx 0.37$, where complete miscibility is obtained. Conversely, the solubility of sodium chloride in the borate phase (corresponding to electrolyte invasion into the exchanger phase) is appreciable even at low $\bar{N}'_{Na_2O}$ and increases with approximately the 1.3 power of it (from 2.5 mole % at $\bar{N}'_{Na_2O} = 0.05$) up to $\bar{N}'_{Na_2O} \approx 0.25$ and then increases rapidly toward the plait point. There is still a considerable composition range where the mutual solubility is low and where the distribution of solutes can give significant information regarding the structure of the melts.

The structure of borate melts has been discussed in several recent publications[186–188] and is related to that of borate glasses[189,190] and molten boron oxide.[191] In the following structural representations, the symbol (O/2) designates an oxygen atom shared between two boron atoms. As alkali oxide is added to boron oxide, the tridimensional network of the latter[189,191] breaks down in two parallel reactions:

$$B(O/2)_3 + \tfrac{1}{2}\,O^{2-} \begin{cases} \longrightarrow B(O/2)_4^- & (52a) \\ \longrightarrow B(O/2)_2O^- & (52b) \end{cases}$$

In reaction (52a) a completely oxygen-bridged tetrahedral borate anion is formed, in which the charge is diffusely distributed over the whole anion,[187,188] whereas in reaction (52b) the network is broken, and the charges are localized on a particular oxygen anion.[186] It has been argued from vapor pressure[185] and viscosity[192] data that at alkali oxide contents higher than the pentaborate composition $M_2O : 5B_2O_3$, the "basic" region B, the nonbridging grouping $B(O/2)_2O^-$ starts to predominate.[27] This tendency is strengthened in the ternary system, that is, the equilibrium $B(O/2)_4^- \rightleftarrows B(O/2)_2O^-$ is shifted to the right and cross-linking bridges are diminished in numbers, as more and more alkali halide invades the borate phase, and requires accommodation of the bulky halide ions. As the phase diagrams show, in region B the solubility of the larger halide ions does not increase as rapidly with increasing oxide content as it does in region A because of the preference of the "harder" $B(O/2)_2O^-$ ions for hard, high field strength cations rather than "soft" anions. Conversely, in region A the diffuse charge distribution is consistent with the presence of large, soft ions, and their preference for the borate phase increases as the cross-linking, that is, the bridging introduced by the alkali oxide, decreases.

5.2.2. Distribution Data

The above considerations are completely borne out by the distribution data, Table IX.[36,37] In region A the softer ions are preferred in the borate phase over the harder ones. When the data are extrapolated to $\bar{N}'_{Na_2O} = 0$, this trend becomes even more pronounced than appears in Table IX at $\bar{N}'_{Na_2O} = 0.05$. In addition to this selectivity, it also should be noted that in region A the distribution ratios are smaller than unity, so that the ions prefer the chloride environment over the bridged $B(O/2)_4^-$ environment. For an ion such as cesium, as $\bar{N}'_{Na_2O}$ increases, D first increases as ion exchange capacity is built into the borate phase by the oxide anions, but then it

TABLE IX. Distribution of Tracer Ions[37] in the B_2O_3–Na_2O–NaCl System at 830°C

Ion	Field strength z/r_c^2	log D in region A at $\bar{N}'_{Na_2O} = 0.05$	log D in region B at $\bar{N}'_{Na_2O} = 0.25$
Cs^+	0.36	−0.32	−0.56
Rb^+	0.46	−0.46	−0.49
K^{+a}	0.58	−1.0	−0.31
Na^{+b}	1.04	−1.00	−0.29
Ba^{2+}	1.17	−1.80	0.23
Sr^{2+}	1.51	−1.80	0.60
Ca^{2+}	2.17	−1.60	1.2
Nd^{3+}	3.06	−1.7	3.25
Eu^{3+}	3.19	−1.7	3.53
Cl^{-b}		−1.66	−0.85
$AgCl_n^{1-n}$		−2.15	−1.35

[a] Potassium is a bulk ion in experiments with B_2O_3–Na_2O–KCl systems where KCl is 54 wt % of the overall composition.[36]
[b] Sodium and chloride are bulk ions in all the experiments.

decreases, as bridging of tetrahedral $B(O/2)_4^-$ increases at the expense of the more open network of $B(O/2)_3$, so that bulky ions are squeezed out. The maximum for cesium is more pronounced than that for rubidium. The high-field ions show very low D values in this region.

As $\bar{N}'_{Na_2O}$ increases and more exchange capacity is built into the borate phase, high-field ions begin to show higher D values, even before the B region is reached. Selectivity reversals occur in the transition from the A to the B region, and very large D values are attained at $\bar{N}'_{Na_2O} = 0.25$—the larger they are, the higher is the field strength. Since mutual miscibility of the phases increases rapidly above $\bar{N}'_{Na_2O} = 0.25$ and complete miscibility is attained near $\bar{N}'_{Na_2O} = 0.38$, where necessarily all D values must extrapolate to unity, it is obvious that ions with $D > 1$ at $\bar{N}'_{Na_2O} = 0.25$ show a maximum around this composition. Rubidium and cesium, which have a maximum near $\bar{N}'_{Na_2O} = 0.10$, as explained above, with $D < 1$, have a minimum D around $\bar{N}'_{Na_2O} = 0.25$.

In addition to the ions shown in Table IX, available information shows americium[27,132] and curium[27] distribution curves similar to, but slightly below, those of the rare earths of similar size. Chloride anions are fairly efficiently excluded from the cation exchanger (borate phase), especially in the more highly cross-linked A region. The even bulkier complex chloro-

argentate anion is even better excluded. So are complex chlorocadmate anions, but as $\bar{N}'_{Na_2O}$ increases cadmium seems to prefer the borate over the chloride phase, and it has a distribution curve like that of barium, with a shallow maximum (that is, $D > 1$) near $\bar{N}'_{Na_2O} = 0.30$. This change in behavior has not been explained.[132]

Experiments at bulk concentrations demonstrate unequivocally that ion exchange takes place in these systems.[36] In the B_2O_3–Na_2O–KCl system it was found that potassium cations not only accompany chloride ions from the salt melt into the boron oxide–borate melt but exceed their concentration there considerably. This can occur only if the potassium ions displace sodium ions from the borate phase into the chloride phase. Indeed, these sodium cations have been found in the chloride melt and, again, at concentrations much higher than can be accounted for by accompanying borate. Such an exchange of sodium for potassium was found for all $\bar{N}'_{M_2O}$ values tested, from 0.05 to the plait point.

5.3. Distribution of Solutes Between Molten Nitrates and Aromatic Solvents

A considerable amount of work has been published by Zangen and by Marcus concerning the distribution of Group IIB metal halides between molten alkali nitrates and certain aromatic solvents.[29,39,150,193–199,207,208] The solvents used were a eutectic mixture of 37 wt % biphenyl, 48 wt % orthoterphenyl, and 15 wt % metaterphenyl as well as pure metaterphenyl. The former solvent has a liquidus point of 22°C and a solidus point of 12°C[31,193] has a vapor pressure less than 50 torr at 200°C,[200] and is stable for many hours at 150–200°C. For application at higher temperatures pure metaterphenyl, with melting point 87°C and boiling point 365°C, should be useful. The lithium nitrate (43 mole %) potassium nitrate (57 mole %) eutectic mixture, melting at 129°C, was used for most experiments, although pure lithium nitrate and several compositions of lithium–sodium, lithium–potassium, and sodium–potassium mixtures were also used.[29,39] The results obtained up to 1966 have already been reviewed[2] and are summarized here only briefly, while more recent results are reviewed in greater detail.

5.3.1. Mercury(II) Halides

Mercury(II) chloride, bromide, and iodide were found to be stable species in alkali nitrate melts, that is, not to undergo dissociation or disproportionation, even in the absence of excess halide.[29] Their distribution constants increase with the atomic number of the halide and with decreasing

temperatures (in the range of 200–150°C). For the reaction

$$HgX_2 \text{ (in salt melt)} \rightleftarrows \overline{HgX_2} \text{ (in aromatic solvent)} \qquad (53)$$

the values of the thermodynamic functions are (in kilocalories per mole): X = Cl, $\Delta G^* = -1.42$, $\Delta H^* = 3.7$; X = Br, $\Delta G^* = -2.55$, $\Delta H^* = 2.3$; X = I, $\Delta G^* = -3.75$, $\Delta H^* = 2.1$. The distribution constants reported previously on a weight basis[2,29] were converted to a mole fractional basis fractional basis for the purpose of calculating ΔG^* by the equation[39]

$$D_{(N)} = D_{(w)} \left(\frac{w_{\text{biph}} + w_{\text{terph}}}{w_{\text{biph}}/M_{\text{biph}} + w_{\text{terph}}/M_{\text{terph}}} \right) (N_{LiNO_3} M_{LiNO_3} + N_{KNO_3} M_{KNO_3}) \qquad (54)$$

The average value of ΔS^* for the three halides, from equation (23), $+12 \pm 2$ cal/deg mole, is rather large, but because of the uncertainty of *ca.* 0.6 kcal/mole in ΔH^* compared with *ca.* 0.04 in ΔG^*, it is impossible to give any significance to the apparent low value for the bromide compared with the chloride and the iodide. The large entropy change shows that mercury halides in the salt melt produce more order than in the aromatic solvent, which is consistent with the view that it is solvated by nitrate anions in the salt melt.[29,150]

The stability of mercury mixed dihalide complexes has now been studied at several temperatures (165, 180, and 200°C)[198] besides the work at 150°C published previously.[194] It was found that the relative destabilization of the species $HgClI(NO_3)_2^{2-}$ and $HgBrI(NO_3)_2^{2-}$ noted at the lower temperature does not persist at the higher ones (Fig. 3). There is no good explanation for

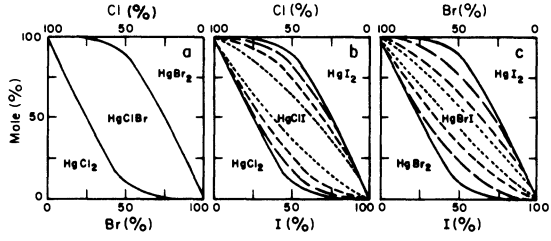

Fig. 3. The dependence of the areas of existence of mixed mercury dihalide species in lithium–potassium nitrate melts on the ratio of the two halide ions (a: chloride–bromide, b: chloride iodide, and c: bromide iodide) and on the temperature [(. . .), 150 °C; (– – –), 165 °C; (— — —), 180 °C; and (———), 200°C]. From Zangen[198] (by permission of Pergamon Press, Ltd., London).

the instability against disproportionation of the above-mentioned species at the lower temperature and for their stabilization as the temperature increases, on the one hand, and for the relative stability of $HgClBr(NO_3)_2^{2-}$ and $HgI_3(NO_3)^{2-}$ at all the temperatures studied on the other band. The contrasting behavior of the corresponding cadmium species (Section 5.3.2) also is puzzling. The large size of the iodide ion, the loosening of the melt structure as the temperature increases, and the degree of covalency of the mercury–halide bonds as the atomic number of the halide increases have probably all to do with the observed phenomena. More specific explanation that have been advanced[2,194,198] are likely to be oversimplified.

The formation of binary mercury halide complexes[29] and ternary (mixed) complexes[194,195] in the alkali nitrate melts, as studied by the distribution method, has been reviewed,[2,201] and the kinetics of the distribution reaction and species interconversion reactions in the salt melt have been discussed earlier in this chapter (Section 4). It is of interest to discuss here the next-nearest-neighbor interactions in which the mercury halides are involved in the alkali metal nitrate melts. Figure 4 shows a schematic representation of a portion of the melt in the vicinity of a mercury diiodide species. The strongly covalent nature of the mercury–iodine bond manifests itself in the negligible effect that the alkali metal cations have on the species

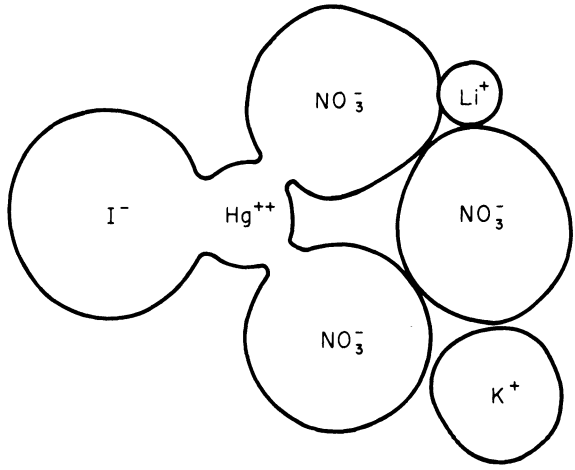

Fig. 4. A schematic representation of mercury iodide in a lithium–potassium nitrate melt. The deformation of the spheres representing ions are intended to suggest polarization effects. Because of the tetrahedral arrangement of the ligands around the mercury ion, the second iodide ion is hidden behind the depicted one.

TABLE X. Thermodynamic Functions of Transfer of Mercury(II) Iodide from Metaterphenyl to Alkali Metal Nitrate Melts at 270°C[39]

N_{Li}	N_{Na}	N_K	ΔH^* (cal/mole)	ΔG^* (cal/mole)	ΔS^* (cal/deg-mole)
1.0			−660	+2280	−5.4
0.5	0.5		−260	+3840	−7.5
0.5		0.5	+110	+4820	−8.7
	0.5	0.5	+220	+3920	−6.8

HgI_4^{2-}. This is seen in the independence of the distribution coefficient D_{Hg} from the lithium-to-potassium ratio in the range 50–65 mole % potassium when 0.5 m excess iodide is present and the species HgI_4^{2-} predominates. The mercury–nitrate bond in the species $Hg(NO_3)_2I_2^{2-}$ however, is, affected by the variation in the lithium-to-potassium ratio, as is shown by a change of D_{Hg} by a factor of three in the above range.[29] Since the nearest neighbors to the mercury atom are the iodide and the nitrate anions, the effect of the alkali metal cations is a next-nearest-neighbor effect, and this has been studied recently in detail.[39] The transfer of mercury iodide from a dilute solution ($\bar{N}_{HgI_2} \approx 2 \times 10^{-4}$) in metaterphenyl into alkali metal nitrates and their mixture was studied from somewhat above their melting points to ~300°. The enthalpy of transfer at 270°C, ΔH^* obtained according to equation (22), and the free energy of transfer, $\Delta G^* = +2.303\,RT \times \log D_{Hg(N)}$, are shown in Table X for lithium nitrate and for equimolar mixtures of lithium–sodium, lithium–potassium, and sodium–potassium nitrates (the melting points of sodium and potassium nitrates were too high for the experimental setup used). Table X shows, again, that a considerable amount of entropy is lost when the mercury iodide changes its aromatic solvent environment to the one occurring in the nitrate melt and that heat may be lost or gained. These results can be explained qualitatively as follows: It is known[202-204] that lithium cations strongly polarize the nitrate anion, and this effect decreases with sodium and potassium. This polarization causes some "order" in the lithium nitrate melt, so when mercury iodide is transferred into it and becomes solvated by the two nitrate anions (Fig. 4), the additional order produced thereby is not as large as when the nitrate melt is initially less ordered, as in the equimolar mixtures. More and more ordering is produced as the difference in polarizing power (proportional to z/r^2) between the two cations increases, since the smaller cation prefers to be located near the large $HgI_2(NO_3)_2^{2-}$ anion. As regards the energy bal-

ance, there could be three processes that would be able to produce the values shown in Table X. One would be the bending of the linear mercury iodide molecule to give the tetrahedral configuration of $HgI_2(NO_3)_2^{2-}$ and is endothermal. Another is solvation of the mercury iodide by the nitrate ions, which is exothermal. The third is the difference in the energies of polarization of two nitrate anions and of the large, soft anion $HgI_2(NO_3)_2^{2-}$ by the cations. This is exothermal—the more so, the harder the cations. Now if the first process is dominant in the sodium–potassium nitrate system and the last in the lithium nitrate system, the sequence of values from $\Delta H^* = +220$ to $\Delta H^* = -660$ cal/mole can be rationalized. That several competing processes occur is evident from the nonlinear dependence of ΔG^* on N_{M+} (Fig. 5), leading to maxima in the lithium-containing systems. A detailed next-nearest-neighbor interaction theory is required to base the above rationalization on firmer grounds.

A further complication is the observation of sharp minima in the curves showing the dependence of D on T, at about 10 to 30°C, above the melting point of the nitrate mixture.[30] (The values shown in Table X and Fig. 5 are well above these minima.) This phenomenon points to sharp structural changes in the molten mixtures just above the melting points. Therefore there might be some justification to compare the melts not isothermally but "isostructurally," that is, at temperatures such as 1.1 T_{melt} or at $T_{melt} + 50$°C. At the latter temperatures, the maxima exhibited by the plot in Fig. 5 are even more pronounced than at $T = 543$°K.

It is thus seen that more experimental information should be helpful and that data for pure sodium and potassium nitrates, and another alkali metal nitrate such as that of cesium, and their mixtures should be obtained. These melt higher than the present limit of 300°C but probably could still be studied with the solvent metaterphenyl, boiling at 365°C. The wider range of temperatures also would permit greater precision for the determination of ΔH^* and ΔS^*.

5.3.2. Cadmium(II) Halides

It may have been expected that the three Group IIB metals, mercury (discussed above), cadmium, and zinc (discussed further below), would show essentially similar behavior in their halide complexes in nitrate melts or at least would show properties varying directly with the atomic number. It appears, however, that cadmium shows exceptional behavior in some respects,[199] reminiscent of such peculiarities in fourth-row elements in

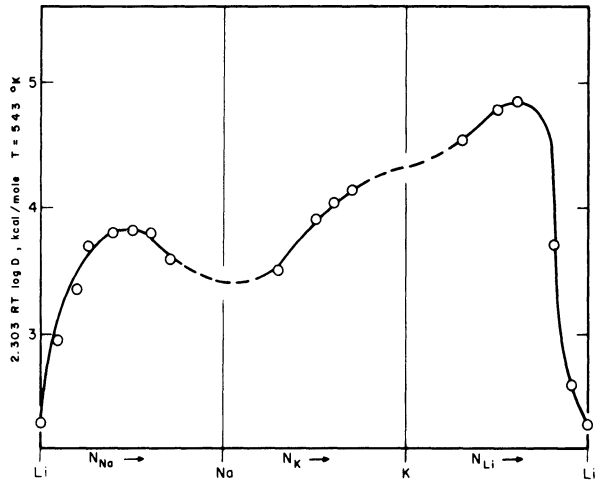

Fig. 5. Free energies of transfer of mercury iodide from a metaterphenyl solution ($\bar{N}_{HgI_2} \simeq 2 \times 10^{-4}$) into alkali metal nitrate melts, as a function of their composition, at 270°C. From Marcus and Zangen[39] (by permission of the International Atomic Energy Agency, Vienna).

other solvents[205,206] and possibility connected with their greater reluctance to forsake the octahedral form and take on tetrahedral coordination.

The distribution of cadmium(II) between the polyphenyl and potassium–lithium nitrate eutectics described on p. 104 has been studied at four temperature between 150 and 200°C as a function of halide molality ($m_X < 0.7$) in the nitrate melt.[199] Since the stability of the first two complexes $CdX(NO_3)_n^{1-n}$ and $CdX_2(NO_3)_n^{n-}$ is relatively low (compare the values in Table XI with those in Table 5 of Marcus,[2] where K_1 and K_2 are $> 10^7$ for all mercury and zinc halide complexes), it also was possible to work at concentrations such that $m_X < m_{Cd}$ in order to obtain their stability con-

TABLE XI. Equilibrium Constants[a] for Cadmium(II) Halide Complexes at 150°C

X	K_1	K_2	K_D	K_3	K_4
Cl	1900	940	0.0049	2.8	2.0
Br	7900	3200	0.0091	3.0	2.2
I	18000	7500	0.0132	3.2	2.3

[a] Molal scale; $K_i = [CdX_i(NO_3)_{n-i}] / [CdX_{i-1}(NO_3)_{n+1-i}] [X^-]$ and $K_D = [\overline{CdX_2}] / [CdX_2(NO_3)_{n-2}]$; precision of K_i for $i = 1$ or 2 is $\pm 10\%$, for $i = 3$ or 4, $\pm 15\%$, and for K_D, $\pm 5\%$.

stants. Thus the regions of low and of high halide concentrations could be treated separately, that is, the first two or the last two terms in the denominator of equation (55) could be neglected in each case.

$$D = K_D/(K_1^{-1}K_2^{-1}m_X^{-2} + K_2^{-1}m_X^{-1} + 1 + K_3m_X + K_3K_4m_X^2) \qquad (55)$$

The values of the constants thus obtained are shown in Table XI. The species $CdX_2(NO_3)_n^{-n}$ has a fairly wide range of existence in the salt melt, but contrary to the corresponding zinc and mercury species it is much less extractable into the polyphenyl phase. This might be due to n being larger than two so that the species interacts more strongly with the cations in the melt and is held there. The enthalpy of complexation is negative for all the equilibria involved in Table XI, though for the distribution constant it is very small indeed and for K_3 and K_4 it is also rather small. The approximate independence of K_3 and K_4 from the nature of X should be noted: It contrasts sharply with the behavior of zinc (see Section 5.3.3) and, also, but less sharply, with that of mercury. As has been argued in the case of mercury,[29] the near equality of K_3 and K_4 suggests that one deals here with replacement reactions of solvating nitrate anions by ligand halide rather than with addition reactions of ligand anions to a nonsolvated species CdX_2.

The mixing constants for the reaction

$$CdX_2 + CdY_2 \rightleftarrows 2CdXY \qquad (56)$$

could not be obtained with any precision from the distribution data, because in these systems K_D for the mixed complex happens to be very near the geometric mean of those for the binary complexes.[201] Estimated values of 25 ± 15 for these constants for both phases and irrespective of the nature of X and Y were found to be consistent with the distribution data.[199]

5.3.3. Zinc(II) Halides

The distribution of zinc(II) halides between the polyphenyl and the lithium–potassium nitrate eutectics has been reported by Zangen in several recent papers.[151,152,197,207] The kinetics of the distribution reaction have been discussed in Section 4, while the formation of binary and mixed complexes has been recently reviewed,[2,201] so that it is unnecessary to discuss them here in detail. It was found that whereas the first two halide complexes are very strong in the nitrate melts, zinc forms the trichloro, tetrachloro, and tribromo species rather reluctantly, and below $1m$ halide in the melt it does not form the tetrabromo and the tri- and tetraiodo species at all.[152]

As far as the mixed dihalide species are concerned, they are formed in the melt at 200°C as expected, but the reactions analogous to (56) have such large negative standard enthalpies (-43 ± 20 kcal/mole) that they are largely inhibited at 150°C.[197] The mixed trihalides are all formed except for $ZnBr_2I(NO_3)^{2-}$ [and $ZnBrI_2(NO_3)^{2-}$ is formed only at 180°C, not at 150°C], while of the mixed tetrahalo complexes, bromo-iodo species are not formed, and of the chloro-iodo, only those containing at least two chloride ions are formed.[207,208] The zinc ion is probably too small and too hard to accommodate around it more than two iodide or three bromide ions.

5.4. Extraction from Molten Salts with Long-Chain Amine Salts

Long-chain amine salts were first used for extraction from ionic melts by Taube and Borkowska[209] and later by them and Mielcarsky.[33] Their extractant was rather unusual: $(C_8H_{17})_3NCu^+Cl^-$, that is, a "copper(I)-ated" instead of the regular protonated onium salt, in biphenyl as a diluent. The molten salt also was unusual: a copper(I)-potassium chloride eutectic—but this permitted work with molten chlorides at the low temperature of 180°C. (The lowest-melting alkali metal chloride eutectic is the lithium potassium one, melting at 352°C.[128]) A rather low temperature is necessary since tertiary amine salts are thermally not very stable. The thermal stability of normal long-chain amine salts has recently been studied.[210] It was concluded that it parallels their melting points so that it decreases with chain length and in the order $Cl^- > HSO_4^- > NO_3^-$ and secondary > primary > tertiary. Secondary dodecylamine nitrate, chloride, and bisulfate showed no decomposition for 3 hr at 200, 230, and 230°C, respectively. At higher temperatures, where most molten salts must be used, rapid decomposition occurred. Therefore, attempts to use long-chain amine salts have concentrated on low-melting salts, particularly nitrates and thiocyanates.

5.4.1. Extraction from Molten Ammonium Nitrate Dihydrate

Molten hydrated salts have been recognized as a special but legitimate subdivision of molten salts, provided the water is closely associated with the ions (generally the cations) and is not "free," that is, it does not constitute a nonionic dielectric medium as it does in the region of concentrated aqueous solutions. Hydrated ammonium nitrate has been the subject of several studies by the emf and solubility methods,[211–213] the range of temperatures available being from 40°C, the melting point of the dihydrate,

to above 170°C, that for anhydrous ammonium nitrate, above which it rapidly decomposes.

Extraction with tetraheptylammonium nitrate, 2×10^{-4} to 0.1 *m* in the diluent 55 mole % biphenyl–45 mole % naphthalene, was applied by Nikolič and Gal[214,215] to molten ammonium nitrate dihydrate at 55, 70, and 85°C. The distribution of tracer chloride, bromide, perrhenate, and silver ions (the latter in the presence of 5×10^{-2} *m* chloride or 1×10^{-2} *m* bromide, that is, as $AgCl_2^-$ and $AgBr_2^-$, respectively[211]) was studied. The order of extractability at a given concentration of the organic extractant is $Cl^- < Br^- \ll AgCl_2^- < ReO_4^- < AgBr_2^-$. At extractant molalities below 10^{-2}, *D* depends linearly on $\bar{m}_{(C_7H_{15})_4NNO_3}$, signifying the occurrence of the anion exchange reaction

$$NH_4^+X^- + \overline{(C_7H_{15})_4NNO_3} \rightleftarrows NH_4^+NO_3^- + \overline{(C_7H_{15})_4NX} \qquad (57)$$

Values of ΔH^* (in kilocalories per mole) for this reaction that could be evaluated from the data are −4.5 for $X = ReO_4$ and −9.7 for $X = AgBr_2$, showing that the distribution coefficients would be lower at 55 to 85°C than they are at room temperature[216] from similar solutions. The values of the distribution coefficients at $\bar{m}_{(C_7H_{15})_4NNO_3} = 5 \times 10^{-2}$, the equilibrium constants for reaction (57), and the derived values of ΔG^* and ΔS^* at 70°C are shown[214] in Table XII.

Nikolič and Gal[214] compared the values of *K* obtained for equilibrium (57) with values calculated from a Born cycle, in which NH_4^+ and X^- are

TABLE XII. Equilibrium Data for Extraction from Molten Ammonium Nitrate Dihydrate

Anion	*D* (kg melt/kg solvent)[a]			*K*[b]	ΔG^{*b} (kcal/mole)	ΔH^* (kcal/mole)	ΔS^{*b} (cal/mole-deg)
	55°C	70°C	85°C				
Cl^-		2.3×10^{-4}		~0.05	+2		
Br^-	4.9×10^{-3}	4.9×10^{-3}	4.6×10^{-3}	1.2	−1.2		
$AgCl_2^-$		1.25		190	−3.6		
ReO_4^-	5.5	3.8	2.8	430	−4.1	−4.5	−1
$AgBr_2^-$	185	86	65	1.8×10^4	−6.7	−9.7	−9

[a] Obtained at $\bar{m}_{(C_7H_{15})_4NNO_3} = 0.05$.
[b] At 343°K.

transferred from the molten salt to the gas phase and then transferred to the organic phase; there the X^- ion pairs with $(C_7H_{15})_4N^+$ cations, and NO_3^- travels the same way in reverse order. Because of uncertainties in the radii used, and in particular since the combination $A(1 - 1/n)$, where A is a "Madelung constant" for the melt and n is the repulsive potential exponent, is essentially a free parameter, the agreement between the calculated and the experimental values of K obtained can be used only in a qualitative sense, as predicting the size effect. This limitation has been stated by the authors themselves. The main criticism against this computation, however, is that the presence of the hydration water has been completely ignored, whereas its interaction with both cations and anions in molten hydrated salts should certainly be recognized.[217]

The distribution of the silver halide complexes was interpreted in terms of the formation of AgX and AgX_2^- in the salt melt, and of $\overline{(C_7H_{15})_4NAg(NO_3)_2}$, $\overline{(C_7H_{15})_4NAgX(NO_3)}$, and $\overline{(C_7H_{15})_4NAgX_2}$ in the organic phase,[215] from experiments where D_{Ag} was measured as a function of m_X. Since the total amine salt concentration in the organic phase was constant at 0.01 m in these experiments, it was assumed that only its monomers need be taken into account, but this is contrary to the observation that at even higher temperatures, and at as low concentrations as $> 10^{-3}$ m, at least dimers of the extractant are present. Notwithstanding, it was also assumed that a constant distribution quotient can be used for each of the three species in the organic phase, D_i, according to the number $i = 0$, 1, or 2 of halide ions in the complex. From the resulting equation

$$(D - D_0)[(K_1 m_X)^{-1} + 1 + K_2 m_X] = (D_1 - D_0) + (D_2 - D_0)K_2 m_X \quad (58)$$

the stability constants (on the molal scale) $K_1 \sim K_2 \sim 10^2$ for X = Cl and $K_1 = 5 \times 10^3$ and $K_2 = 1 \times 10^3$ for X = Br were obtained, in agreement with values obtained by the solubility method.

5.4.2. Extraction from Molten Alkali Metal Nitrates

Gal and co-workers[35] examined in addition to ammonium nitrate dihydrate melts also the lithium–potassium nitrate melt with respect to extraction with tetraheptylammonium nitrate solutions in the polyphenyl diluent. This permitted the use of a higher temperature, 150°C, at which the crystalline extractant is relatively stable (0.6 ± 0.5% of weight and assay was lost in 1 hr).

For the extraction of chloride, experiments were made in the range 0.06–1.0 m_{Cl} and 0.001–0.1 $\bar{m}_{(C_7H_{15})_4NNO_3}$. The concentration on the molal

scale of the extractant monomer $\overline{[(C_7H_{15})_4NNO_3]}$ was calculated from independent experiments (from the perrhenate distribution, see below), and it was found that D_{Cl} was proportional to it at a constant m_{Cl}. It was concluded that species such as $\overline{[(C_7H_{15})_4NCl]_2}$ and

$$\overline{(C_7H_{15})_4NCl \cdot (C_7H_{15})_4NNO_3}$$

can be neglected,† so that the dependence of D_{Cl} on N_{Cl} is due to changing activity coefficients at the higher chloride concentrations. Assuming regular solution behavior, equations (57) and (34) lead to

$$\frac{\log D\, m_{(Li,K)NO_3}}{\overline{[(C_7H_{15})_4NNO_3]}} = \log K = \frac{2\lambda_{(Cl,NO_3)}N_{Cl}}{2.303RT} \tag{59}$$

from which the value $\lambda_{(Cl,NO_3)} = 1.65$ kcal/mole is obtained for the interaction parameter in lithium–potassium chloride–nitrate mixtures. This is also the standard free energy of transfer of chloride from (hypothetical, supercooled at 423°K) lithium–potassium chloride to the infinitely dilute state in lithium–potassium nitrate. Since 2.1 ± 0.2 is the value of K for the latter reference state, the value 0.43 ± 0.04 given for the former standard state must be a misprint, as the correct value is a factor of ten smaller, 0.043.

In the extraction of perrhenate, the participation of the species $\overline{(C_7H_{15})_4NReO_4 \cdot (C_7H_{15})_4NNO_3}$ is demonstrated by the curvature of the distribution curve, log D against log $\overline{[(C_7H_{15})_4NNO_3]}$, that is, the monomer concentration.[35] This was obtained from the expression

$$\bar{m}_{(C_7H_{15})_4NNO_3} = \overline{[(C_7H_{15})_4NNO_3]} + 2K_d\overline{[(C_7H_{15})_4NNO_3]^2} \tag{60}$$

(neglecting the fraction of the extractant bound to the perrhenate, at the low concentrations of the latter used), and the dimerization constant K_d was adjusted, so that the distribution data for chloride, perrhenate, and dichloroargentate could be accommodated. Unfortunately, independent data available on the aggregation of long-chain amine salts at the temperatures involved here[218,219] do not pertain to the particular extractant used, nor can low-temperature data,[216] which do, be extrapolated to the higher tem-

† Although there is no doubt that this conclusion is warranted by the data, it is not easy to explain why these species, or those containing $AgCl_2^-$, are not formed in view of formation of corresponding species with perrhenate instead of chloride or of dichloroargentate.

perature to provide an independent check on $K_d = 50 \pm 5$ obtained in the above way. This procedure then leads to $K = 420 \pm 20$ for the appropriate anion exchange reaction (57) and to a constant for the mutual association of the perrhenate and the nitrate ion pairs in the organic phase $K = 60 \pm 12$. From experiments at 140 to 160°C, extrapolated to zero extractant concentration, ΔH^* for the anion exchange reaction (57) was found to be -12 kcal/mole.

In the extraction of silver from chloride-containing nitrate melts, it was demonstrated that two chloride ions accompany each silver ion into the organic melt, beyond the chloride that is extracted independently.[35] Over the range 3×10^{-4} to 3×10^{-2} in $\bar{m}_{(C_7H_{15})_4NNO_3}$, D_{Ag} was found to be proportional to the extractant monomer concentration, as is the case with chloride discussed above, so that $\overline{(C_7H_{15})_4NAgCl_2}$ is the only silver species important in the organic phase (but see footnote on p. 114). The dependence of D_{Ag} on m_{Cl} (or N_{Cl}) was interpreted in terms of the successive equilibria forming $AgCl_2^-$ in the nitrate melt $K_1 = 310$ and $K_2 = 125$ on the molal scale, in the range of m_{Cl} from $3 = 10^{-3}$ to 6×10^{-2}. The data at higher m_{Cl}, up to 1.0 m, were interpreted in terms of activity effects, leading however to an improbably large interaction parameter (more than 10 kcal/mole for the difference in interaction parameters of $AgCl_2^-$ with nitrate and with chloride). Because of this difficulty at the higher concentration range, the value of K_2 obtained at the lower range also may need revision.

The extraction of lanthanides from the lithium–potassium nitrate eutectic with dioctylammonium nitrate in tetralin at 150°C[220,221] showed distribution coefficients increasing appreciably with their atomic number. Lutetium showed first power dependence of D on $\bar{m}_{(C_8H_{17})_2NH_2NO_3}$, while lanthanum, samarium, gadolinium, and terbium showed second power dependence, in the range of 0.01 to 0.20 m. Since the aggregation of the amine salt in the organic solvent[218,219] was neglected, the interpretation given[221] of the distribution data in terms of the number of extractant molecules associated with each lanthanide nitrate probably needs reconsideration.

5.4.3. Extraction from Molten Alkali Metal Thiocyanates

A number of alkali metal salts, such as nitrates, nitrites, bisulfates, chlorates, and thiocyanates, form low-melting eutectics,[28] but only a few of these anions are known to give thermally stable amine salts.[210] Thiocyanates form reasonably stable dialkyl and tetraalkyl salts[219] and have been used to extract some lanthanides, cobalt(II), and the perrhenate anion

from the molten sodium–potassium nitrate eutectic (70 mole % KSCN, m.p. 123°C).

Attempts to extract cobalt(II) with dioctylammonium thiocyanate in tetralin showed rapid catalytic decomposition, with precipitation of cobalt sulfide. When 1-chloronaphthalene was used as a diluent, decomposition was less rapid, and an absorption spectrum that could be attributed to $Co(SCN)_4^{-2}$ could be observed in the organic phase. However it was impossible to obtain quantitative distribution data.[219]

The extraction of perrhenate with either dioctyl- or tetraisopentylammonium thiocyanate gives reproducible distribution data. Preliminary data showed that, as in the case of the nitrate system, aggregation of the extractant and participation of perrhenate anions in mixed aggregates must be taken into account. Vapor pressure data on the organic solute–diluent systems, obtained by differential thermal osmometry, are useful for the interpretation of the distribution data.[219]

The distribution of terbium, holmium, thulium, and lutetium between the thiocyanate salt eutectic and solutions of dioctylammonium thiocyanate in tetralin has been studied as a function of the extractant molality at 150, 170, and 190°C.[222] The distribution coefficients depend strongly on the atomic number of the lanthanide, the separation factors relative to terbium being at 170°C and $\bar{m}_{(C_8H_{17})_2NH_2SCN} = 0.1\ m$: $\alpha_{Tb}^{Ho} = 11$, $\alpha_{Tb}^{Tm} = 26$, and $\alpha_{Tb}^{Lu} = 130$. In plots of log D against log $\bar{m}_{(C_8H_{17})_2NH_2SCN}$ the slopes obtained were between 1.0 and 1.4, the initially linear curve bending down above 0.1 m extractant. The distribution data could be fitted to the equation

$$D = K_1\alpha\bar{m}_{(C_8H_{17})_2NH_2SCN} + K_2\alpha^2\bar{m}^2_{(C_8H_{17})_2NH_2SCN} + K_3(1 - \alpha)\bar{m}_{(C_8H_{17})_2NH_2SCN} \tag{61}$$

where α is the fraction of the monomer, using the values $K_d = 1.0 \pm 0.3$ [cf. equation (60)], $K_3 \simeq K_1$, and $K_2 \simeq 10 \times K_1$, the values of K_1 increasing from 0.07 for Tb to 7 for Lu (at 170°) and decreasing about fivefold from 150 to 190°C. The best extracted lanthanide (lutetium) at the highest extractant concentration used (0.165 m) and the lowest temperature (150°C) gave $D \sim 4$, which is somewhat lower than what obtained in the nitrate system under comparable conditions ($D \sim 10$).

5.5. Miscellaneous Systems Recently Studied

The survey in Sections 5.1 to 5.4 deals with selected distribution systems, falling into four categories according to the liquid phase opposing the molten salt phase. These are a liquid metal, for which bismuth serves as an illustra-

tion; a molten salt–sodium borate and boron oxide; a more or less inert hydrocarbon; and a diluted extractant— long-chain amine salts. Although the publications in the field of extraction from molten salts are not numerous, several reports, which could not be covered by the systems used to illustrate the categories described above, were recently published and merit review.

The category of extraction with liquid metals encompasses many metals besides bismuth (see Table I). Molten uranium has been used in an extractive oxydation–reduction system, where plutonium is transferred between it and molten calcium chloride:

$$\overline{Pu}[\text{in U}(l)] + UCl_3[\text{in } CaCl_2(l)] \rightleftharpoons PuCl_3[\text{in } CaCl_2(l)] + \overline{U}(l) \qquad (62)$$

The equilibrium constant is 189 (at 1200°C)[223] or 187 (at 1150°C) and 203 (at 1200°C)[224] in the concentration range of 0.2–4.2 wt % plutonium. With plutonium metal as the liquid extracting solutes from a molten salt, sodium–potassium chloride eutectic at 700–780°C, containing 0.6–2.0 mole% plutonium trichloride, the equation analogous to (62) gave distribution data for americium consistent with $PuCl_3$ and $AmCl_2$ as the species in the molten chloride phase.[20] A close examination of the data shows that they do not exclude other possible species, such as $PuCl_4$ and $AmCl_3$ or in general plutonium(III to IV) and americium(II to III), without specifying the number of chloride ions associated directly with the actinide cations in a melt where chloride anions would in any case be the nearest neighbors of metal cations. Thus the distribution data cannot be construed as proving the existence of otherwise unknown compounds (such as $AmCl_2$ or $PuCl_4$).

The metals magnesium, zinc, and cadmium and their alloys (including those with copper) also have been used as the extracting liquids with melts, such as 50 mole % $MgCl_2$, 30 mole % NaCl, 20 mole % KCl; 50 mole % $CaCl_2$, 50 mole % $MgCl_2$; 47.5 mole % $CaCl_2$, 47.5 mole % $MgCl_2$, 5 mole % CaF_2; 59 mole % LiCl, 41 mole % KCl; 50 mole % $MgBr_2$, 30 mole % NaBr, 20 mole % KBr; and x mole % $CaCl_2$, x mole % NaCl, $(100 - 2x)$ mole % $MgCl_2$.[224,225] Typical temperatures used are 600–750°C. As an oxidant, cadmium chloride is effective, but when cadmium metal is the extractant, cadmium(I) species are formed, which are solvated by excess cadmium(II) chloride, namely, $Cd(CdCl_2)_2^+$ or Cd_3^{+5}, the solubility of the cadmium increasing from (Li, K)Cl to LiCl to (Mg, Na, K)Cl melts. Changing from chloride to bromide melts produces small effects on the distribution of solutes. When at 600°C 10 wt % magnesium in cadmium was used in the ternary (Mg, Na, K) halide melts, the value of $D_{Pr(N)}$

decreased and $D_{U(N)}$ and $D_{Pu(N)}$ increased somewhat when bromide replaces chloride, while if $D_{Pr(w)}$ is considered, the difference in formula weights of the molten salts makes it increase.[224] A much more profound effect is caused by changing the metal with which the magnesium is alloyed in the molten metal phase, replacing the cadmium with zinc or with copper: at 600°C and 30 mole % Mg α_{Pu}^{Pr} varies from 25 to 80 to 280.[225] A salt transport process has recently been described in detail[226] where uranium is transported from a donor alloy, via a magnesium choride-containing melt, to an acceptor alloy. The considerations discussed above are found to be important for such a process, too, of course. These effects are all connected with the interactions of the solutes in the molten salt and the molten metal phases, which can be, and have been, expressed formally in terms of activity coefficients. These quantities by themselves do not explain the effects and, since they cannot be derived theoretically yet, have no predictive value as regards new distribution systems.

The category of molten salt–molten salt distribution systems includes many others besides boron oxide.[2] A recent publication by Ammon[34] on the aluminium–potassium bromide system that shows a miscibility gap (system 10 in Table III) complements earlier results of Moore[26] on the aluminium–potassium–lithium chloride system (1 in Table III), as regards the distribution of solutes. The data are compared in Table XIII, and at a first glance only a weak correlation between the chloride and bromide systems in seen. There are obvious reversals in preference, cesium being a glaring case. However, it must be noted that the difference between the two phases in the bromide system is much smaller than in the chloride one and that the more "ionic" phase in the former is as soft as the more "covalent" phase in the latter. The principle that soft solutes prefer the softer environment and the hard ones the harder solvent is kept in the examples in Table XIII. Some of the hard ions form strong halide complexes that are soft, like iron(III), zirconium, uranium(IV), and plutonium(IV), and therefore find themselves in the "wrong" phase. There are a few cases that are difficult to explain even with these considerations [cf. tellurium(IV), which seems to be hard in the bromide system], and more complete data would have been very helpful.

The category of extracting solutes from molten salts with organic extractants recently has been enriched by the work of Vittori,[30] who extracted cobalt and nickel from the lithium–potassium nitrate eutectic at 160°C with solutions of extractants in a polyphenyl diluent. The extractants were triphenylphosphine, triphenylphosphine oxide, triphenylarsine, and triphenylarsine oxide, and the diluent was biphenyl 27%, orthoter-

TABLE XIII. Distribution of Solutes Between the Immiscible Phases in Aluminium Halide–Alkali Metal Halide Systems

Solute	log D	
	$LiCl–KAlCl_4$[a]	$KAlBr_4–AlBr_3$[b]
Cs^{I}	1.26[c]	−1.75
Na^{I}	−0.25	
Ag^{I}		−1.18
Ba^{II}		−1.69
Sr^{II}	−1.85	
Co^{II}		−0.30
Fe^{II}	−0.12	
Sn^{II}	−0.05	
Ru^{II}	−0.62	
Ru^{III}		−0.48
Fe^{III}	0.96	
Ce^{III}	−1.05	−1.18
Pu^{III}	−1.6	
U^{III}	−1.6	
Pu^{IV}	0.28	
U^{IV}	0.21	−0.60
Zr^{IV}		0.35
Te^{IV}		−0.73
Nb^{V}		−0.29
Mo^{V}		0.15
Ta^{V}		0.05
U^{VI}	−0.08	

[a] At 625°C; "ionic" phase is 84 mole % LiCl, 15 mole % KCl, and 1 mole % $AlCl_3$; "covalent" phase is 90 mole % $KAlCl_4$, and 10 mole % LiCl; concentration of solute is extrapolated to zero.

[b] At 200°C; "ionic" phase is 19 mole % KBr and 81 mole % $AlBr_3$; "covalent" phase is 99.6 mole % $AlBr_3$, and 0.4 mole % KBr; concentration of solute 0.5–1.0 wt %.

[c] At macroconcentrations of cesium, so that the "covalent" phase is mainly $(Cs, K)AlCl_4$.

phenyl 54%, and metaterphenyl 18% (it was not specified whether mole or wt % were meant, and this diluent is different in composition from the one used in many other studies, p. 104). It was found that triphenyl-phosphine and triphenyl-arsine do not extract by themselves; that they do, however, on addition of acetic acid, but that they are converted in the process to the corresponding oxides. Triphenylphosphine oxide extracts $Co(NO_3)_2 \cdot [(C_6H_5)_3PO]_2$ and $CoCl_2[(C_6H_5)_3PO]_2$, as found from the absorption spectra of the organic phases, from the dependence of D on the extractant concentration, and from saturation of the extractant with cobalt(II). As

potassium chloride is added to the nitrate melt, the extraction of cobalt decreases, since the cobalt chloride species has a smaller distribution factor. The arsine oxide extracts cobalt about 40 times better than the phosphine oxide but otherwise behaves quite similarly, except that D is less sensitive to chloride. Nickel, again, is extracted similarly to cobalt, although somewhat less efficiently, so that cobalt is enriched in the organic phase and nickel in the salt melt when both are present. All these results are very much in line with what has been found[32] and reviewed[2] for tributylphosphate as extractant.

A new liquid anion exchanger was recently examined for the purpose of extraction from molten salts: tetraoctylphosphonium nitrate.[227] It was used in the usual polyphenyl diluent mixture (p. 104) for extracting from the lithium–potassium nitrate eutectic at 150–170°C the chloride, perrhenate, dichloro argentate, and nitrato argentale complex anions. Another diluent, 1-nitronaphthalene, also was used successfully for this purpose, but another extractant, triphenyl tin nitrate, does not have sufficient thermal stability. The results with tetraoctylphosphonium nitrate are essentially similar to those obtained with tetraheptylammonium nitrate (p. 113).

6. CONCLUDING REMARKS

The information provided in Section 5 of this chapter is an ample illustration of the power of distribution measurements to give useful thermodynamic information on the system studied, as suggested in Section 2. Association constants, activity coefficients, and thermodynamic functions of transfer have been calculated for several systems. What is still lacking, however, is a theory capable of quantitatively relating these quantities to molecular parameters of the system. Molten salts have the advantage over other systems that interactions in them are largely Coulombic, with only second-order perturbations caused by polarization effects. It should be possible to assign numerical values to the hardness and softness of ions[228] and to add terms for second-nearest-neighbor polarization effects to the Coulombic potential of ion interactions.[41] Since mainly short-range effects are involved, it might be unnecessary to conduct a full statistical mechanical analysis leading to a radial distribution function rather to depend on probable geometrical arrangements of the few ions involved. A difficulty that will be encountered in such calculations is the assignment of numerical values to the radii of the ions involved, in particular multiatomic ions such as nitrate. It is probably unsatisfactory to treat these radii as free param-

eters to be determined from the distribution data, since these already carry the burdens of other quantities. It should be possible to arrive at valid estimates of the radii from independent data that still have the same operational significance as the radii to be used in the theory.

A further defect in the few correlations that have been tried to date between thermodynamic data and molecular parameters is too heavy a reliance on free energy data. A much more severe test (in which, moreover, many approximate theories for comparable interactions fail) is the separate correlation of energy and of entropy terms. Although the regular solution theory has considerable success for binary molten salt mixtures,[42] implying the approximation of random mixing of ions of a given sign, estimates of the entropy of mixing that permit nonrandomness should be used[41] for the correlation of data obtained from distribution measurements.

Finally, although the problem of demixing of molten salts is only indirectly connected with liquid–liquid distribution studies of solutes, it was found instructive to include an extensive discussion of it in this chapter. High temperature distribution applications, in particular those involving the thermally stable halide salts, will probably concentrate on immiscible molten salt systems. The limitation of the present theory, discussed in Section 3, to the calculation of an upper critical consolute temperature prevents the prediction of immiscibility in reciprocal systems with unfavorable melting points, of the size of the miscibility gap, or of gaps in binary systems. The theory should be developed to also cover these variables.

Nevertheless, the main thesis developed in this chapter, that apart from technological applications distribution between a molten salt and another liquid yields important chemical information on the species formed and on their interactions, stands even without the desirable theoretical advances. More laboratory studies of such systems certainly will be of great importance in the field of molten salt chemistry.

REFERENCES†

1. D. M. Moulton, W. R. Grimes, and J. H. Shaffer, in: *Molten Salts* (G. Mamantov, ed.), pp. 479–527, Marcel Dekker, New York (1969).
2. Y. Marcus, in: *Solvent Extraction Chemistry* (D. Dyrssen, J. O. Lilienzin, and J. Rydberg, eds.), pp. 555–580, North-Holland, Amsterdam (1967).
3. Y. Marcus and A. S. Kertes, *Ion Exchange and Solvent Extraction of Metal Complexes*, John Wiley (Interscience), London (1969).
4. A. S. Kertes and G. Markovits, *J. Phys. Chem.* **72**:4202 (1968).

† References 126, 127, and 134–139 have been omitted.

5. Y. Marcus, *Pure Appl. Chem.* **18**:459 (1969).
6. D. W. Bareis, R. H. Wiswall, Jr., and V. E. Winsche, *Nucleonics* **12**(7):16 (1954).
7. O. E. Dwyer, R. J. Teitel, and R. H. Wiswall, Jr., in: *Proceeding of International Conference on Peaceful Uses of Atomic Energy, Geneva* 1955, Vol. 9, p. 604, United Nations, New York (1956).
8. W. S. Ginell, *Ind. Eng. Chem.* **51**:185 (1959).
9. C. J. Raseman, H. Suskind, and C. H. Waide, *Chem. Eng. Progr.* **53**(2):86-F (1957).
10. R. H. Wiswall, Jr., and J. J. Egan, in: *Thermodynamics of Nuclear Materials, Proceedings of I.A.E.A. Symposium 1962*, pp. 345–364, I.A.E.A., Vienna (1962).
11. C. F. Baes, Jr., cited by W. R. Grimes, *U.S.A.E.C. Rep. ORNL* **3708**:311 (1964).
12. L. M. Ferris, J. C. Mailen, F. J. Smith, E. D. Nogueira, J. H. Shaffer, D. M. Moulton, C. J. Barton, and R. G. Ross, in: *Proceedings of the Third International Protactinium Conference*, Elmau (1969).
13. R. J. Heus and J. J. Egan, *J. Electrochem. Soc.* **107**:824 (1960).
14. R. H. Moore, *U.S.A.E.C. Rep.* **HW-67574** (1960).
15. P. Chiotti, and J. S. Klepfer, *148th American Chemical Society Meeting, Chicago*, 1964, Abstract 39.
16. D. L. G. Rowlands, J. D. Wilson, C. A. J. McInnes, and P. G. Watson, in: *Thermodynamics of Nuclear Materials, Proceedings of I.A.E.A.. Sumposium 1967*, pp. 181–194, I.A.E.A., Vienna (1968).
17. S. Yamagishi and Y. Kamemoto, *Nippon Genshiryoku Gakkaishi* **5**:210 (1963) [in Japanese, cf. *Nucl. Sci. Abstr.* **17**:21683 (1963)].
18. S. Yamagishi and Y. Kamemoto, *Nippon Genshiryoku Gakkaishi* **6**:158 (1964) [in Japanese, cf. *Nucl. Sci. Abstr.* **18**:19983 (1964)].
19. S. Yamagishi and Y. Kamemoto, *Nippon Genshiryoku Gakkaishi* **6**:500 (1964) [in Japanese, cf. *Nucl. Sci. Abstra.* **18**:43498 (1964)].
20. L. J. Mullins, A. J. Beaumont, and J. A. Leary, *J. Inorg. Nucl. Chem.* **30**:147 (1968).
21. I. N. Belyaev, *Ups. Khim.* **29**:899 (1960), *Russ. Chem. Rev.* **29**:428 (1960).
22. G. J. Janz, *Molten Salt Handbook*, pp. 97–101, Academic Press, New York (1967).
23. C. Sinistri, P. Franzosini, and M. Rolla, *An Atlas of Miscibility Gaps in Molten Salt Systems*, University of Pavia, Italy (1968).
24. R. F. Guenther, *J. Inorg. Nucl. Chem.* **27**:1427 (1965).
25. J. H. Kennedy, *J. Phys. Chem.* **65**:1030 (1961).
26. R. H. Moore, *J. Chem. Eng. Data* **9**:502 (1964).
27. E. C. Freiling, in: *Thermodynamics of Nuclear Materials, I.A.E.A. Symposium, 1965*, pp. 435–457, I.A.E.A., Vienna (1966).
28. P. V. Clark, *Physical Properties of Fused Salt Mixtures*, Vol. 1 and 2, Clearinghouse of Federal Scientific and Technical Information, U. S. Department of Commerce, Washington, D. C., (1965 and 1966).
29. M. Zangen and Y. Marcus, *Isr. J. Chem.* **2**:49 (1964).
30. O. Vittori, Doctoral dissertation, Université de Lyon, France, 1968; C. Gonnet, O. Vittori, and M. Porthault, *Compt. Rend.* **267**:714 (1968).
31. N. M. Isaac, P. R. Fields, and D. M. Gruen, *J. Inorg. Nucl. Chem.* **21**:152 (1961).
32. D. Herzog, *French A.E.C. Rep. CEA-R* **2628** (1964).
33. Z. Borkowska, M. Mielcarski, and M. Taube, *J. Inorg. Nucl. Chem.* **26**:359 (1964).
34. R. V. Ammon, *J. Inorg. Nucl. Chem.* **26**:2569 (1966).
35. I. J. Gal, J. Mendez, and J. W. Irvine, Jr., *Inorg. Chem.* **7**:985 (1968).
36. R. C. Scheidt and E. C. Freiling, *J. Phys. Chem.* **69**:1784 (1965).

37. M. H. Rowell, *Inorg. Chem.* **4**:1802 (1965).
38. M. Temkin, *Acta Physicochim. U.R.S.S.* **20**:411 (1945).
39. Y. Marcus and M. Zangen, in: *Thermodynamics of Nuclear Materials*, 1967, pp. 155–165, International Atomic Energy Agency, Vienna (1968).
40. D. L. Manning, R. C. Bansal, J. Braunstein, and M. Blander, *J. Amer. Chem. Soc.* **84**:2028 (1962).
41. M. Blander, in *Molten Salt Chemistry*, (M. Blander, ed.), p. 127, John Wiley (Interscience), New York (1964).
42. M. Blander and L. E. Topol, *Inorg. Chem.* **5**:1641 (1966).
43. M. Blander and S. J. Yosim, *J. Chem. Phys.* **39**:2610 (1963).
44. I. A. Kablukov, *Zh. Russ. Khim. Obshchest.* **37**:577 (1905); **39**:914 (1907).
45. J. E. Ricci, in: *Molten Salt Chemistry* (M. Blander, ed.), pp. 326–339, John Wiley (Interscience), New York (1964).
46. J. H. Hildebrand, *J. Amer. Chem. Soc.* **38**:1470 (1916).
47. J. Kendall, E. J. Crittenden, and H. K. Müller, *J. Amer. Chem. Soc.* **45**:963 (1923).
48. M. L. Sholokhovich and G. V. Barkova, *Zh. Obshch. Khim.* **26**:1433 (1956).
49. I. N. Belyaev, *Zh. Neorg. Khim.* **1**:1501 (1956).
50. D. S. Lesnykh and A. G. Bergman, *Uch. Zap. Rostov Univ. 20, Tr. Khim. Fak.* (6):19 (1954).
51. R. H. Moore, *J. Chem. Eng. Data* **8**:164 (1963).
52. O. N. Brensov, G. Trapp, A. V. Novoselova, and Yu. P. Simanov. *Zh. Neorg. Khim.* **4**:671 (1959).
53. D. F. Kirkina, A. V. Novoselova, and Yu. P. Simanov, *Zh. Neorg. Khim.* **1**:125 (1956).
54. O. R. Gavrilov and L. A. Niselson, *Zh. Neorg. Khim.* **11**:114 (1966).
55. K. Huber, E. Jost, E. Neuenschwander, M. Studier, and B. Roth, *Helv. Chim. Acta* **41**:2411 (1958).
56. P. I. Fedorov, A. G. Dudareva, and M. S. Nosova, *Zh. Neorg. Khim.* **12**:140 (1967).
57. G. Herrmann, *Z. Anorg. Chem.* **71**:257 (1911).
58. H. M. Davis and M. A. Knight, *J. Amer. Ceram. Soc.* **28**(4):100 (1945).
59. E. T. Carlson, *J. Res. Nat. Bur. Stand.* **9**:825 (1932).
60. E. M. Levin and G. W. Gleek, *J. Amer. Ceram. Soc.* **41**(5):175 (1958).
61. P. F. Konovalov, *Dokl. Akad. Nauk SSSR* **70**(5):847 (1950).
62. E. M. Levin and S. Block, *J. Amer. Ceram. Soc.* **40**(3):99 (1957).
63. E. Ingerson, G. W. Morey, and O. F. Tuttle, *Amer. J. Sci.* **246**:31 (1948).
64. D. E. Harrison and F. A. Hummel, *J. Electrochem. Soc.* **103**:491 (1956).
65. E. C. Subbaras and F. A. Hummel, *J. Electrochem. Soc.* **103**:29 (1956).
66. R. F. Geller and E. N. Bunting, *J. Res. Nat. Bur. Stand.* **18**(5):585 (1937).
67. E. M. Levin, C. R. Robbins, and J. L. Waring, *J. Amer. Ceram. Soc.* **44**(2):87 (1961).
68. E. M. Levin and C. McDaniel, *J. Amer. Ceram. Soc.* **45**(8):355 (1962).
69. D. E. Rase and G. Lane, *J. Amer. Ceram. Soc.* **47**(1):48 (1964).
70. J. W. Greig, *Amer. J. Sci.* **13**(5):1 (1927).
71. F. P. Glasser, *Amer. J. Sci.* **256**:398 (1958).
72. J. W. Greig, *Amer. J. Sci.* **13**(5):133 (1927); **14**:473 (1927).
73. A. S. Berezhnoi, L. I. Karyakin, and D. E. Dudovskii, *Dokl. Akad. Nauk SSSR* **83**:399 (1952).
74. E. N. Bunting, *J. Res. Nat. Bur. Stand.* **4**:131 (1930).

75. M. L. Keith, *J. Amer. Ceram. Soc.* **37**(10):490 (1954).
76. F. P. Glasser, *J. Phys. Chem.* **63**:2085 (1959).
77. N. A. Toropov and F. Yu. Galakhov, *Izv. Akad. Nauk SSSR Otd. Khim. Nauk* 160 (1956).
78. M. Ibrahim and N. F. H. Bright, *J. Amer. Ceram. Soc.* **45**:221 (1962).
79. C. R. Robbins and E. M. Levin, *Amer. J. Sci.* **257**:65 (1959).
80. T. Baak, *Acta Chem. Scand.* **8**:1727 (1954).
81. I. N. Belyaev and A. G. Belyaeva, *Zh. Neorg. Khim.* **10**:252 (1965).
82. N. M. Sokolov, *Zh. Obshchei. Khim.* **24**:1151 (1954).
83. E. W. Roedder, *Amer. J. Sci.* **249**(2):81 (1951).
84. G. W. Morey and N. L. Bowen, *J. Soc. Glass Technol.* **9**:226 (1925).
85. G. W. Morey, F. C. Kracek, and N. L. Bowen, *J. Soc. Glass Technol.* **14**:149 (1930); **15**:57 (1931).
86. E. M. Levin, C. R. Robbins, H. F. McMurdie, and M. K. Reser *Phase Diagrams for Ceramicists*, American Ceramic Society, Columbus, Ohio (1969).
87. E. P. Flint and L. S. Wells, *J. Res. Nat. Bur. Stand.* **17**:745 (1936).
88. R. F. Geller and E. N. Bunting, *J. Res. Nat. Bur. Stand.* **23**:279 (1939).
89. E. W. Roedder, *Amer. J. Sci., Bowen Vol.* Pt. 2:435 (1952).
90. E. M. Levin and S. Block, *J. Amer. Ceram. Soc.* **41**(2):49 (1958).
91. A. Muan, *Trans. Amer. Inst. Mining Met. Eng.* **203**:965 (1955).
92. M. A. Zakharchenko and A. G. Bergman, *Sb. Statei Obshch. Khim. Akad. Nauk SSSR* **1**:131 (1953).
93. M. A. Zakharchenko and A. G. Bergman, *Tr. Novocherkassk. Politekh. Inst.* **27**:3 (1956).
94. G. M. Lifshits, *Zh. Obshch. Khim.* **26**:20 (1956).
95. G. Flor and C. Sinistri, *Ric. Sci.* 38 (1968).
96. G. G. Diogenov, *Sb. Statei Obshch. Khim. Akad. Nauk SSSR* **2**:1227 (1953).
97. M. A. Zakharchenko and A. G. Bergman, *Zh. Obshch. Khim.* **25**:867 (1955).
98. I. N. Belyaev, *Zh. Neorg. Khim.* **3**:2805 (1958).
99. D. S. Lesnykh and A. G. Bergman, *Zh. Obshchei Khim.* **23**:383 (1953).
100. *Tekhnicheskaya Entsiklopediya, Spravochnik*, Vols. VI, VII (1930 and 1931).
101. D. S. Lesnykh, and A. G. Bergman, *Zh. Fiz. Khim.* **30**:1959 (1956).
102. D. S. Lesnykh, and A. G. Bergman, *Zh. Obshch. Khim.* **26**:1749 (1956).
103. J. H. Kennedy, *J. Phys. Chem.* **67**:1432 (1963).
104. M. A. Zakharchenko and A. G. Bergman, *Tr. Novocherkassk. Politekh. Inst.* **27**:19 (1956).
105. M. Rolla, unpublished results, cf. Sinistri *et al.*[23]
106. A. G. Bergman and A. S. Arabadzhan, *Zh. Neorg. Khim.* **8**:1122 (1963).
107. N. S. Dombrovskaya and Z. A. Koloskaya, *Izv. Sekt. Fiz. Khim. Anal. Inst. Akad. Nauk SSSR* **22**:178 (1953).
108. P. P. Platonov, *Tr. Mosk. Sel'skokhoz. Akad.* (36):13 (1946).
109. V. P. Radishev, *Zh. Russ. Fiz. Khim. Obshchest* **62**:1063 (1930).
110. C. Sinistri, G. Flor, P. Franzosini, and M. Rolla, *Z. Naturforsch* **22a**:53 (1967).
111. A. G. Bergman and M. L. Sholokhovich, *Zh. Obshch. Khim.* **25**:423 (1955).
112. C. Sinistri, P. Franzosini, A. Timidei, and M. Rolla, *Z. Naturforsch* **20a**:561 (1965); **21a**:595 (1966).
113. C. Sinistri, P. Franzosini, and G. Flor, *Gazz. Chim.* (*Rome*) **97**:275 (1967).
114. A. P. Rostkorskii, *Zh. Russ. Fiz. Khim. Obshchest* **61**:89 (1929).

115. V. I. Posypaiko, N. V. Khakhlova, E. A. Alekseeva, and N. S. Dombrovskaya, *Zh. Neorg. Khim.* **6**:719 (1961).
116. V. I. Posypaiko and N. S. Dombrovskaya, *Zh. Neorg. Khim.* **6**:361, 722 (1961).
117. A. P. Palkin, *Tr. Voronezh, Gos. Univ.* **17**:3 (1950).
118. A. P. Palkin and T. A. Polivanova, *Zh. Neorg. Khim.* **8**:492 (1963).
119. T. A. Polivanova, *Zh. Neorg. Khim.* **7**:737 (1962).
120. D. S. Lesnykh and A. G. Bergman, *Zh. Obshch. Khim.* **23**:557 (1953).
121. D. S. Lesnykh and A. G. Bergman, *Uch. Zap. Rostov Univ.* 20, *Tr. Khim. Fak.* (6):19 (1954).
122. M. L. Sholokhovich, D. S. Lesnykh, and G. A. Buchalova, *Dokl. Akad. Nauk SSSR* **103**:261 (1955).
123. N. N. Volkov and L. A. Dubinskaya, *Izv. Fiz. Khim. Nauch.-Issled. Inst. Irkutsk. Univ.* **2**:45 (1953).
124. K. A. Bolshakov and P. I. Federov, *Izv. Vyssh. Ucheb. Zaved. Tsvet. Met.* **2**:52 (1959).
125. D. M. Gruen, S. Fried, P. Graf, and R. C. McBeth, *Proc. U. N. Int. Conf. Peaceful Uses At. Energy*, **28**:112 (1958).
128. B. L. Dunicz and R. C. Scheidt, *U.S.A.E.C. Rep. USNRDL-TR-752* (1964).
129. M. H. Rowell, *U.S.A.E.C. Rep. USNRDL-TR-760* (1964).
130. B. L. Dunicz and R. C. Scheidt, *J. Chem. Eng. Data* **11**:566 (1966).
131. B. L. Dunicz and R. C. Scheidt, *J. Chem. Eng. Data* **13**:220 (1968).
132. E. L. Freiling and M. H. Rowell, in: *Ion Exchange* (J. A. Marinsky, ed.), Vol. 2, pp. 43–88, Marcel Dekker, New York (1969).
133. N. P. Nies, *J. Electrochem. Soc.* **107**:817 (1960).
140. Z. P. Ershova and Yu. I. Olshanskii, *Geochimiya* (3):257 (1957).
141. Yu. I. Olshanskii, *Dokl. Akad. Nauk SSSR* **70**(2):246 (1950).
142. M. L. Pearce and J. F. Beisler, *J. Amer. Ceram. Soc.* **48**:40 (1965).
143. L. Hillert, *Acta Chem. Scand.* **19**:1516 (1965).
144. N. M. Sokolov, N. M. Tsindrik, and O. I. Dmitrevskaya, *Zh. Obshch. Khim.* **31**:1051 (1961).
145. N. M. Tsindrik and N. M. Sokolov, *Zh. Obshch. Khim.* **28**:1729 (1958).
146. G. G. Diogenov, *Dokl. Akad. Nauk SSSR* **78**:697 (1951).
147. G. G. Diogenov, *Zh. Obshch. Khim.* **23**:24 (1953).
148. Reference 3, pp. 432–437.
149. Reference 27, pp. 447–448.
150. M. Zangen, *J. Phys. Chem.* **69**:1835 (1965).
151. M. Zangen, *J. Phys. Chem.* **74**, in press (1970).
152. M. Zangen, *Inorg. Chem.* **7**:133 (1968).
153. R. H. Wiswall, Jr., and J. J. Egan, *Nucleonics* **15**(7):104 (1957).
154. F. J. Salzano and F. B. Hill, *U.S.A.E.C. Rep. BNL-639*, 19 pp. (1962).
155. O. F. Dwyer, *Amer. Inst. Chem. Eng. J.* **2**:163 (1956).
156. R. H. Wiswall, Jr., J. J. Egan, W. S. Ginell, F. T. Miles, and J. R. Powell, in: *Proc. U. N. Conf. Peaceful Uses At. Energy, Geneva*, 1958 **17**:421 (1958).
157. O. E. Dwyer, A. M. Eshaya, and F. S. Hill, in: *Proc. U. N. Conf. Peaceful Uses At. Energy, Geneva*, 1958 **17**:428, Geneva (1958).
158. J. A. Lane, H. G. MacPherson, and F. Maslan, eds., *Fluid Fuel Reactors*, Chap. 22, p. 791, Addison-Wesley, Reading (1958).

159. T. Miyauchi and M. Takata, *Kagaku Kogaku* **26**:991 (1962) [in Japanese, cf. *U.S.A. E.C. Rep.* (*trans.*) *ORNL-tr-1665*, and *Nucl. Sci. Abstr.* **21**:24093 (1967)].
160. R. J. Teitel, *U. S. Patent* (to Dow Chemical Co.) 3, 251,745 (1966).
161. I. N. Nichkov, S. P. Raspopin, and O. A. Ryzhik, *Tr. Vses. Soveshch. Fiz. Khim. Rasplav. Solei, 2nd, Kiev* 258 (1965).
162. H. A. Laitinen and W. S. Ferguson, quoted by C. H. Liu, K. E. Johnson and H. A. Laitinen, in: *Molten Salt Chemistry* (M. Blander, ed.), p. 708, John Wiley (Interscience), New York (1964).
163. Yu. K. Delimarskii and B. F. Markov, *Electrochemistry of Fused Salts* (A. Peiperl and R. Wood, transl.-eds.), pp. 297–330, Sigma Press, Washington, D. C. (1961).
164. N. Nachtrieb and M. Steinberg, *J. Amer. Chem. Soc.* **70**:2613 (1948).
165. M. Steinberg and N. Nachtrieb, *J. Amer. Chem. Soc.* **72**:3558 (1950).
166. E. Colichman, *Anal. Chem.* **27**:1559 (1955).
167. J. Randles and W. White, *Z. Elektrochem.* **59**:666 (1955).
168. J. H. Christie and R. A. Osteryoung, *J. Amer. Chem. Soc.* **82**:1841 (1960).
169. D. Inman and J. O'M. Bockris, *Trans. Faraday Soc.* **57**:2308 (1961).
170. H. S. Swofford and H. A. Laitinen, *J. Electrochem. Soc.* **110**:814 (1963).
171. H. S. Swofford, Jr., and C. L. Holifield, *Anal. Chem.* **37**:1509, 1513 (1965).
172. D. Inman, D. G. Lovering, and R. Narayan, *Trans. Faraday Soc.* **63**:3017 (1967).
173. D. Inman and J. O. M. Bockris, *J. Electrochem. Anal.* **3**:126 (1962).
174. J. J. Egan. *J. Phys. Chem.* **65**:2222 (1961).
175. D. E. Ferguson, *U.S.A.E.C. Rep. ORNL-4272* 10–21 (1968) and *ORNL-4422*, 1–36 (1969).
176. W. R. Grimes, *U.S.A.E.C. Rep. ORNL-3708* 214–51 (1967).
177. W. R. Grimes, *U.S.A.E.C. Rep. ORNL-4076* 34–37 (1967).
178. W. R. Grimes, *U.S.A.E.C. Rep. ORNL-4229* 43–46 (1968).
179. Reference 3, pp. 551–558.
180. A. G. Kotlova, Yu. I. Olshanskii, and A. I. Tsvetkov, *Tr. Inst. Geol. Rud. Mestorozhd. Petrog. Mineral. Geokhim.* **42**:3 (1960).
181. B. Stalhane, *Z. Elektrochem.* **35**:486 (1929), **36**:404 (1930).
182. Reference 129, quoted with three detailed figures in Freiling and Rowell,[132] pp. 64–66.
183. C. E. Adams and J. T. Quan, *J. Phys. Chem.* **70**:331 (1966).
184. B. D. McSwain, N. F. Borelli, and G. J. Su, *J. Phys. Chem. Glasses* **4**:1 (1963).
185. C. F. Adams and J. T. Quan, *J. Phys. Chem.* **70**:340 (1966).
186. J. Krogh-Moe, *J. Phys. Chem. Glasses* **3**:101 (1962) and **6**:51 (1965).
187. A. H. Silver and P. J. Bray, *J. Chem. Phys.* **29**:984 (1958).
188. S. E. Svanson, E. Forslind, and J. Krogh-Moe, *J. Phys. Chem.* **66**:174 (1962).
189. J. Biscoe and B. Warren, *J. Amer. Ceram. Soc.* **21**:287 (1938).
190. B. Ottar and W. L. Ruigh, *J. Phys. Chem. Glasses* **3**:95 (1962).
191. J. Goubeau and H. Keller, *Z. Anorg. Chem.* **272**:303 (1953).
192. L. Shartsis, W. Capps, and S. Spinner, *J. Amer. Ceram. Soc.* **36**:35, 319 (1953).
193. Y. Marcus, M. Liquornik, L. F. Friedman, and M. Zangen, *Isr. A.E.C. Rep. IA-864* (1963).
194. M. Zangen, *Isr. J. Chem.* **2**:91 (1964).
195. M. Zangen and Y. Marcus, *Isr. J. Chem.* **2**:155 (1964).
196. Y. Marcus, I. Eliezer, and M. Zangen, *Proc. Symp. Coord. Chem. Tihany, Hungary*, 1964 (M. T. Beck, ed.), Akad. Kiado, Budapest (1965), p. 409.

197. M. Zangen, *Inorg. Chem.* **7**:138 (1968).
198. M. Zangen, *J. Inorg. Nucl. Chem.* **31**:867 (1969).
199. M. Zangen, in: *Solvent Extraction Research* (A. S. Kertes and Y. Marcus, eds.), p. 151, John Wiley (Interscience), New York (1969).
200. M. Zangen, unpublished results (1963).
201. Y. Marcus and I. Eliezer, *Coord. Chem. Rev.* **4**:273 (1969).
202. C. Thomas and J. Braunstein, *J. Phys. Chem.* **68**:957 (1964).
203. J. Braunstein and A. S. Minano, *Inorg. Chem.* **5**:942 (1966).
204. S. C. Wait, Jr., A. T. Ward, and G. J. Janz, *J. Chem. Phys.* **45**:133 (1966).
205. J. Penciner, I. Eliezer, and Y. Marcus, *J. Phys. Chem.* **69**:2955 (1965).
206. Y. Marcus, *Coord. Chem. Rev.* **2**:215 (1967).
207. M. Zangen, in: *Solvent Extraction Chemistry* (D. Dyrssem, J. O. Liljenzin, and J. Rydberg, eds.), p. 581, North-Holland, Amsterdam (1967).
208. M. Zangen, *Inorg. Chem.* **7**:1202 (1968).
209. M. Taube and Z. Borkowska, *Nature* **192**:745 (1961).
210. H. Gutmann and A. S. Kertes, *J. Inorg. Nucl. Chem.* **31**:205 (1969).
211. I. J. Gal. *Inorg. Chem.* **7**:1611 (1968).
212. J. M. C. Hess, J. Braunstein, and H. Braunstein, *J. Inorg. Nucl. Chem.* **26**:811 (1964).
213. M. Peleg, private communication.
214. R. M. Nikolic and I. J. Gal. *J. Inorg. Nucl. Chem.* **30**:1963 (1968).
215. I. J. Gal and R. M. Nikolic, in: *Solvent Extraction Research* (A. S. Kertes and Y. Marcus, eds.), p. 211, John Wiley (Interscience), New York (1969).
216. G. Scibona, J. E. Byrum, K. Kimura, and J. W. Irvine, Jr., in: *Solvent Extraction Chemistry* (D. Dyrssen, J. O. Liljenzin, and J. Rydberg, eds.), North-Holland, Amsterdam (1967), p. 398.
217. J. Braunstein and H. Braunstein, *Inorg. Chem.* **8**:1558 (1969).
218. H. Gutmann unpublished results, Hebrew University, Jerusalem, 1968–1969.
219. J. David, unpublished results, Soreq Nuclear Research Center, Yavne, 1968–1969.
220. J. David, M. Zangen, and A. S. Kertes, *Isr. J. Chem.* **5**:2p (1967).
221. J. David, M. Zangen, and A. S. Kertes, *Isr. A.E.C. Rep. IA*-1168, 96–99 (1968).
222. J. David and M. Zangen, in: *Solvent Extraction Research* (A. S. Kertes and Y. Marcus, eds.), p. 219, John Wiley (Interscience), New York (1969).
223. D. E. McKenzie, W. L. Elsdon, and J. W. Fletcher, *Can. J. Chem.* **36**:1233 (1958).
224. R. C. Vogel, *U.S.A.E.C. Rep. ANL*-7175 (1967).
225. R. C. Vogel, *U.S.A.E.C. Rep. ANL*-7350 (1968).
226. J. B. Knighton, I. Johnson, and R. K. Steunenberg, *U.S.A.E.C. Rep. ANL-7524* (1969).
227. Z. C. H. Tan, Ph. D. Thesis, Massachussetts Institute of Technology, Cambridge (1969).
228. S. Ahrland, *Chem. Phys. Lett.* **2**:303 (1968); Y. Marcus, unpublished results, 1970.
229. R. E. Thoma, H. Insley, H. A. Friedman, and G. M. Herbert, *J. Nucl. Mater.* **27**:166 (1968).

Chapter 3

MOLTEN SALT CHEMISTRY OF THE HALOALUMINATES[†]

C. R. Boston
Metals and Ceramics Division
Oak Ridge National Laboratory
Oak Ridge, Tennessee

1. INTRODUCTION

This review covers the molten salt chemistry of the aluminum halides and their mixtures with other metal halides. These materials have extremely interesting properties from the molten salt point of view. They are almost unique in their wide range of acid–base properties. In addition, they form low melting liquids with good thermal stabilities. These facts together with recent studies showing the existence of unusual dissolved species suggest a vast potential for the haloaluminates as molten salt solvents.

The fluoroaluminates differ quite markedly from other haloaluminates. For this reason and since the fluorides have been discussed in a recent review,[(1)] they are treated only briefly here. This is certainly not to imply a lack of importance. Much work has been done on the fluorides, and they are quite important industrially, particularly in aluminum production.

Studies of molten haloaluminate salts have undoubtedly been deterred by their extreme sensitivity to moisture and organic contaminants. Recently improved techniques for the preparation and handling of haloaluminate melts together with the gradual recognition of their unique properties should make them a popular class of molten salts during the next few years.

[†] Research sponsored by the U. S. Atomic Energy Commission under contract with the Union Carbide Corporation.

2. THE ALUMINUM HALIDES

Even though the Al–X bond is largely ionic[2–5] (65% for Al–Br), the aluminum halides do not melt to form ionized liquids. For example, the specific conductance[6] of liquid aluminum chloride is of the order of 10^{-7} $(\text{ohm-cm})^{-1}$. This apparent anomaly as well as many other unusual liquid properties is due to the strong tendency for AlX_3 molecules to form very stable dimeric Al_2X_6 molecules. This property is discussed in Section 2.2.

Another outstanding feature of the aluminum halides is their behavior as strong Lewis acids as demonstrated by their vigorous reaction with halides to form the anion AlX_4^-. Thus by virtue of such behavior, non-conducting liquid Al_2X_6 will react with many halogen compounds to form highly ionic liquid mixtures.

2.1. Physical and Thermodynamic Properties

Some of the more important physical properties of the aluminum halides are listed in Table I. Aluminum fluoride is obviously in a class by itself. It sublimes at a very high temperature, and no measurements of liquid properties have been reported since these would require both very high temperatures and pressures. The remaining aluminum halides are fairly similar, having low melting and boiling points and other characteristic properties of molecular liquids.

Thermodynamic properties of the aluminum halides are listed in Table II. Most of these data come from the JANAF tables[7] or were calculated from data therein. Again, aluminum fluoride has quite different properties from the other halides. The large heat and entropy of fusion of aluminum chloride reflects the large structural change that occurs on melting this compound but does not occur on melting the bromide and iodide—a point that is discussed in more detail later. The entropies of vaporization are normal for the chloride, bromide, and iodide, as expected since the dimeric molecule exists in both the liquid and vapor.

Surface tension as a function of temperature was measured[8] for liquid Al_2Cl_6. The linear relationship $\sigma = 23.88 - 0.0733t$ was observed, where σ is the surface tension in dynes per centimeter and t is the temperature in degree Celcius.

Vapor pressures have been measured for molten aluminum halides, the results can be expressed as $\log P\ (\text{atm}) = A - B/T(^\circ\text{K})$, where A and B have the values 4.797, 2.07×10^3 for $AlCl_3$[9]; 4.6688, 2.4519×10^3

TABLE I. Physical Properties of Aluminum Halides

	Melting point (°C)	Boiling point (°C)	Critical constants			Liquid properties				
						Specific conductivity at 200°C (ohm-cm^{-1})	Density $d = A - Bt$		Viscosity $\eta = A - Bt$	
			Temperature (°C)	Pressure (atm)	Density (g/cm^3)		A (g/cm^3)	$B \times 10^3$ (g/cm^3/°C)	A (cP)	$B \times 10^3$ (cP/°C)
AlF_3	445[a,b]	1272[a,c]								
$AlCl_3$	192.4[a]	187[a,c]	350 ± 3[d]	28 est.	0.51[e,f]	1×10^{-7} [d]	1.733[e-g]	2.33[e-g]	0.9183[e]	2.899[e]
			347 ± 3[f]							
			354[e]							
$AlBr_3$	97.5[a]	255[h]	490 ± 2[i]	28.5[h]	0.8605[i]	1×10^{-7} [k]	i	i	3.23[l]	18.7[l]
			495	26.7[j]	0.8875[j]		2.905[j]	2.49[j]		
AlI_3	191[m]	386[n]				2×10^{-6} [k]	3.700[o]	2.50[o]	6.09[p]	17.5[p]

[a] From Stull.[7] [b] Transition temperature. [c] Sublimes, 1 atm. [d] From Boston *et al.*[6] [e] From Nisel'son and Sokolova.[8]
[f] J. W. Johnson, W. J. Silva, and D. Cubicciotti (private communication). [g] From Boston.[57] [h] From Johnson *et al.*[10]
[i] J. W. Johnson, W. J. Silva, and D. Cubicciotti, *J. Phys. Chem* **72**; 1664–1668 (1968). $d = 2.8568 - 3.1422 \times 10^{-3} t + 2.9431 \times 10^{-6} t^2 - 3.1121 \times 10^{-9} t^3$.
[j] D. I. Zhuravlev, *J. Phys. Chem. USSR* **10**; 325–329 (1937). [k] From Biltz and Voigt.[15]
[l] K. H. Grothe and P. Kleinschmit, *Naturwissenschaften* **54**; 43 (1967), viscosity also given by $\eta = (35.9 \times 10^{-3})^{-3.11/RT}$.
[m] W. Fischer, *Z. Anorg. Chem.* **200**; 332 (1931).
[n] F. D. Rossini, D. D. Wagman, W. H. Evans, S. Levine, and I. Jaffe, *Selected Values of Chemical Thermodynamic Properties*, National Bureau of Standards, Washington, D.C. (1952).
[o] W. Biltz and W. Klemm, *Z. Anorg. Chem.* **152**; 225, 267 (1926).
[p] P. Kleinschmit, thesis, Clearinghouse for Scientific and Technical Information, N68-37352 (1968).

TABLE II. Thermodynamic Properties of Aluminum Halides[a]

	$\Delta H°$(kcal-mole^{-1})					$C_p°$ (cal mole^{-1} deg^{-1})	$S°$ (cal mole^{-1} deg^{-1})	ΔS (cal mole^{-1} deg^{-1})	
	Formation (solid)	Fusion	Sublimation (to dimer)	Vaporization $[Al_2X_6(l) = Al_2X_6(g)]$	Dissociation $[Al_2X_6(g) = 2AlX_3(g)]$			Fusion	Vaporization
AlF_3	-360.8 ± 1.7	0.16[b]	71.2 ± 0.5[c]			17.951	15.881		
$AlCl_3$	-168.58 ± 0.2	8.44	28.0 ± 0.5	10.1 ± 0.5	29.4[d,e]	21.951	26.45 ± 0.15	18.1	21.7
		(192.4°C)		(192°C)				(192.4°C)	(192°C)
$AlBr_3$	-126.0 ± 3	2.69	20.5 ± 0.6	11.6	29.3	24.040	43.08 ± 0.26	7.3	22.0
		(97.4°C)		(256°C)				(97.4°C)	(256°C)
AlI_3	-73.9 ± 1.5	3.8	26.8 ± 0.6	14.9	23.0	23.640	(45.3 ± 2.0)	8.2	22.6
		(191.0°C)		(386°C)				(191.0°C)	(386°C)

[a] From Stull,[7] unless otherwise indicated.
[b] Transition at 445°C.
[c] To monomer.
[d] G. E. Vrieland and D. R. Stull, *J. Chem. Eng. Data* **12**; 532–535 (1967).
[e] V. B. Nesterenko, A. V. Zinov'ev, and M. A. Bazhin, *Vestsi Akad. Navuk Belarus. SSR, Ser. Fiz.-Tekh. Navuk* (2); 32–41 (1967).

for $AlBr_3$[10]; and 5.6403, 3.6976×10^3 for AlI_3.[11] Thus at 200°C the vapor pressures are approximately 2.6, 0.31, and 6.7×10^{-3} atm for aluminum chloride, bromide, and iodide, respectively.

2.2. Structure

Several studies[12–14] have been made of the structure of aluminum halides. Table III compares the structure for the solid, liquid, and gas. The dimeric Al_2X_6 is the dominant structure and consists of two (AlX_4) tetrahedra that share an edge, as shown in Fig. 1.

Aluminum chloride is the most interesting member of this series. Its melting point is anomalously high compared with the bromide and iodide (Table I), and its molar volume nearly doubles on melting.[15,16] A large decrease in electrical conductivity on melting also has been reported,[14,15,17] but impurity effects[6] may account for part of this. As mentioned above, aluminum chloride has an anomalously high heat and entropy of fusion compared with the other halides. All of these effects can be explained by the pronounced structural changes that occur on melting.[14,18] Solid aluminum chloride is essentially an ionic crystal,[18,19] with

TABLE III. Aluminum Halide Structures

	Solid	Liquid	Gas
AlF_3	Ionic crystal[a] (AlF_6 octahedra joined at all corners)	—	Monomer[b]
$AlCl_3$	Ionic crystal[c–e] (Monoclinic, layer lattice; octahedral coordination of Cl)	Dimer[f]	Dimer[b,g]
$AlBr_3$	Molecular crystal[c,h] (Al_2Br_6 molecules; monoclinic; tetrahedral coordination of Br)	Dimer[i]	Dimer[b,g]
AlI_3	Molecular crystal[c] (Al_2I_6 molecules)	Dimer[i]	Dimer[g] Monomer (85%)[b]

[a] From Hanic *et al.*[20]
[b] From Akishin *et al.*[22]
[c] From Semenenko and Naumova.[14]
[d] From Sasvari.[18]
[e] From Ketelaar *et al.*[19]
[f] From Harris *et al.*[13]
[g] From Palmer and Elliott.[12]
[h] From Renes and MacGillavry.[21]
[i] No direct evidence.

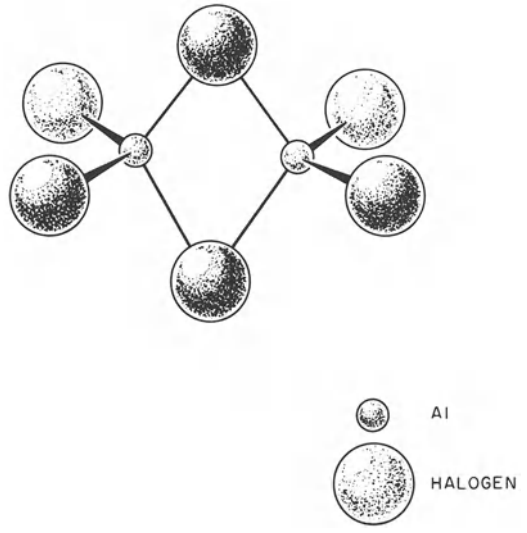

Fig. 1. Structure of Al_2Cl_6, Al_2Br_6, and Al_2I_6 molecules.

the aluminum atom surrounded octahedrally by chlorine atoms to form a layer lattice (octahedra-sharing faces). When this crystal melts, the aluminum atoms move from octahedral to tetrahedral sites to form dimeric Al_2Cl_6 molecules. Thus the change is form an ionic crystal to a molecular liquid. Since the layers of the crystal lattice are held together only by van der Waals forces, the melting point, though high when compared with the bromide and the iodide, is still much lower than the fluoride.[20] The latter forms an ionic, three-dimensional array of AlF_6 octahedra that share corners.

Aluminum bromide[21] and iodide[14] form molecular crystals of Al_2X_6 molecules. These persist in the liquid and to a large extent in the vapor[12,22] so as to give normal entropies of fusion and vaporization.

The nature of Al–X bonds in solid Al_2X_6 has been studied by means of nuclear quadrupole resonance measurements.[2–5] These compounds are particularly well suited for such measurements since both the aluminum and halogen nuclei can be observed. Nuclear quadrupole resonance spectra have been determined for Al^{27} in aluminum chloride[2] and aluminum bromide;[4] Br^{79}, Br^{81} in aluminum bromide;[3] and I^{127} in aluminum iodide.[5] The results for solid aluminum bromide indicate dimeric Al_2Br_6, in agreement with *x*-ray evidence, and also indicate 65% ionic character for nonbridging Al–Br bonds.[3] A similar analysis of the results for solid aluminum chloride indicates a crystal with nearly two-third ionic and one-third covalent character.[2]

2.3. Solvent Properties

The pure aluminum halides seldom have been used as solvents. Their high vapor pressures and reactivities have probably discouraged their use. Decomposition potentials have been measured for various cations in $AlCl_3$,[23] $AlBr_3$,[24] and AlI_3.[25] Solubility studies in aluminum iodide also have been reported.[26] More recently the absorption spectra of divalent, 3*d* metal ions in aluminum chloride at 227°C and 5.6 atm have been reported.[27] In all cases the spectra indicated an octahedral configuration of chlorides around the metal ions.

2.4. Electrical Conductivity

Electrical conductivities have been measured by Biltz and Voigt[15] for liquid Al_2Cl_6, Al_2Br_6, Al_2I_6, and solid aluminum chloride. Specific conductivities of the order of 10^{-7} to 10^{-6} were reported. The measurements on solid aluminum chloride were particularly interesting. Large increases in conductivity with temperature were observed beginning near 140–150°C (m.p. 192°C). A sharp drop in conductivity occurred on melting followed by the usual increase with temperature for the liquid. More recent measurements[14,17] show a similar premelting effect. Since no changes in crystal structure were observed from room temperature to 150°C, Semenenko and Naumova[14] suggest that undetectable changes in structure allow some of the aluminum ions to move from octahedral to unoccupied tetrahedral sites. A free movement of aluminum ions in these randomly destributed sites, according to these authors, would enhance the crystal conductivity. It recently has been suggested[6] that these premelting effects are due to trace impurities (for example, H_2O or reaction products thereof). These authors[6] remeasured the conductivity of aluminum chloride liquid and supercritical vapor using high purity samples and obtained specific conductivity values (at 220°C) almost an order of magnitude lower than those previously reported. This fact, together with the lack of reproducibility in the solid conductivity measurements, suggests that these effects indeed are due to impurities.

2.5. Subvalent Species

Subvalent compounds of aluminum are well known, and the subject has been reviewed by Emmons and Hasselbarth.[28] Both the +1 and +2 oxidation states have been reported. The +1 state is well established,

particularly in the gas phase at high temperatures. The absorption spectra of AlX vapors have been studied in detail for the fluoride,[29] chloride,[30–32] and bromide.[32–34] Lide[35] has studied the microwave spectrum of AlF and AlCl in the gas phase. The +2 oxidation state is apparently much less stable if, indeed, it exists at all. Since divalent aluminum would have a single *s* electron, one might expect it to occur as the dimer as observed for Hg_2^{2+} and Cd_2^{2+}. Recent indications of the dimer $(AlCl)_2$ in the gas phase were reported by Chai *et al.*[36]

The equilibrium, $2Al(l) + AlX_3(g) = 3AlX(g)$, has been studied for the fluoride[37-40] and chloride[40–47] using a transpiration technique at temperatures usually in the range of 800–1200°C. This reaction is of commercial importance as a method for obtaining aluminum metal of high purity as discussed later. Most of these studies indicate that AlX is the only product. Thermodynamic properties of $AlX(g)$ have been calculated from studies of this type and are listed in the JANAF tables.[7] A kinetic study of this reaction for the chloride also has been reported.[49]

The AlX compounds are highly reactive,[50] attacking most structural metals and silica. High purity aluminum oxide, graphite, SiC, TiC, tungsten, and molybdenum are among the materials that are fairly inert.

The existence and nature of Al(I) compounds in liquid and solid phases is less certain. Thonstad[51] reported solubilities of Al metal in Al_2Br_6 and Al_2I_6 of about 0.2 mole % at temperatures near 300°C, while Corbett and von Winbush[52] found a solubility of 0.3 mole % in AlI_3 near 400°C. The nature of the dissolved species is still in doubt but presumably is the monovalent halide. Schumb and Rogers[53] report a buff-colored solid monoiodide $(AlI)_n$. Both Midorikawa[54] and Notoya[55] observed mass transfer of aluminum metal in molten $AlCl_3$–NaCl eutectic at 100–400°C, presumably via Al(I). The important roll of univalent aluminum in metallurgy is discussed by Belyaev.[56]

3. PHYSICAL PROPERTIES OF SALT MIXTURES CONTAINING ALUMINUM HALIDES

Densities, viscosities, and vapor pressures have been determined for molten mixtures containing aluminum halides, as indicated in Table IV. Many of these measurements were made in conjunction with conductivity studies, which will be discussed later. Large negative deviations in molar volume with composition were observed for both the $AlCl_3$–NaCl[57] and $AlCl_3$–KCl[58] systems.

TABLE IV. Reference Physical Properties of Haloaluminate Melts

System	Reference		
	Density	Viscosity	Vapor pressure
AlF_3–LiF		(64)	
AlF_3–NaF	(65, 66)		
$AlCl_3$–LiCl	(67)		
–NaCl	(67–70, 72)	(82, 84)	(59–62)
–KCl	(58, 67, 69–71)		(60)
–$BiCl_3$	(72)		(85)
–ICl	(73)		
–NH_4Cl	(67)		
–KCl–LiCl			(60)
–KCl–NaCl	(70)		(60)
–KCl–$MgCl_2$			(60)
–KCl–$ZrCl_4$			(86)
–KCl–LiCl–$MgCl_2$			(60)
$AlBr_3$–NaBr	(74, 75)	(74)	
–KBr	(74, 76, 81)	(74, 76)	
–IBr	(79, 80)	(79, 80)	
–NH_4Br	(75, 77)	(77)	
–$ZnBr_2$	(75, 76)	(76)	
–$HgBr_2$	(77, 81)	(77)	
–$SbBr_3$	(75, 76, 81)	(76)	
–$SbBr_3$–$AsBr_3$	(78)	(78)	
–$SbBr_3$–$SnBr_4$		(83)	
–$AsBr_3$–$SnBr_4$		(83)	
–KCl	(75)	(75)	

Vapor pressure studies[59–62] on $AlCl_3$–NaCl show very large reductions in vapor pressure as NaCl is added to liquid aluminum chloride. This suggests the formation of stable polymeric anions in the liquid such as $Al_2Cl_7^-$ in addition to the well-established monomer $AlCl_4^-$. Øye and Gruen[27] discuss this point and compare equilibrium constants for the formation of chloroaluminate complexes using the vapor pressure data of Dewing[61] for NaCl–$AlCl_3$ and the distribution data of Moore *et al.*[63] for KCl–$AlCl_3$ mixtures. These authors[27] conclude that although the evidence indicates $Al_2Cl_7^-$ ions there is a great need for precise measurements to identify anionic species and their formation constants for aluminum halide-rich mixtures.

TABLE V. References to Phase Studies

System	Reference	System	Reference
$AlCl_3$–LiCl	(92)	$AlCl_3$–$ThCl_4$	(127)
–NaCl	(92–96)	–NH_4Cl	(92, 128)
–KCl	(92–95)	–NOCl	(129)
–RbCl	(97–98)	–$POCl_3$	(130)
–CsCl	(97–99)	–$PSCl_3$	(131)
–CuCl	(92)	–$VOCl_3$	(132)
–AgCl	(92)	–$SOCl_2$	(133)
–$BeCl_2$	(100)	–KBr	(134, 135)
–$MgCl_2$	(92, 102)	–AgBr	(134, 136)
–$CaCl_2$	(101)	–$HgBr_2$	(134, 136)
–$BaCl_2$	(92)	–$AlBr_3$	(137, 138)
–$ZnCl_2$	(103)	–$SbBr_3$	(134)
–$HgCl_2$	(92)	$AlBr_3$–LiBr	(92)
–$GaCl_3$	(104, 105)	–NaBr	(92)
–InCl	(106)	–KBr	(92, 139)
–TlCl	(92, 107)	–RbBr	(139, 140)
–$SiCl_4$	(108)	–CsBr	(139, 140)
–$TiCl_3$	(109)	–AgBr	(141)
–$TiCl_4$	(110)	–$MgBr_2$	(92)
–$ZrCl_4$	(111–113)	–$ZnBr_2$	(92)
–$HfCl_4$	(113, 114)	–$CdBr_2$	(92)
–$SnCl_2$	(92)	–Hg_2Br_2	(92)
–$SnCl_4$	(92, 115)	–$HgBr_2$	(92)
–$PbCl_2$	(116)	–BBr_3	(142)
–PCl_5	(117, 118)	–TlBr	(92)
–$SbCl_3$	(92)	–$SnBr_2$	(92)
–$BiCl_3$	(85)	–$SnBr_4$	(92, 138)
–VCl_2	(102)	–$PbBr_2$	(92)
–$NbCl_5$	(119, 120)	–$TiBr_4$	(143)
–$TaCl_5$	(99, 120, 121)	–PBr_3	(92)
–S_2Cl_2	(122)	–$AsBr_3$	(92, 138)
–$SeCl_4$	(123)	–$SbBr_3$	(92)
–$TeCl_4$	(123)	–$BiBr_3$	(92)
–$CrCl_2$	(102)	–Br_2	(138)
–$MoCl_5$	(124)	–IBr	(144)
–WCl_6	(124)	–$MnBr_2$	(92)
–$MnCl_2$	(92, 102)	–NH_4Br	(92)
–ICl	(73)	–NaCl	(145)
–$FeCl_2$	(102, 125)	–KCl	(134, 135, 145)
–$FeCl_3$	(125, 126)	–AgCl	(134, 136)
–$CoCl_2$	(102)	–$HgCl_2$	(136)
–$NiCl_2$	(102)	–$SbCl_3$	(135)

TABLE V. (*Continued*)

System	Reference	System	Reference
$AlBr_3$–NaI	(146)	$AlCl_3$–CsCl–$TaCl_5$	(99)
AlI_3–LiI	(97)	–$SnCl_4$–$NbCl_5$	(115)
–NaI	(88)	–$SnCl_4$–$TaCl_5$	(115)
–KI	(88, 97, 147)	–$SnCl_4$–$FeCl_3$	(115)
–RbI	(88, 97)	–$TiCl_4$–$NbCl_5$	(110)
–CsI	(88, 97)	–$TiCl_4$–$TaCl_5$	(110)
–HgI_2	(147)	–$TiCl_4$–$FeCl_3$	(159, 160)
–SnI_4	(147)	–$NbCl_5$–$TaCl_5$	(126)
–AsI_3	(147)	–$NbCl_5$–$FeCl_3$	(126)
–SbI_3	(147)	–$TaCl_5$–$FeCl_3$	(126)
–I_2	(147)	–$MoCl_5$–$FeCl_3$	(161)
–NH_4I	(97)	–WCl_6–$FeCl_3$	(162)
$AlCl_3$–LiCl–KCl	(148, 149)	–$FeCl_2$–$FeCl_3$	(125)
–NaCl–KCl	(93, 149, 150, 151)	–$POCl_3$–$NbCl_5$	(163)
–NaCl–$ZrCl_4$	(152)	–$POCl_3$–$TaCl_5$	(163)
–NaCl–$HfCl_4$	(149, 153)	–LiCl–KCl–$MgCl_2$	(149)
–NaCl–$BiCl_3$	(85)	–NaCl–KCl–$NbCl_5$	(164)
–NaCl–$NbCl_5$	(120)	–NaCl–KCl–$TaCl_5$	(164)
–NaCl–$TaCl_5$	(120)	–NaCl–$NbCl_5$–$TaCl_5$	(165)
–NaCl–$MoCl_5$	(154)	–NaCl–$BiCl_3$–$FeCl_3$	(166)
–NaCl–WCl_6	(155)	–KCl–$NbCl_5$–$TaCl_5$	(165)
–NaCl–$FeCl_3$	(156)		
–KCl–$MgCl_2$	(149)		
–KCl–$ZrCl_4$	(86)		
–KCl–$HfCl_4$	(153)		
–KCl–$NbCl_5$	(157, 158)		
–KCl–$TaCl_5$	(157)		

4. PHASE STUDIES AND THERMODYNAMIC PROPERTIES OF SALT MIXTURES CONTAINING ALUMINUM HALIDES

4.1. Phase Studies

Aluminum halide-containing systems for which phase equilibrium studies have been reported are listed in Table V. A critical examination of this extensive work will not be undertaken here. Complete phase diagrams have not been determined for any systems containing aluminum halides, and many of those listed have been measured only at one or two compositions.

4.2. Alkali Metal Halide–Aluminum Halide Mixtures

The alkali metal halide–aluminum halide mixtures have been studied more than any others. A typical phase diagram of this type is shown in Fig. 2 for $AlCl_3$–KCl. The two-liquid region at high $AlCl_3$ compositions occurs frequently in these systems. This feature has been utilized for distribution studies, as discussed in Section 7.5.

Another common feature of these systems is a low melting eutectic on the AlX_3-rich side of the phase diagram. In Fig. 2 this occurs near 67 mole % $AlCl_3$ and 128°C. Since these are convenient compositions to use for molten salt studies, selected values from the references in Table V are listed by mole % AlX_3 and melting points as follows: $AlCl_3$–LiCl, 58%, 105°C; $AlCl_3$–NaCl, 61%, 108°C; $AlCl_3$–CsCl, 75%, 148°C; $AlBr_3$–NaBr, 76%, 95°C; $AlBr_3$–KBr, 74%, 88°C; $AlBr_3$–RbBr, 75%, 83°C; AlI_3–NaI 70%, 123°C; AlI_3–KI, 67%, 105°C; AlI_3–RbI, 71%, 135°C.

For AlX_3–MX mixtures with mole ratios of 3 : 1, 2 : 1, 1 : 1, and

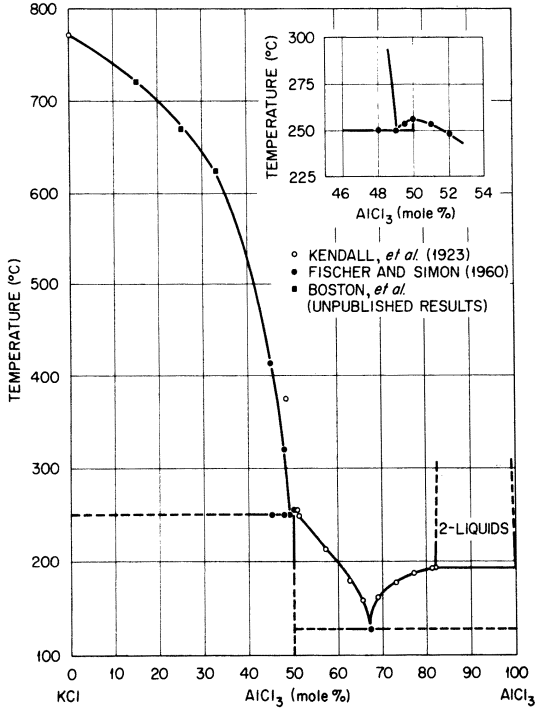

Fig. 2. Typical phase diagram for alkali halide–aluminum halide mixtures.

1 : 3 and corresponding anionic species, $Al_3X_{10}^-$, $Al_2X_7^-$, and AlX_6^{3-} may occur. Of these, AlX_4^- is certainly the most firmly established, having been observed in the solid for X = F, Cl, Br, and I. The alkali metal tetrachloroaluminates have high thermal stabilities and actually can be distilled without decomposition (to aluminum chloride and the alkali metal halide) at temperatures near 1000°C.[61,87] The AlX_6^{3-} ion has been reported only for fluorides, for example, in solid and liquid cryolite. The 2 : 1 compound occurs quite often as an incongruently melting compound in these systems, and congruently melting $CsAl_2I_7$ was reported recently.[88] As mentioned earlier, the abnormally low vapor pressures of melts with this composition also are indicative of fairly stable $Al_2Cl_7^-$ anions. The suggestion of Al_3X_{10} ions and larger ions of this type is much more tenuous, even though phase diagrams give indications of 3 : 1 compounds, as shown in Table VI.

From a consideration of ion radii, Kryagova[89–91] calculated the most probable coordination numbers for aluminum in AlX_3–alkali metal halide mixtures. This study indicated that only coordination numbers 4 and 6 were possible and that 4 was most probable for all halides. Coordination numbers of 4 and 6 were equally probable for X = F. From ion radii considerations the occurrence of AlX_6^{3-} ions for halides other than fluoride, though less probable, appear to be possible for chloride. However, there is no indication of $AlCl_6^{3-}$ in phase diagrams or other studies reported so far.

Thermodynamic data for the haloaluminates are scarce. Table VII lists data from the JANAF tables,[7] most of which is based on very old work. An exception is cryolite, Na_3AlF_6, which has been studied recently by several authors.

5. SPECTROSCOPY AND STRUCTURE

5.1. Raman Spectroscopy

The tetrachloroaluminate ion in molten mixtures containing $AlCl_3$ has been fairly well established by Raman spectroscopy.[167–174] The which appear to clarify some previous discrepancies in band assignments. This work is discussed in another chapter in this volume. The larger anionic species such $Al_2X_7^-$ should be detectable by Raman techniques, but as yet no measurements have been made in the composition range where these species might occur. The most likely configuration for this ion would be two tetrahedral $AlCl_4$ groups sharing a corner analogous to the structure observed for the $Cr_2O_7^-$ ion in $(NH_4)_2Cr_2O_7$.[176] Peach *et al.*[177] report the

TABLE VI. Melting Points (°C) of Alkali Metal Haloaluminate Compounds

M	Fluoride		Chloride		Bromide			Iodide		
	M_3AlF_6	$MAlF_4$	$MAlCl_4$	MAl_2Cl_7	$MAlBr_4$	MAl_2Br_7	MAl_3Br_{10}	$MAlI_4$	MAl_2I_7	MAl_3I_{10}
Li	790[a]		144[e]	No[e]	197[e]			237[g]	No[g]	No[g]
Na	1006[b]	775[d]	151[f]	No[e]	201[e]	105[e,k]	(95)[e,k]	220[l]	164[g,k]	160[g,k]
									No[l]	No[l]
K	1020[c]		256[f]	No[e]	191.5[e]	96[e,i,k]	No[e,i]	207[g]	No[g,l]	No[g,l]
					192.5[i]			210[l]		
Rb			331[g]		285[j]	98[j,k]	(95)[j,k]	179[g]	No[l]	No[l]
					278[i]	110[i,k]		205[l]		
Cs			364[g]	No[h]	340[j]	149[j,k]	(130)[j,k]	259[g]	205[l]	No[l]
			377[h]		357[i]	154[i,k]		250[l]		

[a] D. L. Hildebrand, *et al.*, Aeronutronic Division, Ford Motor Company, Report No. U-2055, Mar. 15, 1963.
[b] W. B. Frank, *J. Phys. Chem. 65*, 2081-7 (1961).
[c] F. P. Hall and H. Insley, *J. Am. Ceram. Soc. 21*, 113 (1938).
[d] K. Grjotheim, Kgl. Norske Videnskab. Selskabs, Skrifter *2*, No. 5, 1–90 (1957).
[e] From Kendall *et al.*[92]
[f] From Fischer and Simon.[93]
[g] From Boef *et al.*[97]
[h] From Morozov and Simonich.[99]
[i] From Cronenberg and van Spronsen.[139]
[j] From Mikheeva *et al.*[140]
[k] Incongruently melting.
[l] From Mikheeva.[88]

TABLE VII. Standard Thermodynamic Properties[a] of Solid Alkali Metal Haloaluminate Compounds at 25°C

	$\Delta H°$ (formation) (kcal mole^{-1})	$C_p°$ (cal mole^{-1} deg^{-1})	$S°$ (cal mole^{-1} deg^{-1})
Li_3AlF_6	-802 ± 5[c]	(48)[j]	(46 ± 4)
Na_3AlF_6	-790 ± 2[d–i]	51.6[d–i]	57.0 ± 0.4[d–i]
K_3AlF_6	(-795 ± 5)	(53)	(68 ± 1)
(Na_3AlCl_6)[b]	-473 ± 1[d]	(58)	(83 ± 2)
$NaAlCl_4$	-273 ± 1[d]	(37)	(45 ± 2)
(K_3AlCl_6)[b]	-500 ± 1[d]	(59)	(90 ± 2)
$KAlCl_4$	-286 ± 3[d]	(37)	(47 ± 2)
$(K_3Al_2Cl_9)$[b]	-684 ± 3[d]	(81)	(112)

[a] From Stull.[7]
[b] Hypothetical compounds.
[c] P. L. Hildebrand *et al.*, Aeronutronic Division, Ford Motor Company, Report No. U-2055 (March 15, 1963).
[d] E. Baud, *Ann. Chim. Phys.* **1**: 8–71 (1904).
[e] J. P. Coughlin, *J. Amer. Chem. Soc.* **80**; 1802–1804 (1958).
[f] P. Gross, C. Hayman, and D. L. Levi, *Physical Chemistry of Process Metallurgy*, Pt. II, John Wiley (Interscience), New York (1961).
[g] E. G. King, *J. Amer. Chem. Soc.* **79**; 2056–2057 (1957).
[h] C. J. O'Brien and K. K. Kelley, *J. Amer. Chem. Soc.* **79**; 5616–5618 (1957).
[i] W. B. Frank, *J. Phys. Chem.* **65**; 2081–2087 (1961).
[j] Parentheses indicate estimated values.

infrared spectrum of acetyl Al_2Cl_7 in acetyl chloride and also find end points in conductometric titrations of tetra-alkylammonium chlorides with Al_2Cl_6 in acetyl chloride corresponding to both $AlCl_4^-$ and $Al_2Cl_7^-$.

5.2. Crystal Structures

Crystal structures have been determined for several fluoroaluminates. For compounds having the general formula $MAlF_4$, Wyckoff[178] lists crystal data with M = Na, K, Rb, Tl, and NH_4 and for the general formula M_3AlF_6 with M = Na, K, and NH_4. The structure of $NaAlCl_4$ was determined by Baenziger[179] and consisted of Na^+ and tetrahedral $AlCl_4^-$ ions. Distances between these ions were normal, but Al–Cl and Cl–Cl distances in the $AlCl_4^-$ tetrahedra were shorter than normal, as might be

expected for the highly polarizing aluminum ion. Ibers[180] determined the crystal structure of $Co(AlCl_4)_2$ and found the dimensions of the $AlCl_4$ tetrahedron to be about the same as observed for $NaAlCl_4$. The cobalt atom was octahedrally coordinated with severe distortion of the $CoCl_6$ group.

The lattice energy has been determined[181] for $NaAlCl_4$. An average value of 138 $\pm$ 7 kcal/mole was calculated, and this corresponded to approximately 50% ionic character for the Al–Cl bond.

6. SOLVENT PROPERTIES

As solvents the haloaluminates have several advantages over most molten salts. Among the more notable are low melting points, a wide range of acidities, optical transparency over wide wavelength ranges, and high decomposition potentials. The frequent occurrence of liquid–liquid miscibility gaps in their phase diagrams also has been utilized for solute distribution studies. The haloaluminates provide suitable media for various chemical syntheses, and this aspect of their solvent properties is considered in Section 8.

6.1. Acid–Base Systems and Solubilities

In considering the solvent properties of haloaluminate melts it is helpful to apply acid–base concepts. This was done recently for the $AlCl_3$–NaCl system by Tremillon and Letisse.[182] These authors assumed the equilibrium $2AlCl_4^- = Al_2Cl_7^- + Cl^-$ for the "acidic" or $AlCl_3$-rich mixtures. With "acids" defined as Cl^- acceptors and "bases" as Cl^- donors the acidity of the system can be expressed in terms of $pCl^- = -\log[Cl^-]$. Using an aluminum microelectrode (rotating) as a pCl indicator, the potentiometric titration curve of Cl^- by the coulometrically produced $Al_2Cl_7^-$ gave the apparent equilibrium constant $K_i = [Al_2Cl_7^-][Cl^-] = 3.40 \pm 0.4 \times 10^{-6}$ mole^2/kg^2 at 175°C. Using a chlorine electrode as a pCl^- indicator gave a similar value for K_i. Thus melts having $pCl^- > 2.7$ are "acid" and those having $pCl^- < 2.7$ are "basic."

This equilibrium also has been measured by more indirect methods for $AlCl_3$–KCl melts by Morrey and Moore,[183] who studied the distribution of uranium between $AlCl_3$–KCl melts and molten aluminum, and more recently by Juvet *et al.*,[184] who used gas chromatography. The latter results gave a value of 3×10^{-4} at 289°C for the constant $K = [Al_2Cl_7^-][Cl^-]/[AlCl_4]^2$, which agreed with the estimates of Morrey and Moore.[183]

Letisse and Trémillon[184] also studied the behavior of H^+ and O^{2-} in molten $NaAlCl_4$ since these ions are formed by reaction with water, which is the most likely contaminant of these melts. They suggest an increase in "basicity" of the melt as water is added because of the reaction

$$2AlCl_4^- + H_2O = 2HCl + Al_2OCl_5^- + Cl^-$$

The molten $AlCl_3$–NaCl eutectic has been used as a solvent for the spectrophotometric determination of equilibria involving the lower oxidation states of bismuth.[186–188] At the eutectic composition, 61 mole % $AlCl_3$, the melts are on the "acidic" side with a high pCl^-. The Cl^- concentration is quite low and buffered, probably by the equilibrium $2AlCl_4^- = Al_2Cl_7^- + Cl^-$. These authors suggest that the buffering capacity of the eutectic melt is sufficient to maintain a constant Cl^- activity when solute concentrations are low. This subject is discussed further in Section 6.2.

Several solubility measurements in molten $NaAlCl_4$ have been reported. Dissolutions of the elements Hg, P, Mn, W, Mo, Cu, Si, and S at 150 to 370°C were determined by Plotnikov and Fortunatov.[189] The solubility of UF_4 was determined by Calkins[190] and the solubility of HCl by Groshev *et al.*[191]

6.2. Stabilization of Subvalent Species

The acidic nature of haloaluminate melts makes them particularly good solvents for studies of lower oxidation states. This point was first emphasized by Corbett, Burkhard, and Druding[192] in their study of Cd(I). Cubicciotti[193] had shown earlier that cadmium dissolution in $CdCl_2$ decreased more rapidly with the addition of KCl than with the more acidic $CeCl_3$. Corbett and co-workers continued their studies on subvalent cadmium measuring Raman spectra,[194] absorption spectra,[195,196] and emf's.[197] This work shows that the Cd_2^{2+} ion is the dominant lower oxidation state species.

A fair amount of information now exists concerning the lower oxidation states of bismuth in molten salt solutions. The early work was done on solutions of bismuth metal in molten bismuth trihalides. Both emf[198,199] and spectrophotometric[200,201] measurements on dilute solutions (<6 mole %) indicated two species, each having an oxidation state lower than three. These results fit the equilibrium $4Bi^+ = Bi_4^{4+}$ or, perhaps more generally, equilibria involving $Bi^+ \cdot xBi^{3+}$ and $Bi_3^+ \cdot yBi^{3+}$, as suggested by Corbett.[202] Since Bi^{3+} is present in large excess, x and y are not easily

determined. This problem was avoided in recent spectrophotometric studies[186,188] by using chloroaluminate melts as solvents and working only at very low concentrations of bismuth species. Both $AlCl_3$–NaCl and the less "acidic" $ZnCl_2$–KCl melts were used as solvents, and the cationic species, Bi^+, Bi_5^{3+}, and B_8^{2+} were identified. The following equilibria were studied:

$$6Bi^+ \rightleftarrows Bi_5^{3+} + Bi^{3+} \quad (1)$$

$$2Bi + Bi^{3+} \rightleftarrows 3Bi^+ \quad (2)$$

$$4Bi + Bi^{3+} \rightleftarrows Bi_5^{3+} \quad (3)$$

$$22Bi + 2Bi^{3+} \rightleftarrows 3Bi_8^{2+} \quad (4)$$

Approximate equilibrium quotients for equation (1) were 1.7×10^{10} l^4/mole^4 for $ZnCl_2$–KCl solvent at 380°C and 4.8×10^8 l^4/mole for $AlCl_3$–NaCl solvent at 130°C. Since this quotient decreases rapidly with increasing temperature (4×10^5 l^4/mole^4 at 190°C), it can be seen that equation (1) is quite sensitive to solvent with several orders of magnitude increase in the equilibrium quotient as the solvent is changed from $AlCl_3$–NaCl to the less acidic $ZnCl_2$–KCl. A similar effect was observed for equation (2), and in both cases an increase in "acidity" favored the formation of Bi^+ at the expense of Bi^{3+}. A ligand field theoretical treatment[187] of the Bi^+ ion assuming $6p^2 \rightarrow 6p^2$ transitions gave good agreement with the observed spectrum.

Corbett and co-workers studied the solid phases occurring in these bismuth systems and identified the unusual cation Bi_9^{5+} in a structural study of the compound $Bi_{12}Cl_{14}$.[203] In chloroaluminate melts Corbett[204] was able to prepare the solid compounds $Bi_5(AlCl_4)_3$ and $Bi_4(AlCl_4)$, which have the same stoichiometry as the polybismuth cations, Bi_5^{3+} and Bi_8^{2+}, identified spectrophotometrically in dilute solutions.[186,188] In addition, mull and reflectance spectra[204] of these solid compounds were similar to solution spectra,[186,188] indicating that the same cations exist in both media.

The lower oxidation states of lead and tin in molten $NaAlCl_4$ were studied electrochemically by Munday and Corbett.[197] The reduced species observed were Pb^+ (or $Pb^+ \cdot mPb^{2+}$) and Sn_2^+ (or Sn_3^{2+} etc.), the identity of the tin species being somewhat less certain.

6.3. Spectroscopy

Haloaluminate melts are particularly good solvents for spectrophotometric studies since they are transparent in the near-infrared, visible, and

ultraviolet (to about 2000 Å for chloroaluminate melts). Their low melting points provide a further advantage for this type of measurement.

In addition to the spectroscopic studies of bismuth and cadmium mentioned in Section 6.2, Øye and Gruen[205] measured the absorption spectrum of Co(II) in $AlCl_3$–KCl mixtures. As solvent composition was varied these authors found evidence for mixed anionic complexes of the type $Co(Al_2Cl_7)(AlCl_4)$, which have a distorted octahedral environment of chloride around cobalt.

With increasing melt "acidity," chloro complexes of both Co(II) and Ni(II) show tendencies toward octahedral relative to tetrahedral configurations. In addition, Ni(II) shows a greater tendency than Co(II) to form octahedral complexes. In the proper "acidity" range one can observe both configurations present in equilibrium. Angell and Gruen found that $ZnCl_2$–KCl mixtures[206] had a suitable "acidity" range for studying the octahedral–tetrahedral equilibrium for Ni(II) whereas Co(II), because of its lower tendency to form octahedral complexes, required the more "acidic" solvent, $AlCl_3$–$ZnCl_2$.[207] The latter solvent should be quite "acidic" at all compositions since $ZnCl_2$ itself is a strong Lewis acid.

In a study of solvent and temperature effects on the absorption spectrum of UCl_4, Morrey[208] used both $AlCl_3$–KCl and $AlCl_3$–CsCl mixtures as solvents. The UCl_6^{2-} ion and another unidentified species were observed. Marked changes in the spectrum occurred with slight changes in $MCl/AlCl_3$ when this ratio was near unity ("neutral" point), indicating large changes in the relative amounts of uranium species with changes in chloride activity.

6.4. Electrical Studies of Solutes

Molten salt mixtures containing aluminum halides have been used as solvents in a great many electrochemical studies. Delimarskii and co-workers[209] have used these solvents for the determination of decomposition[210–212] and electrode[213–215] potentials of a large number of metal ions. Graphite or platinum was the usual electrode material, but an Na-glass indicator electrode[213] also was used. Yntema and co-workers,[216–218] using similar solvents and aluminum reference electrodes, also measured decomposition potentials of several metal ions. The ordering of metals according to their potentials varies with the solvent. Delimarskii and co-workers[209–212] relate this to complex formation.

Measurements of cell emf's using molten $AlBr_3$–NaBr mixtures as solvents also have been reported.[219–220] The metals studied in order of increasing nobility were Al, Mn, Zn, Cn, Pb, Sn, Cu, Ag, Sb, and Bi.

As mentioned earlier, molten $NaAlCl_4$ has been used as a solvent for emf studies of lower oxidation states of lead, cadmium, and tin.[197] This same solvent was also used by Plotnikov *et al.*[221] to measure cell emf's. The order of potentials was Al, Mn, Zn, Fe, and Cu, similar to the order in the corresponding bromide melt.

A number of polarographic studies using haloaluminate solvents have been reported. A polarographic study[222] of Nb^{5+} and Ta^{5+} in molten $AlCl_3$–NaCl–KCl mixtures gave a double wave for Nb^{5+} ($\rightarrow Nb^{4+} \rightarrow Nb^{3+}$) and a single wave for $Ta^{5+}(\rightarrow Ta^{3+})$. Delimarskii *et al.*[223] used a polarographic method to determine decomposition potentials of a large number of metal ions in $AlCl_3$–NaCl mixtures. Chovnyk and co-workers made similar measurements in $AlBr_3$–NaBr[224,225] and $AlBr_3$–NaCl[225–229] mixtures. The reduction of bismuth in the latter solvent[228] occurred in steps, the first being $Bi^{3+} + 2\varepsilon = Bi^{+}$. This lends further support to the existence of Bi^{+} in these melts in agreement with spectrophotometric results.[186]

6.5. Immiscible Liquid Studies

As pointed out in the discussion of phase diagrams, aluminum halide-containing systems frequently form immiscible liquid phases. This characteristic presents the possibility of an extractive separation process that has been explored to some extent. Moore[230] has determined distribution coefficients for several actinide and fission product chlorides between the two nearly immiscible liquid phases, LiCl and $KAlCl_4$, at 625°C. Ammon[231] made a similar study of the distribution of several metal ions between the two liquid phases in the $AlBr_3$–KBr system at 200°C. In Ammon's work the less ionic bromides showed a preference for the more "molecular" ($AlBr_3$-rich) liquid phase. When Moore examined an ion in two different oxidation states, the one having the higher oxidation state usually showed a preference for the $KAlCl_4$-rich phase. The highest separation factor observed by Moore was 1300 for Cs–Sr, while Ammon found a maximum value of 126 for Cs–Zr. Distribution coefficients for the actinide elements also were determined using $AlCl_3$–KCl mixtures as one liquid phase and molten aluminum metal as the second liquid phase.[232] The distribution coefficients were strongly influenced by $AlCl_3$–KCl ratios in the salt phase and went through sharp maxima (metal phase preference) at mole ratios near unity. One of the higher separation factors observed was 800 for Th–Pa.

7. ELECTROCHEMISTRY

In the electrochemical measurements described earlier the haloaluminates were used primarily as solvents. In addition to this type of measurement the aluminum halide mixtures themselves have been studied[233] by a variety of electrochemical techniques, and some of these will be described.

The large number of electrochemical studies of haloaluminate melts is probably due to their low melting points, good solvent properties, high decomposition potentials, and possible industrial use. Bromoaluminates have been studied to a greater extent than chloroaluminates, probably because pure $AlBr_3$ has a lower melting point and vapor pressure than $AlCl_3$. Most of this work falls into three general types: conductivity, decomposition potentials, and electrolysis. Table VIII lists references according to system and type of study.

7.1. Conductivity

Most conductivity measurements on these systems have been limited to compositions between 50 and 80 mole % AlX_3, since below 50 mole % the liquidus curve rises very rapidly and above 80 mole % a two-liquid phase region usually occurs. Furthermore, most measurements have been made below 300°C because of the high vapor pressures characteristic of the AlX_3-rich mixtures. An exception is the work of Grothe,[71] who observed increasing conductivities for 36, 39, and 48 mole % $AlCl_3$–KCl at moderately high temperatures and vapor pressures of less than 1 atm. Recently Boston, Grantham, and Yosim[234] made a complete study of this system. They measured conductivities at compositions from 15 to 80 mole % $AlCl_3$, at temperatures to 1080°C, and at pressures up to about 30 atm. Pronounced minima and maxima in equivalent conductance isotherms occurred at 33 and 50 mole % $AlCl_3$, respectively, as shown in Fig. 3. The compound, $KAlCl_4$, had a maximum specific conductance with a temperature near 1000°C. The KCl–$AlCl_3$ system was considered as comprising the two binary systems KCl–$KAlCl_4$ and $KAlCl_4$–Al_2Cl_6. Large negative deviations from linearity of conductivity isotherms for the KCl–$KAlCl_4$ system were apparently due to differences in anion polarizabilities, while positive deviations for the $KAlCl_4$–Al_2Cl_6 system were attributed to basic changes in melt structure.

Conductivities of molten MBr_n–$AlBr_3$ mixtures were measured by Gorenbein and co-workers[74–77] for M = NH_4^+, Na^+, K^+, Zn^{2+}, Hg^{2+}, and Sb^{3+}. Measurements were made at low temperatures ($\leq$ 170°C)

TABLE VIII. References to Electrochemical Studies

System	Reference		
	Conductivity	Decomposition potentials	Electrolysis
$AlCl_3$–LiCl	(67, 71, 233)		(245)
–NaCl	(67, 70, 233, 238, 259)	(243)	(245, 246, 247)
–KCl	(67, 70, 71, 233)	(71)	(245, 247)
–RbCl	(233)		
–$MgCl_2$	(71)		
–$CaCl_2$			(245)
–$SbCl_3$		(23)	
–ICl	(73)		
–NH_4Cl	(67)		
–S_2Cl_2	(260)		
–$POCl_3$	(261)		(239)
–NaBr	(233)		
$AlBr_3$–NaBr	(74, 75)	(240)	
–KBr	(74, 76, 81)	(240)	
–AgBr		(241)	
–$ZnBr_2$	(75, 76)	(240, 241)	
–$HgBr_2$	(77, 81)		
–TlBr		(240)	
–$SnBr_2$	(23)	(23)	
–$PbBr_2$		(240, 241)	
–$SbBr_3$	(75, 76, 81)	(23, 240, 241)	
–IBr	(79, 80)		(235)
$AlCl_3$–NH_4Br	(75, 77)		
–LiCl	(242)	(240, 242)	
–NaCl	(242)	(242)	
–KCl	(75, 242)	(240, 242)	
–AgCl		(242)	
$AlBr_3$–ICl	(79, 80)		
AlI_3–HI	(262)		
$AlCl_3$–NaCl–KCl	(70)		(244)
$AlBr_3$–$AsBr_3$–$SbBr_3$	(78)		
$AlCl_3$–LiCl–KCl–$MgCl_2$	(71)		
AlX_3–MX_n (in organic solvents)	(249–258)	(249, 250, 255, 258)	(250–255, 258)

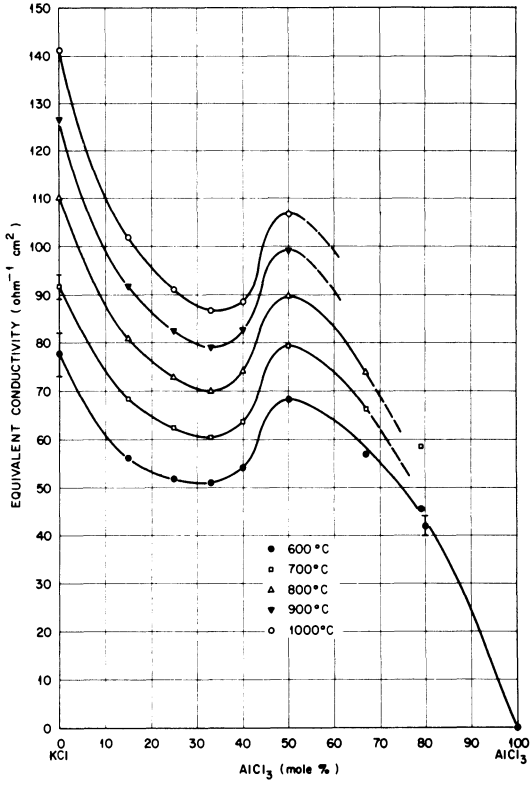

Fig. 3. Equivalent conductivity isotherms for a KCl–$AlCl_3$ system.

and were further limited to a single composition or very narrow composition ranges. Viscosities and densities also were measured. Molar conductivities were "corrected" for viscosities in the belief that a direct relationship existed between these two properties. However, Delimarskii and Markov[209] suggest that this is an erroneous assumption. Compounds having the general formula $MBr_n \cdot Al_2Br_6$ were indicated for $M = NH_4^+$, Na^+, K^+, Zn^{2+}, and Hg^{2+}. These authors also studied[78] the system $SbBr_3$–$AlBr_3$ in $AsBr_3$ as solvent.

A considerable amount of work has been done by Fialkov and coworkers[73,79,80,235] on IX–$AlBr_3$ mixtures (X = Br and Cl) as well as ICl–$AlCl_3$ mixtures. In addition to conductivities this work often included measurements of densities, viscosities, and liquidus temperatures. Conductivity isotherms showed maxima near 10–14 mole % AlX_3 for all three systems. The compounds $AlCl_3 \cdot ICl$, $AlCl_3 \cdot 2ICl$, and $AlBr_3 \cdot IBr$ were indi-

cated, and transference measurements[73,235] suggested the existence of $I(AlCl_4)$ and $I(AlBr_4)$.

Transport properties were determined for $AlBr_3$–KBr by Isbekow[236] and later interpreted in terms of interionic friction coefficients by Laity.[237] Transference numbers also have been measured for the $AlCl_3$–NaCl system.[238] and the $AlCl_3$–$POCl_3$ system.[239] In all cases transference numbers for AlX_4^- were quite small as expected for such large anions.

7.2. Decomposition Potentials, Electrolysis, and Other Electrochemical Studies

Decomposition potentials and electrolysis behavior have been reported for a number of chloro- and bromoaluminate melts, as indicated in Table VIII. Most of the decomposition potential measurements were done by Gorenbein and co-workers[240,241] on $AlBr_3$-containing mixtures. Mezhenni[242] along with Izbekov and Chovnik[23] also measured these mixtures. Similar measurements for aluminum chloride with NaCl,[243] KCl,[235] and $SbCl_3$[23] also have been reported.

Electrolysis behavior of $AlCl_3$-containing mixtures has been the subject of several studies.[244–247] Some of this work[245] was motivated by the prospect of developing a low temperature process for the commercial production of aluminum.

A polarographic study of $AlBr_3$–NaBr mixtures was recently reported by Chovnyk *et al.*[248] An Ag–AgBr electrode was used, and the limiting currents indicated 1 : 1 compound formation.

Various electrochemical studies of haloaluminates in organic solvents have been reported.[249–258] They deal mainly with conductivity and electrolysis in benzene or nitrobenzene, and in general the behavior in organic solvents is similar to what is observed in melts. Again, evidence for stable 1 : 1 compounds was observed. Plotnikov[258] has reviewed this subject.

8. TECHNOLOGICAL APPLICATIONS

From an applied point of view perhaps the most promising use of haloaluminate melts is as media for both inorganic and organic syntheses. The use of molten salts as media for chemical synthesis has recently been reviewed by Sundermeyer,[263] who points out the advantages of these liquids and how little they have been exploited.

Inorganic reactions in haloaluminate melts that have been studied are

mainly reduction processes involving a metal halide and a metal with the emphasis here being on total reduction to the metal rather than partial reduction to intermediate oxidation states as described in Section 6.2. The metal is usually present as a liquid or suspended solid and, presumably, is in solution to a very slight extent. Typical of this type of reaction are those studied by Moore and co-workers that involved the reduction of UX_3 by liquid aluminum in AlX_3–KX solvents for X = Cl and Br. The reduction of UCl_3 in $AlCl_3$–KCl was measured[264] as a function of solvent composition, with uranium reduction being quite sensitive to $AlCl_3$/KCl ratios. The optimum mole ratio was found to be about unity. This same equilibrium was measured[265] with chloride replaced by bromide and found to be much less favorable for reduction of uranium. These results were explained[266] in terms of acid–base equilibria involving the complex species $Al_2Cl_7^-$, $AlCl_4^-$, and UCl_6^{3-}. Delimarskii[267] also studied reduction equilibria between liquid metals and molten halides. He examined the systems $PbBr_2$ + Cd, $SnBr_2$ + Cd, and $SnBr_2$ + Pb using $AlBr_3$–KBr mixtures as solvents. The reduction of $ZnCl_2$ by Al also has been measured.[268] The disproportionation of $ZrCl_2$ to Zr metal and $ZrCl_4$ was observed[269] in several molten salt mixtures. The fastest reaction rate was found for $AlCl_3$–NaCl melts

The chlorination of Nb, Ti, and Ta oxides by $NaAlCl_4$ and $KAlCl_4$ has been studied.[270] Here the solvent also was a reactant, and the progress of reaction was followed by measuring vapor pressure increases.

A great deal of synthetic work has been done by Sundermeyer and co-workers using molten salts as reaction media. Much of this work deals with organic reactions with particular emphasis on the silanes. Molten LiCl–$AlCl_3$,[271] NaCl–$AlCl_3$,[272,273] KCl–$ZnCl_2$,[272,274–276] LiCl–KCl eutectic,[277–279] and LiF–NaF–KF eutectic[280,281] were used as solvents. These authors point out that fused salts are particularly well suited as media for organic reactions. This becomes most apparent when the catalytic behavior of molten salts is compared with solid catalysts. High thermal conductivities help dissipate the heat of reaction rapidly in melts, thus avoiding the serious problem of local overheating that often occurs with solid catalysts. In addition, the catalytic activity of the melt does not deteriorate with time as is often the case with solid supports where the active material is either lost with the reaction products or is blocked by adsorbed decomposition products. Typical of the types of reactions studied by Sundermeyer and co-workers are the preparation of SiH_3Cl by bubbling a gaseous, equimolar mixture of SiH_4 and HCl through molten LiCl–$AlCl_3$ at 120–130°C and the preparation of ethyl benzene by passing an equimolar mixture of benzene and ethyl chloride through this same melt at 150–160°C. Catalytic chlorina-

tions of hydrocarbons proceed smoothly in melts because of the efficient dissipation of heat and the high solubility of chlorine. Several patents have been issued for the isomerization of *n*-paraffins to branched-chain compounds in melts containing Friedel–Crafts catalysts (for example, $AlCl_3$), a process of interest for increasing octane ratings of hydrocarbon fuels. For further discussion of this highly promising field the reader is referred to the recent, comprehensive review by Sundermeyer.[263]

Bruce, Sorrie, and Thomson[282] have studied intramolecular cyclizations, Fries rearrangements, and condensations of p-$C_6H_4(OH)_2$ with various mono- and dibasic acids using molten $AlCl_3$–NaCl at 180–200°C as a solvent.

The suitable process mentioned in Section 2.5 for the purification of aluminum appears promising from the technological point of view. Impure aluminum is reacted with gaseous aluminum chloride at temperatures above 1000°C to form $AlCl(g)$, which is then cooled to form pure aluminum metal. The reaction also can be run in alkali chloride–$AlCl_3$ melts at lower temperatures.[54,55]

Other technological uses suggested for haloaluminate melts are as electrolytes in batteries[283] and heat exchange fluids in nuclear reactors.[284]

9. MELT PREPARATION AND HANDLING

From this brief review of haloaluminates it becomes apparent that these systems are of interest in themselves and have great potential as molten salt solvents. As pointed out earlier, the difficulties encountered in the preparation and handling of the haloaluminates and especially the pure aluminum halides have doubtless been the major deterrent to their more extensive use. Their relatively high vapor pressures also may be a handicap.

The pure aluminum halides are extremely reactive. They form strong addition compounds with many organics and react vigorously with even trace amounts of ambient moisture. For precise work they should be handled only in sealed systems or, as a second choice, in extremely clean, inert atmosphere glove boxes. Purification of contaminated aluminum halides is extremely difficult so that most workers have found that the best procedure is to prepare them from the elements using high-purity starting materials.

The most common impurities of haloaluminate melts are water, organics, and iron. The sensitivity of these melts to these and other contaminants increases with aluminum halide concentration, so the discussion here primarily, considers the pure aluminum halides.

Although these materials react vigorously with moisture, this contaminant may not be as serious as in other molten salts. Instead of forming soluble (and corrosive) oxides and/or hydroxides, water reacts with aluminum halides to give insoluble (and inert) aluminum oxide with perhaps small amounts of soluble oxychlorides.[185]

Contamination by organics can be more serious than water contamination for certain measurements, for example, spectrophotometric, since aluminum halides form stable, often highly colored, addition compounds with many organic materials. One fairly common source of organic contamination is back-diffusing oil vapor from mechanical vacuum pumps. Once contaminated by organics, removal can be extremely difficult. Distillation helps very little, and thermal decomposition requires equipment that will withstand substantial vapor pressures and even then is surprisingly ineffective.

Contamination by iron usually as FeX_3 can be avoided by synthesis and/or distillation in a reducing environment, for example, with excess aluminum metal present. Whereas $FeCl_3$ will distill with $AlCl_3$, the presence of excess aluminum metal keeps iron in the $+2$ state, which is much less volatile.

The preparation of high purity aluminum chloride by the reaction of aluminum metal with hydrogen chloride gas recently has been described.[27,186] Although high purity aluminum metal is readily available, most commercial HCl contains excessive amounts of organic (largely acetylene) impurities. Either laboratory-generated or special, high purity (99.99%) commercial HCl should be used.

ACKNOWLEDGMENTS

The author would like to thank Dr. G. P. Smith for many helpful suggestions to improve the text and his encouragement of the work in general. Thanks also are due Dr. J. Brynestad for many helpful discussions.

REFERENCES

1. J. F. Gall, in: *Kirk-Othmer Encyclopedia of Chemical Technology*, 2nd ed. Vol. 9, pp. 529–48, John Wiley (Interscience), New York (1966).
2. P. A. Casabella and N. C. Miller, *J. Chem. Phys.* **40**:1363–1368 (1964).
3. R. G. Barnes and S. L. Segel, *J. Chem. Phys.* **25**:180 (1956).
4. P. A. Casabella, P. J. Bray, and R. G. Barnes, *J. Chem. Phys.* **30**:1393–1396 (1959).

5. S. L. Segel and R. G. Barnes, *J. Chem. Phys.* **25**:578–579 (1956).
6. C. R. Boston, S. J. Yosim, and L. F. Grantham, *J. Chem. Phys.* **51**:1669–1671 (1969).
7. D. R. Stull, ed., *JANAF Thermochemical Tables*, Dow Chemical Co., Midland, Michigan (1965).
8. L. A. Nisel'son and T. D. Sokolova, *Zh. Neorg. Khim.* **10**:1516–19 (1965).
9. A. Smits and J. L. Meijering, *Z. Phys. Chem.* **B41**:98–111 (1938).
10. J. W. Johnson, W. J. Silva, and D. Cubicciotti, *J. Phys. Chem.* **72**:1669–1672 (1968).
11. E. Moles and A. Vian, *An. Soc. Espan. Fis. Quim.* **34**:782–786 (1936).
12. K. J. Palmer and N. Elliott, *J. Amer. Chem. Soc.* **60**:1852–1857 (1938).
13. R. L. Harris, R. E. Wood, and H. L. Ritter, *J. Amer. Chem. Soc.* **73**:3151–3155 (1951).
14. K. N. Semenenko and T. N. Naumova, *Zh. Neorg. Khim.* **9**:1316–1322 (1964).
15. W. Biltz and A. Voigt, *Z. Anorg. Allg. Chem.* **126**:39–53 (1923).
16. H. Schinke and F. Sauerwald, *Z. Anorg. Allg. Chem.* **287**:313–324 (1956).
17. B. F. Markov and A. F. Polishchuk, *Ukr. Khim. Zh.* **31**:1065–1071 (1965).
18. K. Sasvari, *Acta Phys. Acad. Sci. Hung.* **9**:195–202 (1958).
19. J. A. A. Ketelaar, C. H. MacGillavry, and P. A. Renes, *Rec. Trav. Chim.* **66**:501–512 (1947).
20. F. Hanic, K. Matiasovsky, D. Stempelova, and M. Malinovsky, *Acta Chim. Acad. Sci. Hung.* **32**:309–313 (1962).
21. P. A. Renes and C. H. MacGillavry, *Rec. Trav. Chim.* **64**:275–283 (1945).
22. P. A. Akishin, N. G. Rambidi, and E. Z. Zasorin, *Kristallografiya* **4**:186–193 (1959).
23. V. O. Izbekov and N. G. Chovnik, *Mem. Inst. Chem. Ukr. Acad. Sci.* **4**:71–83 (1937).
24. W. Isbekow, *Z. Phys. Chem.* **116**:304–312 (1925).
25. Yu. K. Delimarskii and A. A. Kolotti, *Zh. Fiz. Khim.* **23**:90–96 and 437–440 (1949).
26. V. Izbekov and O. Nizhnik, *J. Gen. Chem. USSR* **7**:1268–1279 (1936).
27. H. A. Øye and D. M. Gruen, *Inorg. Chem.* **3**:836–841 (1964).
28. H. H. Emons and H. Hasselbarth, *Chem. Tech. (Berlin)* **14**:621–624 (1962).
29. R. F. Barrow, I. Kopp, and R. Scullman, *Proc. Phys. Soc.* **82**:635–636 (1963).
30. D. Sharma, *Astrophys. J.* **113**:210–218 (1951).
31. M. Heise and K. Wieland, *Helv. Chim. Acta* **34**:2182–2197 (1951).
32. E. Miescher, *Helv. Phys. Acta* **9**:693–706 (1936).
33. D. Maeder, *Helv. Phys. Acta* **16**:503–528 (1943).
34. D. Sharma, *Astrophys. J.* **113**:219–221 (1951).
35. D. R. Lide, Jr., *J. Chem. Phys.* **42**:1013–1018 (1965).
36. B. J. Chai, H. C. Ko, M. A. Greenbaum, and M. Farber, *J. Phys. Chem.* **71**:3331–3336 (1967).
37. A. I. Belyaev, *Izv. Akad. Nauk SSSR Met. Gorn. Delo* (4):22–31 (1963).
38. H. C. Ko, M. A. Greenbaum, J. A. Blauer, and M. Farber, *J. Phys. Chem.* **69**:2311–2316 (1967).
39. V. Pozsgai and E. Balazs, *Kohasz. Lapok* **99**:227–233 (1966).
40. E. Balazs and V. Pozsgai, *Femip. Kut. Intez. Kozlem.* **7**:275–288 (1964).
41. R. Heimgartner, *Schweiz. Arch. Angew. Wiss. Tech.* **18**:241–255 (1952).
42. P. Weiss, *Z. Erzbergbau Metallhuettenw.* **3**:241–244 (1950).
43. A. S. Russell, K. E. Martin, and C. N. Cochran, *J. Amer. Chem. Soc.* **73**:1466–1469 (1951).

44. T. Kikuchi, T. Kurosawa, and T. Yagihashi, *Trans. Jap. Inst. Metals* **5**:122–127 (1964).
45. M. A. Frisch, M. A. Greenbaum, and M. Farber, *J. Phys. Chem.* **69**:3001–3005 (1965).
46. D. B. Rao and V. V. Dadape, *J. Phys. Chem.* **70**:1349–1353 (1966).
47. H. Mitani and H. Nagai, *Nippon Kinzoku Gakkaishi* **31**:1296–1300 (1967).
48. W. Klemm, K. Geiersberger, B. Schaeler, and H. Mindt, *Z. Anorg. Chem.* **225**:287–293 (1948).
49. W. Hirschwald and O. Kacke, *Z. Erzbergbau Metallhuettenw.* **11**:99–104 (1958).
50. S. A. Semenkovich, *Zh. Prikl. Khim.* **33**:552–559 (1960).
51. J. Thonstad, *Can. J. Chem.* **42**:2739–2743 (1964).
52. J. D. Corbett and S. von Winbush, *J. Amer. Chem. Soc.* **77**:3964–3966 (1955).
53. W. C. Schumb and H. H. Rogers, *J. Amer. Chem. Soc.* **73**:5860–5868 (1951).
54. R. Midorikawa, *Denki Kagaku* **25**:13–16 (1957).
55. T. Notoya, *Electrochim. Acta* **13**:2194–2195 (1968).
56. A. I. Belyaev, *Sb. Nauch. Tr. Mosk. Inst. Tsvet.* Metal. Zolota (31):46–63 (1958).
57. C. R. Boston, *J. Chem. Eng. Data* **11**:262–263 (1966).
58. J. R. Morrey and D. G. Carter, *J. Chem. Eng. Data* **13**:94 (1968).
59. I. I. Naryshkin, *J. Phys. Chem. USSR* **13**:690–692 (1939).
60. H. Grothe, *Z. Elektrochem.* **54**:216–219 (1950).
61. E. W. Dewing, *J. Amer. Chem. Soc.* **77**:2639–2641 (1955).
62. T. Narita, T. Ishikawa, and R. Midorikawa, *Denki Kagaku* **36**:300–305 (1968).
63. R. H. Moore, J. R. Morrey, and E. E. Voiland, *J. Phys. Chem.* **67**:744 (1963).
64. M. M. Vetyukov and G. I. Sipriva, *Zh. Prikl. Khim.* **36**:1905–1909 (1963).
65. J. D. Edwards, C. S. Taylor, L. A. Cosgrove, and A. S. Russell, *J. Electrochem. Soc.* **100**:508 (1953).
66. W. B. Frank and L. M. Foster, *J. Phys. Chem.* **64**:95–98 (1960).
67. Y. Yamaguti and S. Sisido, *J. Chem. Soc. Jap.* **62**:304–307 (1941).
68. A. I. Kryagova, *J. Gen. Chem. USSR* **9**:1755–1758 (1939).
69. R. Midorikawa, *J. Electrochem. Soc. Jap.* **23**:310 (1954).
70. R. Midorikawa, *J. Electrochem. Soc. Jap.* **23**:352–355 (1955).
71. H. Grothe, *Z. Elektrochem.* **53**:362–369 (1949).
72. C. R. Boston, *J. Chem. Eng. Data* **13**:117 (1968).
73. Ya. A. Fialkov and O. I. Shor, *J. Gen. Chem. USSR* **19**:a235–a249 (1949).
74. E. Ya. Gorenbein and E. E. Kriss, *J. Gen. Chem. USSR* **19**:1978–1986 (1949).
75. E. Ya. Gorenbein, *Zh. Obshch. Khim.* **18**:1427–1439 (1948).
76. E. Ya. Gorenbein, *J. Gen. Chem. USSR* **15**:729–744 (1945).
77. E. Ya. Gorenbein, *J. Gen. Chem. USSR* **17**:873–886 (1947).
78. E. Ya. Gorenbein and E. E. Kriss, *J. Phys. Chem. USSR* **25**:791–797 (1951).
79. Ya. A. Fialkov, *Zap. Inst. Khim., Akad. Nauk SSSR.* **6**:235–260 (1940).
80. Ya. A. Fialkov and N. I. Gol'dman, *J. Gen. Chem. USSR* **11**:910–924 (1941).
81. B. A. Isbekov and V. A. Plotnikov, *Z. Anorg. Chem.* **71**:328–346 (1911).
82. A. I. Kryagova, *J. Gen. Chem. USSR* **9**:1759–1763 (1939).
83. E. Ya. Gorenbein, *J. Phys. Chem. USSR* **25**:1160 (1951).
84. N. A. Trifonov, *Akad. Nauk SSSR Otd. Tekh. Nauk, Inst. Mashinoved. Soveshch. Vyazkosti Zhidk. Kolloid. Rastvorov* **2**:76–84 (1944).
85. B. G. Korshunov, N. I. Kaloev, L. A. Nisel'son, and O. R. Garvilov, *Zh. Neorg. Khim.* **13**:1956–1961 (1968).

86. I. S. Morozov and L. Tsegledi, *Zh. Neorg. Khim.* **6**:2766–2775 (1961).
87. I. S. Morozov and D. Y. Toptygin, *Bull. Acad. Sci. USSR Div. Chem. Sci.* 1832–1839 (1959).
88. V. I. Mikheeva, S. M. Arkhipov, and T. V. Revzina, *Zh. Neorg. Khim.* **13**:1946–1949 (1968).
89. A. I. Kryagova, *J. Gen. Chem. USSR* **17**:23–26 (1947).
90. A. I. Kryagova, *J. Gen. Chem. USSR* **17**:421–424 (1947).
91. A. I. Kryagova, *Zh. Prikl. Khim.* **21**:561–572 (1948).
92. J. Kendall, E. D. Crittenden, and H. K. Miller, *J. Amer. Chem. Soc.* **45**:963–996 (1923).
93. W. Fischer and A. Simon, *Z. Anorg. Allg. Chem.* **306**:1–12 (1960).
94. R. Midorikawa, *J. Electrochem. Soc. Jap.* **23**:72–76 (1955).
95. U. I. Shvartsman, *J. Phys. Chem. USSR* **14**:253–256 (1940).
96. A. Chretien and E. Lous, *Compt. Rend.* **217**:451–453 (1943).
97. G. Boef, H. B. Slot, R. A. W. D. van Leeuwen, H. Wessels, and J. W. van Spronsen, *Z. Anorg. Allg. Chem.* **353**:93–102 (1967).
98. L. K. Van der Kamp and J. W. van Spronsen, *Z. Anorg. Allg. Chem.* **361**:328–332 (1968).
99. I. S. Morozov and A. T. Simonich, *Zh. Neorg. Khim.* **2**:1907–1914 (1957).
100. K. N. Semenenko, T. N. Naumova, L. N. Gorokhov, and A. V. Novoselova, *Dokl. Akad. Nauk SSSR* **154**:648–649 (1964).
101. V. S. Balikhin and V. A. Reznichenko, *Titan. Ego Splavy, Akad. Nauk SSSR, Inst. Met.* (9):225–229 (1963).
102. R. F. Belt and H. Scott, *Inorg. Chem.* **3**:1785–1788 (1964).
103. A. P. Palkin and O. K. Belousov, *Zh. Neorg. Khim.* **2**:1620–1628 (1957).
104. A. P. Palkin and N. V. Ostrikova, *Zh. Neorg. Khim.* **7**:2635–2636 (1962).
105. P. I. Fedorov and S. K. Nedev, *Zh. Neorg. Khim.* **10**:2717–2719 (1965).
106. T. N. Larionova and E. P. Vognikova, *Zh. Neorg. Khim.* **12**:2184–2185 (1967).
107. I. P. Palyura and A. P. Palkin, *Zh. Neorg. Khim.* **9**:2668–2669 (1964).
108. G. V. Seryakov and L. A. Nisel'son, *Zh. Prikl. Khim.* **35**:482–486 (1962).
109. E. G. M. Tornqvist, J. T. Richardson, Z. W. Wilchinsky, and R. W. Looney, J. Catal. **8**:189–196 (1967).
110. I. S. Morozov and D. Ya. Topygin, *Zh. Neorg. Khim.* **2**:1915–1921 (1957).
111. N. D. Denisova, E. K. Safronov, and O. N. Bystrova, *Zh. Neorg. Khim.* **11**:2412–2413 (1966).
112. A. J. Shor, W. T. Smith, Jr., and M. A. Bredig, *J. Phys. Chem.* **70**:1511–1515 (1966).
113. O. R. Gavrilov, A. S. Krivoshein, and L. A. Nisel'son, *Zh. Neorg. Khim.* **11**:2392–2393 (1966).
114. I. S. Morozov, V. A. Tverskov, and G. I. Kurapova, *Zh. Neorg. Khim.* **9**:2196–2202 (1964).
115. I. S. Morozov and C. Li, *Zh. Neorg. Khim.* **8**:2733–2736 (1963).
116. G. Jander and K. H. Swart, *Z. Anorg. Allg. Chem.* **301**:54–79 (1959).
117. Ya. A. Fialkov and Ya. B. Bur'yanov, *Dokl. Akad. Nauk SSSR* **92**:585–588 (1953).
118. W. Fischer and O. Jübermann, *Z. Anorg. Allg. Chem.* **235**:337–351 (1938).
119. L. A. Nisel'son, A. I. Pustil'nik, O. R. Gavrilov, and V. A. Rodin, *Zh. Neorg. Khim.* **10**:2339–2346 (1965).
120. I. S. Morozov, B. G. Korshunov, and A. T. Simonich, *Zh. Neorg. Khim.* **1**:1646–1657 (1956).

121. A. I. Pustil'nik, O. R. Gavrilov, V. A. Rodin, and L. A. Nisel'son, *Zh. Neorg. Khim.* **12**:2186–2189 (1967).
122. B. A. Boitovich, A. S. Barabanova, and N. Kh. Tumanova, *Zh. Neorg. Khim.* **6**:2545–2549 (1961).
123. H. Houtgraaf, H. J. Rang, and L. Vollbracht, *Rec. Trav. Chim.* **72**:978–988 (1953).
124. B. G. Korshunov and V. I. Gol'din, *Zh. Neorg. Khim.* **6**:1642–1644 (1961).
125. B. G. Korshunov, G. A. Lovetskaya, and A. A. Palant, *Zh. Neorg. Khim.* **12**:203–209 (1967).
126. I. S. Morozov, *Zh. Neorg. Khim.* **1**:2792–2802 (1956).
127. B. G. Korshunov, V. I. Ionov, T. A. Baklashova, and V. V. Kakorev, *Izv. Bysshikh Ucheb. Zaved., Tsvet. Met.* (6):114–118 (1960).
128. Y. Li, *Zh. Neorg. Khim.* **5**:2804–2807 (1960).
129. H. Houtgraff and A. M. de Roos, *Rec. Trav. Chim.* **72**:963–977 (1953).
130. V. Gutmann, *Z. Anorg. All. Chem.* **269**:279–291 (1952).
131. R. C. Paul, K. C. Malhotra, and G. Singh, *J. Indian Chem. Soc.* **37**:105–110 (1960).
132. B. F. Markov, B. A. Voitovich, and A. S. Barabanova, *Ukr. Khim. Zh.* **27**:580–584 (1961).
133. H. Spandau and E. Brunneck, *Z. Anorg. Allg. Chem.* **270**:201–214 (1952).
134. V. A. Plotnikov and U. I. Shvartsman, *J. Phys. Chem. USSR* **12**:120–130 (1938).
135. V. A. Plotnikov and U. I. Shvartsman, *Mem. Inst. Chem., Ukr. Acad. Sci.* **4**:137–151 (1937).
136. V. A. Plotnikov and U. I. Shvartsman, *Mem. Inst. Chem. Ukr., Acad. Sci.* **4**:299–308 (1937).
137. J. D. Corbett and N. W. Gregory, *J. Amer. Chem. Soc.* **75**:5238–5242 (1953).
138. N. A. Pushin and J. Makuc, *Z. Anorg. Allg. Chem.* **237**:177–182 (1938).
139. C. T. H. M. Cronenberg and J. W. van Spronsen, *Z. Anorg. Allg. Chem.* **354**:103–110 (1967).
140. V. I. Mikheeva, S. M. Arkhipov, and T. V. Revzina, *Zh. Neorg. Khim.* **13**:1697–1698 (1968).
141. V. A. Plotnikov and V. I. Mikhailovskaya, *Mem. Inst. Chem., Ukr. Acad. Sci.* **4**:121–124 (1937).
142. R. F. Adamsky and C. M. Wheeler, Jr., *J. Phys. Chem.* **58**:225–227 (1954).
143. L. N. Eingorn, *Ukr. Khim. Zh.* **16**:404–413 (1950).
144. Ya. A. Fialkov and O. I. Shor, *Zh. Obshch. Khim.* **23**:357–363 (1953).
145. E. L. Starokadomskaya, *J. Gen. Chem. USSR* **9**:840–844 (1939).
146. J. L. Daniel and N. W. Gregory, *J. Amer. Chem. Soc.* **72**:3801–3803 (1950).
147. A. T. Nizhnik, *J. Gen. Chem. USSR* **7**:1935–1947 (1937).
148. R. H. Moore, *J. Chem. Eng. Data* **8**:164–167 (1963).
149. H. Grothe and C. A. Piel, *Z. Elektrochem.* **54**:210–215 (1950).
150. V. A. Plotnikov and U. I. Shvartsman, *Mem. Inst. Chem. Acad. Sci. Ukr. SSR* **3**:387–400 (1936).
151. R. Midorikawa, *J. Electrochem. Soc. Jap.* **23**:127–129 (1955).
152. B. G. Korshunov, A. M. Reznik, and I. S. Morozov, *Tr. Mosk. Inst. Tonkoi Khim. Tekhnol. M. V. Lomonosova* (7):127–139 (1958).
153. I. S. Morozov, V. A. Tverskov, and G. I. Kurapova, *Zh. Neorg. Khim.* **9**:2196–2202 (1964).
154. B. G. Korshunov and E. D. Lapkina, *Zh. Neorg. Khim.* **8**:2585–2588 (1963).
155. B. G. Korshunov and L. A. Vyrskaya, *Zh. Neorg. Khim.* **7**:1403–1407 (1962).

156. B. A. Il'ichev and A. M. Vladimirova, *Titan Splavy, Akad. Nauk SSSR, Inst. Met.* (5):148–166 (1961).
157. N. D. Chikanov, A. P. Palkin, and M. K. Bizyaeva, *Izv. Vyssh. Ucheb. Zaved., Khim. Tekhnol.* **6**:355–360 (1963).
158. I. S. Morozov and V. A. Krokhin, *Zh. Neorg. Khim.* **7**:2400–2410 (1962).
159. N. K. Druzhinina, *Titan Splavy, Akad. Nauk SSSR, Inst. Met.*, (5):225–232 (1961).
160. I. S. Morozov and D. Ya. Toptygin, *Zh. Neorg. Khim.* **2**:2129–2135 (1957).
161. B. G. Korshunov, E. D. Lidina, and Z. N. Shevtsova, *Zh. Neorg. Khim.* **8**:1531–1532 (1963).
162. B. G. Korshunov and L. A. Vyrskaya, *Zh. Neorg. Khim.* **6**:2815–2816 (1961).
163. A. S. Barabanova and B. A. Voitovich, *Ukr. Khim. Zh.* **30**:1298–1304 (1964).
164. N. D. Chikanov and A. A. Dubyanskaya, *Zh. Neorg. Khim.* **12**:3187–3191 (1967).
165. N. D. Chikanov and A. A. Ivanova, *Zh. Neorg. Khim.* **12**:2219–2224 (1967).
166. B. G. Korshunov and N. I. Kaloev, *Zh. Neorg. Khim.* **13**:2547–2551 (1968).
167. H. Gerding and H. Houtgraaf, *Rec. Trav. Chim.* **72**:21–38 (1953).
168. H. Gerding and H. Houtgraaf, *Rec. Trav. Chim.* **73**:759–770 (1954).
169. H. Gerding, *Rec. Trav. Chim.* **75**:589–593 (1956).
170. A. E. van Arkel, *Chem. Weekbl.* **52**:193–197 (1956).
171. D. A. Long and R. T. Bailey, *Trans. Faraday Soc.* **59**:594–598 (1963).
172. G. L. Carlson, *Spectrochim. Acta* **19**:1291–1307 (1963).
173. C. D. Schmulbach, *J. Inorg. Nucl. Chem.* **26**:745–749 (1964).
174. K. Balasubrahmanyam and L. Nanis, *J. Chem. Phys.* **42**:676–680 (1965).
175. D. E. H. Jones and J. L. Wood, *Spectrochim. Acta* **23A**:2695–2697 (1967).
176. A. Byström and K. A. Wilhelmi, *Acta Chem. Scand.* **5**:1003–1010 (1951).
177. M. E. Peach, V. L. Tracy, and T. C. Waddington, *J. Chem. Soc.* (*A*) 366–367 (1969).
178. R. W. G. Wyckoff, *Crystal Structures*, 2nd ed., Vol. 3. John Wiley (Interscience), New York (1965).
179. N. C. Baenziger, *Acta Cryst.* **4**:216–219 (1951).
180. J. A. Ibers, *Acta Cryst.* **15**:967–972 (1962).
181. R. H. Wood and L. A. D'Orazio, *Inorg. Chem.* **5**:682–684 (1966).
182. B. Trémillon and G. Letisse, *J. Electroanal. Chem. Interfacial Electrochem.* **17**:371–386 (1968).
183. J. R. Morrey and R. H. Moore, *J. Phys. Chem.* **67**:748–752 (1963).
184. R. S. Juvet, V. S. Shaw, and M. A. Khan, *J. Amer. Chem. Soc.* **91**:3788–3792 (1969).
185. G. Letisse and B. Trémillon, *J. Electronal. Chem. Interfacial Electrochem.* **17**:387–394 (1968).
186. N. J. Bjerrum, C. R. Boston, and G. P. Smith, *Inorg. Chem.* **6**:1162:1172 (1967).
187. H. L. Davis, N. J. Bjerrum, and G. P. Smith, *Inorg. Chem.* **6**:1172–1178 (1967).
188. N. J. Bjerrum and G. P. Smith, *Inorg. Chem.* **6**:1968–1972 (1967).
189. V. A. Plotnikov and N. S. Fortunatov, *Mem. Inst. Chem. Ukr. Acad. Sci.* **3**:123–128 (1936).
190. V. P. Calkins, *U. S. At. Energy Comm.* **TID-5290**:765–769 (1958).
191. G. L. Groshev, S. M. Danov, and V. S. Shinyaeva, *Tr. Khim. Khim. Tekhnol.* (3):30–33 (1965).
192. J. D. Corbett, W. J. Burkhard, and L. F. Druding, *J. Amer. Chem. Soc.* **83**:76–80 (1961).
193. D. Cubicciotti, *J. Amer. Chem. Soc.* **74**:1198–1200 (1952).
194. J. D. Corbett, *Inorg. Chem.* **1**:700–704 (1962).

195. R. D. Barnes, *U. S. At. Energy Comm.* **Ts-T-36**:1–51 (1965).
196. R. A. Potts, R. D. Barnes, and J. D. Corbett, *Inorg. Chem.* **7**:2558–2565 (1968).
197. T. C. F. Munday and J. D. Corbett, *Inorg. Chem.* **5**:1263–1268 (1966).
198. L. E. Topol, S. J. Yosim, and R. A. Osteryoung, *J. Phys. Chem.* **65**:1511–1516 (1961).
199. L. E. Topol and R. A. Osteryoung, *J. Phys. Chem.* **66**:1587–1591 (1962).
200. C. R. Boston and G. P. Smith, *J. Phys. Chem.* **66**:1178–1181 (1962).
201. C. R. Boston, G. P. Smith, and L. C. Howick, *J. Phys. Chem.* **67**:1849–1852 (1963).
202. J. D. Corbett, F. C. Albers, and R. A. Sallach, *Inorg. Chim. Acta* **2**:22–26 (1968).
203. A. Hershaft and J. D. Corbett, *Inorg. Chem.* **2**:979–985 (1963).
204. J. D. Corbett, *Inorg. Chem.* **7**:198–208 (1968).
205. H. A. Øye and D. M. Gruen, *Inorg. Chem.* **4**:1173–1180 (1965).
206. C. A. Angell and D. M. Gruen, *J. Phys. Chem.* **70**:1601–1609 (1966).
207. C. A. Angell and D. M. Gruen, *J. Inorg. Nucl. Chem.* **29**:2243–2247 (1967).
208. J. R. Morrey, *Inorg. Chem.* **2**:163–169 (1963).
209. Yu. K. Delimarskii and B. F. Markov, *Electrochemistry of Fused Salts*, Sigma Press, Washington, D. C. (1961).
210. Yu. K. Delimarskii, E. M. Skobets, and V. D. Ryabokon, *J. Phys. Chem. USSR* **21**:843–848 (1947).
211. Yu. K. Delimarkii, L. S. Berenblyum, and I. N. Sheiko, *Ukr. Khim. Zh.* **16**:254–263 (1950).
212. Yu. K. Delimarskii, *Zh. Fiz. Khim.* **29**:28–38 (1955).
213. Yu. K. Delimarskii and R. S. Khaimovich, *Ukr. Khim. Zh.* **15**:340–350 (1949).
214. Yu. K. Delimarskii, *Ukr. Khim. Zh.* **16**:414–437 (1950).
215. Yu. K. Delimarskii, L. S. Berenblyum, and I. N. Sheiko, *Zh. Fiz. Khim.* **25**:398–403 (1951).
216. W. H. Wade, G. O. Twellmeyer, S. J. Yntema, and L. F. Yntema, *Trans. Electrochem. Soc.* **78**:77–90 (1940).
217. R. G. Verdieck and L. F. Yntema, *J. Phys. Chem.* **46**:344–352 (1942).
218. R. Wehrman and L. F. Yntema, *J. Phys. Chem.* **48**:259–268 (1944).
219. Yu. K. Delimarskii, *J. Phys. Chem. SSSR* **19**:465–468 (1945).
220. Yu. K. Delimarskii, *Zap. Inst. Khim., Akad. Nauk SSSR* **8**:23–30 (1946).
221. V. A. Plotnikov, E. I. Kirichenko, and N. S. Fortunatov, *Zap. Inst. Khim., Akad. Nauk SSSR* **7**:159–171 (1940).
222. R. Gut, *Helv. Chim. Acta* **43**:830–842 (1960).
223. Yu. K. Delimarskii, E. M. Skobets, and L. S. Berenblyum, *Zh. Fiz. Khim.* **22**:1108–1115 (1948).
224. N. G. Chovnyk, *Dokl. Akad. Nauk SSSR* **87**:1033–1034 (1952).
225. N. G. Chovnyk, *Zh. Fiz. Khim.* **30**:277 (1956).
226. N. G. Chovnyk, *Dokl. Akad. Nauk SSSR* **95**:599–601 (1954).
227. N. G. Chovnyk, *Dokl. Akad. Nauk SSSR* **100**:495 (1955).
228. N. G. Chovnyk and V. V. Vashchenko, *Zh. Neorg. Khim.* **1**:710–712 (1956).
229. N. G. Chovnyk, *Tr. Chetvertogo Soveshch. Elektrokhim.*, Moscow 358–361 (1956).
230. R. H. Moore, *J. Chem. Eng. Data* **9**:502–505 (1964).
231. R. V. Ammon, *J. Inorg. Nucl. Chem.* **28**:2569–2578 (1966).
232. R. H. Moore and W. L. Lyon, *U. S. At. Energy Comm.* **HW-59147**:1–36 (1959).
233. R. H. Moss, thesis, University Microfilms (Ann Arbor, Michigan), Publ. No. 12,730; *Diss. Abstr.* **15**:1325 (1955).
234. C. R. Boston, L. F. Grantham, and S. J. Yosim, *J. Electrochem. Soc.* **117**:28–31 (1970).

235. Ya. A. Fialkov and O. I. Shor, *J. Gen. Chem. USSR* **23**:369–373, 375–382, (1953).
236. W. Isbekov, *Z. Anorg. Allg. Chem.* **158**:87–93 (1926).
237. R. W. Laity, *Ann. N. Y. Acad. Sci.* **79**:997–1022 (1960).
238. Yu. V. Baimakov and V. I. Shelomov, *Trans. Leningrad Ind. Inst.* Sect. Met. (1):36–48 (1938).
239. V. Gutmann and R. Himml, *Z. Physik. Chem.* **4**:157–164 (1955).
240. E. Ya. Gorenbein and M. A. Abramova, *Zh. Obshch. Khim.* **20**:749–754 (1950).
241. E. Ya. Gorenbein and M. S. Kavet'skii, *Zh. Fiz. Khim.* **37**:174–176 (1962).
242. Ya. P. Mezhennii, *Mem. Inst. Chem. Acad. Sci. Ukr. SSR* **4**:413–424 (1938).
243. M. G. Kher and P. S. Mene, *Indian J. Chem.* **1**:185–186 (1963).
244. G. A. Abramov and N. A. Emel'yanov, *Trans. Leningrad Ind. Inst.* Sect. Met., (4):54–59 (1940).
245. C. G. Fink and D. N. Solanki, *Trans. Electrochem. Soc.* **91**:203–219 (1947).
246. R. Piontelli, G. Sternheim, and M. Francini, *J. Chem. Phys.* **24**:1113–1114 (1956).
247. R. Piontelli, G. Sternheim, and F. Fumagalli, *Ric. Sci.* **28**:160–172 (1958).
248. N. G. Chovnyk, V. V. Vashchenko, and M. S. Polyantseva, *Ukr. Khim. Zh.* **32**:454–456 (1966).
249. E. Ya. Gorenbein, *Univ. Kiev., Bull. Sci., Rec. Chim.* **2**, 115–28 (1936).
250. V. A. Plotnikov and E. Ya. Gorenbein, *Mem. Inst. Chem. Ukr. Acad. Sci.* **3**:471–487 (1936).
251. V. A. Plotnikov and O. K. Kudra, *Mem. Inst. Chem. Ukr. Acad. Sci.* **3**:147–151 (1936).
252. V. A. Plotnikov and I. B. Barmashenko, *Mem. Inst. Chem. Ukr. Acad. Sci.* **3**:177–187 (1936).
253. J. P. Mezhennii, *Mem. Inst. Chem. Ukr. Acad. Sci.* **3**:211–236 (1936).
254. V. A. Kikets, *Mem. Inst. Chem. Ukr. Acad. Sci.* **3**:489–507 (1936).
255. A. M. Ruban, *J. Gen. Chem. USSR* **7**:1419–1426 (1937).
256. E. Ya. Gorenbein, *J. Gen. Chem. USSR* **9**:2041–2047 (1939).
257. E. Ya. Gorenbein, *J. Gen. Chem. USSR* **11**:925–933 (1941).
258. V. A. Plotnikov, *Rab. Khim. Rastvorov Kompleks. Soedin., Akad. Nauk Ukr. SSR* (2):3–71 (1959).
259. A. I. Kryagova, *J. Gen. Chem. USSR* **9**:2061–2066 (1939).
260. V. Gutmann and G. Schöber, *Monatsh. Chem.* **87**:792–793 (1956).
261. V. Gutmann and M. Baaz, *Monatsh. Chem.* **90**:729–743 (1959).
262. F. Klanberg and H. W. Kohlschutter, *Z. Naturforsch.* **16b**:69–71 (1961).
263. W. Sundermeyer, *Angew. Chem.* **77**:241–258 (1965). For English translation see, *Angew. Chem. Int. Edit.* **4**:222–238 (1965).
264. R. H. Moore, J. R. Morrey, and E. E. Voiland, *J. Phys. Chem.* **67**:744–747 (1963).
265. R. H. Moore, *Inorg. Chem.* **3**:1738–1740 (1964).
266. J. R. Morrey and R. H. Moore, *J. Phys. Chem.* **67**:748–752 (1963).
267. Yu. K. Delimarskii, *J. Gen. Chem. USSR* **11**:1081–1091 (1941).
268. A. P. Palkin and O. K. Belousov, *J. Inorg. Chem. USSR* **2**(7):273–285 (1957).
269. I. N. Sheiko and V. T. Barchuk, *Ukr. Khim. Zh.* **30**:577–581 (1964).
270. B. G. Korshunov and D. A. Rokhlenko, *Zh. Prikl. Khim.* **37**:1941–1946 (1964).
271. W. Sundermeyer and O. Glemser, *Angew. Chem.* **70**:625–627 (1958).
272. W. Sundermeyer, *Berichte* **97**:1069–1074 (1964).
273. W. Sundermeyer and W. Verbeek, *Angew. Chem. Int. Ed.* (*Engl.*) **5**:1–6 (1966).

274. W. Sundermeyer, O. Glemser, and K. Kleine-Weischede, *Berichte* **95**:1829–1831 (1962).
275. W. Sundermeyer, *Angew. Chem.* **74**:717 (1962).
276. W. Sundermeyer, *Berichte* **96**:1293–1297 (1963).
277. W. Sundermeyer, German Patent 1,080,077 (April 21, 1960) (Cl. 12 i).
278. W. Sundermeyer, *Z. Anorg. Allg. Chem.* **313**:290–295 (1961).
279. M. Fild, W. Sundermeyer, and O. Glemser, *Berichte* **97**:620–621 (1964).
280. W. Sundermeyer and W. Meise, *Z. Anorg. Allg. Chem.* **317**:334–342 (1962).
281. W. Verbeek and W. Sundermeyer, *Angew. Chem. Int. Ed.* (*Engl.*) **5**:314 (1966).
282. D. B. Bruce, A. J. S. Sorrie, and R. H. Thomson, *J. Chem. Soc.* 2403–2406 (1953).
283. A. K. Hoffmann, Belgian Patent 669,396 (March 9, 1965).
284. M. Taube, M. Mielcarski, A. Kowalew, and S. Porturaj-Gutniak, *Nukleonika* **10**:639–640 (1965).

Chapter 4

MOLTEN SALT BATTERIES AND FUEL CELLS

D. A. J. Swinkels
Principal Research Officer
Broken Hill Proprietary Co., Ltd.
Central Research Laboratory
Shortland, New South Wales, Australia

1. INTRODUCTION

1.1. Scope

This chapter describes recent work on batteries and fuel cells using molten salt electrolytes. This entails a comparison with other batteries and fuel cells utilizing aqueous and organic electrolytes; for further details of these low-temperature systems a number of reference works are available[1,2] General background in molten salt properties may be found in several books,[3–7] some recent reviews,[8,9] and of course in other parts of the current series.

High temperature batteries and fuel cells using solid electrolytes are covered because many of their characteristics and problems are similar to those encountered in molten salt systems.

In theory the subject of molten salt batteries covers a large range of possible systems utilizing many electrolytes over a temperature range that could extend well over 1000°C, in which any electropositive element on the left-hand side of the periodic table could be combined with any more electronegative element, or compound containing that element, to form an electrochemical cell.

In practice, work on molten salt batteries has been limited to a temperature range of less than 500°C using a few of the alkali halides as elec-

trolytes, and the number of electropositive and electronegative elements that have received serious consideration is limited to about half a dozen of each. This does not include the many molten salt cells that have been investigated to obtain basic thermodynamic or kinetic data.[10]

Only systems that have some potential for energy conversion or energy storage applications and have been studied in some detail are discussed here. This eliminates many of the possible electrode materials for reasons of availability (and hence cost) or electrode properties. In fact, any proposed molten salt system must show some potential advantage over the available low-temperature batteries in terms of performance, life, convenience, or cost.

1.2. Advantages of Molten Salt Electrolytes

The advantages of molten salt electrolytes over aqueous or organic electrolytes are threefold. First, the electrical conductivity of molten salts is generally an order of magnitude higher than that of the aqueous electrolytes and several orders of magnitude higher than that of the organic electrolytes. Recently some solid electrolytes have been found with conductivities as high as aqueous electrolytes at readily accessible temperatures, for example, $RbAg_4I_5$,[11] but most solid electrolytes show conductivities even lower than the organic electrolytes. The reason for the high electrical conductivities found in many fused salts is the high temperature, resulting in high mobility for the ions and the complete ionization of many of the simple fused salts. The absence of any solvent also increases the conductivity.

The second advantage of molten salts is the high temperature of operation, although at times this also may be a drawback. The advantage arises from the fact that electrode reactions generally proceed faster and hence with less polarization at higher temperatures. This results in a higher voltage for a given combination of electrodes than in an aqueous or organic electrolyte or, alternatively, a higher current density at the same output voltage. In one case this improves the energy capacity of the system, while in the other case an improvement in the power capacity occurs.

The third but possibly most significant advantage of molten salt electrolytes is their high decomposition potential. Aqueous electrolytes are basically limited by the decomposition potential of water of about 1.23 V, and it is only because of kinetic limitation that batteries of higher open-circuit voltage (OCV) are possible. Molten salts, on the other hand, typically have decomposition voltages of 3 V or more so that more reactive electrode materials can be considered. Table I shows relevant properties of the

TABLE I. Electrolyte Properties

Electrolyte (mole %)	Melting point (°C)	Conductivity $\Omega^{-1} \cdot cm^{-1}$	Reference
LiCl	610	5.92 (620°C)	(3)
NaCl	808	3.73 (850°C)	(3)
KCl	772	2.42 (800°C)	(3)
LiCl–KCl (58.8–41.2)	353	1.57 (450°C)	(8)
LiCl–LiF (71–29)	485		(3)
LiF–LiCl–LiI (11.7–29.1–59.2)	341	2.3 (375°C)	(44, 45)
Li_2CO_3	754	5.66 (800°C)	(3)
Na_2CO_3	854	3.03 (900°C)	(3)
K_2CO_3	896	2.18 (950°C)	(3)
Li_2CO_3–Na_2CO_3 (53.3–46.7)	496	0.85 (600°C)	(119)
Li_2CO_3–Na_2CO_3–K_2CO_3 (43.5–31.5–25.0)	397	0.75 (500°C)	(119)
Modified β–Al_2O_3	Decomposes 1300+	0.25 (300°C)	(95)
$(ZrO_2)_{0.88}(CaO)_{0.12}$	2500	0.05 (1000°C)	(134)
$(ZrO_2)_{0.9}(Y_2O_3)_{0.1}$	2500	0.1 (1000°C)	(133)
$(ZrO_2)_{0.9}(Sc_2O_3)_{0.1}$	2500	0.25 (1000°C)	(132)

electrolytes most commonly used. Organic electrolytes also have high decomposition potentials but are very limited in their conductivities and electrode kinetics, so that high energy capacity systems can result, but only when discharged at low rates and hence these are low power systems.

1.3. Disadvantages of Molten Salt Electrolytes

The problems associated with molten salt electrolytes are in two main areas, viz., materials and self-discharge.

The materials of construction for molten salt batteries and fuel cells must be capable of operating at elevated temperature in the presence of very reactive electrode materials for extended periods of time. The high temperature not only speeds up electrode processes but also corrosion processes, and hence the development of materials and structures for molten salt batteries is the main development task that must be completed before the systems now in the laboratory can find many applications. The only exceptions to this general statement are short-life primary batteries, which are required to

give a high power output for periods of less than an hour. Because of this limited active life much higher rates of corrosion can be tolerated.

The second problem area for molten salt batteries is self-discharge of the batteries in the widest sense. Since energy is required to keep the molten salt batteries hot, when insufficient waste heat is available from charge and discharge processes to maintain cell temperature, this can be regarded as a self-discharge. Since diffusion coefficients increase with temperature, any solubility of electrode materials in the electrolytes will result in higher self-discharge than in the corresponding low temperature system. Finally, a number of metals when dissolved in molten salts result in significant electronic conductivity in the electrolyte, which places a constant current drain on the system. These various forms of self-discharge are discussed in more detail in a later section.

2. GENERAL DISCUSSION

2.1. Cell emf's

The open-circuit cell emf's of many molten salt cells have been calculated from thermodynamic data,[12,13] or emf measurements have been used to determine thermodynamic data.[10] For a simple formation cell in which only pure phases are present such as

$$\mathrm{Li}(l)/\mathrm{LiCl}(l)/\mathrm{Cl_2}(g)\ \text{(carbon or graphite)}$$

the thermodynamic open-circuit voltage is given by

$$E^\circ = \frac{-\Delta G^\circ}{nF} \tag{1}$$

where ΔG^0 is the standard free energy given out in the reaction

$$\mathrm{Li}(l) + \tfrac{1}{2}\mathrm{Cl_2}(g) \rightarrow \mathrm{LiCl}(l) \tag{2}$$

at the cell temperature, n is the number of electrons involved in reaction (2), and F is the Faraday constant:

$$F = 96{,}487\ \mathrm{C/g\text{-}equiv}$$
$$= 23.06\ \mathrm{kcal/V \cdot g\text{-}equiv}$$

Some emf's calculated from thermodynamic data are shown in Table II.

TABLE II. Calculated Open Circuit Voltage for Hypothetical Cell at 500°C

	F	Cl	Br	I	O	S
Li	5.56	3.65	3.21	2.57	2.14	
Na	5.12	3.52	3.16	2.59	1.62	1.82
K	5.02	3.76	3.48	2.98	1.27	
Be	4.41	2.14	1.58	0.91	2.70	1.15
Mg	5.01	2.68	2.26	1.61	2.68	
Ca	5.60	3.53	3.06	2.48	2.88	2.33
Al	3.87				2.48	

However, many electrolytes of practical interest are not pure fused salts. Mixtures of salts may be used to achieve lower operating temperatures or to increase the electrical conductivity of the electrolyte by the addition of more conductive salt, for example, LiCl. Furthermore, the electrode may not be pure but may be an alloy [for example, Li(Al)] or a mixture of gases (for example, air, air + CO_2). We therefore write in more general terms for the reaction

$$mM + xX \rightarrow M_mX_x \tag{3}$$

$$-nEF = \mu_{MX} - m\mu_M - x\mu_X \tag{4}$$

where μ_{MX}, μ_M, μ_X are the chemical potential of the product, and the two electrode reactants, respectively.[10,14] A good example is the cell

$$Li(Al) + \tfrac{1}{2}Cl_2(C) \rightarrow LiCl(KCl) \tag{5}$$

in which a LiAl alloy negative electrode, a Cl_2 adsorbed on charcoal positive electrode, and a LiCl–KCl mixed electrolyte are used. A number of concentration cells have been studied that consist of a pure metal at one electrode and an alloy or compound at the other electrode. These are best analyzed in terms of chemical potential or activity of one species at both electrodes.

There are perhaps half a dozen favorite molten salt electrolytes in which most electrochemical work has been carried out. Enough data are available to set up an electromotive force series for each of these electrolytes. Although each electrolyte has its own series because of the variations in temperature and interactions of the MX product with the different solvent

electrolytes, the series of course must generally run parallel. Hence the emf of a cell taken from one series gives a fair approximation of what could be expected in another electrolyte at the same temperature. There is no universally accepted defined reference system such as the standard hydrogen electrode in aqueous electrolytes. However, the Pt^{2+}/Pt electrode seems to be suitable for most fused salts. Even this electrode has been defined in three ways using standard states of unit mole fraction (E_x^0), unit molarity (E_M^0), and unit molality (E_m^0) for Pt^{2+} in the electrolyte.[15] Since mole fraction is readily calculated and is independent of temperature it will be used here. Table III shows part of the emf series in several electrolytes.[16]

From the data in Tables II and III it is clear that the open circuit voltage (OCV) of many molten salt cells will be more than 2 V and often in excess of 3 V. The next question is how much of this voltage is available at practical current densities.

2.2. Electrode Polarization

The terminal voltage of a battery or fuel cell during discharge is given by the OCV minus all the resistance and polarization losses throughout the cell,[1,17,18] while during recharge of a secondary battery these terms must be added to the OCV. Thus we have for discharge

$$V_D = \text{OCV} - I\Sigma R - \eta_{c,a} - \eta_{c,c} - \eta_{a,a} - \eta_{a,c} \tag{6}$$

where V_D is discharge voltage; OCV is open circuit voltage; I is current; ΣR is the sum of electrolyte, electrode, and lead resistance; $\eta_{c,a}$, $\eta_{c,c}$ are concentration polarization at the anode and at the cathode; and $\eta_{a,a}$, $\eta_{a,c}$ are activation polarization at the anode and at the cathode. For simplicity, all polarizations are here taken as positive quantities.

The concentration polarization at each electrode is due to the concentration gradients necessary to move reactants from the supply zone to the region where electron transfer can occur and to move products from the electron transfer region to the product storage volume. The relationship between concentration polarization η_c and current density is of the form[18]

$$\eta_c = \frac{2.303RT}{nF} \log \frac{i_L}{i_L - i} \tag{7}$$

where R is the gas constant equals 8.314 joules/deg-mole; T is temperature in degrees Kelvin; n is the number of electrons; and F is the Faraday.

The limiting current density i_L is the maximum current density that can

TABLE III. Electromotive Force Series (E_x^0)[4,13,14,16]

Electrode	LiCl–KCl Eutectic (450°C)	NaCl–KCl Equimolar (700°C)	$MgCl_2$–NaCl–KCl Eutectic (475°C)	$AlCl_3$ NaCl–KCl (218°C)	Calculated decomposition potential of chloride (500°C)
Li(+1)–Li(0)	−3.410	Exceeds electrolyte decomposition potential			3.646
Mg(+2)–Mg(0)	−2.580		−2.646		2.680
Al(+3)–Al(0)	−1.767		−1.914	−2.09	
Ti(+3)–Ti(0)	−1.64	−1.046			1.836
Zn(+2)–Zn(0)	−1.566	−0.860	−1.550	−1.75	1.603
Co(+2)–Co(0)	−1.316	−0.620	−1.312	−1.63	1.403
Fe(+2)–Fe(0)	−1.172	−0.520	−1.183	−1.52	1.267
Cr(+3)–Cr(0)	−1.160	−0.425	−1.159		1.336
Fe(+3)–Fe(0)	−0.928		−0.880		
Ni(+2)–Ni(0)	−0.795	−0.140	−0.792	−1.19	1.070
Ag(+1)–Ag(0)	−0.637	0.0	−0.680	−1.24	0.896
Cu(+2)–Cu(0)	−0.448	+0.170	−0.519		0.528
Pt(+2)–Pt(0)	0.0		0.0		0.27
Cl_2(0)–Cl(−1)	+0.216	+0.845	+0.076	0.0	

be obtained. It is typically given by

$$i_L = \frac{nFDC}{x} \tag{8}$$

where C = concentration of the rate-limiting reactant in the supply zone, D = diffusion coefficient of the rate-limiting species, and x = a characteristic distance equal to or simply related to the distance between the supply zone and the electron transfer region.

It is clear from equation (7) that in order to minimize η_c one must maximize i_L. This, in turn, means maximizing D and C and minimizing x. Generally, little can be done about increasing D except by increasing the temperature, whereas the concentration C is usually determined by solubility, which may be increased by increasing the temperature or, in the case of a gaseous reactant, by increasing the pressure. It is the diffusion distance x that one often has a good deal of control over the limiting current density. In a porous gas electrode x is usually related to the particle size or the pore size[19] and the wetting characteristics of the electrode, whereas in solution x can be reduced by convection or stirring.

The activation polarization (η_a) is the polarization more directly related to the electron transfer processes, although surface diffusion of reactant or intermediates may be involved. It is related to the current density as follows:[18]

$$i = i_0\left[\exp\frac{(1-\beta)F\eta_a}{RT} - \exp\frac{-\beta F\eta_a}{RT}\right] \tag{9}$$

where i_0 is the exchange current density and β is the symmetry factor.

There is no simple way of expressing η_a in terms of the other parameters except in special cases. When β equals the often-observed value of 0.5, we have

$$\eta_a = \frac{RT}{0.5F}\sinh^{-1}\frac{i}{2i_0} \tag{10}$$

An approximate relationship can be written for polarization values less than RT/nF when

$$\eta_a = \frac{RT}{nF}\frac{i}{i_0} \tag{11}$$

whereas for polarization larger than RT/nF we have the Tafel equation[18]

$$\eta_a = \frac{2.303RT}{nF}\log\frac{i}{i_0} \tag{12}$$

A comparison of molten salt system with either aqueous or organic electrolyte cells shows that the various losses are generally lower for molten salt cells. The main resistance term in most cells is the electrolyte resistance, which for molten salts is low; temperatures are high, resulting in higher diffusion coefficients and hence lower concentration polarization losses in molten salt electrolytes, and finally the exchange current densities observed in molten salts are typically 10^0 to 10^2 A/cm^2 compared to exchange current densities of less than 10^{-3} A/cm^2, which are common in aqueous and organic electrolytes. This means lower activation polarization in molten salt cells so that the linear approximation, equation (11), is usually satisfactory.

The smaller polarization losses together with the higher OCV in molten salt systems results in higher voltage efficiencies compared to aqueous and organic electrolyte batteries.

The voltage efficiency of a rechargeable battery is defined as

$$\eta_v = \frac{V_{\text{discharge}}}{V_{\text{charge}}}$$

while for a primary battery or fuel cell we have

$$\eta_v = \frac{V_{\text{discharge}}}{\text{OCV}} \tag{14}$$

η_v is multiplied by the current efficiency to give the total electrical efficiency of the system.

2.3. Energy and Power Limits

The maximum amount of energy can be drawn from a battery if it is withdrawn at a very show rate so that the voltage is close to the OCV. This assumes that self-discharge processes are negligible. In selecting potential electrode combinations it is useful to calculate a maximum energy capacity based on operation at the OCV, 100% current efficiency, and the weight of reactants only. Experience has shown that in a practical system about 15–30% of this theoretical energy capacity generally can be attained. The theoretical maximum energy capacity is given by

$$\text{Max energy capacity} = \frac{\text{OCV} \times F}{3600 \times \text{equiv. wt}} \text{ kwh/kg} \tag{15}$$

Table IV shows values calculated for the OCV data of Table II.

TABLE IV. Some Theoretical Energy Capacities (kwh/kg) Calculated from OCV Data of Table II (500°C)

	F	Cl	Br	I	O	S
Li	5.74	2.31	0.99	0.57	3.84	
Na	3.27	1.61	0.82	0.50	1.40	1.25
K	2.32	1.35	0.78	0.52	0.72	
Be	5.03	1.44	0.50	0.20	5.79	1.50
Mg	4.31	1.51	0.66	0.34	3.56	
Ca	3.84	1.70	0.82	0.49	2.75	1.73
Al	3.71				3.91	

The combinations with fluorine give the highest energy capacity, but since no suitable electrode material is available at high temperatures, the fluorine systems are eliminated for practical reasons. The next highest group is the oxygen group. However, the oxide reaction products have very high melting points, as do any fused salts in which oxides have significant solubilities. If instead of O_2 only, one considers $O_2 + H_2O$, then the reaction products are hydroxides and lower temperature systems could result. However, several of the metals react with their hydroxides, forming oxides and hydrides leading to significant self-discharge. The sulfides formed with sulfur also have high melting points, but lower melting polysulfides can be formed. This leads to lower energy capacities than those shown in Table IV, but at least two systems using sulfur have shown considerable promise.

The other group showing high energy capacities is the chlorine group, Li–Cl_2 in particular, and this system is the highest energy and power capacity system currently under development.

We can define a power limit for the various systems based on resistance only.

If the current voltage relationship for a cell is linear, then the maximum power is delivered at half the OCV and the maximum power is given by

$$\text{Max power} = \frac{(\text{OCV})^2}{4R} \text{ W/cm}^2 \tag{16}$$

where R is cell resistance for 1 cm^2 of electrode surface. Thus high OCV is of paramount importance in achieving high power densities. By operating at half the OCV the energy capacity of course also is halved. Thus the final

system must be a trade off between energy capacity and power capacity and is determined by the cost structure of the application. The battery must be able to supply the maximum power required by the application, must meet possible size and weight limitations imposed, and must be able to store the required amount of energy. Within these limits the most economical system can be designed by optiziming cost over the life of the system in terms of original capital cost and operating cost.[20]

2.4. Self-Discharge

One potential problem area in molten salt batteries and fuel cells is the loss of energy due to various self-discharge processes. The first and most obvious process by which energy is lost is inherent in molten salt systems, viz., heat lost to the surroundings and to any gases continuously passed through the system. Since the amount of heat lost to the surroundings is proportional to the temperature difference and the surface area of the system, it follows that the higher the temperature of the cell, the larger the volume of the system should be before heat losses no longer represent a significant loss. It therefore is not surprising that the solid oxide type of fuel cell, which operates at about 1000°C, is considered only for large, stationary power supplies of 100 kW all the way up to 1000-MW central power stations.[21]

The amount of thermal insulation that can be placed around the battery or fuel cell is largely governed by the economics of the application so that low power molten salt systems (<10 kW) only find use under special conditions such as military or space applications. Also it should be noted that since molten salt batteries are generally high power density systems, when these systems are operated at a high rate, large amounts of waste heat will become available from $T\Delta S$, I^2R, and $I\eta$ terms in the overall energy balance. Since it generally is not desirable to allow large temperature fluctuations to occur, provision must be made to allow heat removal during these periods of high rate operation while conserving heat during standby periods.

Several other self-discharge sources can occur in molten salt systems. Electrode materials may dissolve in the electrolyte and diffuse toward the opposite electrode to react chemically, or in the case of alkali metal electrodes the dissolved metal may generate a degree of electronic conductivity in the electrolyte that acts as a load placed across the cell terminals. Impurities in the electrolyte may be alternately reduced and oxidized at the negative and positive electrodes, respectively.

The energy efficiency of a rechargeable battery, defined as the ratio of electric energy taken out during discharge to electric energy put in during the charging process, can be expressed as the product of a current efficiency and a voltage efficiency. The voltage efficiency is determined by the rate of charge and discharge and the electrode kinetics of the particular system. The higher the rate of charge or discharge, the lower the voltage efficiency. The current efficiency, on the other hand, can increase or decrease as the rate of charge or discharge is increased, depending on what causes the coulombic loss. If the coulombic loss is due to a side reaction that starts to occur when the voltage reaches a certain value (for example, gassing in aqueous electrolyte systems), then a lower rate of charge will result in a higher coulombic efficiency. However, if the coulombic loss is due to a reactant solubility in the electrolyte and chemical combination, then the cell self-discharges at essentially a constant rate and hence the higher the average rate of charge and discharge, the higher the coulombic efficiency.

Energy losses, whether due to electronic conductivity, to reactant solubility, or to energy required to keep the cell hot during standby periods, can be expressed as a self-discharge current. The practical coulombic or current efficiency then becomes

$$\text{Current efficiency} = \frac{I_D t_D}{I_C t_C} = \frac{I_D t_D}{I_D t_D + I_{SD} t_{SD}} \tag{17}$$

where I_D is average discharge current, t_D is discharge time, I_C and t_C are charge current and time, and I_{SD} and t_{SD} are self-discharge current and time.

If we define a "use factor" for a particular battery or fuel cell application as the fraction of time during which it supplies useful power, then we can relate self-discharge to current efficiency in the following way:

$$\text{Current efficiency} = 1 \Big/ \left[1 + \frac{I_{SD}}{I_D} \frac{1}{\text{use factor}}\right] \tag{18}$$

Figure 1 shows a plot of equation (18) for various use factors. A use factor of 1.0 can be achieve only in a primary battery or fuel cell, which, after activation, is discharged continuously. Under these conditions quite high self-discharge rates can be sustained without serious effects on the current efficiency.

The lower use factors apply to secondary batteries that must be recharged regularly. A battery in industrial use might be discharged 8 hr a day and recharged every night for a use factor of 0.33, whereas a battery for a personal electric vehicle that is driven about an hour a day would have a

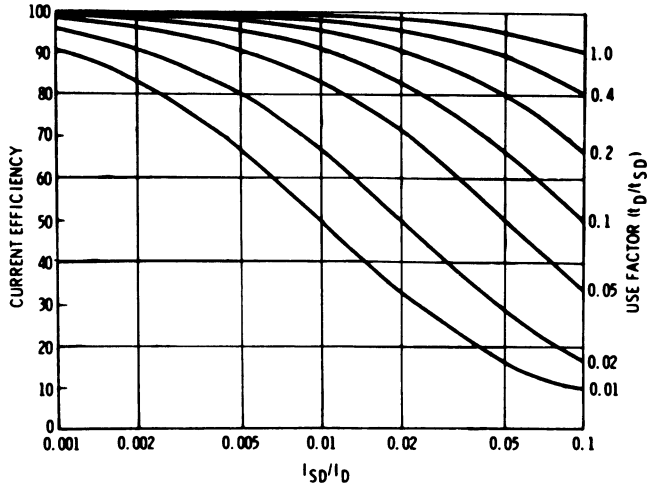

Fig. 1. Current efficiency as a function of self-discharge and use factor.

use factor of about 0.04. In the latter case the effective self-discharge current clearly must be kept low to give reasonable current efficiencies.

Since the self-discharge current for a given system is generally directly proportional to the electrode area, it appears advantageous to reduce the electrode area to a minimum. However, this increases the charge and discharge current densities with a loss in voltage efficiency.

Thus the optimum design of a battery or fuel cell is a complicated function of current–voltage relationship, self-discharge factors, and fuel and material costs with possibly overriding system weight and volume limitations.

The lowest self-discharge system is therefore not necessarily the optimum system. Thus Takahashi *et al.*[22] considered the efficiency of solid electrolyte fuel cells with some electronic conductivity. They showed that even if the electrolyte has some electronic conductivity, a cell can give fairly high efficiency together with high power levels if its total conductivity is sufficiently high and the ionic transference number is not below 0.9. The selection of an electrolyte is then based on the relative importance (cost or weight and volume) of the fuel or the fuel cell structure (that is, electrodes, electrolyte, and case). Takahashi *et al.*[22] showed that for a cell in which

$$E = E_0 t_i - \frac{i}{\sigma} \tag{19}$$

where E is the cell voltage, E_0 is the theoretical OCV, t_i is the ionic transport

number, i is the current density, and σ is the electrolyte conductivity, the maximum energy efficiency occurs when

$$i = \sigma E_0[\sqrt{1 - t_i} - (1 - t_i)] \tag{20}$$

The energy efficiency at this current density is independent of total conductivity and theoretical emf and is given by

$$\eta_{\max} = \frac{1 - \sqrt{1 - t_i}}{1 + \sqrt{1 - t_i}} \times 100\% \tag{21}$$

where $\eta_{\max}$ = maximum energy efficiency. It should be noted, of course, that in the absence of any electronic conductivity, $t_i = 1$ and hence $i = 0$, that is, maximum energy efficiency is obtained when the process occurs at an infinitesimal rate, a well-known but not very practical result. However, for $t_i < 1$ these equations allow us to calculate the current density at which maximum energy is obtained. The power density at the maximum efficiency point (W at $\eta_{\max}$) is given by

$$W \text{ at } \eta_{\max} = \sigma E_0^2 \sqrt{1 - t_i}\,(1 - \sqrt{1 - t_i})^2 \tag{22}$$

This, however, is not the maximum power point. It occurs at a higher current density than the maximum energy efficiency operating point. Thus the optimum operating point will be determined again by the relative importance of fuel and converter cost (or weight). This determination may be further complicated by the fact that polarization losses other than ohmic (or quasi-ohmic) losses may be present and by the fact that the converter may be required to operate at different levels for different periods of time. In that case it becomes simpler to use computer iteration techniques to define the optimum system rather than developing detailed analytical equations.

Thus the transport number, which was taken to be a constant in the above equations, in fact generally varies across the electrolyte and the resulting self-discharge rate varies with current density. The variation of the transport number across the electrolyte is due to the fact that in a solid electrolyte such as $(ZrO_2)_{0.85}$ $(CaO)_{0.15}$ the electronic conductivity at any point is affected by the local oxygen potential.

It is generally assumed that the electronic conductivity is due to the process

$$2O_0 \rightarrow O_2 + 2V_{0^{\cdot\cdot}} + 4e^- \tag{23}$$

where O_0 is an oxygen atom in a regular oxygen site, $V_{0^{\cdot\cdot}}$ is a doubly ionized oxygen vacancy, and e^- is an excess electron.[23–25] Since the number of

oxide ions and the number of vacancies are fixed by the electrolyte composition, more free electrons are generated at low oxygen potentials and hence the electronic conductivity increases in going from the air to the fuel side of the electrolyte. At a given temperature we then have

$$\sigma_e = \sigma_e^0 P_{O_2}^{-1/4} \tag{24}$$

where σ_e is the electronic conductivity, σ_e^0 is the electronic conductivity at $P_{O_2} = 1$, and P_{O_2} is the partial pressure of O_2. Hence $t_i = \sigma_i/(\sigma_i + \sigma_e)$ varies across the electrolyte.

The cell OCV is given by

$$E = \frac{1}{nF} \int_{\mu_1}^{\mu_2} t_i d\mu \tag{25}$$

where μ_1, μ_2 are the chemical potential of oxygen at the anode and the cathode, respectively. Assuming ideal gas behavior and using equations (24) and (25), we find

$$E = \frac{RT}{F} \ln \left[\frac{P_\ominus^{1/4} + P_2^{1/4}}{P_\ominus^{1/2} + P_1^{1/4}} \right] \tag{26}$$

where $P_\ominus$ is the partial pressure of O_2 at which $\sigma_e = \sigma_i$ and P_2, P_1 are the partial pressures of O_2 at the two electrodes.

A similar treatment can be applied to the battery system using alkali metals, which are known to impart a degree of electronic conductivity to the electrolyte. Hesson *et al.*[26] have treated the self-discharge of the alkali metal cells in detail for the case of the sodium–bismuth cell.

Neglecting heat losses and other external self-discharge processes, three modes of self-discharge through the electrolyte can be distinguished in this case. These are

1. Self-discharge due to the diffusion of sodium atoms (that is, nuclei + electrons) due to the concentration gradient from the sodium electrode to the bismuth electrode.
2. When there is a concentration gradient of sodium, then since we have the equilibrium $Na \rightleftharpoons Na^+ + e^-$ there will be a concentration gradient in electrons and hence a diffusion of electrons in the same direction as the diffusion of Na atoms. This is not to say that electrons have a long independent life in the electrolyte. The mechanism is more likely the jumping of electrons from a Na atom to a nearby Na^+ ion with jumps in the direction of decreasing Na concentration being statistically favored.

3. The electron movements are affected not only by the concentration gradient but also by the local electrical gradient. Hence as the cell is charged or discharged the varying electrical gradient in the electrolyte will result in changes in the self discharge rate due to the change in electric field gradient across the cell.

The above three processes can be summarized as follows:

$$i_{SD} = -FD_{\mathrm{Na}} \frac{dC_{\mathrm{Na}}}{dx} - FD_e \frac{dC_e}{dx} - K_e \frac{d\psi}{dx} \tag{27}$$

where D_{Na} is the diffusion coefficient of Na atoms, D_e is the diffusion coefficient of electrons, K_e is the partial electronic conductivity of the electrolyte, C_{Na}, C_e are the concentration of Na atoms and electrons, respectively, and ψ is the local electric potential in the electrolyte.

After some substitutions and rearrengement Hesson *et al.*[26] find

$$i_{SD} = \frac{-FD_{\mathrm{Na}}\varrho}{M} \frac{dX_{\mathrm{Na}}}{dx} - \frac{K_e RTK_i}{F(K_i + K_e X_{\mathrm{Na}})} \frac{dX_{\mathrm{Na}}}{dx} - \frac{K_e X_{\mathrm{Na}} i}{(K_i + K_e X_{\mathrm{Na}})} \tag{28}$$

where ϱ is the electrolyte density, M is the molecular weight of the electrolyte, X_{Na} is the mole fraction of Na in the electrolyte, K_i is the partial ionic conductivity of the electrolyte, and i is the current density.

The dependence of the self-discharge rate on current density is clear in equation (28). The higher the rate of discharge (that is, the more negative i), the lower the absolute magnitude of the self-discharge, while during charging of the cell the self-discharge will increase.

An additional degree of complication arises from the fact that temperature changes occur as a result of high rates of charge and discharge, resulting in changes in many of the quantities in equation (28). Thus in a multi cell rechargeable battery it is likely that not all cells will be equivalent, some getting warmer than others due to their location in the stack. The hotter cells will have a higher self-discharge rate, generating more waste heat. Since in a series-connected stack all cells receive the same charge, the lower self-discharge cells will become fully charged before the high self-discharge cells, and this effect will be cumulative until a point is reached where some cells are fully charged while other may be less than half-charged. At some point it therefore would become necessary to test all cells individually and bring them all to the same state of charge.

3. SPECIFIC BATTERY SYSTEMS

3.1. Concentration Cells

Although many batteries and fuel cells can be treated as concentration cells in one of the two reactant materials, the description is more apt for cells using alloy electrodes such as, for example, the potassium–mercury cell

$$K(Hg)/K^+ \text{ electrolyte}/K(Hg) \tag{29}$$

and similar cells. The work on these cells was motivated by a need for systems that could convert heat to electrical energy in an efficient manner. The concentration cells are suitable since the alloy formed in the electrochemical cell can be separated into its components by distillation at a higher temperature. Since there obviously must be an upper limit to the temperature at which the distillation can be done, there is a clear limit to the electrode materials that can be used, since one of the electrode materials must have a boiling point close to the temperature of the distillation unit. Also, there is a limit to the strength of the bond formed between the components of the alloy, since it must be possible to break down the alloy thermally within the temperature range available. This, then, also infers a limit to the cell voltage, since it will be proportional to the free energy given out in the formation of the alloy at the cell operating temperature.[27]

In a desire to increase the power and energy capacity of systems of this type, ever more reactive combinations of electrodes have been investigated, including systems that cannot be practically separated thermally but can only be recharged electrically. However, these systems are all discussed under the present heading since they grew out of work on the alloy cells and since most of this work is carried out by a single group of workers at Argonne National Laboratory.[28]

Because of the original aim of thermal separation of the reactants this class of cells has been called "thermally regenerative cells" or simply "regenerative cells."[29]

These cells consist of an anode of Li, Na, or K coupled with a cathode from the group Hg, Sn, Pb, Bi, and more recently S, Se, and Te. In the cells using Hg the cathode metal Hg is the more volatile component, and hence it is distilled off and returned to the cathode compartment while the alkali-rich residue is returned to the anode. In all the other systems that are thermally regenerated the anode material is more volatile, and it is distilled off and returned to the anode.[27,30]

For the general case

$$A(a_1)/A^+/A(a_2) \text{ in } B \tag{30}$$

the emf of the concentration cell is given by

$$E = \frac{RT}{nF} \ln \frac{a_1}{a_2} \tag{31}$$

where a_1 and a_2 are the activity of A at the anode–electrolyte and the cathode–electrolyte interfaces, respectively. If the anode metal is essentially pure A, as is often the case, then $a_1 = 1$ and hence

$$E = \frac{-RT}{nF} \ln a_2 = \frac{-RT}{nF} \ln \gamma N_A \tag{32}$$

where γ is the activity coefficient and N_A is the mole faction of A in B. If A formed a simple ideal solution in B, then $\gamma = 1$ and very low emf's would be observed. In fact, ideal solutions are not formed and very low values of γ are found due to the formation of compounds of the form A_xB_y. This results in very low activities of free A in B and hence in practical voltage levels. It is clear that the cell voltage will decrease as the concentration of A in B increases so that cell performance will go down as the cell is discharged unless a steady state is reached by continuous thermal regeneration at the same time.

Self-discharge may be expected to be an important parameter in these cells because of the solubility of alkali metals in alkali halides and the resulting electronic conductivity. The solubility and the electronic conductivity at a given concentration generally decrease in going from Cs to Li so that Li is the most desirable anode material not only because of its lower self-discharge characteristics but also because of its low equivalent weight and high reactivity. Furthermore, the Li salts are generally more conductive than the other alkali halides, resulting in lower resistance losses. It therefore is not surprising that power densities as high as 5 W/cm^2 have been obtained in the Li/Te cell.[31] This power density is only exceeded by another Li system operating at higher temperature, viz., the Li–Cl_2 cell at 650°C[32] (Section 3.3). Self-discharge transfer of alkali metal from the negative to the positive electrode can be corrected by thermal or electrical regeneration. However, transfer of the cathode material to the alkali metal electrode cannot be rectified so readily. When this occurs to any significant extent, the only solution is a periodic removal of the contaminated anode material

and external separation of the components. Fortunately the solubility of the cathode materials in the electrolyte is generally quite low.

Since both electrodes and the electrolyte are normally liquid at cell operating temperatures, the mechanical stability of the interfaces must be considered in designing practical cells based on these systems. This is achieved by restraining one or more of the liquids in a porous solid matrix. Thus a ceramic matrix or paste has been used to contain the electrolyte[28] while metal or graphite matrices may be used to contain the electrode materials. This is necessary in any case for Te, Se, and S, since these are increasingly poor electronic conductors and hence must be contained in a porous metal or graphite mesh to give adequate conductivity to the electrode. Of the regenerative cells the Na–Bi system probably has been studied most thoroughly. Single cells have been operated for periods up to 17 months with electrical recharging.[33] Discharge current densities were 90 and 110 mA/cm^2 at cell voltages of 0.5 and 0.45 V, respectively. In this life test the average cathode composition was about 20 atom % Na in Bi, giving an OCV of 0.7 V. The cell was constructed of type 304 stainless steel with a high purity alumina insulator ring, which was protected, however, from attack by sodium by a layer of frozen electrolyte. The electrolyte for the Na–Bi cell consists of a mixture of sodium halides that melts at 529.4°C.[33] Cell operating temperature is typically 550°C, and for the geometry used in the life test the average self-discharge rate on open circuit was equivalent to 23.6 mA/cm^2 or about one-fourth of the average discharge current density. This is clearly too high a self-discharge rate for applications involving significant periods in a standby condition, that is, applications with a use factor of less than 0.5.

The liquid–vapor equilibria for the Na–Bi system have been studied by the transpiration method at 900°C.[34] The low activity of Na in liquid Bi is due to the formation of NaBi and of Na_3Bi, which also exists as a solid phase. From the vapor composition data at 900°C the equilibrium constants for the formation of these compounds in the liquid were found to be

$$K_1 = \frac{X_{NaBi}}{X_{Na} \cdot X_{Bi}} = 300 \tag{33}$$

$$K_2 = \frac{X_{Na_3Bi}}{X_{Na_3} \cdot X_{Bi}} = 2 \times 10^5 \tag{34}$$

The Na–Bi cell can be charged and discharged at much higher rates than the 100 mA/cm^2 reported for the life test (see Fig. 2), and current

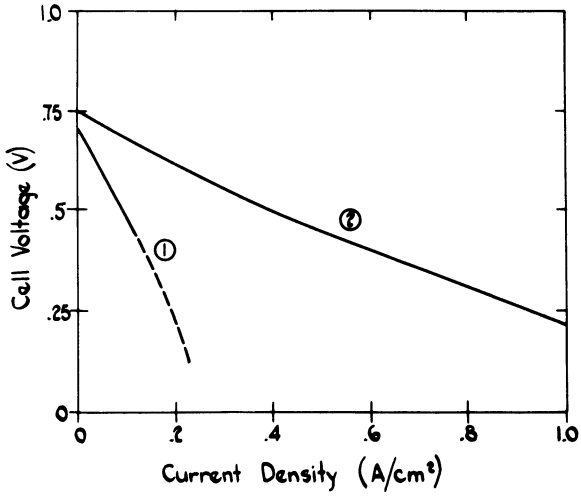

Fig. 2. Sodium–bismuth cell performance. 1: Life cell, 550°C, 2.5-cm-thick electrolyte. 2: Power cell, 575°C, 0.4-cm-thick electrolyte. Electrolyte is NaF–NaCl–NaI (15.2–31.6–53.2 mole %).

densities in excess of 1 A/cm^2 have been reported using a much smaller electrode spacing.[35] However, this results in significant concentration polarization due to concentration gradients in the alloy, and the cell terminal voltage falls rapidly as the cell discharges. In a thermally regenerative mode a steady state would be set up determined by the current and the rate of distillation, but in an electrically rechargeable mode the cell voltage drops continuously as the cell is discharged. This means that power and energy capacities quoted for the Na–Bi system probably only refer to a fully charged cell and will decrease as the cell is discharged as opposed to the simple Li–Cl_2 cell, which has the same performance at all charge levels. Several other bimetallic cells using sodium have been studied including Na–Sn,[36,37] Na–Pb,[28,38] and Na–Hg.[39-41] The emf's of these cells are lower then the emf of the Na–Bi cell at the same composition.[38] In addition, in the case of Na–Hg the mercury is the more volatile component. Hence the cathode metal is continuously distilled and returned to the cathode. Since it is necessary to keep the Na concentration in the cathode low to maintain a high voltage, the major component of the cathode alloy is distilled off, requiring a much greater heat input. The same comment applies to the K–Hg system,[42] which is the only potassium system that has been investigated in some detail.

The best performance can be obtained from systems using Li as the alkali metal because of the high reactivity of Li, its low equivalent weight, and the high conductivity of its halide salts. Also, the Li halides have lower melting points, thus allowing lower operating temperatures. The main problem associated with Li-containing cells is the fact that Li will attack most ceramic insulators, forming electrolyte-soluble or electronically conducting products. However, if the material problems can be overcome through material development and clever design, then the Li batteries certainly will become the energy storage systems of the future. Table V shows a comparison of several lithium and sodium batteries with more conventional ambient temperature systems. Lithium is more abundant than lead and not much more expensive. Since the lead acid battery presently satisfies most of our electrical energy storage requirements, an order of magnitude improvement should be possible.

The lithium systems are generally not thermally regenerative because of the high strengths of the bonds formed between Li and the various cathode materials used. This is reflected in the high cell voltages shown in Table V. The electrolytes used in these Li cells are LiCl–LiF (m.p. = 485°C), LiCl–KCl (m.p. = 353°C), or LiF–LiCl–LiI (11.7–29.1–59.2 mole %). The latter electrolyte melts at 341°C and at 375°C has a conductance of 2.3 Ω^{-1} cm^{-1}.[45] Using this electrolyte held in a paste form with $LiAlO_2$ filler, a Li–Bi cell was operated at 380 to 485°C.[45] The performance increased with temperature, and at 485°C a maximum power density of 0.57 W/cm^2 at 0.6 V was obtained. A similar Li–Te cell yielded 1 W/cm^2 at 0.9 V,[45] while in a cell using liquid electrolyte power densities of 5 W/cm^2 have been demonstrated.[31] A Li–Se cell has been reported to deliver 7.8 W/cm^2 at 1.2 V using liquid electrolyte,[46] and current densities in excess of 10 A/cm^2 are possible without significant voltage losses other than resistance losses. Figure 3 shows typical current voltage curves for a number of Li cells.

In addition to the high performance of the Li batteries, their self-discharge is generally lower than for the corresponding Na systems. Thus, although quite high solubilities of Li_3Bi have been found in LiCl–LiF at elevated temperatures (1 mole % at 900°C).[47] at cell operating temperatures of less than 500°C the solubility is reduced 100-fold and essentially 100% coulombic efficiencies have been reported for both Li–Bi and Li–Te.[45] The Li–Se cell has advantages of higher voltage than the Li–Te cell (2.3 V *vs.* 1.75 V) lower equivalent weight (39.5 *vs* 63.8 g/equiv.) and lower operating temperature (375 *vs* 475°C) due to the lower melting point of selenium, yielding a cell of high specific energy and high specific power.[44]

TABLE V. Electrical Energy Storage Cells[35,38,43,44]

	Temperature (°C)	Electrolyte resistivity (Ω-cm)	Cell voltage (V)	Typical discharge current density (A/cm²)	Power capacity (W/kg)	Energy capacity (w-hr/kg)	Energy density (w-hr/cm³)	Cycle life
Lead–acid	Ambient	1.5	2.1–1.5	0.01	6–30	20–30	0.08	10–400
Nickel–iron	Ambient	2.0	1.3–0.8		7–40	30–35	0.07	100–3000
Nickel–cadmium	Ambient	2.0	1.3–0.8	0.01	7–45	36–40	0.06	100–2000
Silver–zinc	Ambient	2.0	1.55–1.1	0.4	25–150	80–100	0.29	100–300
Zinc–air	Ambient	2.0	1.4–1.0	0.1	40–60	100–150		
Sodium–air	130	3.6	2.6–1.8	0.1	80–100	180–275	0.4	
Sodium–bismuth	550	0.24	0.8–0.4	0.6	80	40	0.08	500
Sodium–sulfur	300	4.0	2.1–1.2	0.7	200–350	180–330	0.35	
Lithium–chlorine (GM)	650	0.17	3.5–3.0	3	200–400	300–400		
Lithium–chlorine (Sohio)	450	0.63	3.4–1.0	1	330–440	100–160	0.5	225
Lithium–tin	400	1.7	0.8–0.4	0.35				
Lithium–tellurium	470	0.26	1.8–1.0	3	550–800	185–265	0.36	
Lithium–selenium	375	0.26	2.2–1.2	5	600–1000	220–330		
Lithium–sulfur	340		2.3–1.2	2.5 (Short term)	550–800	250–360		

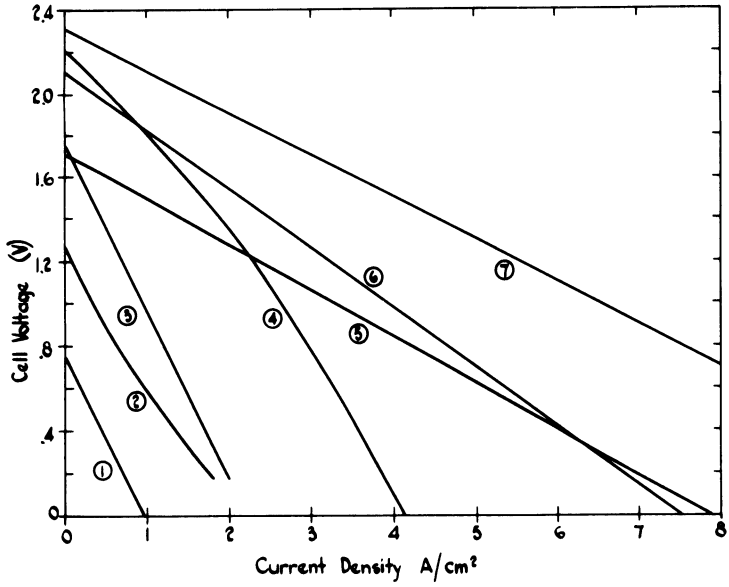

Fig. 3. Cell performance for some Li systems. 1: Li–Sn, 50 wt % filler, 0.39-cm-thick electrolyte, 510°C. 2: Li–Bi, 50 wt % filler, 0.34-cm-thick electrolyte, 485°C. 3: Li–Te 50 wt % filler, 0.32-cm-thick electrolyte, 475°C. 4: Li–Se, 40 wt % filler, 0.26-cm-thick, electrolyte, 375°C. 5: Li–Te, no filler, 0.5-cm-thick electrolyte, 470°C. 6: Li–S, no filler 0.5-cm-thick electrolyte, 347°C. 7: Li–Se, no filler, 0.5-cm-thick electrolyte, 375°C.

The main limitation of systems based on Se or Te is an economic one. Te has about the same terrestrial abundance as gold, and although Se and Te are not expensive now, this is only because the demand is low. Thus a major application of these systems, such as electric vehicles, could not be envisaged without major new sources of Se or Te. This, however, is not the case for the Li–S system. Sulfur is economically more attractive, yields a high open-circuit voltage (2.4 V) with Li, and has a low equivalent weight (16 g/equiv).[44] Since S is an insulator it requires a porous matrix current collector of metal or graphite to reduce the cathode resistance losses. Because of the solubility of S in fused salts some self-discharge problems may occur.[48] However, the potential energy and power capacity of this system together with its economic promise seems to justify a thorough investigation of this system.[43] The corresponding Na–S system is being developed using an Na^+-ion conductive solid electrolyte.[49] Since this solid electrolyte is a pure Na^+ ion conductor no self-discharge occurs except through thermal losses. A similar Li^+-ion conductive electrolyte with high

conductivity and essentially zero solubility for Li and S species, which is compatible with the more reactive Li, would make the Li–S battery a very powerful energy storage system.

3.2. Thermal Batteries

Thermal batteries are reserve-type primary batteries that can be activated by heating them.

They contain an inorganic or organic solid electrolyte, which is essentially nonconducting until the temperature is raised sufficiently to melt the electrolyte. Electrical energy then may be withdrawn from the system. This type of cell been investigated since World War II for military and aerospace applications. These cells generally are used when high currents are required for short periods of time after possibly years of inactive waiting. Once activated, their life is usually measured in minutes. To be able to deliver high currents and store as much energy as possible a fused salt cell is an obvious choice. Before the electrolyte is molten a very inactive, extremely low self-discharge system can be obtained. Although in the early days of thermal cell investigations almost any molten salt electrolyte was considered, only the halide mixtures have been found practical and most work has been done with LiCl–KCl eutectic electrolytes.[50]

Anode materials most often used are Mg and Ca. The latter is the more active electrode material and when used with an LiCl–KCl electrolyte the Ca will displace some of the Li from the electrolyte, forming a liquid Ca–Li alloy on the surface of the electrode.[51] Since this surface is continuously renewed a very low polarization electrode system results. Thermal cell performance therefore depends largely on the cathode materials used. Cathode performance depends, of course, on the oxidizing nature of the cathode material, and the rate of reaction is often determined by its solubility in the electrolyte.[1] Cathodes generally consist of compounds containing large amounts of not too strongly bound oxygen, so that the overall cell discharge reaction is

$$x\mathrm{Ca} + \mathrm{MO}_x \rightarrow x\mathrm{CaO} + \mathrm{M} \tag{35}$$

where MO_x is typically CuO,[52] Fe_2O_3,[53] V_2O_5,[54] WO,[50,55] or $CaCrO_4$ and K_2CrO_4.[50,56] Much of the art of making high-performance cathodes is described in classified reports and also in the patent literature. For example, one patent[57] describes cathodes consisting of electrolyte, a conductive material such as C or Cu, and depolarizing salts such as an aluminate, borate, carbonate, phosphate, silicate, sulfate, or alumino-silicate with a Ni current collector. A cell consisting of a Ca anode and a cathode

made up of 40% $Fe_2(SO_4)_3$, 14% graphite, 12% Cu powder, and 34% KCl–LiCl electrolyte gave an open-circuit voltage of 2.52 V at 560°C.[57] However, the electrochemistry of these systems is not well understood, and discussion therefore will be limited to those materials which have been studied in some detail. Generally, the cell reaction is not as simple as indicated by equation (35). For example, a study of V_2O_5 in LiCl–KCl at 450°C[58] showed that V_2O_5 is first partially reduced to form a mixed lithium vanadium oxide of the composition $Li_2O \cdot 2V_2O_4 \cdot 4V_2O_5$, which was insoluble in the electrolyte and formed a coating on the electrode. Further reduction of the V_2O_5 can occur but at a lower voltage and at a much lower rate due to the insoluble precipitate formed. It therefore is not surprising in a comparison of a number of cathode materials in actual thermal cells that although V_2O_5 gives the highest initial voltage its energy capacity is low and hence very short lives are obtained.[50] This is due not only to the above-mentioned passivation but also to a high self-discharge rate when hot because of the high solubility of V_2O_5. This allows rapid diffusion of V_2O_5 to the anode followed by chemical reaction.

Chromate cathode materials can be reduced to a larger extent than V_2O_5 before producing insoluble passivating precipitates. From a chronopotentiometric study it was concluded that in LiCl–KCl at 450°C primary reduction product was CrO_4^{-5}, which then decomposed to give CrO_3^{-3} and O^{-2}.[59]

$$CrO_4^{-2} + 3e^- \rightarrow CrO_4^{-5} \rightarrow CrO_3^{-3} + O^{-2} \tag{36}$$

At sufficiently high concentrations Li_5CrO_4 was deposited, while in the presence of Mg^{2+} or Ca^{2+}, as would be the case in thermal cells using these anode materials, black and very stable precipitates were formed. The composition suggested a compound $2Li_2O \cdot CaO \cdot Cr_2O_3$,[50,60] in the presence of Ca^{2+} and compounds of the form $Li_xMg_yCrO_4$ where $x + 2y = 5$ have been found when Mg^{2+} was present.[61] Nevertheless, a three electron change per molecule of K_2CrO_4 or $CaCrO_4$ occurs, resulting in the highest energy output in a series of thermal cells tested under identical conditions except for the cathode active material. (See Table VI).

Cell geometry of thermal cells is generally a stack of flat disks of current collector, cathode material, electrolyte, anode material, and current collector. This is repeated until the necessary current and voltage capacity are built up. The large area, flat geometry assists in getting heat into the battery rapidly to start it up as well as giving a large electrode area so that high power levels can be obtained. However, it also results in a fairly high self-discharge after activation so that only short-life applications are possible.

TABLE VI. Comparison of Cathode Materials in Thermal Cells at 600°C and Constant Current Discharge (i = 0.31 A-cm²)[50]

Cathode material	Peak voltage[a]	$t(90\%)^b$ (sec)	$t(80\%)^c$ (sec)	Energy (90%)[d] (W-sec)	Energy (80%) (W-sec)
CuO	1.49 ± 0.01	24 ± 2	32 ± 1	194	259
$CaCrO_4$	1.65 ± 0.01	46 ± 1	62 ± 1	412	557
WO_3	1.71 ± 0.05	44 ± 6	50 ± 3	410	465
Fe_2O_3	1.48 ± 0.06	27 ± 6	41 ± 3	216	328
V_2O_5	2.07 ± 0.06	22 ± 10	40 ± 2	248	450

[a] Peak voltage is the maximum voltage recorded under load.
[b] $t(90\%)$ = service time above 90% of peak working voltage.
[c] $t(80\%)$ = similarly above 80%.
[d] Energy (90%) = energy output above 90% of peak working voltage in watt-seconds.

When longer life (days) is required a cylindrical geometry with the top portion of the cylinder making up the anode and the bottom portion the cathode mix is necessary.[62] Using this type of geometry, cells of the type

$$Mg/LiCl - KCl/CuO,\ Cu_2O/Ni \tag{37}$$

were discharged at 425–535°C over periods of up to 6 days with an electrode efficiency of 73%, while over a period of 1 day the efficiency was 93%.[52] The cell voltage shows a clear two-plateau behavior, the first plateau corresponding to $Cu^{2+} \rightarrow Cu^{+}$ and the second plateau to the reduction to Cu^0.

Another cathode material that has been studied in some detail is iron oxide, usually Fe_2O_3. Using LiCl–KCl electrolyte and a Mg anode one study compared the performance of cells with Fe_2O_3 or Fe_3O_4 from different sources.[53] Marked differences were observed that could be largely ascribed to variations in electrical conductivity. Since Fe_2O_3 is not very soluble in the electrolyte we have mainly a solid electrode reaction. Hence the conductivity of the solid is important. Impurities that increase the conductivity of the solid such as Ti^{4+} were found to result in higher cell voltages when present in otherwise poorly conducting α-Fe_2O_3. Similarly, the more conductive γ-Fe_2O_3 gave better performance than α-Fe_2O_3 and simple mixing of carbon with α-Fe_2O_3 resulted in improved performance. However, in that case the improvement only occurred in the initial stage of discharge

and a fairly rapid drop in voltage occurs. This may be due to the chemical reduction of Fe_2O_3 by C which would remove the cathode reactant and possibly the conductive path by forming CO-filled voids in the electrode. Thus the type of iron oxide selected may be determined by the cell discharge characteristics required. For a high voltage output γ-Fe_2O_3 or Fe_3O_4 would be used, but if a longer, constant output is more important α-Fe_2O_3 without additives may be more desirable. The end product of the cathode reduction is a water-insoluble mixed oxide of Li and Fe, possibly of the form $Li_2O \cdot (FeO)_x$, but this has not been positively identified.[53] The anode reaction therefore is not the formation of MgO but simply the formation of Mg^{2+} ions that dissolve in the electrolyte.

A recent comparison of several cathode materials in the two cell designs at various temperatures and current loadings allows some selection of materials for particular applications.[50] The cells consisted of a Ca anode, an LiCl–KCl electrolyte, and the following cathode materials: CuO, $CaCrO_4$, Fe_2O_3, WO_3, and V_2O_5. The most successful cell design consisted very simply of a calcium-coated nickel plate that was the negative lead, a two-layer disk pressed in one operation by feeding into the die first a layer of electrolyte mixed with some Florida–Kaolin and then a layer of the cathode material mixed with some electrolyte, and finally another nickel plate that was the positive lead. These layers were then pressed together, and electrically heated and the cells were discharged at constant current. Table VI shows some of the results obtained.

Thermal cells are not limited to the disk-type geometry or the oxide cathode materials. The Li–Cl_2 cell or any of the Li–chalcogen systems could make very high energy, thermally activated cells of much longer life than the cells discussed above, and we are not limited to fused salts. Several high-melting organic materials have been studied for this purpose. However, many of the organic electrolytes react chemically either with the anode or with the cathode material. Several cells using acetamides have been tested, but electrolyte conductivities are at least an order of magnitude below those of molten salts and significant reduction of the acetamide by the high energy anode metals was observed.

3.3. Lithium–Chlorine Cells

The combination of Li with any of the elements in the top right-hand corner of the periodic table results in a high energy battery system. However, practical considerations of container and electrode materials have eliminated Li–F_2 because there is no known electrode material that will

withstand F_2 at elevated temperatures and Li–O_2 because of the high melting point of the Li_2O reaction product as well as its corrosive nature toward ceramic insulators. The Li–S system already has been mentioned under the heading of "Concentration Cells" (Section 3.1) since it has evolved from thermally regenerative systems of the Na–Bi type. The next combination is Li–Cl_2, and this cell has several advantages over the systems mentioned above. The reaction product LiCl serves as the electrolyte. LiCl melts at 608°C, which is lower than any of the other Li halides. Cell operating temperature is therefore in the range 625–650°C, and in this range the electrolyte conductivity is higher than that of any other fused salt. The cell open-circuit voltage is also the highest of any of the fused salt batteries being seriously investigated, and it therefore is not surprising that the highest power density of any battery system (40 W/cm^2) has been demonstrated in this system.[63] The Li–Cl_2 cell in its simplest form consists of liquid Li (m.p. 183°C) held in a porous stainless steel matrix, LiCl electrolyte, and a Cl_2 on porous graphite cathode. Since Cl_2 of course will attack all metals at 650°C, the metal parts of the cell must be maintained at the Li potential and Cl_2 must see only carbon or graphite and glass or ceramic materials. The biggest technical problem associated with the Li–Cl_2 cell is the insulator, which must be stable with respect to both Li and Cl_2. Solid LiCl of course is such a material, but the heat loss associated with maintaining this solid region represents a serious self-discharge. High purity BeO has shown considerable promise as a suitable material. There are several means of reducing the demands placed on the insulator. One is to lower the temperature using mixed electrolytes, such as LiCl–KCl eutectic (m.p. 353°C). Since additional LiCl is formed during discharge, the cell of course will be operated well above this temperature to prevent the early precipitation of solid LiCl. These mixed electrolytes are used in the production of Li by electrolysis[64] and have a lower conductivity than pure LiCl, but this is in part compensated for by a higher open circuit voltage.[65] An additional step in lowering the insulator requirements is to lower the activity of Li by alloying, as has been done in the Sohio version of the Li–Cl_2 cell.[66]

The self-discharge aspects of the Li–Cl_2 system caused some concern initially,[67] but the problem does not seem to be severe. The biggest self-discharge loss is the heat loss associated with the high operating temperature of the system. Although the Li–Cl_2 cell can be frozen and restarted without damage, it would not appear to be practical to do this regularly, and in a vehicle application it would be preferable to keep the cell hot continuously by using its own stored energy as required.

The simple Li–Cl_2 cell has another distinct advantage over the concen-

tration cells and the Sohio version: its performance is essentially independent of the level of charge, provided high purity Cl_2 is used. This is desirable in many applications and reduces the amount of power conditioning equipment that otherwise might be needed.

The open-circuit voltage of the Li–Cl_2 cell has been determined from the melting point of LiCl to about 850°C and is given by

$$E = 3.4906 - 5.64 \times 10^{-4}(t - 608) \text{ [volts]} \tag{38}$$

where t is temperature in degrees centigrade.[32] These data are about 100 mV lower than the OCV calculated from thermodynamic data by Hamer[13] but are in good agreement with more recent thermodynamic data.[68] The measured OCV's are about 7 mV above the emf calculated from the JANAF Themochemical Data, which indicates that electronic conductivity losses are small.

The lithium electrode behaves ideally in that it has not been possible to detect any polarization at current densities of 40 A/cm^2. However, mechanically the Li electrode presents some problems. Since Li is a liquid at cell operating temperature and is less dense than LiCl, it normally floats on top of the electrolyte. Since Cl_2 gas of course is also less dense, any Cl_2 gas escaping from the Cl_2 electrode would rise and chemically react with the Li. In addition, since the Li–Cl_2 cell has good potential for vehicle applications, free Li sloshing around close to the Cl_2 electrode is clearly not desirable. There are two ways in which this can be overcome. One is to contain the Li in a porous metal matrix similar to those used as current collectors for Se, Te, and especially S. The purpose here is not to improve electrical conductivity, since Li is good electrical conductor, but simply to act as a sponge to soak up the liquid Li and hold it against the buoyancy forces by capillarity. Since Li generally wets metals preferentially over LiCl a simple stainless steel, felt metal matrix serves the purpose well.

Alternately the Li may be stored as a free liquid remote from the Cl_2 electrode and transported to the electrode region via capillary forces in a porous wick. The maximum depth to which Li will travel down the wick can be found by equating the capillary forces and the hydrostatic forces,[69] which leads to

$$h_0 = \frac{2\gamma \cos\theta}{rg\,\Delta\varrho} \tag{39}$$

where h_0 is the maximum depth in centimeters, γ is the Li–LiCl interfacial tension, θ is the contact angle between Li and the pore wall, r is the pore radius (centimeters) at the interface, g is the acceleration due to gravity

(981 cm/sec^2), and $\Delta\varrho$ is $\varrho_{LiCl}-\varrho_{Li}$, the density of LiCl minus the density of Li in grams per cubic centimeter. At 650°C, $\gamma = 157$ dynes/cm, $\varrho_{LiCl} = 1.484$ g/cm^3, and $\varrho_{Li} = 0.469$ g/cm^3. Hence, for Li–LiCl at 650°C, equation (39) reduces to $h_0 = 0.3153\ (\cos\theta)/r$. If the wall of the pore is preferentially wetted by the Li to a high degree, then $\theta \to 0$ and $\cos\theta \to 1$. The rate at which Li can be transported to any depth $h < h_0$ expressed in terms of amperes per square centimeter of wick cross section (I) is given by

$$I = \frac{nF\varrho_{Li}\varphi}{M}\left(\frac{r^2}{8\eta\tau h}\right)\left(\frac{2\gamma\cos\theta}{r} - gh\,\Delta\varrho\right) \tag{40}$$

where n is the number of electrons per molecule (here equal to 1), F is the Faraday, φ is the wick porosity, M is the molecular weight of Li, η is the viscosity of Li $= 3.03 \times 10^{-3}$ poise at 650°C and τ is the tortuosity of the pores. Inspection of equation (40) shows that for a given required wicking depth there is an optimum pore size (r_{opt}) that is readily obtained by differentiating equation (40) with respect to r and setting $dI/dr = 0$. This leads to

$$r_{opt} = \frac{\gamma\cos\theta}{gh\,\Delta\varrho} \tag{41}$$

For pore sizes smaller than the optimum the rate is limited by the flow resistance, while for pores larger than the optimum the capillary driving force is reduced. Actual wicks do not have a single pore size but rather a pore size distribution. The net effect would be a complex average of the effects for individual pores with the larger pores contributing more to the flow and the smaller pores more to the depth of wicking. Fairly good agreement between caculated and experimental wicking rates has been obtained by approximating the pore size distribution by a number of steps, applying equation (40) to each step, and summing the contributions[69] (see Fig. 4).

The chlorine electrode consists of a thin-walled, highly porous piece of porous carbon or graphite that is exposed to Cl_2 gas on one side. Since carbon and graphite are not wetted by clean dry LiCl, electrolyte only penetrates a short distance into the porous electrode. This means that the models developed for aqueous fuel cell electrodes that are wetted by the electrolyte do not apply here, since it has been demonstrated for the wetted electrodes that most of the electrode reaction occurs in the thin film of electrolyte just beyond the point to which the electrolyte completely fills the pores. The overall Cl_2 electrode process in LiCl can be separated into four steps:

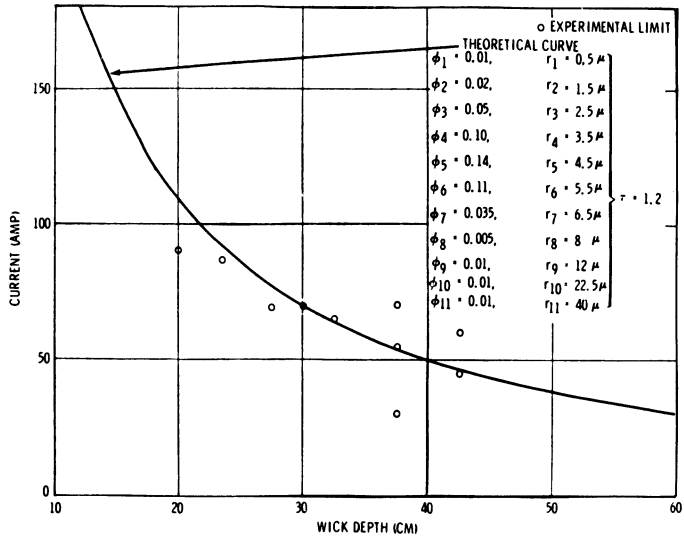

Fig. 4. Limiting current as a function of wick depth for Type 347 stainless steel Feltmetal (Huyck Corp.). Wicking cross section = 0.16 cm^2; total porosity = 0.5; and nominal pore radius = 5 μ. (With permission of the Electrochemical Society.[69])

1. Chlorine transport through the porous electrode due to a pressure difference ΔP.
2. Dissolution of Cl_2 in LiCl.
3. Diffusion of Cl_2 to the graphite–LiCl interface.
4. Electron transfer and migration of Cl^-.

The second step is fast compared with the others, and the fourth step has an exchange current density of about 0.2 A/cm^2 associated with it, which means that at practical current densities of 2–4 A/cm^2 an activation polarization of about 0.2 V may be expected. Steps 1 and 3 are the main rate-determining steps, depending on the structure of the porous electrode. The diffusion-limited current density[32] associated with Step 3 is given by

$$i_L = \frac{8nFDKP_2\varphi}{r} \tag{42}$$

where n is the number of electrons (here equal to 2), F is the Faraday, D is the diffusion coefficient for Cl_2 in LiCl, K is the Henry's law constant, φ is the porosity, and r is the pore radius.

The partial pressure of Cl_2 at the gas–liquid interface (P_2) is determined by the pressure drop (ΔP) across the porous electrode and the buildup of electroinactive impurities (P_i), which are invariably present in the Cl_2[70,71]

P_2 is then given by

$$P_2 = P_T - \Delta P - P_i \tag{43}$$

in which

$$\Delta P = \frac{i_L RTL}{nF\varphi}\left\{\frac{16\mu}{1.013r^2(2P_T - \Delta P)} + \frac{3}{4\delta r}\left(\frac{\pi M}{1.6634T}\right)^{1/2}\right\} \tag{44}$$

$$P_i = N_0 P_T \exp\frac{iRTL}{nFP_T\varphi D'} \tag{45}$$

In equations (44) and (45), μ is gas viscosity, δ is a constant equal to 0.9, M is molecular weight of $Cl_2 = 71$, N_0 is mole fraction of impurities in the incoming gas, and D' is diffusion coefficient in the gas.

The plot of i_L vs. pore radius shows a maximum, indicating an optimum pore size.[32] For pores smaller than the optimum size, flow through the porous graphite is the main limiting process, whereas for pores larger than the optimum size, diffusion of Cl_2 in the electrolyte is the main rate-limiting step. Figures 5 and 6 show the effects of electrode thickness, total pressure, and impurity level.

Similar to the wick electrode, the porous carbon or graphite does not have a single unique pore size but rather a pore size distribution. This

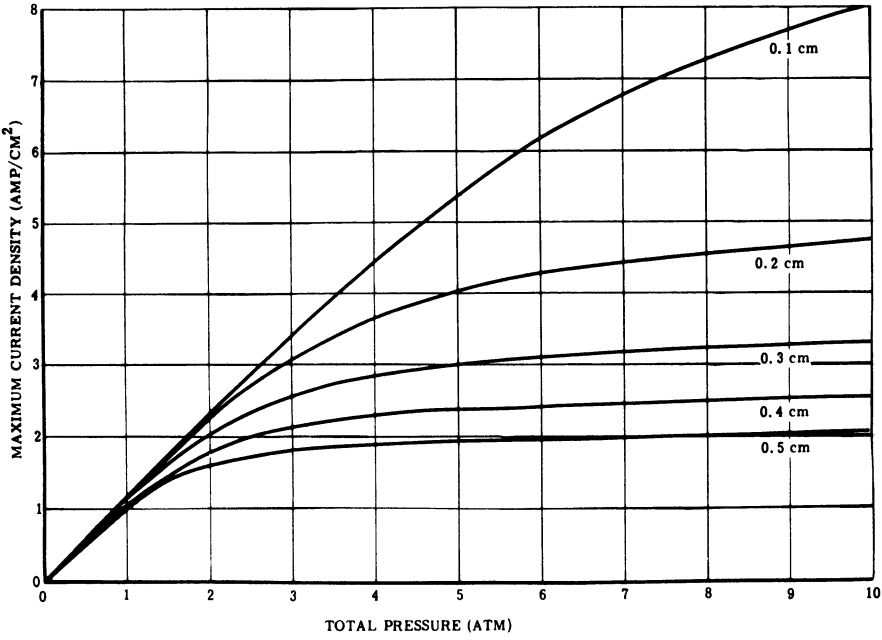

Fig. 5. Maximum current density (i_L) calculated for FC-11 porous graphite as a function of electrode thickness and total pressure at a 1% impurity level. (With permission of the Electrochemical Society.[70])

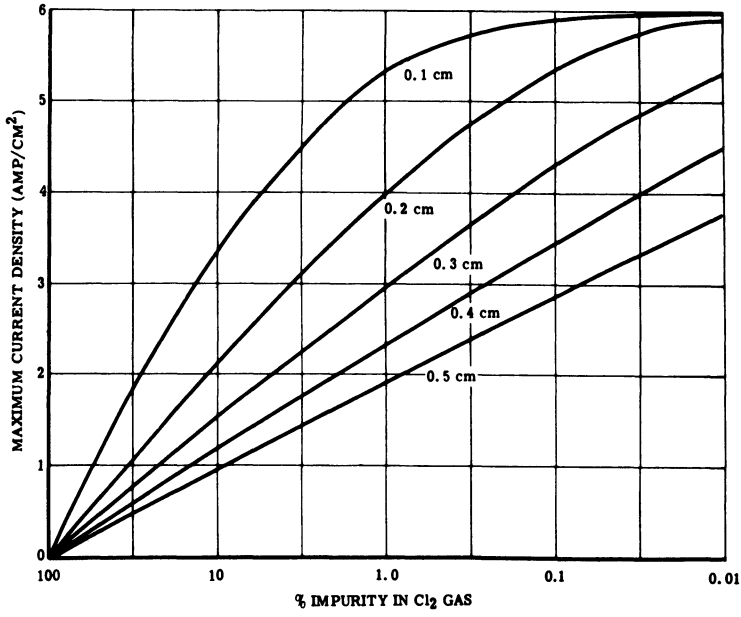

Fig. 6. Maximum current density (i_L) calculated for FC-11 porous graphite at a total pressure of 5 atm. (With permission of the Electrochemical Society.[70])

distribution is again approximated by a series of steps, and the contributions of all steps are summed.[71] In spite of the flow and impurity limitations of the Cl_2 electrode, current densities in excess of 10 A/cm^2 are readily obtained using porous graphite of high porosity and optimum pore size distribution,[71] while in complete Li–Cl_2 cells power densities of 40 W/cm^2 have been demonstrated.[63]

On recharge, Cl_2 is evolved from the porous graphite electrode and bubbles up through the electrolyte. This means that there is a minimum electrode separation in rechargeable cells below which self-discharge during the recharge cycle becomes intolerably high due to physical contact between the Cl_2 bubbles and the Li electrode. This problem can be overcome and the cell can be simplified if the Cl_2 can be forced to flow back through the porous graphite electrode and return to the storage tank via the same route used on discharge. Since the electrode is not wetted by pure LiCl and most ceramics are wetted by LiCl, this effect can be achieved by using the surface tension forces. It is not practical to hold the electrolyte in a porous matrix unless very intimate contact with the electrode is achieved. This is because any significant voids between the electrode and the matrix will fill with Cl_2 and contact between the electrode and the electrolyte will

be lost. However, intimate contact between a porous ceramic and the graphite electrode can be obtained by flame or plasma spraying the ceramic onto the electrode. Such an electrode can withstand pressure differences in both directions without the interface moving significantly, the magnitude of these pressure differences being dependent on the wetting properties and the pore sizes of the two layers. Such an electrode has been called a "valve electrode"[72] by analogy to Justi's electrode of similar properties in aqueous electrolytes. Paste electrolytes may serve the same purpose but, as pointed out earlier, a ceramic that is compatible with both Li and Cl_2 at 650°C for extended periods of time is still the main development problem associated with the Li–Cl_2 cell.

The compatibility problem may be reduced by operating at a lower temperature or by reducing the Li activity by alloying. Both these approaches have been adopted in the Sohio version of the Li–Cl_2 system.[66,73] The system uses a LiCl–KCl mixed electrolyte and typically operates at 450–500°C. The anode consists of a solid Li–Al alloy of which only the Li is the electroactive metal. The Li–Al phase diagram shows a Li-rich β-phase and a lower Li content α-phase.[74] Conversion from one phase to the other with removal or addition of Li is rapid above about 400°C,[75] and charge and discharge rates of 2 A/cm^2 can be obtained.[73] The current capacity per unit weight of such an alloy electrode is about one-fifth that for pure Li but is similar to that of a matrix electrode. The Sohio system also avoids the use of free gaseous Cl_2 by adsorbing and reacting the Cl_2 within the cell.[76] Adsorption of Cl_2 on high surface area charcoals has been proposed as a safe method of carrying large quantities of Cl_2,[77] but the amount of Cl_2 that can be stored at 450–500°C is rather small. Plain porous carbon was found to have a current capacity $\leq$ 1 A-hr/in^3,[78] but activated charcoals of high surface area gave current capacities of 2–3 A-hr/in^3 and for a given type of material the current capacity was proportional to area.[79,80] Very high surface area carbons can be made from polymer precursors such as Saran[80] and B.E.T. N_2 surface areas of 1000 m^2/g can readily be obtained. The total current capacity of these electrodes arises from a number of processes that include physical and chemical adsorption of chlorine, double layer charging, and cation adsorption.[81] However, these processes occur at different voltages so that the OCV of this cell, which is 3.25–3.4 V when fully charged, will decrease as the cell is discharged. The cell can be discharged to an OCV of about 1 V. At lower voltages irreversible damage to the cathode starts to occur until finally Li_2C_2 is formed. The activated carbon cathodes have been cycled for 200 cycles over a period of 90 days, demonstrating good reversibility.[81] However, further improvements in the

current capacity are needed to achieve the stated goal of 220 (W-hr/kg).[79] Various additives to the activated carbon therefore were investigated to increase the energy storage. The incorporation of metals in the cathodes has resulted in the formation of metal chlorides, many of which are known to form intercalation compounds with graphite.[82] Thus for these compounds to be formed the graphite layer structure must be at least partially developed. The current capacity of such electrodes has been investigated in both fused salt and organic electrolytes.[76] Carbon–tungsten composites have been demonstrated with current capacities as high as 8 A-hr/in^3 and energy capacities vs the Li–Al anode of 12 W-hr/in^3[78]. Very fast recharge rates are possible with these cells, for example, 60% efficiency has been demonstrated in a 3-min recharge.[78]

Although the chemistry of this system is much more complex than that of the straight Li–Cl_2 cell, the physical construction is certainly simpler. The total cell consists of a pancake-type layer structure of anode alloy, LiCl–KCl electrolyte in a porous separator, and an electrolyte-filled porous cathode[66,83] (see Fig. 7). Although carbon and graphite are not normally

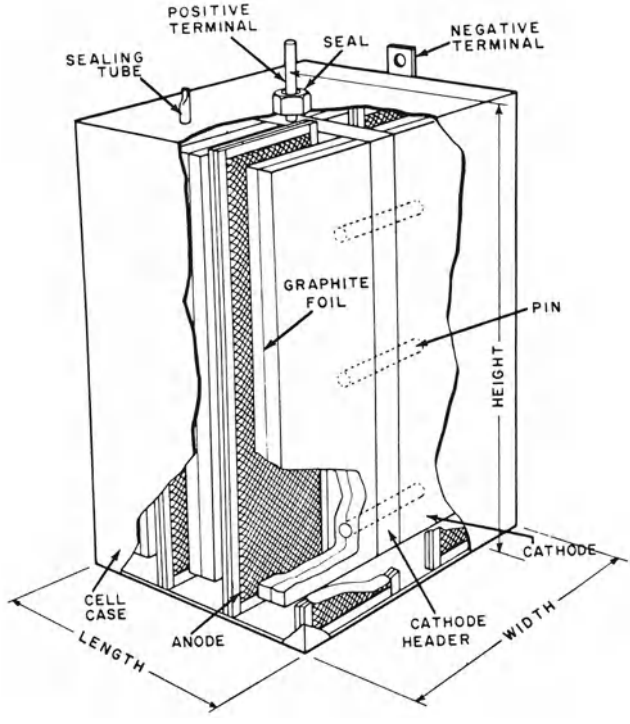

Fig. 7. Sohio design[66,83] for the cell Li(Al)/LiCl–KCl/Cl_2(C).

wetted by many fused halides, additives, surface pretreatment, or potential control can be used to cause wetting.[84] Self-discharge in this cell can be quite low (40 μA/cm^2[78]), but it varies quite a bit from cell to cell. The self-discharge processes seem to be due to impurities introduced into the system with the electrolyte or the activated carbon, which of course is an excellent scavenger for any impurities around. Significant improvements in cell performance were observed when the cathodes were pretreated in large volumes of purified electrolyte and the cells were assembled in a dry box in which O_2, N_2, and H_2O levels were kept below 1 ppm.[83]

3.4. Sodium–Sulfur Cell

The use of sulfur in positive battery electrodes is quite recent, although several advantages can be cited for sulfur. It is readily available and cheap in terms of battery materials. It is a liquid at fused salt temperatures (b.p. 445°C) and hence is readily stored within the battery, and it is less corrosive towards a number of metals than the halogens. The latter is probably due to the formation of protective sulfide films on the metal surface. However, sulfur has one big disadvantage: a potentially high rate of self-discharge due to the formation of polysulfides. Sulfur will react with alkali metals to form compounds of the form Na_2S_x, where x ranges from 1 to 5. Thus it is impossible to use the cell reaction product as the only electrolyte. The Li–S cell using a mixed halide electrolyte has shown good current–voltage behavior (Fig. 3), but little is known regarding its self-discharge rate. The ideal electrolyte for this type of cell has a high conductivity for Li ions and a very low solubility for sulfur and sulfide ions. Very few data are available on the solubility of sulfur and polysulfide ions in low temperature fused salt mixtures that are compatible with alkali metals and sulfur.[48] However, there are solid electrolytes that will conduct alkali ions and will not pass any sulfur species.[85] The most obvious materials are soda glasses, but their resistivities are typically in the range of 100–1000 Ω-cm at 300°C. Thus, to obtain acceptable cell performance very thin, large area electrolyte geometries such as a bundle of thin-walled capillaries must be used. If a minor break occurs anywhere in the solid electrolyte, Na and S will contact and the break may be sealed off by the formation of the high-melting Na_2S (m.p. 950°C). Further self-discharge is then limited by the diffusion through the solid Na_2S.

Another class of solid electrolytes are the porcelains,[86] but again the conductivity below 450°C is generally too low for power-producing purposes.

Cells have been operated at higher temperatures using Li or Na alloyed with Sn to reduce its activity so that attack on the solid electrolyte was minimized.[87] It was not until the discovery of β-Al_2O_3 and its derivatives that a power-producing Na–S cell became a practical possibility. Beta-alumina was known as early as 1935[88,89] and was known to contain some alkali metal ion. Its preparation[89] and its conversion to alpha-alumina by heating[88] were studied, and its chemical formula was tentatively established as $Na_2O \cdot 12Al_2O_3$ or $K_2O \cdot 12Al_2O_3$. Commercial materials based on β-Al_2O_3 have been developed for use in glass manufacture,[90] and its structure and properties have been determined.[91] The currently accepted formula for β-Al_2O_3 is $Na_2O \cdot 11Al_2O_3$, although considerable x-ray and chemical evidence for $Na_2O \cdot 6Al_2O_3$ has been presented.[92] Subsequently, the existence of two distinct but similar phases of compositions nominally $Na_2O \cdot 11Al_2O_3$ and $Na_2O \cdot 5Al_2O_3$ has been demonstrated.[93,94] Their structures are layer structures with the alkali ions situated between layers of Al_2O_3 held apart by Al–O–Al props. The Na^+ ions are quite free to move in these planes but not across from one plane to the next. Hence the conductivity of single crystals across the planes is many orders of magnitude smaller than along the planes. The resistivity along the planes is about 30 Ω-cm at 25°C and about 3.5 Ω-cm at 300°C.[49] The high two dimensional mobility of the Na^+ ions has been demonstrated by diffusion experiments,[91] which also showed that many other monovalent and divalent ions could displace the Na^+ ions by soaking the Na form of β-Al_2O_3 in a suitable fused salt of the ion that was to replace Na. However, the highest self-diffusion coefficient was found for the Na–β-Al_2O_3,[91] and hence it many be inferred that this would also give the highest ionic conductivity. Because of the large difference in conductivity between the different directions in the single crystal, a polycrystalline body of β-Al_2O_3 would be expected to have a significantly lower conductivity than the single crystals. This was indeed observed, but the addition of small amounts of B_2O_3 and Li_2O or MgO[85] to improve conductivity and aid sintering has resulted in a modified material that is impervious and at 300°C still has a resistivity of 3–5 Ω-cm. Using an electrolyte thickness of 0.7 mm, we can obtain a resistance of 0.21 to 0.35 Ω/cm^2. This is comparable with fused salt resistances since thicker electrolyte layers are usually required there. The Na–S cell performance obtained with this type of electrolyte is as follows[49,95]: The OCV is 2.08 V at 300°C from the fully charged condition until the cathode composition reaches Na_2S_5 since up to that point two immiscible phases are present. After that the OCV drops linearly as the cathode composition changes from Na_2S_5 to Na_2S_3, the fully discharged condition of the cell. At 300°C the lower sulfur content

mixtures are solid. The overall cell reaction is therefore

$$2Na(l) + 3S(l) \rightarrow Na_2S_3(l) \tag{46}$$

which has a theoretical energy density of 346 W-hr/lb. The solid electrolyte separator results in a 100% current efficiency for the cell so that only the energy associated with keeping the system hot contributes to the self-discharge. The voltage losses are associated mainly with the sulfur electrode since sulfur is an insulator. Hence a large area porous matrix of carbon or graphite is required to give low effective current density and hence low polarization of the sulfur electrode. Power densities approaching 1 W/cm^2 have been demonstrated, and energy densities of about 60 W/lb have been obtained in laboratory cells. System studies have indicated potential systems of 150 W-hr/lb, which is rather a high fraction of the theoretical energy capacity of the system. However, structural simplicity and low temperature of operation compared to some other systems may well make this possible.

The use of solid ionically conductive membranes of course is not limited to sulfur electrodes. An all solid state electrochemical cell based on β-Al_2O_3 has been proposed.[96] Solid state electrodes containing a redox couple and mobile Na^+ ions and having sufficient electronic conductivity may be used in the following way:

$$\text{Cathode reaction } Fe^{3+} + e^- + Na^+ \rightarrow Fe^{2+} \cdot Na^+ \tag{47}$$

$$\text{Anode reaction } Fe^{2+} \cdot Na^+ \rightarrow Fe^{3+} + e^- + Na^+ \tag{48}$$

$$\text{Net cell reaction } (e^- + Na^+)\,\text{anode} \rightarrow (e^- + Na^+)\,\text{cathode} \tag{49}$$

Thus the cell is basically a concentration cell in Na. Since no phase changes occur at either electrode the cell voltage does not exhibit any kind of plateau and the cell behaves essentially like a capacitor.

In general, β-Al_2O_3 may be considered for any cell that uses Na as one electrode, which can operate in the temperature range 250–450°C and in which the other electrode reactant is compatible with β-Al_2O_3. Systems discussed under the heading of thermal batteries, which suffer from high self-discharge rates, may be suitable as well as the following type of cell:

$$nNa + MX_n \rightarrow nNaX + M \tag{50}$$

where X is the halogen. Since all monovalent metal ions and many divalent ions will exchange with Na in the β-Al_2O_3 with a reduction in conductivity n must be 2 or more likely 3 to meet the compatibility requirement.

A particularly attractive system from the energy capacity point of view would be

$$2Na + \tfrac{1}{2}O_2 + H_2O \rightarrow 2NaOH \quad (51)$$

However, not enough is known about the compatibility of β-Al_2O_3 with NaOH or many other fused salts to determine the practicability of these systems.

4. FUEL CELLS

4.1. Carbonate Fuel Cell

Of the many fuel cells under investigation only one significant molten salt system is being investigated: the molten carbonate system.[97] Its history has been traced back to Gore, who in 1864[98] made a molten Na_2CO_3 based cell. However, it was the work of Ketelaar and Broers in the 1950's that really started the work on carbonate fuel cells.[99,100] Several types of carbonate fuel cell have been studied. These are as follows.

4.1.1. The Free Electrolyte Cell

The molten carbonate is contained between two electrodes that give the structural strength to the system. The electrodes are dual porosity electrodes with the fine pore layer flooded by electrolyte, and the gases are pressurized sufficiently to prevent flooding of the coarse pore layer but not enough to blow gas through the fine pore layer. Although this system has the highest electrolyte conductivity for a given temperature and electrolyte mixture, the sealing problems encountered have resulted in the development of various methods of containing the electrolyte in some form of porous support.

4.1.2. The Matrix Cell

Porous ceramic bodies, mainly of MgO, which have shown good compatibility with carbonate melts, are strongly wetted by molten carbonates and hence will asorb the electrolyte. The matrix filled with electrolyte has enough structural strength to support the electrodes in this case, which may be directly deposited on the electrolyte-filled matrix. This generally gives a much better contact than making a separate electrode structure and clamping the two rigid structures together. The main problem associated

with the matrix-type electrode is the fact that somewhat conflicting requirements are placed on it. To obtain high conductivity a high porosity is desirable, but it is difficult to make very small pores at high porosity levels. The small pores are required to limit the loss of electrolyte by creep. To achieve high porosity as well as small pore size the paste electrolytes have been developed.

4.1.3. Paste Electrolytes

When very fine inert particles are mixed with just enough liquid to fill the voids between the particles a fairly rigid paste similar to clay may be formed.[101] The filler used is typically submicron size MgO powder, and recipes for making suitable electrolytes have been published by several groups. These generally consist of intimately mixing the MgO filler and the carbonate electrolyte (for example, in a ball mill) and then heating the mixture to above the highest temperature it is likely to experience in later service. The mixture is then ground and cold pressed and sintered or for higher density hot pressed at a temperature just below the melting point of the carbonate mixture.[102] In the same step electrodes may be hot pressed onto the paste electrolyte, ensuring intimate contact with the electrolyte. Electrolytes made with 30–65% filler of MgO, ZnO, Al_2O_3, ZrO_2, or ThO_2 have been patented.[103] The paste electrolytes exhibit resistances that are about three times the pure electrolyte resistance. However, in long-life tests, electrolyte is still lost by creep or evaporation. To overcome this a "slurry" electrolyte has been proposed with a reservoir of electrolyte to replace any electrolyte lost.

4.1.4. Slurry Electrolyte

In this system the structural strength is provided by the electrodes and the space between the electrodes is filled with a fine MgO powder. The electrolyte is placed in a reservoir below the cell and is drawn up into the interelectrode space by capillary forces. Excess electrolyte is placed in the reservoir to replace salt lost. Since the electrolyte does not support the electrodes a higher ratio of liquid phase to solid filler can be used than in the "solid" paste electrolyte with corresponding improvements in conductivity. Yet the electrolyte is held sufficiently to avoid electrode flooding problems observed in free electrolyte cells.

Workers on carbonate fuel cells seem to have standardized on two electrolytes, the binary eutectic of Li_2CO_3 and Na_2CO_3 (m.p. 500°C) and

the tertiary eutectic of Li_2CO_3, Na_2CO_3, and K_2CO_3 (m.p. 396°C). The purpose of using the mixed carbonates is of course to lower the minimum temperature of operation, although performance is always better at the higher temperatures. Typical operating temperatures therefore range from 550 to 750°C. Above this range electrolyte losses become significant.

The overall reaction for the fuel cell run, for example, on methane is

$$CH_4 + 2O_2 \rightarrow CO_2 + 2H_2O$$

However, at the cell operating temperature CH_4 and other hydrocarbons are not stable and will deposit carbon in the electrode.

Carbon deposition can be prevented by reducing the carbon potential of the fuel gas by adding H_2O and/or CO_2. The amount of oxygen that must be added can be calculated from thermodynamic data.[104,105] Also, the cell performs much better on a mixture of H_2 and CO than on CH_4, so the hydrocarbons are generally reformed either external to the cell[106] or within the cell by mixing steam with the fuel and passing the mixture over a suitable catalyst. Such a catalyst (typically Ni on MgO) may be deposited right on the anode, and such a double duty anode has several advantages.[102B]

1. The waste heat of the electrode reaction is used directly by the endothermic reforming reaction:

$$CH_4 + H_2O \rightarrow 3H_2 + CO \tag{53}$$

2. The H_2O formed in the electrode reaction can be used in the reforming reaction.
3. A more extensive conversion of CH_4 can be obtained than in an external reformer since the reaction products are continuously removed by the electrode reaction.

As a result the thermal efficiency of a system with internal reforming is predicted to be about 5% higher than for external reforming.[102G] Most of the fuel cell and electrode studies therefore have been done with mixtures of H_2 and CO_2, which at the cell temperature will form an equilibrium mixture of H_2, H_2O, CO, and CO_2 similar to what could be obtained from refined hydrocarbons. Several equilibria exist with the carbonate electrolyte such as

$$CO_3^{2-} \rightleftharpoons CO_2 + O^{2-} \tag{54}$$

$$CO_3^{2-} + H_2O \rightleftharpoons CO_2 + 2OH^- \tag{55}$$

and the combination of (54) and (55) gives

$$O^{2-} + H_2O \rightleftharpoons 2OH^- \tag{56}$$

However, the equilibrium is heavily on the carbonate side in (54) ($K = 10^{-7.5}$[102F]) so that the concentration of O^{2-} is quite low. Therefore, if pure O_2 or air is used as the oxidant, then the only electrode reaction possible is

$$O_2 + 4e^- \rightarrow 2O^{2-}$$

and a large concentration gradient of O^{2-} will occur. The performance of carbonate fuel cells on O_2 or air therefore is very poor; in practice CO_2 is always added to the air so that the ratio CO_2/O_2 is at least equal to 1, and a value of 2.5 has been recommended.[107]

The overall cathode reaction then is

$$2CO_2 + O_2 + 4e^- \rightarrow 2CO_3^{2-} \tag{58}$$

The O_2/CO_2 and CO/CO_2 electrodes on gold have been studied in detail by Borucka.[104,108–110]

Superior cell performance has been claimed for the use of H_2O in place of CO_2.[102F] The overall cell reaction is then

$$2H_2O + O_2 + 4e^- \rightarrow 4OH^- \tag{59}$$

with the formation of alkali hydroxides. However, no data on the life of cells using H_2O in place of CO_2 at the cathode is available. Since the alkali hydroxides are generally more corrosive, a high concentration of these in the electrolyte may not be desirable. However, a mixture of CO_2 and H_2O is probably the only practical additive to the cathode air stream since it may be obtained directly from the anode exhaust gas. Electrode materials for the carbonate cell are selected not for their catalytic properties as in low temperature fuel cells but for their compatibility with the system and low cost. The anode is almost always porous Ni, made either of sintered powder or of sintered fibers. An activation process consisting of partial oxidation of the electrode followed by reduction is sometimes used. However, the effects of this activation disappear after a few days.[102A] In fact, the statement has been made that measurements on carbonate cells during the first few days of operation have little significance since the cell has not yet reached its steady state. Quite large changes in the anode structure have been observed after some 625 hr of operation at 100 mA/cm^2 at 700°C[102B] During this initial period additional sintering of the electrode occurs, with small pores disappearing and consolidating into fewer large pores.

Other anode materials that have been used are porous graphite with a small amount of Pd (0.1 mg/cm^2)[102E] and Ag–Pd alloys.[102A,102F] The latter of course is well known for its high solubility and diffusion of hydrogen and hence may be expected to give better performance than an Ni electrode, but this is at a considerably increased cost.

The anode process may be written

$$H_2 + CO_3^{2-} \rightarrow H_2O + CO_2 + 2e^- \tag{60}$$

$$CO + CO_3^{2-} \rightarrow 2CO_2 + 2e^- \tag{61}$$

with several chemical reactions occurring between the gases and the electrolyte. Although both H_2 and CO can react at the anode, the rate of reaction for H_2 is about ten times faster than for CO.[111] Polarization of the anode is mainly due to the slow diffusion of reaction products H_2O and CO_2 away from the reaction site, and at high current density the diffusion of H_2 to the reaction sites also may become a significant factor. The latter process is much faster in the Pd–Ag electrodes, and this results in the improved performance compared with Ni electrodes.

The cathodes in the carbonate fuel cell are generally porous Ag- or Ag-containing mixtures. At the operating temperatures of 550–750°C, the precious metals (Pt group, Au) and Ag are the only metals not oxidized by air. Some electronically conductive oxides such as copper oxide also have been used, or mixtures of Ag and oxides such as Ag–Cu_2O–ZnO (25–2.5–72.5 wt %) have been studied.[102A] Ag-coated, porous, stainless steel electrodes[102F] have been used to reduce the quantity of Ag required. Ceramics such as Al_2O_3 or ZnO have been used as a support for Ag to reduce sintering of the metal.[112]

The overall anode reaction may be split up into an adsorption and dissociation step on the silver

$$\tfrac{1}{2}O_2 + n\mathrm{Ag} \rightarrow \mathrm{Ag}_n\mathrm{O} \tag{62}$$

followed by fast electron transfer to form O^{2-} which then reacts chemically with CO_2 or H_2O in the cathode gas to form CO_3^{2-} or OH^-, respectively. The magnitude of the various contributions to the overall cell polarization decrease in the order resistance losses > anode polarization > cathode polarization. The resistance losses occur not only in the electrolyte since cell resistances are often two to three times higher than can be accounted for by the bulk resistance of the paste or matrix. It therefore is assumed that there is a significant resistance associated with the electrodes due to mismatching of pores in the electrode and the electrolyte and due to the re-

sistance in the thin film of electrolyte, where an electrochemical reaction occurs. Experiments with solid foils of Pt have shown that the thin film of electrolyte near the region of three-phase contact represents a significant barrier to the diffusion of reactants and products through the electrolyte. This tends to widen the area of electrochemical activity, and hence the resistance losses associated with ion transport along the film can be significant.[113] The various contributions to the cell polarization can be distinguished by current interruption techniques.[114,115] If during steady state operation of the cell the current is suddenly reduced to zero, the cell voltage is immediately reduced by an amount equal to the resistance drop in the cell. By having a third electrode in the system through which no current is passed, a so-called "idling electrode," the total resistance drop can be split into a component associated with each electrode and a portion of the electrolyte that depends on the geometry of the system.

Any activation polarization would be expected to decay away in about 100 μsec following current interruption. Since no decay has been observed in this time scale[114] activation polarization may be considered negligible for at least the fuel–electrode combinations examined. However, it is not surprising that for simple one- or two-electron processes at temperatures of 600°C or higher no significant activation polarization is observed at current densities up to 200 A/ft², since exchange current densities under these conditions are typically 10–100 A/cm².

Any concentration polarization would decay away next as reactants diffuse to the electrode–electrolyte interface to establish equilibrium conditions and as products diffuse away. These processes have been found to be the main source of polarization at both electrodes of the carbonate fuel cell.[116] The detailed treatment of the mass transfer problem in porous electrodes is rather complex. The electrodes in the carbonate system are wetted by the electrolyte so that the pores either will be flooded or will have a film of electrolyte extending into the pore. Clearly when the pore radius becomes equal to the thickness of this film the pore will be flooded. Calculations of the limiting current density based on a flooded pores model have been found to be less than experimentally observed current densities.[117] The thin-film model has given quantitative agreement with experimental anode polarization data when suitable values were assumed for film thickness, effective pore length, and pore radius.[118] The current density of the thin-film model, which was found applicable, is given by

$$I = \frac{nFC^0\beta AD}{\delta(1 + W)} \tag{63}$$

where I is the current density per geometrical square centimeter, C^0 is the initial concentration of H_2 in moles per cubic centimeter, β is the hydrogen solubility equals (moles/cc in the gas phase)/(moles/cc in the liquid phase), A is the area, D is the diffusion coefficient of H in the electrolyte in square centimeters per second, δ is the film thickness, and W is the dimensionless parameter related to D, δ, and a kinetic parameter k.

The above expression only considers the diffusion of reactant H_2 to the reaction sites and hence has only a limited range of applicability. One of the main limitations found in the detailed study of concentration polarization is the lack of data on the solubility of the various gases in the fused salts and their diffusion coefficients. Estimates of these quantities can be made,[118] but experimental data are clearly to be preferred. The solubility of O_2 in carbonates has been determined by titration with Na_2SO_3[119] for the two commonly used electrolytes over the temperature range of 600–800°C. The solubilities for both electrolytes over that temperature range fall between 10^{-7} moles/cm^3 at about 600°C and 10^{-6} moles/cm^3 at 800°C, with slightly higher solubilities being observed in the ternary eutectic (43.5 mole % Li_2CO_3, 31.5 mole % Na_2CO_3, and 25 mole % K_2CO_3, m.p. 397°C). The ternary also was found to have the higher enthalpy of solution of 17.7 kcal/mole vs 14.9 kcal/mole for the binary. Because of the increase in gas solubility with temperature, the increase in diffusion coefficients and the increase in electrolyte conductivity, cell performance increases markedly with temperature. Thus in raising the temperature from 530 to 735°C the current density at 0.5 V could be raised from 40 to 140 mA/cm^2.[118] However, as the temperature is increased heat losses also increase, placing greater demands on heat recovery processes to maintain overall efficiency. Cell life is also reduced because of electrolyte losses and increased silver electrode corrosion.[107]

Cell performance is determined not only by electrode and electrolyte parameters and temperature but also by the fuel and oxidant mixture used. In a battery of cells it is common to feed both the fuel and the oxidant stream sequentially through a number of cells so that the fuel stream becomes progressively poorer in H_2 and richer in CO_2 while the oxidant stream becomes poorer in O_2 and CO_2 and richer in inerts (N_2).[120] Electrically, the cells may be in series or in parallel. In the first instance the same current passes through all cells and hence the voltage contribution becomes less, while in the second case all cells have the same voltage but the current contribution decreases as the cell feed is degraded. Of course it is not practical to extract all the energy potentially available from a fuel, but the optimum level of fuel depletion is determined by the relative costs of fuel

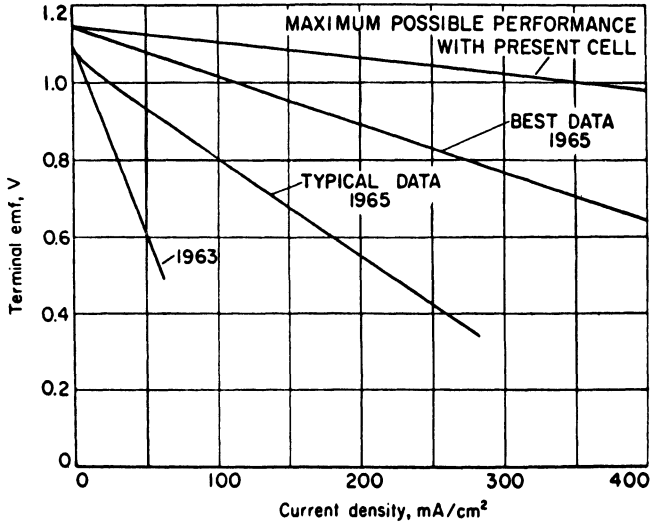

Fig. 8. Performance characteristics of IGT molten carbonate fuel cell.[102] (With permission of Academic Press).

and battery and by what other potential uses there are for the partially spent fuel. Single-cell performance therefore cannot be directly translated into battery performance, and also battery performance may decrease with time. It is not likely that cell performance will be improved much beyond the best performance available in 1965, which was 0.25 W/cm^2,[102G] but if the average cell performance can be brought to approach this level (Fig. 8) and if this can be maintained for a life of several years, the carbonate fuel cell will no doubt find many applications.

4.2. Solid Oxide Fuel Cell

Although this chapter is primarily concerned with molten salt systems, the high temperature solid oxide fuel cell in many ways is similar to the fused salt systems. However, to achieve low cell resistance even higher temperatures are required (typically 1000°C) and very thin electrolyte layers are used (to 0.001 in.).

Because of the very high temperatures involved the heat losses of the system are large unless a large capacity system is used. As a result the main potential application of solid electrolyte fuel cells lies in central power station applications, generating a megawatt or more of electrical power. The heart of these cells, the solid, electrically conductive oxides, date back to Nernst, and one of the most useful materials (15 wt % Y_2O_3, and 85

wt % ZrO_2) bears his name.[121] A student of Nernst in 1902 studied an electrolyte consisting of 90% ZrO_2 and 10% MgO[122] that was one of several solid electrolytes studied in fuel cells by Baur and Preis in 1937.[123]

Kiukkola and Wagner in 1957 showed that the conductivity in these materials was due entirely to oxide ion mobility under most conditions.[124] However, no major development occurred in this area until about 10 years ago when General Electric Co.[125,126] and Westinghouse Corp.[127–129] started devoting significant efforts to the development of these materials in high temperature fuel cells. The early cells consisted of tubes or disks of the solid oxide electrolyte with electrodes applied to opposite sides and exposed to air or oxygen on one side and H_2 or H_2/CO mixtures on the fuel side. In a practical system mixtures of H_2 and CO derived from coal gasification or hydrocarbon reforming would be used.

The electrodes in the early cells generally were made of platinum, and although as recently as 1968[130] Pt has been seriously considered as an electrode material, it is not economic in a large-scale industrial plant. However, several other metals can be used on the fuel side, while electronically conductive oxides or mixtures of oxides have been used on the air side.[131] This, together with modern techniques of thin-film deposition, has resulted in large improvements in the performance and the cost of these cells, and publicly owned central power stations producing 345 kV ac at a bus bar cost of 2.21 mills/kW-hr (that is, U.S. $0.00221/kW-hr) have been predicted.[21]

The basic electrolyte material is zirconia, to which about 10–15 mole % of an aliovalent oxide such as CaO, MgO, Y_2O_3, Sc_2O_3, or rare earth oxide is added to achieve suitable conductivity and thermal stability. The substitution of these lower valency cations for Zr^{4+} creates a corresponding number of O^{2-} vacancies, thus allowing the movement of the oxide ions. The value of the oxide ion conductivity obtained depends on both the amount of the stabilizer added and its cation size.[132–134] There is considerable disagreement in the literature regarding the exact magnitude of the conductivity, but the most representative data are shown in Fig. 9. The lowest resistivity is shown by Sc_2O_3-stabilized ZrO_2, but to date this has not been used in fuel cells because of the cost of Sc_2O_3 (about $500 per pound). However, with the development of thinner electrolyte layers the cost becomes less significant. Y_2O_3-stabilized ZrO_2 represents a good compromise between cost and performance and is used in most work. If with thin-film techniques it is possible to make impervious electrolyte layers 0.01 cm thick, an electrolyte resistance of 0.1 Ω/cm^2 should be possible. At a current density of 1 A/cm^2 this results in a resistance drop of 0.1 V. Since the open-

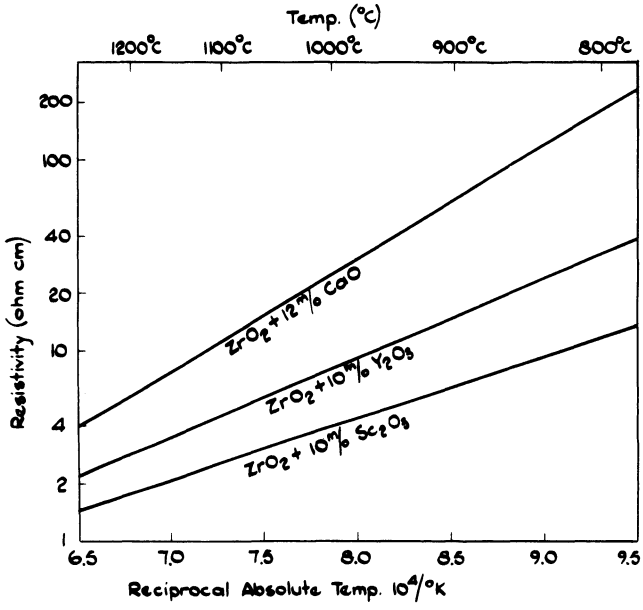

Fig. 9. Resistivities of some solid oxide electrolytes.

circuit voltage at 1000°C is typically 1 V and allowing 0.15 V for electrode losses, a power density of 0.75 W/cm² should be possible.

The electrode reactions in the solid oxide fuel cell are particularly simple, and because of the high temperature low polarization can be achieved.

At the air electrode we have

$$O_2 + 4e^- \rightarrow 2O^{2-} \tag{64}$$

while at the fuel electrode we have

$$H_2 + O^{2-} \rightarrow H_2O + 2e^- \tag{65}$$

$$CO + O^{2-} \rightarrow CO_2 + 2e^- \tag{66}$$

At the fuel side the electrode can be made of any of a number of high melting point metals. Since this electrode is always in a reducing atmosphere, oxide formation is not a problem, and the main limitation to electrode life becomes the evaporation of the metal. Metals that have been found to be suitable are iron, nickel, and cobalt,[135] with cobalt in particular[125] costing less than 0.1% as much as Pt for the same conductivity. Since the thermal expansion coefficient of Co is about 50% greater than that of the

electrolyte it is mixed with electrolyte before being applied to the impervious electrolyte, resulting in a porous electrode with good adhesion to the substrate.

The selection of an alternate material to Pt on the air side is more difficult. The only metals not oxidized are the Pt group metals and gold and silver. Although silver is much cheaper and makes an excellent oxygen electrode due to the high solubility of oxygen in the metal,[125] it is eliminated because of its high vapor pressure. Hence metals are generally excluded as cheap air electrode materials. However, there are a number of simple oxides and mixed oxides that are excellent electronic conductors at cell temperatures. Materials that have been used are tin-doped indium oxide[136] and the perovskite-type material $PrCoO_3$.[131,137] Again, mixing with electrolyte is required to anchor the electrode firmly to the electrolyte.

The requirements for electronically conductive oxide electrodes in magnetohydrodynamic power generation are similar, and if anything are more demanding than in the solid oxide fuel cell. Therefore, materials developed for this application also may be suitable for use in the fuel cell.[138]

There is no doubt that further development is required to improve electrode structures and methods of manufacture, but it is also clear that the cost of Pt is no longer a limiting factor in the development of economically competitive solid electrolyte fuel cells.

The cell performance that may be obtained depends mainly on the electrode and electrolyte resistance. Typical cell performances are shown in Fig. 10. An early cell[127] that consisted of an 0.5-mm thick disk of electrolyte with Pt electrodes had a resistance of about $4\Omega/cm^2$. Maximum power output was about 0.08 W/cm^2. Early cell performance is typified by curve 1 in Fig. 10. More recent cells consisting of batteries of 10–20 cylindrical cells placed electrically in series have shown performances two to four times better, as shown by curves 2 and 3 in Fig. 10.[128] The life of these systems also has increased significantly. One cell consisting of a porous Ni anode, a Y_2O_3–ZrO_2 electrolyte, and a $PrCoO_3$ cathode delivered 0.5 W/cm^2 initially and after 316 days of operation at 1100°C still delivered 0.47 W/cm^2.[137]

Reasonable extrapolations of present cell performance to a "thin-film cell" (curve 4, Fig. 10) have been made, and system studies based on this cell are very promising indeed.[21] In the thin-film cell it is proposed to start with a porous alumina or CaO-stabilized zirconia tube. Techniques such as flame or plasma spraying, chemical vapor deposition, and sputtering then are used to successively deposit the cathode, the electrolyte, and the anode

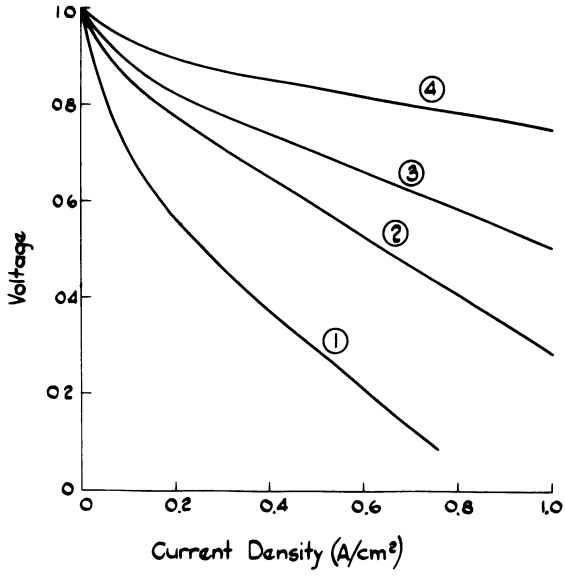

Fig. 10. Solid electrolyte fuel cell performance. 1: Early cells. 2,3: Range of current technology demonstrated for 100 hr. 4: Extrapolated "thin-film cell" performance.

with suitable masking between each step so as to finish with up to 100 cells in series in one set of operations. Such a tube is expected to deliver 1.76 A at 80 V or 140 W when fed with gasified coal.[21]

Two detailed studies have been made of the economics of dc power generation using solid electrolyte fuel cells. One of these only considered the use of Pt electrodes and Au–Pt alloy intercell connectors.[130] Even with such an unreasonable assumption the cost of fuel cell electricity to the customer was calculated to be 9–11 mills/kW-hr, depending on the location in the United States. The variation in cost is due to the variation of the cost of transmission and distribution of natural gas. This cost may be compared to an average cost of 9 mills/kW-hr paid by the electrolytic industries in the United States in 1967.[139] Since electrode materials costing less than 1% of the cost of Pt have been demonstrated for a cell life approaching 1 year it seems unreasonable not to consider these cheaper electrode materials.

A detailed review and evaluation of the Westinghouse work on solid oxide fuel cells has been made by the Jackson and Moreland Division of United Engineers and Constructors, Inc.[21] Since the Westinghouse work in recent years has been sponsored by the Office of Coal Research the work

is aimed at using coal as the raw material and converting it to a useful gaseous fuel consisting mainly of H_2 and CO. However, the fuel cell of course would work equally well on reformed natural gas.

This could significantly reduce the capital cost of the power plant while the operating cost would depend largely on the location with respect to natural gas sources. The final cost of the power produced is a function not only of capital and fuel costs but also of the method of financing and the load variations that must be absorbed. The ideal application of a fuel cell power plant would appear to be in the electrometallurgical industries such as Al or Mg production that require a large constant source of dc power.

5. OTHER SYSTEMS

There are a number of high-temperature battery and fuel cell studies that do not conveniently fit into any of the previous groups discussed or do not yet look sufficiently promising to justify major development work.

Some thermally regenerative systems were discussed under the heading of concentration cells, but the lithium hydride cell does not conveniently fit into this latter classification. The lithium hydride cell is unusual in that hydrogen, which is generally thought of as an anodic reactant, is in this case the cathodic reactant. The system consists of an Li electrode, a Li-halide electrolyte in which the LiH reaction product is dissolved, and an H_2 electrode that can consist of a thin metal foil through which hydrogen diffuses at a sufficient rate to support the desired current density. Operating temperature depends on the electrolyte chosen but falls typically in the range of 350–550°C. The cell voltage is determined by the temperature and the concentration of LiH in the electrolyte and is of the order of 0.5 V. The voltage decreases as the temperature increases and becomes zero at 900–1000°C. At this temperature the LiH therefore thermally breaks down into $Li + H_2$, thus regenerating the reactants.[140] The electrochemistry of the H_2/LiH electrode has been studied in some detail in LiCl–KCl eutectic electrolyte at 375°C by voltammetric and chronopotentiometric methods.[141] An exchange current density of about 1 mA/cm^2 was found for the H_2/hydride electrode, which is low for a fused salt system at this temperature. The diffusion coefficient of LiH in this system was determined as $1.67 \pm 0.04 \times 10^{-5}$ cm^2 sec^{-1} by chronopotentiometric measurements. Although there was much early interest in this system (see references given in Plambeck *et al.*[141]) for converting heat from nuclear sources to electrical

energy, this interest seems to have largely lapsed due to the low performance of this system.

Several other systems have been studied in LiCl–KCl eutectic electrolyte. The Li–Cl_2 cell and several thermal battery systems were mentioned previously. Fuel cells using this electrolyte have been proposed using Cl_2 as the cathodic reactant with H_2[142] or hydrocarbons[143] at the anode. The electrolyte acts as a Cl^- conductor, and the reaction products formed at the anode are HCl and chlorinated hydrocarbons such as CH_3Cl, CH_2Cl_2, $CHCl_3$, and CCl_4. The relative amounts depend on current density. Current efficiencies for the reaction

$$CH_4 + Cl_2 \rightarrow CH_3Cl + HCl$$

were found to be 20, 91, 79.5, and 59.8% at 4, 10, 20, and 50 mA/cm^2, respectively. Performance of these cells as energy converters has been low, but this is not necessarily their primary purpose. If it is desired to use by-product Cl_2 to make HCl or chlorinated hydrocarbons, then this can be done by reacting the necessary materials directly, in which case the heat of reaction is generally wasted. However, by doing this in a fuel cell, some of the free energy liberated in the reaction may be recovered as useful electric power. Aqueous HCl solution of course can be used also as an electrolyte, and 0.5 V at 0.1 A/cm^2 has been demonstrated in such a system,[144] but if anhydrous HCl is the desired reaction product, then a fused salt system would be more useful.

Chlorine has been coupled with other metals besides Li to make energy storage or energy conversion systems. A high-temperature energy conversion scheme based on the Na–Cl_2 cell has been suggested.[145] Two Na–Cl_2 cells are operated at different temperatures. The cell at the lower temperature (810–900°C) has a higher emf, and hence it electrolyzes NaCl in the high-temperature cell (900–1400°C) and has power to spare to supply useful energy. The Na and Cl_2 vapors produced in the high-temperature cell are transported to the low-temperature cell to supply the reactants for the low-temperature cell. The system has a low efficiency because of heat losses and electronic conductivity due to dissolved Na in the electrolyte at these high temperatures.

Magnesium and chlorine have been combined using a KCl–NaCl–$MgCl_2$ electrolyte with a melting point of 430°C.[146] Open-circuit voltage at 480°C was 2.65 V, and the cell performance was studied as a function of Cl_2 pressure at the porous carbon electrode. Power densities of 1.15–2.1 W/cm^2 were obtained. However, energy densities of such a system using a

mixed electrolyte cannot be very high. The system should be rechargeable, but no data are given on recharge characteristics.

Magnesium cells with a carbon–MnO_2 cathode have been studied using a variety of low-melting fused salts such as nitrates and hydroxides.[147] Best performance was obtained using NaOH. These cells are basically thermal batteries and are not rechargeable.

The electrochemistry of other low-melting fused salts has been studied, for example, KNO_3–$NaNO_3$ eutectic at 250°C[148–150] and KSCN–NaSCN in the temperature range of 150–325°C.[151] Thermal batteries using the latter electrolyte were demonstrated at temperatures from 150 to 250°C, using Li-alloy anodes and a variety of oxides and organic nitrocompounds as cathodes.

A number of batteries with solid electrolytes have been studied. The advantage of simplicity and ruggedness of these batteries is generally reduced by the need to make the solid electrolyte very thin to reduce its resistance to a useful level. The zirconia-based solid electrolytes used in the fuel cells can be used to make a variety of metal–air or metal–metal oxide cells. Anode materials that have been investigated vs a Pt/air cathode include Fe, Ni, Mn, Co, Cr, Mo, Zr, Y, and a Zr-Y mixture.[152] The first four of these were reasonably successful in that discharge times of a few minutes were demonstrated. To have a life longer than a few minutes the metal oxide reaction product formed in each case must not interfere with the progress of the reaction, that is, the oxide must possess a high mobility of either the metal or oxygen so that equilibrium can be maintained across the oxide layer.

Various glasses and porcelains have been used with alkali metals or metals or alloys containing alkali metals as anodes and Cl_2 or Ni–$NiCl_2$ cathodes.[87] In this case the solid electrolytes have mobile alkali metal ions and the overall cell reduction is, for example,

$$2Li(Sn) + NiCl_2 \rightarrow Ni + 2LiCl \qquad (67)$$

Alloying of the Li is necessary to reduce its activity sufficiently to make it compatible with the lithium aluminosilicate solid electrolyte. Cells using Fe and Al alloy anodes, an Li-conductive porcelain enamel, and a silver cathode also have been demonstrated[153] and were shown to be rechargeable. The temperature of operation of the solid electrolytes mentioned above is in the range of 600–1000°C, the temperature required to obtain sufficient ionic conductance in these materials to allow current to be drawn from the cells.

Sufficient conductivity is available at lower temperatures in beta-

alumina, and an all-solid cell based on this electrolyte has been described.[96] However, this electrolyte does not yet seem to have been fully exploited since it makes possible the combination of Na with many cathode materials at reasonable temperatures.

Finally, in the area of solid electrolytes there are the silver conductive electrolytes, many of which show excellent conductivity down to room temperature.[11,154,155] However, these low-temperature systems are outside the scope of this chapter.[156]

REFERENCES

1. R. Jasinski, *High-Energy Batteries*, Plenum Press, New York (1967).
2. D. Collins, ed., *Batteries*, Macmillan, New York (1963).
3. G. J. Janz, *Molten Salts Handbook*, Academic Press, New York (1967).
4. J. Lumsden, *Thermodynamics of Molten-Salt Mixtures*, Academic Press, New York (1966).
5. M. Blander, ed., *Molten Salt Chemistry*, John Wiley (Interscience), New York (1964).
6. B. R. Sundheim, ed., *Fused Salts*, McGraw-Hill, New York, (1964).
7. G. Mamantov, *Molten Salts: Characterization and Analysis*, Marcel Dekker, New York (1969).
8. T. B. Reddy, *Electrochem. Techn.* **1**:325–351 (1963).
9. D. Inman and S. H. White, *Annual Report on the Progress of Chemistry for 1965*, pp. 106–130, Chemical Society of London (1966).
10. C. Dijkhuis, R. Dijkhuis, and G. J. Janz, *Chem. Rev.* **68**:253–275 (1968).
11. J. N. Bradley and P. D. Greene, *Trans. Faraday Soc.* **63**:2516–2521 (1967).
12. W. J. Hamer, M. S. Malmberg, and B. Rubin, *J. Electrochem. Soc.* **103**:8–16 (1956).
13. W. J. Hamer, M. S. Malmberg, and B. Rubin, *J. Electrochem. Soc.* **112**:750–755 (1965).
14. H. C. Gaur and H. L. Jindal, *Electrochim. Acta* **13**:835–842 (1968).
15. H. A. Laitinen and C. H. Liu, *J. Amer. Chem. Soc.* **80**:1015–1020 (1958).
16. J. A. Plambeck, *J. Chem. Eng. Data* **12**:77–82 (1967).
17. J. O'M. Bockris and S. Srinivasan, *J. Electroanal. Chem.* **2**:350–389 (1966).
18. J. O'M. Bockris and A. K. N. Reddy, *Modern Electrochemistry*, Plenum Press, New York (1970).
19. S. Srinivasan, H. D. Hurwitz, and J. O'M. Bockris, *J. Chem. Phys.* **46**:3408–3422 (1967).
20. J. Verstraete, D. Lefevre, R. Lefort, and J. Henry, *Handbook of Fuel Cell Technology*, C. Berger (ed.), Prentice-Hall, Englewood Cliffs, New Jersey (1968).
21. H. F. White, *Review and Evaluation of Project Fuel Cell*, O.C.R. Rep. 17, Contract 14-01-001-500 (1966).
22. T. Takahashi, K. Ito, and H. Swahara, *Electrochim. Acta* **12**:21–30 (1967).
23. H. Schmalzried, *Z. Elektrochem.* **66**:572–576 (1962).
24. H. Schmalzried, *Z. Phys. Chem. N. F.* **38**:87–102 (1963).

25. J. W. Patterson, E. C. Bogren, and R. A. Rapp, *J. Electrochem. Soc.* **114**:752–758 (1967).
26. J. C. Hesson, M. S. Foster, and H. Shimotake, *J. Electrochem. Soc.* **115**:787–790 (1968).
27. A. K. Fisher, in: *Regenerative EMF Cells*, Advances in Chemistry Series 64, pp. 121–135, American Chemical Society, Washington, D. C. (1967).
28. E. J. Cairns, C. E. Crouthamel, A. K. Fisher, M. S. Foster, J. C. Hesson, C. E. Johnson, H. Shimotake, and A. D. Tevebaugh, *Galvanic Cells with Fused Salt Electrolytes*, Argonne National Laboratory, Rep. ANL-7316 (1968).
29. H. A. Liebhafsky, in: *Regenerative EMF Cells*, Advances in Chemistry Series 64, 1–10, American Chemical Society, Washington, D. C. (1967).
30. M. S. Foster, in: *Regenerative EMF Cells* Advances in Chemistry Series 64, pp. 136–147, American Chemical Society, Washington, D. C. (1967).
31. H. Shimotake, G. L. Rogers, and E. J. Cairns, Presented at ECS Meeting, Chicago, October 15–19, 1967.
32. D. A. J. Swinkels, *J. Electrochem. Soc.* **113**:6–10 (1966).
33. H. Shimotake and J. C. Hesson, *J. Electrochem. Soc. Jap.* **36**:118–122 (1968).
34. A. K. Fisher, S. A. Johnson, and S. E. Wood, *J. Phys. Chem.*, **71**:1465–1472 (1967).
35. H. Shimotake and E. J. Cairns, in: *Advances in Energy Conversion Engineering*, pp. 951–962, ASME (1967). Presented at 1967 Intersociety Energy Conversion Engineering Conference, August 1967, Miami Beach, Florida.
36. B. Agruss, *J. Electrochem. Soc.* **110**:1097–1103 (1963).
37. R. D. Weaver, S. W. Smith, and N. L. Willmann, *J. Electrochem. Soc.* **109**:653 (1962).
38. H. Shimotake and E. J. Cairns, Presented at the 1968 Intersociety Energy Conversion Engineering Conference, August 13–17, 1968, Boulder, Colorado.
39. L. A. Heredy, M. L. Inerson, G. D. Ulrich, and H. L. Recht, in: *Regenerative EMF Cells*, Advances in Chemistry Series 64, American Chemical Society, Washington, D. C. (1967).
40. I. J. Groce and R. D. Oldenkamp, in: *Regenerative EMF Cells*, Advances in Chemistry Series 64, American Chemical Society, Washington, D. C. (1967).
41. R. D. Oldenkamp, L. A. Heredy, and H. L. Recht, in: *Proceedings of the 1st Intersociety Energy Conversion Engineering Conferences*, American Institute of Aeronautics and Astronautics, New York (1966).
42. B. Agruss and H. R. Karas, in: *Regenerative EMF Cells*, Advances in Chemistry Series 64, pp. 62–81, American Chemical Society, Washington, D. C. (1967).
43. E. J. Cairns and H. Shimotake, *Science* **164**:1347–1355 (1969).
44. H. Shimotake and E. J. Cairns, Presented at the 4th Advances in Battery Technology Symposium, December 1968, Los Angeles.
45. H. Shimotake, G. L. Rogers, and E. J. Cairns, *Ind. Eng. Chem., Process Design Develop.* **18**:51–56 (1969).
46. H. Shimotake, and E. J. Cairns, Presented at the CITCE Meeting, September 1968, Detroit.
47. M. S. Foster, C. E. Crouthamel, D. M. Gruen, and R. L. McBeth, *J. Phys. Chem.* **68**:980–981 (1964).
48. F. G. Bodewig and J. A. Plambeck, *J. Electrochem. Soc.* **116**:607–611 (1969).
49. N. Weber and J. T. Kummer, *Proc. 21st Ann. Power Sources Conf.* 37–39 (1967).
50. H. Goldsmith and J. T. Smith, *Electrochem. Techn.* **6**:16–19 (1968).

51. S. M. Selis and L. P. McGinnis, *J. Electrochem. Soc.* **108**:191–195 (1961).
52. L. H. Thaller, *J. Electrochem. Soc.* **113**:309–312 (1966).
53. S. M. Selis, L. P. McGinnis, E. S. McKee, and J. T. Smith, *J. Electrochem. Soc.* **110**:469–476 (1963).
54. G. F. Zellhoefer, U. S. Patent 3, 311, 503; C. A. 66:101108j.
55. R. B. Goodrich and R. C. Evans, *J. Electrochem. Soc.* **99**:207C–208C (1952).
56. S. M. Selis, J. P. Wondowski, and R. F. Justus, *J. Electrochem. Soc.* **111**:6–13 (1964).
57. S. Senderoff and E. M. Klopp, U. S. Patent 3, 361, 596; C. A. 68:74641k.
58. H. A. Laitinen and D. R. Rhodes, *J. Electrochem. Soc.* **109**:413–419 (1962).
59. H. A. Laitinen and R. D. Bankert, *Anal. Chem.* **39**:1790–1795 (1967).
60. S. M. Selis and L. P. McGinnis, *J. Electrochem. Soc.* **106**:900 (1959).
61. J. H. Propp and H. A. Laitinen, *Anal. Chem.* **41**:644–649 (1969).
62. L. H. Thaller, *J. Electrochem. Soc.* **115**:116–122 (1968).
63. E. H. Hietbrink, J. J. Petraits, and G. M. Craig in: *Advances in Energy Conversion Engineering*, pp. 933–941, ASME (1967).
64. G. T. Motock, *Electrochem. Techn.* **1**:122–127 (1963).
65. R. G. Anthony, B. J. Welch, and R. J. Steele, *Aust. J. Chem.* **21**:789–792 (1968).
66. R. A. Rightmire, J. W. Sprague, W. N. Sorensen, T. H. Hacha, and J. E. Metcalfe, Paper presented at the International Automotive Engineering Congress, 1969, Detroit.
67. R. N. Snyder and J. J. Lander, *Electrochem. Techn.* **4**:179–181 (1966).
68. *JANAF Thermochemical Tables*, CFSTI, Springfield, Va.
69. D. A. J. Swinkels and S. B. Tricklebank, *Electrochem. Techn.* **5**:327–331 (1967).
70. D. A. J. Swinkels, J. *Electrochem. Soc.* **114**:812–816 (1967).
71. D. A. J. Swinkels and R. N. Seefurth, *J. Electrochem. Soc.* **115**:994–999(1968).
72. D. A. J. Swinkels, *Electrochem. Techn.* **5**:396–399 (1967).
73. R. A. Rightmire and A. L. Jones, *Proc. 21st Ann. Power Sources Conf.* 42–45 (1967).
74. M. Hansen, *Constitution of Binary Alloys*, McGraw-Hill, New York (1958).
75. L. P. Costas and R. P. Marshall, *Trans. Met. Soc. AIME* **224**:970–974 (1962).
76. E. S. Buzzelli. Presented at the ECS Meeting, October 11, 1968, Montreal, Quebec.
77. J. Werth and E. J. Zeitner, *Advances in Energy Conversion Engineering*, pp. 927–932, ASME (1967).
78. E. S. Buzzelli. Paper presented at the Southern California–Nevada Section of the ECS, December 1967.
79. R. A. Rightmire, *Development of Electrochemical Energy Storage Unit for Vehicle Propulsion*, USAERDC Contract DA-44-009-AMC-1843T, Final Rep. 1967.
80. S. M. Selis, paper presented at the ECS Meeting, February, 1970, Los Angeles, California.
81. J. W. Sprague, D. L. Boos, D. L. Beals, R. L. Rowland, and R. A. Rightmire. Paper Presented at the ECS Meeting, October 1966, Philadelphia.
82. R. C. Croft, *Aust. J. Chem.* **9**:184–200 (1956).
83. J. W. Sprague, *Development of Electrochemical Energy Storage Unit for Vehicle Propulsion*, USA ERDC Contract DA-44-009-AMC-1531(T), Final Report 1968.
84. J. L. Benak and T.B. Selover, Presented at the 8th Biennial Conference on Carbon, June 1967, Buffalo, New York.
85. J. T. Kummer, and M. E. Milberg, *Chem. Eng. News* **47**:90–99 (May 1969). See also U. S. Patents 3,404,036 and 3,413,150.

86. R. J. Labrie and V. A. Lamb, *J. Electrochem. Soc.* **106**:895–899 (1959).
87. D. C. Hamby, B. W. Steller and J. B. Chase, *J. Electrochem. Soc.* **111**:998–1002 (1964).
88. J. Gallup, *J. Amer. Ceram. Soc.* **18**:144–148 (1935).
89. R. R. Ridgway, A. A. Klein, and W. J. O'Leary, *Trans. Electrochem. Soc.* **70**:71–88 (1936).
90. K. H. Sandmeyer and W. A. Miller, *Ceram. Bull.* **44**:541–544 (1965).
91. Y. Y. Yung-Fang, and J. T. Kummer, *J. Inorg. Nucl. Chem.* **29**:2453–2475 (1967).
92. R. Von Scholder and M. Mansmann, *Z. Anorg. Allg. Chem.* **321**:246–261 (1963).
93. M. Bettman and C. R. Peters, *J. Phys. Chem.* **73**:1774–1780 (1969).
94. R. C. De Vries and W. L. Roth, *J. Amer. Ceram. Soc.* **52**:364–369 (1969).
95. N. Weber and J. T. Kummer, in: *Advances in Energy Conversion Engineering*, pp. 913–916, ASME (1967).
96. K. O. Hever, *J. Electrochem. Soc.* **115**:830–836 (1968).
97. C. G. Peattie, *IEEE Spectrum* 69–76 (June 1966).
98. J. Gore, *Phil. Mag.* **27**(4):641 (1964).
99. M. L. Kronenberg, *J. Electrochem. Soc. Jap.* **33**:203–213 (1965).
100. G. H. J. Broers and M. Schenke, *Rev. Energ. Primaire* **1**:54–62 (1965).
101. G. H. J. Broers, M. Schenke, and G. G. Piepers, *Advan. Energy Convers.* **4**:131–147 (1964).
102. *Hydrocarbon Fuel Cell Technology* (B. S. Baker (ed.), Academic Press, New York (1965): (A) A. D. S. Tantram, A. C. C. Tseung, and B. S. Harris, pp. 187–212; (B) R. W. Hardy, W. E. Chase, and J. McCallum, pp. 213–224; (C) G. H. J. Broers and M. Schenke, pp. 225–250; (D) I. Trachtenberg, pp. 251–266; (E) A. Salvadori, pp. 267–284; (F) J. Millet and R. Buvet, pp. 285–292; and (G) B. S. Baker, L. G. Marianowski, J. Zinner, and G. Price, pp. 293–307.
103. B. S. Harris and A. D. S. Tantram, U. S. Patent 3,351,491; C. A. 68:353272.
104. A. Borucka, *Electrochim. Acta* **13**:295–297 (1968).
105. E. J. Cairns, A. D. Tevebaugh, and G. J. Holm, *J. Electrochem. Soc.* **110**:1025–1030 (1963).
106. J. Meek and B. S. Baker, in: *Fuel Cell Systems*, Advances in Chemistry Series 47, pp. 221–231, American Chemical Society, Washington, D. C. (1965).
107. I. Trachtenberg and D. F. Cole. Paper Presented at the ACS Symposium on Fuel Cells, September 1967, Chicago.
108. A. Borucka, in *Fuel Cell Systems II, Advances in Chemistry No. 90*, American Chemical Society, Washington, D.C. (1969), p. 242–268.
109. A. Borucka and C. M. Sugiyama, to be published in *Electrochim. Acta.*
110. A. Borucka and C. M. Sugiyama, *Electrochim. Acta* **13**:1887–1897 (1968).
111. A. N. Webb, W. B. Mather, Jr., and R. M. Suggitt, *J. Electrochem. Soc.* **112**:1059–1063 (1965).
112. A. C. C. Tseung and A. D. S. Tantram, *Sci. Ceram.* **4**:367–379 (1967).
113. J. T. Cobb, Jr., and L. F. Albright, *J. Electrochem. Soc.* **115**:2–6 (1968).
114. I. Trachtenberg, in: *Fuel Cell Systems*, Advances in Chemistry Series 47, pp. 232–246, American Chemical Society, Washington, D. C. (1965).
115. L. Reid, D. F. Cole, and I. Trachtenberg, *J. Electrochem. Soc.* **113**:954 (1966).
116. I. Trachtenberg, *J. Electrochem. Soc.* **111**:110–113 (1964).
117. D. T. Wasan, T. Schmidt, and B. S. Baker, *Chem. Eng. Progr. Symp. Ser.* **63**:16–25 (1967).

118. E. S. Argano, T. Schmidt, and D. T. Wasan, *Chem. Eng. Progr. Symp. Ser.* **63**:26–31 (1967).
119. M. Schenke, G. H. J. Broers, and J. A. A. Ketelaar, *J. Electrochem. Soc.* **113**:404 (1966).
120. F. L. Gray, *Proc. 21st Ann. Power Sources Conf.* 29–32 (1967).
121. W. Nernst, *Z. Elektrochem.* **6**:41 (1900).
122. H. Reynolds, dissertation, University of Güttingen (1902).
123. E. Baur and H. Preis, *Z. Elektrochem.* **43**:727–732 (1937).
124. K. Kiukkola and C. Wagner, *J. Electrochem. Soc.* **104**:379–387 (1957).
125. D. W. White, *Rev. Energ. Primaire* **2**:10–18 (1966).
126. D. W. White, *Progress in High-Temperature, Zirconia–Electrolyte Cell Technology at General Electric*, G. E. Rep. 68-C-254 (1968).
127. D. H. Archer, J. J. Alles, W. A. English, L. Elikan, E. F. Sverdrup, and R. L. Zahradnik, in: *Fuell Cell Systems*, Advances in Chemistry Series 47, 332–342, American Chemical Society, Washington, D. C. (1965).
128. E. F. Sverdrup and D. H. Archer. *Proceedings of the 3rd Annual Conference on Energy Conversion and Storage*, pp. 1-1 to 1-6 (1965).
129. D. H. Archer, L. Elikan, and R. L. Zahradnik, in: *Hydrocarbon Fuel Cell Technology* (B. S. Baker, ed.), pp. 51–78, Academic Press, New York (1965).
130. R. H. Boll and R. K. Bhada, *Energy Convers.* **8**:3–18 (1968).
131. C. S. Tedmon, Jr., H. S. Spacil, and S. P. Mitoff, *J. Electrochem. Soc.* **116**:1170–1175 (1969).
132. D. W. Strickler and W. G. Carlson, *J. Amer. Ceram. Soc.* **48**:286–289 (1965).
133. D. W. Strickler and W. G. Carlson, *J. Amer. Ceram. Soc.* **47**:122 (1964).
134. T. Y. Tien, *J. Amer. Ceram. Soc.* **47**:430 (1964).
135. O. Antonsen, W. Baukal, and W. Fischer, *Brown Boveri Rev.* **53**:21–30 (1966).
136. E. F. Sverdrup, D. H. Archer, and A. D. Glasser, in *Fuel Cell Systems II, Advances in Chemistry No. 90*, American Chemical Society, Washington, D.C. (1969), p. 301–314.
137. C. S. Tedmon, Jr., S. P. Mitoff, and H. S. Spacil, "Materials Limitations and Performance of High-Temperature Zirconia Electrolyte Fuel Cells. I. Cathodes and Cathode Leads," Paper Presented at the Fall 1968 Meeting of the Electrochemical Society.
138. D. B. Meadowcroft, *Energy Convers.* **8**:185–190 (1968).
139. J. H. Sullivan and R. R. Dukes, *Electrochem. Techn.* **6**:365–370 (1968).
140. C. E. Johnson and R. E. Heinrich, in: *Regenerative EMF Cells*, Advances in Chemistry Series 64, pp. 105–120, American Chemical Society, Washington, D. C. (1967).
141. J. A. Plambeck, J. P. Elder, and H. A. Laitinen, *J. Electrochem. Soc.* **113**:931–937 (1966).
142. S. Yoshizawa and Z. Takehara, *Asahi Garasu Kogyo Gijutsu Shorei kai Kenkyu Hokoku* **12**:39–55 (1966); C. A. 68:55856t.
143. S. Yoshizawa, Z. Takehara, Y. Ito, and Y. Koyama, *Denki Kagaku* **35**:784–788 (1967).
144. C. Bianchi, *Rev. Energ. Primaire* **1**:60–63 (1965).
145. J. J. Lander, S. W. Smith, and R. D. Weaver, U. S. Patent 3,370,983.
146. P. Drossbach and H. Hoff, in: *Performance Forecast Selections of Static Energy Conversion Devices*, (G. W. Sherman, ed.), pp. 741–762, Air Force Aero Propulsion Laboratory, Dayton, Ohio (1968).

147. W. J. Hamer and J. P. Schrodt, *J. Amer. Chem. Soc.* **71**:2347–2352 (1949).
148. H. S. Swofford and H. A. Laitinen, *J. Electrochem. Soc.* **110**:814–820 (1963).
149. P. G. Zambonin and J. Jordan, *J. Amer. Chem. Soc.* **89**:6365–6366 (1967).
150. P. G. Zambonin and J. Jordan, *Anal. Lett.* **1**:1–10 (1967).
151. R. E. Panzer and M. J. Schaer, *J. Electrochem. Soc.* **112**:1136–1143 (1965).
152. D. P. Clark and R. E. Meredith, *Electrochem. Techn.* **5**:446–448 (1967).
153. B. W. King, W. A. Hedden, A. B. Tripler, D. J. Bowers, and B. O. Austin, *Ceram. Bull.* **43**:117–121 (1964).
154. B. B. Owens and G. R. Argue, *J. Electrochem. Soc.* **117**:898–900 (1970).
155. B. B. Owens, paper presented at the ECS Meeting, October 1970, Atlantic City, New Jersey.
156. T. Takahashi and O. Yamamoto, *J. Electrochem. Soc.* **117**:1–5 (1970).

Chapter 5

THERMODYNAMIC STUDIES, BY MASS SPECTROMETRY, OF MOLTEN MIXED HALIDE SYSTEMS

John W. Hastie
National Bureau of Standards
Washington, D. C.

1. INTRODUCTION

The solid and liquid states of mixed halide systems have received considerable continued attention over the past 50 years.[1] Thermodynamic and spectroscopic studies have indicated that many halides interact strongly on mixing to form new solid compounds[2] and very nonideal molten salt mixtures.[3] However, until more recently the vapor state of halide and mixed halide systems was believed to be ideal in that no chemical interaction occurred between the monomers. The expectation appeared to be that, at the elevated temperatures and low pressures used, the entropy contribution to free energy would be significant and would naturally favor the dissociation of complex or polymeric species.

From the pioneering mass spectrometric experiments of Ionov (1948),[4] Chupka and Inghram (1955),[5] and others, it was evident that high-temperature vapors, such as those of the alkali halides and graphite, were appreciably polymeric and, that the presumption of ideality for molten salt vapors should be seriously questioned. Subsequent work over the past 15 years has indicated the nonideality of molten salt vapors to be a widespread phenomenon. The purpose of the present article is to review the thermodynamic properties of such complex vapors and to develop criteria from which the behavior of unstudied systems may be predicted.

Complex vapor species, besides being important to the evaluation of condensed state thermodynamic properties, are of interest due to their possible formation in rocket systems, molten salt breeder reactors,[6] and other practical high-temperature situations. They also serve as positive test cases for theories of bonding and proposed potential functions and provide insight into the nature of the condensed phase from which they are derived.

Other applications are likely for these molecules. One may take advantage of the ability to vaporize, at low temperatures, relatively involatile molecules such as the alkali halides in the form of a more volatile complex species. For example, by complexing with $AlCl_3$ mixtures of the relatively involatile rare earth chlorides can be separated by gas chromatography at temperatures of less than 250°C.[7] A less obvious use is provided by the ability to produce, by electron impact, negative ions of the component molecule which otherwise may not be possible.[8]

A few of these molecules have been studied by nonmass spectrometric methods, but we shall include them in the text to facilitate a more complete evaluation of chemical trends. Also, the evidence for some of these species is not unequivocal, and they might receive more detailed study by the mass spectrometric method.

Earlier reviews of halide vapors have appeared.[9,10] However, experimental techniques have improved and the increased number of studies in subsequent years allow a more unified discussion and interpretation of the complex vaporization phenomenon.

2. EXPERIMENTAL TECHNIQUES

The basic techniques of high temperature mass spectrometry are well known, and detailed descriptions are readily available in the existing literature.[11–13] A synopsis is therefore adequate for the present discussion. Molten salt thermodynamic data are usually obtained by mass spectrometry with the following procedures:

(1) *Sampling the Molten Salt System.* The salt sample is usually contained by a Knudsen cell that has the characteristic property of allowing a representative portion of the sample vapor to effuse as a molecular beam without destroying the *in situ* equilibrium. The molecular beam is then ionized by electron impact, and the ions are mass analyzed.

(2) *Identification of Molecular Species.* For multicomponent systems an unambiguous assignment of the observed ions to their molecular pre-

cursors may not be straightforward as the ion may form either as a fragment or as a parent. Also a particular fragment–ion may be common to several molecular species. A careful analysis of ionization efficiency curves, use of isothermal vaporization techniques, or temperature dependence studies are used to resolve these problems.

(3) *Partial Pressure Determination.* From the measured positive ion intensity I, the partial pressure P of its molecular precursor is given by the relation

$$P = kIT, \tag{1}$$

where T is the sample (that is, Knudsen cell) temperature and k is a proportionality term that contains factors such as ionization cross section, multiplier efficiency, ionizing-electron energy, and instrument sensitivity. Molecular ionization cross sections usually are not well known, which commonly leads to absolute pressure uncertainties of a factor of two or three. However, accurate relative pressure data may be obtained with the use of a dual,[14] or even higher multiplicity, Knudsen cell system where the k factors cancel.

For Knudsen effusion, and with the use of present-day mass spectrometers, it is possible to measure pressures over the range of 10^{-3} to 10^{-12} atm. This relatively low pressure capability is advantageous for studies on molten salt mixtures as the mass of material vaporized during an experiment is sufficiently low for essentially constant composition conditions to exist.

For some mixed systems, one of the components may have a partial pressure that is outside of the mass spectrometric range. Hence, in order to study the vapor phase interaction between the components, it is necessary to vaporize each salt at a different temperature such that their vapor pressures are more compatible. This requires the use of separately heated double (or higher multiplicity) Knudsen cells, linked so that the more volatile species effuses from the relatively cooler to the hotter cell, which contains the normally less volatile component.[15,16]

(4) *Thermodynamic Data Evaluation.* From the basic partial pressure and temperature data one may derive thermodynamic activities and the related partial molar free energy properties. Also from the second or third laws of thermodynamics one obtains free energy, enthalpy, and entropy of vaporization (or sublimation) data and the corresponding ΔG_T, ΔH_T, and ΔS_T quantities for vapor phase equilibria. Details of these procedures may be obtained elsewhere.[13,17] The combined difficulties of measuring or estimating ionization cross sections and obtaining isothermal condi-

tions and true temperature readings result in uncertainties of about ± 2 kcal/mole and ± 2 cal/deg-mole for ΔH_T and ΔS_T, respectively.

With mixed systems, the problems of assigning ions to molecular precursors and of obtaining accurate relative cross section and hence partial pressure data are effectively dealt with by use of total vaporization isotherms.[18] This recently developed technique is of sufficient novelty and importance to warrant a general outline as presented below. The arguments are essentially those originally outlined by Sidorov and Akishin.[18]

2.1. Use of Total Vaporization Isotherms for Mass Spectrometric Determination of the Partial Pressure and Relative Ionization Cross Sections of Molecules

2.1.1. Case 1

Consider a system of molecules A and B in equilibrium at temperature T. The total vaporization isotherm of q g of sample containing q_1 g of A and q_2 g of B is related to the time dependence of the ion currents of $A^+(I_1)$ and $B^+(I_2)$ by the following equations:

$$P = kIT \tag{1}$$

The proportionality k, between ion intensity I and pressure P, can be obtained by the usual method of weight-loss measurement from a Knudsen cell as given by

$$q = aP\sqrt{\frac{M}{2\pi RT}} \cdot t$$

where M is molecular weight, t is time and R is the gas constant. Hence,

$$q = a\sqrt{\frac{MT}{2\pi R}} \cdot k\int_0^t Idt = Bk\int_0^t Idt \tag{2}$$

where a is the product of the Clausing factor and the orifice area. Similarly,

$$q_1 = B_1k_1\int_0^t I_1\,dt \tag{2a}$$

and

$$q_2 = B_2k_2\int_0^t I_2\,dt \tag{2b}$$

Equations (2a) and (2b) may be solved for k_1 and k_2 by graphical integration of I vs t curves. For Faraday collection of ions (that is, no multiplier discrimination effects present) these constants are related to the ionization cross sections σ_1 of A and σ_2 of B by the relation:

$$\frac{\sigma_1}{\sigma_2} = \frac{k_2}{k_1} \tag{3}$$

Thus, from the experimental I vs t curves and equation (1) we are able to follow the time variation of pressure for each species.

The time dependence also can be related to concentration dependence (condensed phase), which is of more interest for a description of the system in terms of a composition–partial pressure diagram. For the conversion of time to a concentration variable consider the area under the I vs t curve S_1 as composed of small segments S_1', S_1'', ..., $S_1^{(k)}$ parallel to the ordinate. Then S_1'/S_1 is the fraction of the substance evaporating at time t and $(S_1' + S_1'')/S_1$ is the fraction evaporating at time t_2, etc. Hence, after a period t the amount of sample remaining is

$$q_1' = q_1 - \frac{S_1'}{S_1} \cdot q_1$$

and after time t_2

$$q_1'' = q_1 - \frac{S_1'' + S_1'}{S_1} \cdot q_1$$

Similarly, the amount of substance B left in the sample can be calculated at various times, and hence the pressure–composition relation can be deduced.

2.1.2. Case 2

Consider the effect of the presence of a third species AB that also can produce A^+, B^+, and $AB^+(I_3)$ in the mass spectrum. The total A^+ intensity I_1 then is given by

$$I_1 = I_{11} + I_{13}$$

where I_{11} is the contribution from A and I_{13} from AB. Similarly,

$$I_2 = I_{22} + I_{23}$$

Then $a_{13} = I_{13}/I_3$ is a coefficient representing the fraction of A^+ relative to AB^+. Similarly, for B^+,

$$a_{23} = \frac{I_{23}}{I_3}$$

These coefficients are obtained as follows: For two different compositions we have

$$I_1 = I_{11} + a_{13}I_3$$

and

$$I_1' = I_{11}' + a_{13}I_3' \tag{4}$$

Also, since

$$K_p = \frac{P_1P_2}{P_3} = \frac{P_1'P_2'}{P_3'} \qquad (T = \text{const})$$

then

$$\frac{I_{11} \cdot I_{22}}{I_3} \equiv \frac{I_{11}' \cdot I_{22}'}{I_3'} \tag{5}$$

The coefficients then can be solved for using equations (4) and (5). For the region rich in component B, where $I_2 \equiv I_{22}$, equation (5) simplifies to

$$I_{11}' = CI_{11} \quad \text{where} \quad C = \frac{I_2 \cdot I_3'}{I_3 \cdot I_2'}$$

By a similar treatment the coefficient a_{23} can be calculated and hence the contribution of AB to the fragment–ion mass spectrum.

The total vaporization of AB is given by $I_3 + I_{23} + I_{13}$ and of A by I_{11} and of B by I_{22}. The total vaporization isotherm integrals are then

$$S_{11} = \int_0^t I_{11}\, dt$$

$$S_{22} = \int_0^t I_{22}\, dt$$

and

$$S_3 = \int_0^t (I_3 + I_{23} + I_{13})\, dt$$

Let q_1^0 and q_2^0 be the amount of substance A and B, respectively, present in the starting sample, and let q_1, q_2, and q_3, be the amount of substance

evaporating in the form of molecules A, B, and AB, respectively. Then

$$q_1 = q_1^0 - \frac{M_1}{M_3} q_3 = B_1 k_1 \int_0^t I_{11}\, dt$$

$$q_2 = q_2^0 - \frac{M_2}{M_3} q_3 = B_2 k_2 \int_0^t I_{22}\, dt \tag{6}$$

$$q_3 = B_3 k_3 \int_0^t (I_3 + I_{23} + I_{13})\, dt$$

For compositions rich in component A the pressure of A is

$$P_1 = k_1 I_{11} T$$

However, if the system forms an azeotrope of known composition, then the weight losses are related by the equation

$$q_1 + q_2 + q_3 = q_1^0 + q_2^0 \tag{7}$$

and

$$\frac{q_1 + (M_1/M_3)q_3}{q_1 + q_2 + q_3} = \frac{q_1^0}{q_1^0 + q_2^0}$$

is the composition of the starting sample. Also,

$$\frac{q_1' + (M_1/M_3)q_3'}{q_1' + q_2' + q_3'}$$

is the composition of the mixture at the end of the vaporization, that is the composition of the azeotrope. q_1, q_2, and q_3 then are obtained as solutions of equation (7).

The ionization cross sections are determined from the coefficients of equation (6), that is,

$$\frac{\sigma_2}{\sigma_1} = \frac{k_1}{k_2} \quad \text{and} \quad \frac{\sigma_3}{\sigma_1} = \frac{k_1}{k_3}$$

Finally, partial pressures are obtained from equation (1), that is,

$$P_1 = k_1 I_{11} T$$

$$P_2 = k_2 I_{22} T$$

and

$$P_3 = k_3 (I_3 + I_{13} + I_{23}) T$$

The transformation from time to concentration dependence is made in an analogous manner to that for the simple A + B system (that is, Case 1).

Examples of specific applications of this technique are provided in Sections 3.3 and 3.5

3. RESULTS FOR BINARY SYSTEMS

3.1. Group IA–IA Halide Systems

The mass spectra and thermodynamic properties of the alkali halide monomers and dimers have been relatively well established,[9,10] and recently interest has centered on binary AX + BX or AX + AY mixtures of these or similar salts.[9,10,19–22] Blander has proposed[23] a dimensional theory that predicts energies of association for the simple alkali halide dimers, and the current studies of mixed dimers have allowed a further test of the theory. Comparison of the theory with measured equilibrium constants for several mixed chloride and mixed bromide systems indicates[24] the energetics of these species to be more complex than implied by the proposed Coulombic model. Possibly higher order polarization, as well as van der Waals, interactions are significant, and refinement of the model is at present under study.[24] Further application of the theory is limited due to the lack of data on molecular dimensions for high temperature species.

Bauer and Porter[9] have reviewed briefly the nature of the mixed binary fluoride systems, while Novikov and co-workers[10,25] have more recently studied the binary chlorides.

The problem of obtaining the enthalpy change (ΔH) for the reaction

$$(AX)_2 + (BX)_2 \rightarrow 2ABX_2$$

is not a direct one because the similarity in the enthalpies for the formation of $(AX)_2$ and $(BX)_2$ implies a small value of ΔH and it, therefore, is not easily obtained from the second law temperature dependence of the equilibrium constant. However, the structures of $(AX)_2$ have been proven, and sufficient molecular constant data are either known or estimated so that third law entropies can be calculated.[9,26] Alternatively, ΔS can be taken as a first approximation to be negligible,[10] and hence ΔG becomes ΔH. Values of ΔG have been measured mass spectrometrically, and Table I presents a summary of the thermodynamic data for the formation of these mixed dimers. The error limits for ΔG and hence ΔH arise mainly from the uncertainty in estimating relative ionization and multiplier efficiency terms.

TABLE I. Group I_A-I_A Halide Mixtures
Thermodynamic Data for the Equilibrium: $(A_2X_2) + (B_2X_2) \rightarrow 2ABX_2$

System	Temperature (°K)	K^b	$-\Delta H_T{}^a$ (kcal/mole, ABX_2)
LiF–NaF	1166–1179	7.1 ± 0.7	2.3
LiF–RbF	897–958	25.3 ± 7	3.0
NaF–KF	891–951	4.9 ± 2.0	1.5
KF–RbF	965–994	4.2 ± 1.0	1.4,0
RbF–CsF	833–925	4.3 ± 1.0	1.3
LiCl–CsCl	923–1173		7.0
NaCl–KCl	946–986	5.2 ± 0.2	
NaCl–RbCl	1073		5.8
NaCl–CsCl	923–1173		5.2
KCl–RbCl	1073		0
KCl–RbCl	978–1066	3.2 ± 0.2	
KCl–CsCl	923–1173		2.7
RbCl–CsCl	917–942	2.8 ± 0.3	
NaOH–KOH	883	4.9 ± 0.3	
NaOH–RbOH	823	2.8 ± 0.3	
KOH–RbOH	693–718	5.2 ± 1	
KOH–CsOH	692	3.5 ± 1	
RbOH–CsOH	673	4.2 ± 0.1	

[a] ΔH values for reactions of the first ten systems were calculated[10] by assuming $\Delta S = 0$.
[b] K values were taken from Schoonmaker *et al.*[21,22] for reactions involving fluoride and hydroxide systems and from Milne and Klein[19] for the chlorides.

It appears that mixed dimers having the smallest mass difference from either of the reactant dimers form with nearly zero enthalpy change. In this case the entropy in terms of the equilibrium constant K is given by

$$\frac{\Delta S}{R} = \ln K$$

The major contribution to ΔS would be due mostly to the effect of a symmetry change on the rotational contribution to the partition function. For this case,

$$\Delta S_{\text{rot}} = R \ln 4 \quad [= 2.77 \text{ cal/deg-mole } (AX)_2]$$

that is, K would be 4. This interpretation agrees well with the data for $CsRbF_2$, $RbKF_2$, $KNAF_2$, and the analogous hydroxide species where cancellation of translational and vibrational entropy is most likely. The symmetry effect also explains the tendency of mixed dimers to have higher association constants than the average of values for the component dimers.[24] On the other hand, for molecules of the type ABX_2 where A and B have very different atomic numbers, such as $CsLiCl_2$, the negative ΔH contributes most to the free energy of formation.

3.2. Group IA–II Halide Systems

Mass spectrometric and other studies on the pure Group II halides indicate a tendency to produce dimers, though not to the same extent as the Group I halides.[9] Even trimers have been observed, in small amount, for BeX_2 and MgX_2. It is not surprising, therefore, that these halides are capable of forming mixed dimers with the alkali halides. The most predominant species has the composition AMX_3, where A is an alkali metal, M is an alkaline-earth metal, and X is a halogen. There also is indirect evidence for the formation, to a lesser extent, of A_2MX_4, $(AMX_3)_2$, and AM_2X_5, as indicated in Table II. These molecules tend to resemble MX_2, rather than AX, in their thermodynamic and spectral[37] properties as well as in their electron impact cracking patterns.

A summary of the existing thermodynamic data for the vapors of these systems is given by Table II. The experimental entropies listed were derived mostly from a combination of the second law enthalpies of reaction with the free energies. As is usual, the largest uncertainty lies in the values of the second law heats, but at the moment insufficient molecular data are known for the complex species to allow a useful third law entropy and hence enthalpy calculation. Of the several ΔS values listed in Table II for the formation of $NaBeF_3$ the higher value (that is, 32 cal/deg-mole) appears to accord more with data for similar systems and with trends discussed in Section 6.

Not readily apparent in Table II is the fact that the AMX_3 species are more volatile than the corresponding chlorides of Be, Mg, Ca, and Sr. Novikov and Kuzmenko[29] have stated that the stabilities of the $KMCl_3$ species increase down the group from Be to Sr. However, the large error limits for ΔH and ΔS do not allow a definite decision on this matter.

The $ABeF_3$ species have unusual fragmentation properties in the mass spectrometer. Usually AMX_3 species fragment, on electron impact, mostly to AMX_2^+ and, to a lesser extent, to AMX^+. However, using a dual crucible

TABLE II. Thermodynamic Data for Vapor Equilibria Over Group I_A-II Systems

Vapor equilibria	Temperature (°K)	$-\Delta H_T$ (kcal/mole)[a]	$-\Delta S_T$ (cal/deg-mole)[a]	Reference
$LiF + BeF_2 \rightarrow LiBeF_3$	900	60	32	(27)
$LiF + BeF_2 \rightarrow LiBeF_3$	900	53		(28)
$LiF + LiBeF_3 \rightarrow Li_2BeF_4$	900	53		(27)
[b]$NaF + BeF_2 \rightarrow NaBeF_3$	1180	52 ± 2	21 ± 3	(29)
[c]$NaF + BeF_2 \rightarrow NaBeF_3$	1084	67.7 ± 3	32 ± 2	(31)
[d]$NaF + BeF_2 \rightarrow NaBeF_3$	1300	67.1	30.5	(32)
[d]$NaF + NaBeF_3 \rightarrow Na_2BeF_4$	1300	100	64.6	(32)
[e]$NaCl + BeCl_2 \rightarrow NaBeCl_3$	720	54 ± 5	23 ± 2	(29)
$Na_2Cl_2 + Be_2Cl_4 \rightarrow 2NaBeCl_3$		22		(10)
$KCl + BeCl_2 \rightarrow KBeCl_3$	720	48 ± 5	24 ± 2	(29)
[f]$KCl + MgCl_2 \rightarrow KMgCl_3$	1080	58 ± 5	31 ± 2	(10)
$KCl + CaCl_2 \rightarrow KCaCl_3$	1100	63 ± 3	30 ± 2	(10, 29)
$KCl + SrCl_2 \rightarrow KSrCl_3$	1100	67 ± 17	32 ± 2	(10)
[g]$2KCl + CdCl_2 \rightarrow K_2CdCl_4$	1100	115 ± 9	67.3 ± 8	(34)
[h]$CsCl + CdCl_2 \rightarrow CsCdCl_3$	923	45 ± 5	29 ± 6	(35)
[i]$CsCl + 2CdCl_2 \rightarrow CsCd_2Cl_5$	923	($\Delta G_T = -7.8 \pm 1.8$)		(35)
[g]$NaCl + ZnCl_2 \rightarrow NaZnCl_3$	800	42	22.5 ± 2.5	(36)
[g]$KCl + ZnCl_2 \rightarrow KZnCl_3$	1100	39.5 ± 3	17 ± 2.7	(34)

[a] Refers to values per mole of complex except for reaction involving $2NaBeCl_3$.
[b] Schoonmaker[30] also has qualitatively verified this equilibrium.
[c] The mass spectrometric data, with the use of total vaporization isotherms, yielded $\Delta G^\circ_{1084} = 32.9$ kcal/mole, and if one assumes $\Delta S^\circ_{1084} = 32 \pm 2$ cal/deg-mole, then $\Delta H^\circ_{1084} = 67.7 \pm 3$ kcal/mole. Also, the $Na_2BeF_3^+$ ion appears to be a fragment of $(NaBeF_3)_2$ and the existence of Na_2BeF_4 is unlikely.
[d] Transpiration vapor pressure method.
[e] Nonmass spectrometric vapor pressure methods used for study of equilibria from here down.
[f] This equilibrium also has been inferred from vapor pressure and activity measurements.[33]
[g] These reactions are postulates based on an observed nonideality of the vapors, and for such cases the exact stoichiometry of the complex species is not readily deduced. The data are more consistent with the formation of $KCdCl_3$.
[h] Proven by both vapor pressure and mass spectrometric studies and $\Delta G_{923} = -17.9 \pm 1.4$ kcal/mole. Analogous NaCl and RbCl species also were found.
[i] The formation of $CsCd_2Cl_5$ is not definite as it was not proven by mass spectrometry.

system Buchler and Stauffer[27] obtained the following fragmentation patterns: For $LiBeF_3$ the following ions and their relative proportions were found: Li^+ (2.9), $LiBeF_2^+$ (1), and LiF^+ (0.06); and for Li_2BeF_4–Li_2F^+ (40) and $Li_2BeF_3^+$ (1). Similarly, for $NaBeF_3$, Sidorov *et al.*[31] found appreciable fragmentation to Na^+. As with organic mass spectra, these fragmentations should have certain implications as to the parent molecule structures and frequency factors. However, with the present lack of structural information for inorganic species, there have been very few attempts to relate mass spectral fragmentation and molecular structure data. It would be of interest if any negative ions resulting from these fragmentations were recorded. One could speculate that as Li^+ is the major ion from $LiBeF_3$ then BeF_3^- also may form, owing to the probable $(Li)^+(BeF_3)^-$ structure for the molecule.

3.2.1. Activity Determination

In addition to the usual mass spectrometric enthalpy and free energy determinations, activities also have been measured in several instances.[27,28] Future studies should show an increased usage of the following techniques for activity determinations:

One technique makes use of the presence of dimers. For example, consider the LiF–BeF_2 system where Li_2F_2 is a significant species. For the dissociation of this dimer,

$$K = \left[\frac{(p_{LiF})^2}{p_{Li_2F_2}}\right]_{\text{pure salt}} = \left[\frac{(p_{LiF})^2}{p_{Li_2F_2}}\right]_{\text{mixed salt}}$$

and the partial and vapor pressures are related through the activity a_{LiF}, that is,

$$a_{LiF} = \frac{(p_{LiF})_{\text{mixed}}}{(p_{LiF})_{\text{pure}}}$$

and as $p \alpha I^+T$ this becomes

$$a_{LiF} = \frac{(I_{Li^+}/I_{Li_2F^+})_{\text{pure}}}{(I_{Li^+}/I_{Li_2F^+})_{\text{mixed}}}$$

and, similarly,

$$a_{BeF_2} = \frac{(I_{BeF_2^+}/I_{Be_2F_3^+})_{\text{pure}}}{(I_{BeF_2^+}/I_{Be_2F_3^+})_{\text{mixed}}}$$

Using this technique Berkowitz and Chupka[28] calculated activity values of $a_{LiF} = 0.0246$ and $a_{BeF_2} = 0.343$ over the equimolar melt at 900°K. As

dimers have been shown to be fairly common in salt vapors, this method can be used for a number of other systems.

The following alternative dual crucible method does not require the presence of dimers, however. Essentially, use is made of adjacent Knudsen crucibles having individual Knudsen orifices but both heated to the same temperature.[27] A pure salt such as BeF_2 is contained in one crucible and the LiF–BeF_2 mixture in the other. A swivel arrangement allows each crucible, in turn, to be focused toward the ion source of the mass spectrometer. The activity then is simply

$$a_{BeF_2} = \frac{(I_{BeF_2^+})_{\text{mixture}}}{(I_{BeF_2^+})_{\text{pure}}}$$

and similarly for LiF. This method relies on the assumption that ions BeF_2^+ or Li^+ have only BeF_2 or LiF as their molecular precursors, which may not always be valid. Values of $a_{BeF_2} = 0.017$ and $a_{LiF} = 1$ for the 74% LiF–BeF_2 and $a_{BeF_2} = 0.91$ and $a_{LiF} = 0.073$ for the 33% LiF–BeF_2 mixtures at 875°K were obtained by this method.

3.3. Group IA–III Halide Systems

Of this series only Al- or La-containing mixtures have been studied (see Table III), but there is no thermodynamic reason why at least B, Ga, Sc, and Y systems should not behave similarly.

$LiAlF_4$ has been found[38] to produce a similar fragmentation, on electron impact, to that found for $LiBeF_3$, that is, Li^+ is one of the major fragment ions. The total vaporization isotherm technique indicates the principal fragment ions produced from M_2AlF_5 (M = Li and Na) and $M_2(AlF_4)_2$ to be M_2F^+ and $M_2AlF_4^+$, respectively.[39]

The structures of these AMX_4 species are unknown, with the recent exception of $NaAlF_4$.[42] However, the most energetically favorable groupings for ions A^+, M^{3+}, and $3X^-$ are those where M^{3+} is tetrahedrally coordinated by X^- and A^+ is bridged to M^{3+} by two or three of these X^- ligands to form either C_{2v} or C_{3v} point-group symmetry species, respectively. Infrared vibrational frequencies observed[37,43] for $LiAlF_4$ support these structures. Such a tetrahedral coordination about Al has been well established for the Al_2Cl_6 molecule[44] and also $NaAlF_4$, as discussed in Section 6.

An interesting approach to the problem of relating fragment ions to molecular precursors for these complex systems is by the method of total vaporization isotherms, outlined in Section 2.1. The fragmentation pattern

TABLE III. Thermodynamic Data for Vapor Equilibria Over Group I_A-III Systems

Vapor equilibria	Temperature (°K)	$-\Delta H_T$ (ckal/mole)[a]	$-\Delta S_T$ (cal/deg-mole)[a]	Reference
$LiF + AlF_3 \rightarrow LiAlF_4$	1000	73 ± 4	37	(38)
$Li_2F_2 + AlF_3 \rightarrow LiF + LiAlF_4$	1000	9.0 ± 2	4.6 ± 2	(38)
[b]$NaF + AlF_3 \rightarrow NaAlF_4$	910	87.5 ± 3	31.5 ± 3	(39)
$2NaAlF_4 \rightarrow (NaAlF_4)_2$	910	42.6 ± 2	27.1 ± 2	(39)
$Na_2Cl_2 + Al_2Cl_6 \rightarrow 2NaAlCl_4$		27		(10, 41)
$NaCl + AlCl_3 \rightarrow NaAlCl_4$		51[c]		
$NaCl + LaCl_3 \rightarrow NaLaCl_4$	1400	69.8	32.8	(10)

[a] Refers to per mole of complex except for the reaction yielding $2NaAlCl_4$.
[b] Evidence of $NaAlF_4$ was obtained prior to the mass spectrometric investigation from vapor pressure measurements.[10,40]
[c] Calculated from the previous reaction data and known Al_2Cl_6 and $(NaCl)_2$ dimer energies of 28 and 48 kcal/mole, respectively.

for $NaAlF_4$, using 82 eV electrons, is Na^+(100), $NaAlF_3^+$ (1.3), and AlF_2^+(3.3). For the dimer $(NaAlF_4)_2$ the pattern is Na^+(100), $Na_2AlF_4^+$(7.2) $NaAlF_3^+$(0.8), and AlF_2^+(3.7).[39]

3.4. Group IA–IVA Halide Systems

Only mixtures of alkali halides and Sn or Pb dihalides are readily studied since the divalent halides of Ge, Si, and C show an increasing reactivity and tendency to disproportionate to tetravalent species. Use of the double Knudsen cell technique could possibly alleviate this difficulty. Table IV summarize available data for the vapor-phase processes.

Activities and other thermodynamic data have been measured for most of the systems presented in Table IV, and the results have indicated considerable non ideality in the liquid as well as in the vapor states. For the liquid state it has been suggested that this non ideality is due mainly to the formation of complex ions such as $[MX_3]^-$ and $[MX_4]^{2-}$. Further, the data suggest that the concentration of these ions appears to increase with the size, or polarizability, of X and with the increasing charge density of M.[35] One might expect similar behavior for the vapor AMX_3 species, and the higher

stabilities of $ASnF_3$ and $ASnCl_3$, as compared with $APbCl_3$, are in accord with the expected stabilizing effect of a smaller M^{2+} ion. A comparison of the enthalpies for $KPbBr_3$ and $KPbCl_3$ reveals, if anything, an opposite stability trend to that found in the liquid state, but the data are in accord with the general lower stability of bromide molecules as compared with chlorides. Similarly, values of ΔH for the formation of $KSnX_3$ decrease with the increasing size of X (see Table IV), which is the same sequence followed by the Sn–X bond energies in SnX_2.

From the relative magnitudes of ΔH for the vaporization of AMX_3, AX, and MX_2, one can predict whether the concentration of complex species will increase with increasing temperature. On this basis the proportion of $NaPbCl_3$ and $KPbCl_3$ species increases with increasing temperature, but $CsPbCl_3$ decreases and $RbPbCl_3$ does not vary significantly as compared with $PbCl_2$.

Appearance potential and ionization efficiency measurements have indicated the fragmentation of AMX_3 to be AMX_2^+, AMX_3^+, and AMX^+ at least up to 20 eV ionizing electron energy.

TABLE IV. Thermodynamic Data for Vapor Equilibria Over Group I_A-IV_A Systems

Vapor equilibria	Temperature (K°)	$-\Delta H_T$[a] (kcal/mole)	$-\Delta S_T$ (cal/deg-mole)	Reference
$NaF + SnF_2 \rightarrow NaSnF_3$	746	60 ± 4	19 ± 3	(45)
$NaF + NaSnF_3 \rightarrow Na_2SnF_4$	746	69 ± 4	32 ± 5	(45)
$SnF_2 + NaSnF_3 \rightarrow NaSn_2F_5$	754	36 ± 12	43 ± 13	(45)
$KF + SnF_2 \rightarrow KSnF_3$	855	54 ± 4	19 ± 3	(45)
[b]$NaCl + SnCl_2 \rightarrow NaSnCl_3$	721	48 ± 2	27 ± 2	(46)
$NaCl + PbCl_2 \rightarrow NaPbCl_3$	740–910	38.0 ± 2	20.0 ± 0.5	(47)
$KCl + PbCl_2 \rightarrow KPbCl_3$	740–910	41.0 ± 2	19.6 ± 0.5	(47)
$RbCl + PbCl_2 \rightarrow RbPbCl_3$	740–910	39.5 ± 2	19.3 ± 0.5	(47)
[c]$CsCl + PbCl_2 \rightarrow CsPbCl_3$	740–910	36.5 ± 2	19.0 ± 0.3	(47)
$KBr + PbBr_2 \rightarrow KPbBr_3$	900	37 ± 2	20 ± 1.5	(48)
[b]$KI + SnI_2 \rightarrow KSnI_3$	680–820	34	24	(49)

[a] ΔG_T values may be back-calculated from ΔH_T and ΔS_T, the uncertainties being less than ±2 kcal/mole.
[b] Transpiration method.
[c] This data also has been verified by nonmass spectrometric vapor pressure measurements.[35,47]

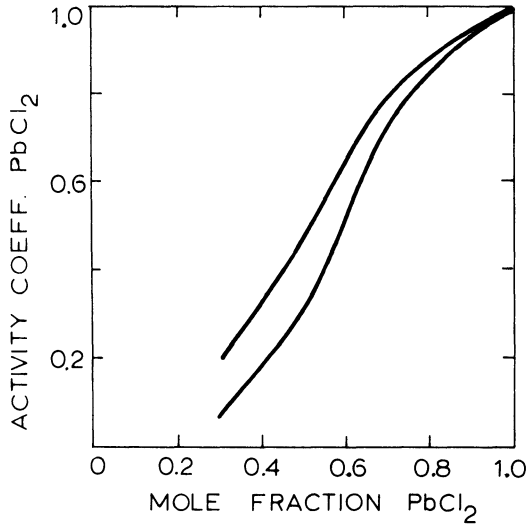

Fig. 1. Effect of vapor-phase complex formation on calculated activity coefficients for the $PbCl_2$ + CsCl system. The lower curve takes into account the presence of $CsPbCl_3$ as a vapor species and the upper curve does not.

The effect of neglecting the vapor phase formation of AMX_3 on activity calculations, from non absolute vapor pressure measurements, is demonstrated in Fig. 1 † for the $PbCl_2$ + CsCl system.[50] Similarly, in the $SnCl_2$–KCl system at 380°C, activity data,[51] based on the assumption of simple vaporization to $SnCl_2$, are in error owing to the formation of $(SnCl_2)_2$ and $KSnCl_3$.

3.5. Group IA–Transition Metal Halide Systems

The transition metal halides are best considered as a group rather than a series of B subgroups to facilitate eventual discussion of possible ligand field effects when more data become available. Transition metal halides have received fairly detailed thermodynamic study by mass spectrometry but mixed systems have not as yet. Because of the characteristic variable valency of transition metals a variety of complex vapor species, such as

† It should be noted that the curves of Fig. 1 may not be extrapolated to zero activity coefficient as the requirement of a finite coefficient for CsCl implies a limiting slope of zero at very low $PbCl_2$ mole fraction.

AMX_3, AMX_4, and others, are possible. Even more complex species are feasible for cases where metal–metal bonding is likely, for example, with Mo- or W-halides. Table V summarizes the available data.

The Group IIIB and IIB metal halides were discussed in their respective subgroups as these halides usually do not (that is, for their normal tri- and divalent states, respectively) involve ligand field stabilizing effects. This transition element series usually allows the formation of AMX_3, AMX_4, etc. only to a minor extent as compared with Groups IIA and IVA. Also mass spectrometric investigation of $KF–CoF_2$ and $KF–MnF_2$ systems failed to detect any significant vapor interaction for pressures of less than 1 torr. The existence of $KCoCl_3$, however, would seem to indicate that chlorides are more favorable than fluorides for the formation of these mixed vapor species. Possibly the tendency for chlorides to be more readily detected than fluorides, at similar total pressures, is a property of the lower temperatures required to vaporize the chlorides. This becomes important when

TABLE V. Thermodynamic Data for Vapor Equilibria Over Group I_A-Transition Metal Halide Systems

Vapor equilibria (unless otherwise indicated)	Temperature (°K)	$-\Delta H_T$ (kcal/mole)	$-\Delta S_T$ (cal/deg-mole)	Reference
$LiCl + FeCl_2 \rightarrow LiFeCl_3$	1023	43		(10, 28)
$NaCl + FeCl_2 \rightarrow NaFeCl_3$	1020			(52)
$KCl + FeCl_2 \rightarrow KFeCl_3$	~935	34.7		(28)
$CsCl + FeCl_2 \rightarrow CsFeCl_3$		24.7		(28)
$KCl + CoCl_2 \rightarrow KCoCl_3$	1020			(52)
$KCl + NiCl_2 \rightarrow KNiCl_3$	1020			(52)
$NaCl + FeCl_3 \rightarrow NaFeCl_4$	970	51.6 ± 2.5	28.9	(10)
$NaCl(s) + FeCl_3 \rightarrow NaFeCl_4$	723	-3.7 ± 1	-6.5 ± 1.5	(53)
$3NaCl + CrCl_3 \rightarrow Na_3CrCl_6$	1180	139 ± 10	74 ± 7	(10)
$3KCl + CrCl_3 \rightarrow K_3CrCl_6$	1180	132 ± 10	76 ± 7	(10)
$KCl + KTiCl_5 \rightarrow K_2TiCl_6$			28	(10)
$2KCl(s) + TiCl_4 \rightarrow K_2TiCl_6(s)$		33.3	26.4	(10)
$KCl + TiCl_4 \rightarrow KTiCl_5$		≤ 32	(28)	(10)
$NaF + ZrF_4 \rightarrow NaZrF_5$	1170	64.4	29	(10)
$NaF + ZrF_4 \rightarrow NaZrF_5$	1167	62.2 ± 4.6		(18)
[a] $NaF + VF_3 \rightarrow NaVF_4$	1151			(54)

[a] The vapor over the equimolar mixture is almost entirely $NaVF_4$.

ΔS is relatively significant and, therefore, $T\Delta S$ contributes to a noticeable reduction in free energy change with increasing temperature.

The $AFeCl_3$ data suggest a marked change in stability for various A, which contrasts with the behavior in the analogous Group IIA and IVA systems.

Molecular beam velocity analysis[52] has indicated that the vapors over equimolar KCl–$FeCl_2$ contain 85% $KFeCl_3$ relative to KCl at an unspecified temperature, while similar rotational magnetic moment experiments indicate about 91% $KFeCl_3$ at 935°K. Thus a significant proportion of the alkali halide evaporates as a mixed complex species, which appears to be a general characteristic for these systems.

The total vaporization isotherm technique[18] has been applied to the NaF–ZrF_4 system by Sidorov and Akishin.[55] The formation of $NaZrF_5$ may be described in the same manner as the formation of AB for the general case given in Section 2.1. Composition vs pressure curves are given in Fig. 2. Analysis of the data indicated relative ionization cross sections of $NaF(\sigma = 1.0)$, $ZrF_4(\sigma = 1.8)$, and $NaZrF_5(\sigma = 2.5)$. This example seems to verify the often-used approximate additivity rule for relative ionization cross sections, that is,

$$\sigma_{AB} \approx \sigma_A + \sigma_B$$

Similarly, the $NaF + VF_3$ system forms a mixed molecule $NaVF_4$ that complicates the fragmentation pattern of NaF and VF_3.[54] For 51 eV ionizing electron energy the vapor at 1151°K produces the mass spectrum

Ion:	Na^+	$NaVF_3^+$	VF_3^+	VF_2^+	VF^+	V^+
Relative intensity:	100	0.88	2.28	8.25	1.75	1.58

The total vaporization isotherms are given in Fig. 3 for the mixture 95% $NaF + 5\%$ VF_3 where it is apparent that the curve for $VF_2^+(NaVF_4)$ is parallel to the curve for $Na^+(NaVF_4)$, that is, VF_2^+ is formed completely from molecular $NaVF_4$. This is possible only if the partial pressure of VF_3 is much lower than that of $NaVF_4$ over the composition range used. Analysis of these curves leads to relative ionization cross sections of $NaF(\sigma = 1.0)$ and $NaVF_4(\sigma = 1.57)$.

It should be noted that the complex mass spectral fragmentation behavior found for the systems studied by this vaporization isotherm method is enhanced by the use of high ionizing electron energies (that is, 50-80 eV) and by using compositions that are rich in one of the components and not

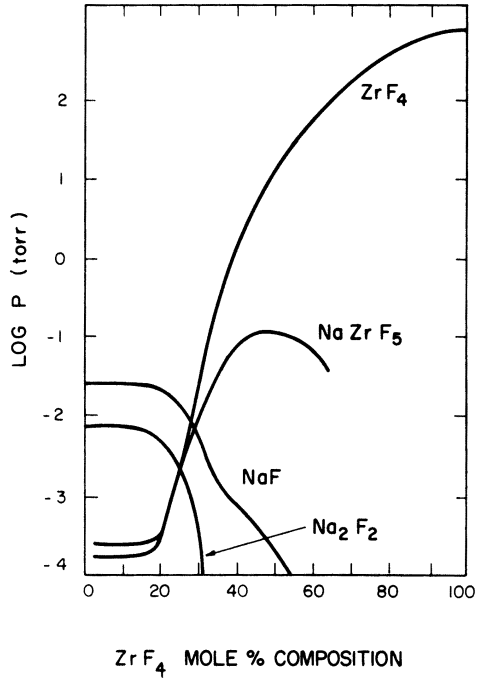

Fig. 2. Isothermal variation of partial pressures with condensed phase composition for the NaF + ZrF_4 system, as derived from the total vaporization–isotherm technique.[55]

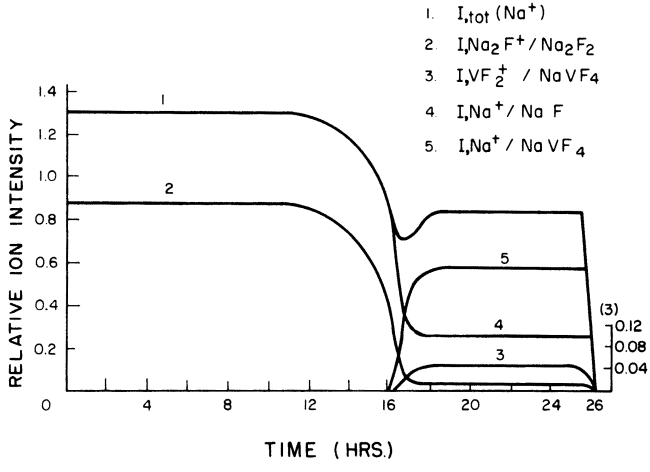

Fig. 3. Variation of fragment ion intensities with time over the system NaF + VF_3 (5 mole %) at 1151°K.[54]

the other. For the equimolar $NaSnF_3$ system at 20 eV, the Na^+ ion could be attributed to NaF only, even though an appreciable amount of $NaSnF_3$ was present.[45]

3.6. Group IA–Rare Earth Halide Systems

This group has received considerable study by Novikov and Gavryuchenkov,[10] and the data (Table VI) appear sufficiently accurate to permit some generalizations to be made. Only the chloride rare earth systems have been studied so far, and these show similarity to those systems involving Group IIIA halides. The thermodynamic properties of these systems have been obtained mainly by vapor pressure and not mass spectrometric methods. However, $KErCl_4$ and analogous species have been definitely established by mass spectrometry,[57,58] and the assumptions of the vapor

TABLE VI. Thermodynamic Data for Vapor Equilibria Over Group I_A–Rare Earth Metal Systems[a]

Vapor equilibria (unless otherwise indicated)	Temperature (°K)	$-\Delta H_T$ (kcal/mole)	$-\Delta S_T$ (cal/deg-mole)
$NaCl + LaCl_3 \rightarrow NaLaCl_4$	1400	69.8	32.8
$NaCl + NdCl_3 \rightarrow NaNdCl_4$	1400	61.3 ± 3	32.6 ± 2
$NaCl + ErCl_3 \rightarrow NaErCl_4$	1400	63.0	34.0
$KCl + LaCl_3 \rightarrow KLaCl_4$	1350	61.4	32.6
$KCl + LaCl_3 \rightarrow KLaCl_4$	~1000	88	47
$KLaCl_3(s) \rightarrow KLaCl_3$	~1000	52	35
$KCl + CeCl_3 \rightarrow KCeCl_4$	1350	61.0	32.6
$KCl + CeCl_3 \rightarrow KCeCl_4$	1350	76	43
$KCeCl_4(s) \rightarrow KCeCl_4$	1350	54	40
$KCl + PrCl_3 \rightarrow KPrCl_4$	1350	59.3	32.6
$KCl + PrCl_3 \rightarrow KPrCl_4$	~1350	71	41
$KPrCl_4(s) \rightarrow KPrCl_4$	~1350	56	40
$KCl + NdCl_3 \rightarrow KNdCl_4$	~1320	66	38
$KNdCl_4(s) \rightarrow KNdCl_4$	~1320	55	40
$KCl + NdCl_3 \rightarrow KNdCl_4$	1350	59.3	32.6
$KCl + ErCl_3 \rightarrow KErCl_4$	~1320	59	32
$KErCl_4(s) \rightarrow KErCl_4$	~1320	57	41
$KCl + ErCl_3 \rightarrow KErCl_4$	1350	59.5	32.6
$CsCl + NdCl_3 \rightarrow CsNdCl_4$	1300	57.2	29.8
$CsCl + ErCl_3 \rightarrow CsErCl_4$	1300	58.0	30.8

[a] Data obtained by Novikov and co-workers[10,56,57] Note that where alternate ΔH and ΔS values are indicated the lower ones are considered to be the more reliable.

pressure method are verified. For $KErCl_4$ the fragment ions $KErCl_3^+$ (1) and $KErCl_2^+$(0.16) were observed at 30 eV and in the indicated relative proportion.

It has been noted that the concentration of $KMCl_4$ in the vapor increases across the row. Also, the stability of $AMCl_4$ increases in the order $Na < K < Cs$.[59] However, as is the case with the other properties of the rare earths, the thermodynamics of vaporization and vapor phase interaction are not very dependent on the nature of M. The similarity between the ΔS values (that is, -32.6 ± 3 cal/deg-mole) for the formation of $AMCl_4$ from ACl and MCl_3 and those found[60] (that is, -30 ± 3 cal/deg-mole) for the dimerization of MCl_3 is worthy of note. Also, the significantly larger ΔH—that is, more negative—values for the formation of $AMCl_3$ as compared with $(MCl_3)_2$ accounts for the higher relative abundance of the former species.

3.7. Group IA–Actinide Halide Systems

Of these systems only Th has been studied,[10] however, from analogy with the rare earth systems, the following example should be typical of the other actinides: For Th,

$$KCl + ThCl_4 \rightarrow KThCl_5$$

$$\Delta H_{1280} = -49.3 \pm 3 \text{ kcal/mole}$$

$$\Delta S_{1280} = -28.0 \pm 3 \text{ ckal/deg-mole}$$

The similarity of ΔS to those for the rare earth systems possibly indicates similar structures for the complex species.

4. RECIPROCAL AND SIMILAR SYSTEMS

Few reciprocal systems, that is, those involving different X and Y and a common cation, have been studied experimentally. However, one expects the mixed dimers to form with the evolution of more heat than is found for the binary species. For example, consider the alkali halide reactions

$$(NaF)_2 + (KF)_2 = 2NaKF_2 \tag{8}$$

and

$$(NaF)_2 + (NaCl)_2 = 2Na_2ClF \tag{9}$$

The heats of dimerization of NaF and KF are 54 and 49.6 kcal/mole, respectively, and to a first approximation the heat of formation of $NaKF_2$ from NaF and KF should be between these values. For NaCl the dimerization energy is only 46.4 kcal/mole, hence Na_2ClF should form, via reaction (9), with a larger enthalpy change than $NaKF_2$ from reaction (8). Generally the mixed dimer is most similar to the dimer having the largest heat of dimerization, and this probably holds for reciprocal systems.

As with the simple alkali halide dimers and monomers, the mixed dimers readily lose a halogen group on electron impact by the process

$$ABX_2 + e \rightarrow ABX^+ + X + 2e$$

which is mostly an effect of the relative instability of the molecule-ion ABX_2^+.[61] The almost unmeasurably low molecule-ion intensities unfortunately do not allow measurement of ionization potential for these species.

Mixed trimers such as Cs_2LiCl_3 also exist[25] but apparently not in sufficient concentration for quantitative mass spectrometric measurements to be made.

Systems involving halides, other than the alkali halides, have been studied to a small extent, mainly for their molten state thermodynamic properties with a view to testing thermodynamic and structural models developed for binary systems. To some degree this work suffered from a lack of knowledge of the vapor state interactions.

It has been established that bromides and chlorides interact in the vapor state to form chlorobromides, for example

$$PbCl_2 + PbBr_2 = 2PbClBr \qquad \Delta S_T \approx 1 \text{ cal/deg-mole } PbCl_2[50]$$

$$CrCl_2 + CrBr_2 = 2CrBrCl \qquad \Delta H_T \approx 0 \text{ kcal/mole } CrCl_2[62]$$

As with the alkali halides, the formation of these mixed halogen species can be predicted solely from the decrease in symmetry, allowing a slightly positive ΔS for the above reactions provided $\Delta H \lesssim 0$ kcal/mole.

Similarly, Cu(I) halides, which vaporize mainly as the trimer, form all possible combinations of the mixed chloro-bromides.[63] The mixed halide Re_3ClBr_8 also has been identified mass spectrochemically.[64]

Similarly, fluoro-chlorides and bromo-iodides are possible. For example, reaction of Br with P_2I_4 in the mass spectrometer[65] produced $PBrI_2$. Also,

$$\tfrac{1}{3}BF_3 + \tfrac{2}{3}BCl_3 = BFCl_2 \qquad \Delta H_{f298} = 0.7 \pm 0.04 \text{ kcal/mole}$$

and

$$\tfrac{2}{3}BF_3 + \tfrac{1}{3}BCl_3 = BF_2Cl \qquad \Delta H_{f298} = 0.49 \pm 0.03 \text{ kcal/mole}^{(66)}$$

As hydroxides behave as pseudohalides, it is not surprising that mixed hydroxide–halide species exist,[66] for example,

$$\tfrac{1}{3}BF_3 + \tfrac{2}{3}B(OH)_3 = B(OH)_2F \qquad \Delta H_{f298} = 0.7 \pm 0.3 \text{ kcal/mole}$$

$$\tfrac{2}{3}BF_3 + \tfrac{1}{3}B(OH)_3 = B(OH)F_2 \qquad \Delta H_{f298} = 0.6 \pm 0.2 \text{ kcal/mole}$$

$B(OH)F_2$ was formed at 25°C and 10^{-6} atm by the reaction of BF_3 with boric acid.

5. MISCELLANEOUS MIXED HALIDE REACTIONS

As with a number of the new species mentioned above, frequently they are products of unintended reactions. For example, a Hg discharge[67] through BCl_3 vapor in a quartz container produced Cl_2BSiCl_3. The mass spectrum showed the following fragment ions: $BSiCl_4^+$, $BSiCl_3^+$, $BSiCl_2^+$, $BSiCl^+$, BSi^+, Si^+, and B^+ among others. A B–Si bond is suggested by the presence of BSi^+ in the mass spectrum.

Indirect evidence of vapor phase interaction between $ZnCl_2 + CuCl_2$ and $PbCl_2 + CuCl_2$ also is indicated in the vapor pressure measurements of these systems.[68] Possibly species such as $CuPbCl_3$ are formed with Cu in its univalent state. Usually binary halide mixtures having both cations with valences greater than unity do not interact to form mixed dimers unless the pure dimers are also present. For example, the $FeCl_2 + LnCl_3$ systems form solutions without forming solid compounds, and no interaction is found in the other physical states either.[69] On the other hand, the volatility of $NdCl_3$ is enhanced markedly by the presence of $AlCl_3$, suggesting the formation of a mixed complex species.[70] Mass spectrometric identification of these species which, from the partial pressure data, appear to be $NdAl_3Cl_{12}$ or $NdAl_4Cl_{15}$ seems desirable.

6. STRUCTURES AND UNIFYING CONCEPTS

In the previous sections we outlined the evidence for the formation of complex mixed halide species and summarized their ΔH_T and ΔS_T values. Analogous data also are available for a number of the simple dimeric species of the type $(AX)_2$, $(MX_2)_2$, and $(MX_3)_2$, and it is instructive to analyze the relation of these data to those of the mixed dimer species.

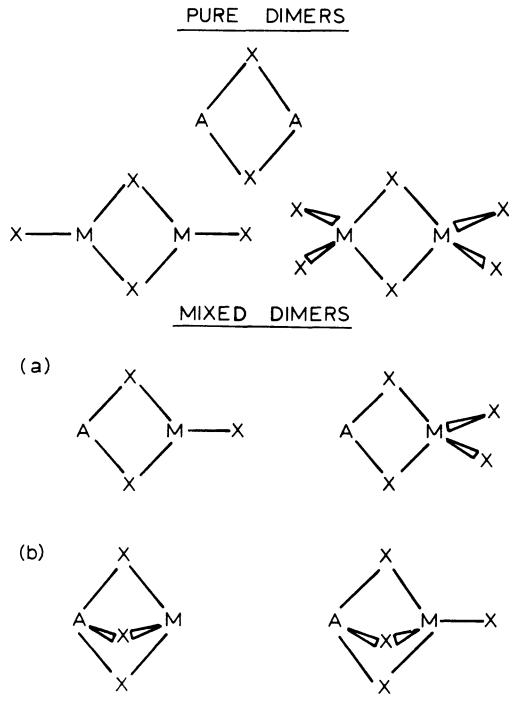

Fig. 4. Structures of complex metal halide species.

First, however, it is necessary to briefly summarize our knowledge regarding the structure of these various complex species. From the electron diffraction study[26] of $(LiCl)_2$, infrared spectra of $(LiF)_2$, etc.[37] and from supporting theoretical calculations,[9] the structure of the alkali halide dimers is well established as rhombohedral with V_h symmetry. Another isomeric form ($D_{\infty h}$) of $(LiF)_2$ is known, however.[71] Infrared spectral studies† for species of the type $(MX_2)_2$, where X is a halogen and M is a Group II, Group IV, or first-row transition element, strongly support C_{2v}-type structures involving four equivalent M–X bridge bonds and two terminal M–X bonds. In the case of the Group IV species, the terminal bonds are probably not coplanar with the $(MX)_2$ ring, though this is not essential to the following discussion. Similarly, for AMX_3- and AMX_4-type species infrared studies indicate the presence of both A–X and M–X bridge bonds. The two possible geometries are described by Fig. 4. In view of the apparently unambiguous evidence of the electron diffraction studies on

† For a recent summary of these studies see Hastie *et al.*[72]

$NaAlF_4$, where structure (a) was found,[42] preference should be given to this configuration as a general model. Species containing a Group IV element may provide a possible exception owing to the stereochemical influence of the lone pair of nonbonding *s* electrons, in which case structure (b) is highly probable. Supporting evidence for these structures is also provided by the known stability and tetrahedral or pseudotetrahedral configurations of the $(MX_4)^-$ and $(MX_3)^-$ species in the condensed molten salt state.[73]

Consider the reaction of dimers to form the mixed complex species, that is,

$$(AX)_2 + (MX_2)_2 = 2AMX_3$$

With model (a) of Fig. 4, it is clear that for this reaction the number of A–X and M–X bridge bonds and M–X terminal bonds remains constant. Thus, providing that the strengths of these bonds remain essentially unaltered in forming the mixed complex, one would expect to observe very little enthalpy change, that is,

$$\Delta H_T \approx 0$$

There is evidence that the M–X bond energies remain essentially constant in various species provided there is no change in valence—for example, with the following groups of species: PbClBr, $PbBr_2$, and $PbCl_2$[50]; LiGaO, Li_2O, and Ga_2O;[74] and WF_6, WOF_4, WO_2F_2, and WO_3.[75] In addition, with $NaAlF_4$ the Al–F bond distances are only slightly greater than those for AlF_3 and probably close to those in $(AlF_3)_2$. Also, the Na–F distance is about what one expects for the $(NaF)_2$ species. Thus the transferability of M–X bonds from one species to another without significant change does appear likely.

The geometrical similarities between the mixed and simple component dimers suggest the following entropy approximations: The number of vibrational modes remains constant. Also, the partitioning of these modes among M–X terminal and bridging bonds remains essentially unaltered, particularly if AMX_3 or AMX_4 have structure type (a). Hence it may be assumed that there are negligible vibrational contributions to entropy change for the above reaction. The effect of molecular weight reduces to the expression

$$\Delta S_{\text{trans}} = 6.86 \log\left[\frac{(M_{AMX_3})^2}{M_{(AX)_2} \cdot M_{(MX_2)_2}}\right]$$

and for the species of interest this results in a translational entropy change of

$$0 \lesssim \Delta S_{\text{trans}} \lesssim 1 \text{ cal/deg-mole } (AX)_2$$

As practically all of the reactions of the above type involve species present in their most stable valence state, and in view of the structural evidence, one expects very little change in electron configuration and hence no electronic contribution to ΔS. Structural similarity between reactants and products suggests little influence from moments of inertia differences to ΔS via the rotational partition function. On the other hand, the symmetry number σ,† that is, the number of indistinguishable configurations into which the molecule can be rotated by simple rigid rotations, varies for each configuration, and the effect on entropy change is given by

$$\Delta S = 4.75 \log \left[\frac{\sigma_{(AX)_2}\sigma_{(MX_2)_2}}{\sigma_{(AMX_3)^2}} \right]$$

where $\sigma_{(AX)_2} = 4$; $\sigma_{(MX_2)_2} = 4$ or 2, depending on whether all atoms are coplanar or alternatively the terminal X groups are out-of-plane as may be the case for the Group IV species; $\sigma_{(AMX_3)} = 2$ for model (a) and 3 for model (b); $\sigma_{(MX_3)_2} = 4$; and $\sigma_{(AMX_4)} = 2$ for model (a) and 3 for model (b). Thus for (AMX_3) model (a) planar $(MX_2)_2$,

$$\Delta S_{rot} = 2.75 \text{ cal/deg-mol } (AX)_2$$

or for model (b),

$$\Delta S_{rot} = 1.14 \text{ cal/deg-mol } (AX)_2$$

and for nonplanar $(MX_2)_2$ and model (b),

$$\Delta S_{rot} = -0.25 \text{ cal/deg-mole } (AX)_2$$

For AMX_4 species one obtains similar values of ΔS_{rot} From these considerations the total ΔS should fall in the region of 1–3 cal/deg-mol $(AX)_2$, depending on the molecular structures, and generally one may assume that

$$\Delta S = +2 \pm 2 \text{ cal/deg-mole } (AX)_2$$

Also, if one assumes that $\Delta H \approx 0$ kcal/mole $(AX)_2$, if follows that at a typical reaction temperature of 1000°K the partial pressure of AMX_3 is 1.65 times the geometric mean of the $(AX)_2$ and $(MX_2)_2$ pressures. Hence it is apparent that the only requirement to the formation of AMX_3 is a reduction in symmetry, and this is analogous to what was found for the case of the mixed alkali halide dimers. To test the applicability of the above ΔH and ΔS approximations it is necessary to relate these quantities to the

† Use of this notation from this point on should not be confused with the ionization cross-section terminology.

corresponding data for the reactions

$$2AX = (AX)_2 \tag{1}$$

$$2(MX_2) = (MX_2)_2 \tag{2}$$

or

$$2(MX_3) = (MX_3)_2 \tag{3}$$

$$AX + MX_2 = AMX_3 \tag{4}$$

or

$$AX + MX_3 = AMX_4 \tag{5}$$

for which data are mostly available. It follows from the above that

$$\Delta H = 2\Delta H_4 - \Delta H_1 - \Delta H_2$$

and similarly for ΔS.

Table VII summarizes the data from which ΔH and ΔS are obtained. The significantly high negative values of ΔH indicate that the AMX_3 or AMX_4 species have formed A–X and M–X bonds that are effectively more stable from those in the corresponding $(AX)_2$ and $(MX_2)_2$ or $(MX_3)_2$ species. This extra stability, as one might expect, increases roughly in proportion to the known M–X bond strength, and the species in Table VII are listed in the order of decreasing M–X average bond dissociation energy.

Based on a point charge model one can rationalize this enhanced stability of the mixed, as compared with the simple, dimers in terms of a reduced cation–cation repulsion through substitution of M^{2+} or M^{3+} by A^+ in the ring.

From the data of Table VII one obtains an average value of $\Delta S = -2 \pm 3$ cal/deg-mole $(AX)_2$, which is in accord with the prediction of $\Delta S = 2 \pm 2$ cal/deg-mole $(AX)_2$. The observed negative sign of ΔS is probably significant as the highly negative ΔH values imply relatively stronger bonds in the mixed dimer and hence higher vibrational frequencies, resulting in a slightly lower entropy for the mixed dimer than was predicted. It should be mentioned that values of ΔS_2 also are available for $(ZnCl_2)_2$ and $(BeCl_2)_2$; however, they result in unreasonably large positive values of ΔS. The data for $(ZnCl_2)_2$ is higly uncertain owing to the experimental technique used of comparing quasi-static and transpiration data.[82] Similarly, the $(BeCl_2)_2$ entropy data is very uncertain as it is based on estimated molecular param-

TABLE VII. Thermodynamic Properties Related to the Formation of Mixed Dimers[a]

Complex	$-\Delta H_1$[b]	$-\Delta H_2$ $-\Delta H_3$	$-\Delta H_4$ $-\Delta H_5$	$-\Delta H$	$-\Delta S_1$[b]	$-\Delta S_2$ $-\Delta S_3$	$-\Delta S_4$ $-\Delta S_5$	$+\Delta S$
$NaBeF_3$[c]	57	33	67	44	31	31	20	2
$NaAlF_4$[d]	57	46	87	71	31	35	31	3
$LiAlF_4$[d]	62	46	73	38	31	35	37	−8
$NaLaCl_4$[e]	48	48	70	44	28	30	32	−6
$NaAlCl_4$[f]	48	28	51	27	28	32	33	−6
$KMgCl_3$[g]	43	39	58	34	27	30	31	−7
$NaSnCl_3$[h]	48	19	48	29	28	26	27	0
$NaPbCl_3$[i]	48	14	38	14	28	$\lesssim 15$	20	$\lesssim 3$
$KSnI_3$[j]	37	36	34	−5	25	20	24	−3

[a] Temperatures are the same as indicated in previous tables. Uncertainties in ΔH and ΔS are about 6 kcal/mole and 6 cal/deg mole $(AX)_2$, respectively.
[b] ΔH_1, ΔS_1 data for alkali halides from Bauer and Porter[9] or *JANAF* tables.[76]
[c] ΔH_2, ΔS_2 from Belousov *et al.*[77]
[d] ΔH_3, ΔS_3 from Krause and Douglas.[78]
[e] ΔH_3, ΔS_3 from Hastie *et al.*[60]
[f] ΔS_5 estimated; other data from Novikov and Gavryuchenkov.[10]
[g] ΔH_2, ΔS_2 from Berkowitz and Marguart.[79]
[h] ΔH_2, ΔS_2 from Karpenko and Novikov.[80]
[i] Because $(PbCl_2)_2$ was not observed as a vapor species,[35] an upper limit to its free energy of formation (ΔG_2) may be calculated from the instrumental detection limitation. ΔH_2 was estimated by comparison with the data for $(SnCl_2)_2$, and then ΔS_2, was obtained from the combination of ΔH_2 with ΔG_2.
[j] ΔH_2, ΔS_2 from Karpenko.[81]

eters.[76] In fact, ΔS_2 for $(BeCl_2)_2$ formation is about double that for the fluoride, which seems very unlikely.

In view of the now apparent extra stability associated with the formation of two M–F bridge bonds at the expense of a single terminal M–F bond, the possibility of further complexing of AMX_3 or AMX_4 is evident. Thus species of the type A_2MX_4, AM_2X_5, $(AMX_3)_2$, etc. are possible and, as indicated in previous tables, evidence exists for their formation.

The similar enthalpy changes for the reactions

$$2AlF_3 = (AlF_3)_2 \qquad \text{(see Table VII)}$$

and

$$2(NaAlF_4) = (NaAlF_4)_2 \qquad \text{(see Table III)}$$

are of note and should allow prediction for analogous systems. For example,

consider

$$2BeF_2 = (BeF_2)_2 \tag{1}$$

$$2NaBeF_3 = (NaBeF_3)_2 \tag{2}$$

and

$$\Delta H_2 \simeq \Delta H_1 = -33 \text{ kcal/mole} \qquad \text{(from Table VII)}$$

As indicated in Table VII, ΔS values for dimerization reactions do not vary significantly for similar systems and hence, from the analogous Al system, $\Delta S_2 = -28$ cal/deg-mole. With these data one predicts that, at a temperature of 1084°K, the abundance of $(NaBeF_3)_2$ is about 10^{-3} relative to $NaBeF_3$. This prediction coincides exactly with the observed[31] total relative ion intensities associated with these two species, thus lending support to the above approximations. The observation[45] of $(NaSnF_3)_2$ also is in accord with these predictions. One also would expect to see $(KMgCl_3)_2$ in a mass spectrometric experiment.

Recently obtained spectroscopic data for the MX_2 and MX_3 species have allowed accurate standard entropies to be calculated and, combined with the measured ΔS_4 or ΔS_5 data, allow $S_T°(AMX_3)$ and $S_T°(AMX_4)$ to be determined. As indicated in Fig. 5, these data follow a smooth trend with increasing molecular weight and, therefore, unknown entropies, and hence ΔS_3, may be interpolated from this relation.

In conclusion it is apparent that if simple molten salts have a tendency to vaporize as dimers, which is frequently the case, then mixtures of these salts will most likely produce mixed dimers and usually with a higher stability. An enhanced volatility of one of the component salts also is usual, a fact that may be of increasing practical importance. The prevalence of this vapor-complexing phenomenon, together with the predictions that can be made based on the ΔH and ΔS relations and by simple analogy with known systems, indicates the absolute necessity of establishing the identity of the vaporizing species. Certainly the application of mass spectrometry to the analysis of molten salt vapors has been a major factor in the understanding of such systems. However, the need for further work is readily apparent, both from the rather large experimental uncertainties in existing data and from the many molten salt systems that are as yet unstudied. It is expected that as more structural data, particularly vibrational frequencies, become available the third-law treatment of data will yield much more accurate ΔH and ΔS properties for these complex systems. The availability of structural data also would permit an extension, and application, of the dimensional theory of association to more complex systems than the alkali halide mixtures.

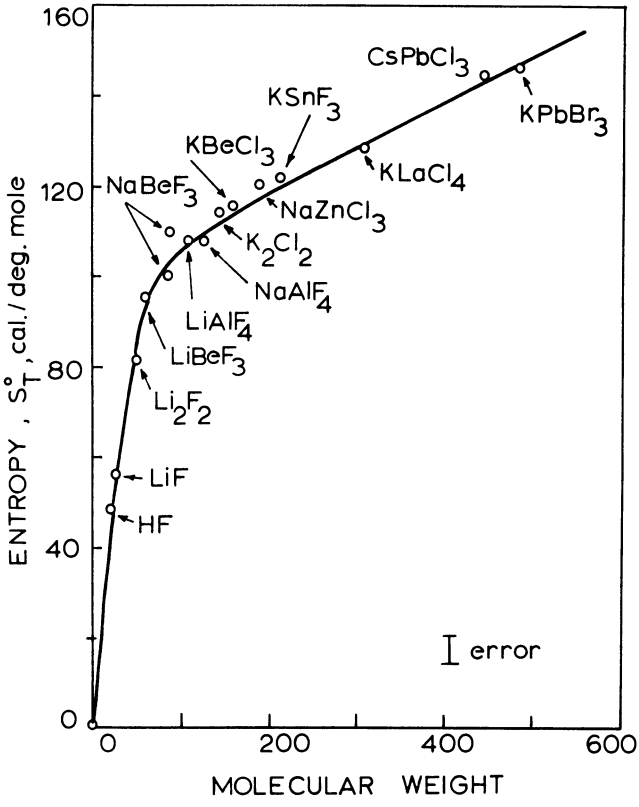

Fig. 5. Correlation of entropy with molecular weight. S_T° relates to the temperature of observation as listed in the tables. The vertical bar indicates the experimental uncertainty. Entropy values for the component species, that is AX, MX_2, or MX_3, were taken from the *JANAF* tables,[76] except for the following: $BeCl_2$ and BeF_2 [A. Snelson, *J. Phys. Chem.* **70**;3208 (1966)]; $ZnCl_2$ [A. Loewenschuss, A. Ron, and O. Schnepp, *J. Chem. Phys.* **49**:272 (1968)]; and $PbCl_2$, $PbBr_2$, SnF_2, and $LaCl_3$ were calculated from unpublished spectroscopic data of J. W. Hastie, R. H. Hauge, and J. L. Margrave (1969). The $NaAlF_4$ value is from Sidorov and Kolosov.[39]

REFERENCES

1. (a) M. Blander, ed., *Molten Salt Chemistry*, John Wiley (Interscience), New York (1964); (b) B. R. Sundheim, *Fused Salts*, McGraw-Hill, New York (1964); (c) J. Lumsden, *Thermodynamics of Molten Salt Mixtures*, Academic Press, New York (1966); (d) G. J. Janz, *Molten Salts Handbook*, Academic Press, New York (1967).

2. M. K. Reser, ed., *Phase Diagrams for Ceramists*, Suppl., American Ceramic Society, Columbus, Ohio (1969).
3. G. Mamantov, ed., *Molten Salts Characterization and Analysis*, Marcel Dekker, New York (1969).
4. N. I. Ionov, *Dokl. Akad. Nauk SSSR* **59**:467 (1948).
5. W. A. Chupka and M. G. Inghram, *J. Phys. Chem.* **59**:100 (1955).
6. J. R. Hightower, Jr., and L. E. McNeese, *Nucl. Sci. Abstr.* **22**:1044 (1968).
7. T. S. Zvarova and I. Svara, Rare-Earth Separation by Gas Chromatography of Chlorides, unpublished data, USSR (1969).
8. H. Bloom and J. W. Hastie, *J. Chem. Phys.* **49**:2230 (1968).
9. S. H. Bauer and R. F. Porter, in: *Molten Salt Chemistry* (M. Blander, ed.), p. 607, John Wiley (Interscience), New York (1964).
10. G. I. Novikov and F. G. Gavryuchenkov, *Russ. Chem. Rev.* **36**:156 (1967).
11. J. Drowart and P. Goldfinger, *Angew. Chem. Int. Ed.* **6**:581 (1967).
12. R. T. Grimley, in: *The Characterization of High Temperature Vapors* (J. L. Margrave, ed.), J. Wiley, New York (1967).
13. R. C. Svedberg, in: *Modern Aspects of Mass Spectrometry* (R. I. Reed, ed.), p. 169, Plenum Press, New York (1968).
14. R. T. Grimley and T. E. Joyce, *J. Phys. Chem.* **73**:3047 (1969).
15. P. A. Akishin, L. N. Gorokhov, and L. N. Sidorov, *Russ. J. Phys. Chem.* **33**:648 (1959).
16. J. W. Hastie, R. H. Hauge, and J. L. Margrave, *J. Chem. Phys.* **51**:2648 (1969).
17. J. L. Margrave, ed., *The Characterization of High Temperature Vapors*, John Wiley, New York (1967).
18. L. N. Sidorov and P. A. Akishin, *Dokl. Akad. Nauk SSSR* **151**:136 (1963).
19. T. A. Milne and H. M. Klein, *J. Chem. Phys.* **33**:1628 (1960).
20. R. F. Porter and R. C. Schoonmaker, *J. Chem. Phys.* **29**:1070 (1958).
21. R. F. Porter and R. C. Schoonmaker, *J. Phys. Chem.* **62**:486 (1958).
22. R. C. Schoonmaker and R. F. Porter, *J. Chem. Phys.* **30**:283 (1959).
23. M. Blander, *J. Chem. Phys.* **41**:170 (1964).
24. J. Guion, D. Hengstenberg, and M. Blander, *J. Phys. Chem.* **72**:4620 (1968).
25. A. V. Tarasov, A. B. Pospelov, and G. I. Novikov, *Vestn. Leningrad. Univ.* **21**, *Ser. Fiz. Khim.* No. 2, 97 (1966); also *C.A.* **65**:11417h (1966).
26. S. H. Bauer, R. M. Diner, and R. F. Porter, *J. Chem. Phys.* **29**:991 (1958).
27. A. Buchler and J. L. Stauffer, in: *Thermodynamics*, Vol. I, p. 271, International Atomic Energy Agency, Vienna (1966).
28. J. Berkowitz and W. A. Chupka, *Ann. N. Y. Acad. Sci.* **79**:1073 (1960).
29. G. I. Novikov and A. L. Kuzmenko, *Vestn. Leningrad Univ.* **19**(16), *Ser. Fiz. Khim.* No. 3, 165 (1964); also *C. A.* **62**:1317b (1965).
30. R. C. Schoonmaker, doctoral dissertation, Cornell University, Ithaca (1960).
31. L. N. Sidorov, V. I. Belousov, and P. A. Akishin, *Russ. J. Phys. Chem.* **43**:39 (1969).
32. K. A. Sense, R. W. Stone, and R. B. Filbert, Jr., *U. S. At. Energy Commi. Rese. Rep., BNI-1186* (1957).
33. E. E. Schrier and H. M. Clark, *J. Phys. Chem.* **67**:1259 (1963).
34. H. J. Moss, *Diss. Abstr.* **21**:3283 (1961).
35. H. Bloom and J. W. Hastie, *Aust. J. Chem.* **19**:1003 (1966); and J. W. Hastie, doctoral dissertation, University of Tasmania (1966).
36. D. W. Rice and N. W. Gregory, *J. Phys. Chem.* **72**:4524 (1968).

37. A. Snelson, *Optical Spectra of Some Low-Molecular Weight Compounds Using the Matrix Isolation Technique*, Rep. IITRI-U6001-13, U. S. Army Research Office (1966).
38. R. F. Porter and E. E. Zeller, *J. Chem. Phys.* **33**:858 (1960).
39. L. N. Sidorov and E. N. Kolosov, *Russ. J. Phys. Chem.* **42**:1382 (1968).
40. E. H. Howard, *J. Amer. Chem. Soc.* **76**:2041 (1955).
41. E. W. Dewing, *J. Amer. Chem. Soc.* **77**:2639 (1955).
42. V. P. Spiridonov and E. V. Erokhin, *Dokl. Akad. Nauk SSSR* **180**:161 (1968).
43. L. D. McCory, R. C. Paule, and J. L. Margrave, *J. Phys. Chem.* **67**:1086 (1963).
44. P. A. Akishin, N. G. Rambidi, and E. Z. Zasorin, *Kristallografiya* **4**:186 (1959).
45. J. W. Hastie, K. F. Zmbov, and J. L. Margrave, *J. Inorg. Nucl. Chem.* **30**:729 (1968).
46. N. V. Karpenko, *Russ. J. Inorg. Chem.* **12**:1556 (1967).
47. H. Bloom and J. W. Hastie, *J. Phys. Chem.* **72**:2706 (1967).
48. H. Bloom and J. W. Hastie, *Aust. J. Chem.* **21**:583 (1968).
49. N. V. Karpenko and T. N. Sevast'yanova, *Vestn. Leningrad. Univ., Fiz. Khim.* **22**:109 (1967).
50. H. Bloom and J. W. Hastie, *J. Phys. Chem.* **72**:2361 (1968).
51. S.-Wu P. and T.-L. Chen, *K'o Hsueh T'ung Pao* **3**:268 (1965); *C. A.* **64**:4290h (1966).
52. P. Kusch, *J. Chem. Phys.* **22**:1203 (1954).
53. R. R. Richards and N. W. Gregory, *J. Phys. Chem.* **68**:3089 (1964).
54. L. N. Sidorov, Yu. M. Korenev, V. B. Sholts, P. A. Akishin, and V. P. Frolov, *Russ. J. Phys. Chem.* **41**:371 (1967).
55. L. N. Sidorov, P. A. Akishin, V. I. Belousov, and V. V. Sholts, *Russ. J. Phys. Chem.* **38**:641 (1964).
56. F. G. Gavryuchenkov and G. I. Novikov, *Zh. Neorg. Khim.* **4**:1515 (1966); *C. A.* **65**:12906h (1966).
57. G. A. Semenov and F. G. Gavryuchenkov, *Russ. J. Inorg. Chem.* **9**:123 (1964).
58. G. I. Novikov and A. K. Baev, *Vestn. Leningr. Gos. Univ.*, Pt. 3(16):3, 89 (1962).
59. F. G. Gavryuchenkov and G. I. Novikov, *Vestn. Leningrad Univ.* **21**(4), *Ser. Fiz. Khim.* **1**:106 (1966); *C. A.***65**:86b (1966).
60. J. W. Hastie, P. J. Ficalora, and J. L. Margrave, *J. Less Common Metals* **14**:83 (1968).
61. J. W. Hastie and J. L. Margrave, *High Temp. Sci.* **1**:1737 (1969).
62. R. C. Schoonmaker, A. H. Friedman, and R. F. Porter, *J. Chem. Phys.* **31**:1586 (1959).
63. H. M. Rosenstock, J. R. Sites, J. R. Walton, and R. Baldock, *J. Chem. Phys.* **23**:2442 (1955).
64. A. Büchler, P. E. Blackburn, and J. L. Stauffer, *J. Phys. Chem.* **70**:685 (1966).
65. A. H. Conley and S. T. Cohen, *Inorg. Chem.* **4**:1221 (1965).
66. R. F. Porter, D. R. Bidinosti, and K. F. Walkerson, *J. Chem. Phys.* **36**:2104 (1962).
67. A. G. Massey and D. S. Urch, *Proc. Chem. Soc. London* 284 (1964).
68. D. W. Tarasenkov and L. L. Klyachko-Gurvich, *J. Gen. Chem. USSR* **6**:305 (1936); *C. A.* **30**:7427.
69. G. I. Novikov, A. K. Baev, and O. G. Polyachenok, *Khim. Redk. Elem. Leningrad Gos. Univ.* 63 (1964).
70. H. A. Oye and D. M. Gruen, *J. Amer. Chem. Soc.* **91**:2229 (1969).
71. A. Snelson, *J. Phys. Chem.* **73**:1919 (1969).

72. J. W. Hastie, R. H. Hauge, and J. L. Margrave, in: *Spectroscopy in Inorganic Chemistry* (J. Ferraro and N. Rao, eds.), Academic Press, New York (1970).
73. V. A. Maroni and E. J. Cairns, in: *Molten Salts Characterization and Analysis* (G. Mamantov, ed.), p. 231, Marcel Dekker, New York (1969).
74. K. F. Zmbov, P. Ficalora, and J. L. Margrave, *J. Inorg. Nucl. Chem.* **30**:2059 (1968).
75. K. F. Zmbov, O. M. Uy, and J. L. Margrave, *J. Phys. Chem.* **73**:3008 (1969).
76. D. R. Stull, ed., *JANAF Thermochemical Tables*, (No. PB-168-370, Clearinghouse for Federal Scientific and Technical Information, Springfield, Virginia (August 1965).
77. V. I. Belousov, L. N. Sidorov, S. A. Komarov, and P. A. Akishin, *Russ. J. Phys. Chem.* **41**:1598 (1967).
78. R. F. Krause, Jr., and T. B. Douglas, *J. Phys. Chem.* **72**:475 (1968).
79. J. Berkowitz and J. R. Marquart, *J. Chem. Phys.* **37**:1853 (1962).
80. N. V. Karpenko and G. I. Novikov, *Vestn. Leningrad. Univ.* **22**, *Fiz. Khim.* No. 1, 72 (1967).
81. N. V. Karpenko, *Zh. Neorg. Khim.* **12**:3248 (1967).
82. F. J. Keneshea and D. Cubicciotti, *J. Chem. Phys.* **40**:191 (1964).

AUTHOR INDEX

Numbers in parentheses are reference numbers for authors whose names are not explicitly given in the text. Underlined numbers indicate the page on which the reference is listed.

FORMULA INDEX

SUBJECT INDEX